Natural and anthropogenic regime variance of a seagrass ecosystem: A late Anthropocene palaeo-reconstruction

By

John Barry Gallagher (B.Sc. (Hons), M.Sc.)

A thesis submitted in total fulfilment of the requirements of the degree of

Doctor of Philosophy

University of Tasmania

February 2013

Looking down on to the entrance of Little Swanport estuary. In the foreground are the estuary's oyster leases. (Photograph by Dr. Francisco Neira).

Declaration

This thesis contains no material which has been accepted for a degree or diploma by the University or any other institution, except by way of background information and duly acknowledged in the thesis, and to the best of the author's knowledge and belief no material previously published or written by another person except where due reference is made in the text of the thesis, nor does the thesis contain any material that infringes copyright.

……..

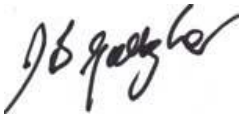

John Barry Gallagher

Authority of Access

This thesis may be made available for loan and limited copying in accordance with the

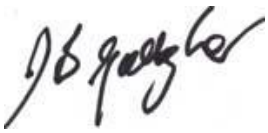

Copyright Act of 1968.

……..

John Barry Gallagher

Acknowledgements

I would like to express my appreciation to the following people for comments that led to improvements to the thesis document:

- My partner Diana Davies for her patience and support in managing the ordeal of proof reading all the chapters.
- Research supervisor Dr. John Gibson, whom I have known for many years, for Chapters 2, 4, 5 and 6, congenial robust and interesting dialectics and for some assistance in the field.
- Dr. Regina Magierowski for Chapter 7 and for many delightful two-way exchanges of knowledge and ideas.
- Program supervisor Dr. Christine Crawford for Chapters 1, 2, and 8.
- Program supervisor Dr. Jeffery Ross for Chapters 2, 3 and 8 and for some assistance in the field.
- Primary program supervisor Professor Ted Lefroy for Chapter 1 and his financial support through the CERF Hub Landscape Logic.
- Dr. Krystyna Saunders for her assistance in identifying fossil diatoms.

Finally, School of Zoology and the Institute of Marine Science for their logistical and financial support.

Contents

List of Figures

List of Tables

List of Abbreviations

ANSTO	Australian Nuclear Science and Technology Organisation
AINSE	Australian Institute of Nuclear Science and Engineering
BSi	biogenic silica
CIC	constant initial concentration
CPN	concentration of potential inorganic nitrogen
CRS	constant rate of supply
CSIRO	Commonwealth Scientific Industrial Research Organisation
CUSUM	cumulative sum of a statistic within an ordered series
WABC	West Australian Biogeochemistry Centre
DB	Depositional Basin
DTOC	diagenetically corrected total organic carbon
DTOC	diagenetically corrected particulate organic carbon
IBE	inference to the best explanation
LOI	loss on ignition
LSPMB*xyy*	Little Swanport estuary's central middle basin, *x* cores number and *yy* a year in the 21st century.
MAR	mass accumulation rate
MB	Middle Basin
NSW	New South Wales
OM	organic matter
PON	particulate organic nitrogen
POC	particulate organic carbon
RA	Robustness Analysis
RD	residual detritus
RMA	reduced major axis
SB	sandy basin of the Marine Flood/Tidal Delta
SC	self-consistency
SM	sediments from salt marsh sampling sites
SNS	soils from steep dry sclerophyll forest sampling sites
SP	soils from eroded pasture sampling sites
SPM	suspended particulate matter
SSA	singular spectrum analysis
SSAM	singular spectrum analysis for missing data

SSS	sediments from shallow slope dry sclerophyll forest sampling sites
BSi	biogenic silica
DBSi	total biogenic silica corrected for loss from dissolution
TOC	total organic carbon
TON	total organic nitrogen
WABC	West Australian Biogeochemistry Centre
WB	Watch House Basin
ZI	westerly wind zonal index

Abstract

Seagrass meadows, such as found in the Little Swanport estuary, Tasmania, Australia, provide a high ecosystem service that typically responds to natural destructive events and nitrogen loading at decadal to inter-decadal scales. Consequently, determining and understanding the effects of anthropogenic impacts, such as the estuary's shellfish aquaculture, requires an ecological time series of sufficient length to develop a long-term predictive theory behind changes to pattern and process and distinguish anthropogenic from natural effects. The aims of this study were to produce the appropriate long-term ecological time series for the Little Swanport estuary by combining sediment core and long term datasets (83 years to 139 years) in a palaeo-reconstruction that includes natural and anthropogenic variability, and to develop a general predictive theory behind pattern and process. The reconstructed time series was designed to include the elements of top down and bottom up control on the reconstructed seagrass–micro-algal assemblage: planktivorous fish predation, copepod feeding, calcareous sessile epifauna, seagrass-mediated nitrogen fixation, and external nutrient supply as the concentration of potential inorganic nitrogen (CPN).

Ecosystem variance in the upper region of the estuary differed from the lower estuary. Within the upper estuary, weight of evidence suggested variability was consistent with decadal periods of seagrass meadow destruction and recovery as two seagrass transient regime states, followed by stable natural and impacted seagrass regime states. The transient regimes appeared to be limited by nitrogen, the natural stable regimes appeared to be limited by light and the impacted regime had a near complete reliance on light mediated nitrogen fixation. The switch between nitrogen and light limiting resources was consistent with a change from a strong to weak top down control by a planktivorous fish–copepod–sestonic–calcareous epifaunal trophic cascade. Comparisons with both temporal and spatial natural patterns and processes indicated the dependence of nitrogen fixation was the result of the lower estuary shellfish aquaculture 'soaking up' the supply of inorganic nitrogen from coastal waters during an extended period of drought.

Within the lower estuary there was no evidence of direct effects of floods, tsunamis or shellfish aquaculture on the long-term pattern and process. Nevertheless, there was an uninterrupted repeatable natural ecosystem periodicity (*i.e.* a neutral model) of 57.9 years for the seagrass and micro-algal assemblage and a planktivorous fish–copepod–sestonic–

calcareous epifaunal trophic cascade with a CPN at twice the biome frequency. The seagrass and micro-algal assemblage was inversely correlated but the trophic cascade was 13 years out of phase, driven by a CPN periodicity at twice the biome frequency in phase with the peaks and troughs of the seagrass and micro-algal assemblage. As a consequence, there was a change from a positive to a negative correlation of the CPN with seagrass abundance that was consistent with a change from seagrass nitrogen to light limitation. This switch was coincident during times of a CPN minimum together with strong and weak top down control respectively. By linking changes in top down control with the evolution of a seagrass meadow's configuration a general theory of seagrass meadow dynamics was developed, constructed, in part, from data and generic postulates taken from other seagrass ecosystems systems.

The theory unified two desperate approaches to seagrass meadow variance, namely light and nutrient limitation, within the framework of landscape ecology and consequently highlighted a number concerns for managers of seagrass ecosystems: (1) the loss of a seagrass meadow by flood damage may produce a seagrass transient regime and not a micro-algal regime, in which recovery of the transient is assisted by a moderate increase and not a reduction in nutrient supply; (3) changes to the extent of the landscape patch configuration can determine the light and nutrient limitation status of the seagrass meadow, consequently, rehabilitation of the seagrass meadow after loss or damage, by replanting or through the control of nutrient supply, may need to take into account the landscape patch configuration of the plantation or the damaged landscape in relation to the dynamics of nutrient supply; (4) the effects on the seagrass meadow from over-harvesting of planktivorous fish fishing or the introduction of piscivorous fish will depend on the light or nutrient limitation status of the seagrass meadows.

Chapter 1. General introduction. Separating and understanding anthropogenic change from natural variability: An ecosystems approach

1.1. Introduction

Around the world, there is a growing realisation that healthy estuary ecosystems hold the key for users of the waterway's sustainable economic and social wellbeing. However, defining what constitutes a healthy and sustainable ecosystem often leads to tension between estuary users, catchment management of water and nutrient resources to the estuary and environmental organisations. In the mid-1990s, the 'Convention on Biodiversity' (CBD, 1998), in recognition of these kinds of problems, endorsed the ecosystems approach and defined a strategy for integrated management of land, water and living resources that promotes conservation and sustainable use in an equitable way. By 1998, 12 guiding principles and operational guidelines had been produced. Of the 12 principles, four were concerned with the nature of the ecosystem:

- Ecosystems must be managed within the limits of their function.
- The approach should be taken at the appropriate spatial and temporal scales.
- Processes and objectives for ecosystem management should be set for the long term.
- Management must recognise that change is inevitable.

These principles are exemplified by the tension between users of Little Swanport's catchment/estuary system, situated on the east coast of Tasmania. Presently, the estuary supports both a lush seagrass ecosystem and a shellfish aquaculture industry. The aquaculture industry's concerns have been focused on a reduction in micro-algal productivity should catchment water and nutrient resources be diverted towards catchment development. In contrast, too much or too little nutrient loading may lead to the loss of seagrass (Duarte, 1995; Nienhuis *et al.*, 1996; Frederiksen *et al.*, 2004a; Duarte *et al*., 2006). Loss of seagrass directly affects both recreational users of the estuary and environmental groups, as healthy seagrass meadows support a high level of biodiversity, habitat for game fish (Black Bream) and relatively clear water.

Management policies that react only to contemporary issues can fail to account for the effect of climate variability. The climate of the east coast of Tasmania has been subject to decadal periods of wet and drought conditions (Khalia *et al.*, 2009) and Little Swanport estuary has

experienced periodic damaging floods that have forced the shellfish industry to relocate to the lower part of the estuary.

Landres *et al.* (1999), and more recently Jackson (2001) using examples from coastal waters, and Willis and Birks (2006), Reeves and Duncan (2009), Duncan *et al.* (2010) from lake river systems respectively, conclude that natural variability is a reality and should be sustained as a precautionary principle in line with the above operational guidelines. Human activities that attempt to stabilise a system in one particular state by removing natural disturbances (*e.g.* river dams) often reduce resilience by eliminating mechanisms that allow the system to adapt to external change, making them more likely to pass thresholds and undergo dramatic shifts to possible undesirable states. For example, the placement of dams on riverine systems removes natural flow variability and, along with that, the ability of many plant and animal populations associated with the recovery from natural flood disturbances (Graf, 2003).

Alternatively, Costanza and Mageau (1999) in their approach to ecosystem assessment of aquatic systems introduced the concept of 'health' by comparing the system's present evolutionary state to what would have been expected under natural conditions. In this way, a healthy aquatic biome is one that will survive over its expected lifespan, while an unhealthy aquatic biome will have its lifespan cut short (*e.g.* oligotrophic to eutrophic and *vice versa*). These approaches to aquatic ecosystem management, Landres *et al.'s* (1999) variability and Costanza and Mageau's (1999) health, are neither contradictory nor disparate in their approach. Aquatic health is complimentary to natural variability by contextualising variability as the aquatic system evolves. That is, from the standpoint of Landres *et al.* (1999), changes in variability as the ecosystem evolves are part of natural variability, but at a longer time scale, and ecosystem health recognises an unnatural anthropogenic acceleration in that evolution. From the standpoint of Costanza and Mageau, a description of natural intra-state variability is required to calibrate a healthy state.

Yet, Costanza and Mageau's (1999) aquatic health concept, linked to a natural evolutionary state, may be too simplistic for practical application. Currently, oligotrophication and eutrophication in seagrass and other benthic systems are marked by the dominance of micro-algae over seagrass (Duarte, 1995; Borum and Sand-Jensen, 1996). However, a complete loss of seagrass can also result from oligotrophication (Nienhuis *et al.*, 1996). Benthic oligotrophic

and mesotrophic systems can also exhibit two alternative stable regimes[1] namely, seagrass or micro-algal at same level of eutrophication, together with their persistent dynamic transient states (Scheffer and Carpenter, 2003; Knowlton, 2004). Further, it appears that at the landscape scale, the seagrass-dominated state can be divided into two separate functional regimes, which are affected in different ways by external forcing factors. These are either light limitation of seagrass growth (*e.g.* Duarte, 1995; Duarte *et al.*, 2006) or nutrient limitation of seagrass (*e.g.* Fourqurean and Zieman, 2002). Hence, natural ecosystem variability may exhibit three hierarchies: (1) variability between different ecosystem regimes, (2) variability in the number of different regimes, (3) variability within each regime.

With the three above hierarchies, there are two potential different impacts from anthropogenic forcing: (1) different effects on different regimes or (2) different variability between regimes. Thus, ideally any assessment of anthropogenic impacts on natural variability should: (1) measure the anthropogenic effects over the range of natural variability and (2) measure the anthropogenic effect across the range of ecosystem regimes. However, the result of anthropogenic impacts can also be dependent on the ecosystem state at the time of impact (*i.e.* historical contingency Strayer *et al.*, 1986). Consequently, and as a matter of practicality, evidence-based studies based on time series need to be augmented by current landscape spatial theories and newly developed theories of long-term ecosystem variance. In this way, predictions on the complete range of natural regimes can be made for anthropogenic impacts.

1.1.1. Temporal and spatial scales

Landres *et al.* (1999) cautioned against using a single *a priori* period to define natural variability. From the standpoint of ecosystem services, it can be argued that the scales of the study are determined by both the temporal and spatial concerns about anthropogenic impacts. For example, a hypothetical genetic harvesting of a species with a distribution at a patch scale, for a limited specific use, may be of concern for a patch ecology that responds over a season (Fonseca and Bell, 1998). In contrast, a seagrass meadow or an aquaculture lease at landscape scales, traditionally a km^2 or more (Allen and Hoekstra, 1990) must maintain itself over decadal economic cycles and human generation times. For aquatic management, Reeves and Duncan (2009) suggest a temporal scale of between 10 and 100 years, which is well within the

[1] Alternative states have independent feedbacks that maintain each regime state expressed by a backwards folding curve (hysteresis) in their response to nutrient loading (Scheffer and Carpenter, 2007). Ecological regime shift: a sudden shift in ecosystem status caused by passing a threshold where core ecosystem functions, structures and processes are fundamentally changed (Andersen *et al.*, 2008).

range of the ecosystem scales imposed on Little Swanport estuary through climatic and coastal current variability (Harris *et al.*, 1987, 1988; Stenseth *et al.*, 2003; Evans *et al.*, 2005; Nunez and McGregor, 2007; Hill *et al.*, 2008), *Zostera* spp meadow dynamics (Larkum and West, 1983; Giese, 1988; Duarte, 1995; Cunha *et al.*, 2005) and the period of aquaculture exposure (from around 1980 to the present).

Wiens (1989), in a classic discussion paper on scale, argued that an appropriate temporal scale for landscape evolution must match any theory developed or used at the landscape configuration scale. Wiens (1989) then warned that applying a theory formulated from just a spatial consideration would likely suffer from pseudo-prediction if applied across the matching temporal scale. That is, a failure to recognise an emerging property due to a long-term non-linear dynamic at shorter time scales. Indeed, it is increasingly realised that the importance of internally generated non-linear dynamics between the ecosystem and/or landscape leads to an emergent long-term dynamic that cannot be predicted at shorter or small spatial scales (*e.g.* Carpenter and Kitchell, 1988; Hastings and Higgins, 1994; Kareiva and Wennergren, 1995; Pastor *et al.*, 1996; Rietkerk *et al.*, 2004; Kendrick *et al.*, 2005; van Nes *et al.*, 2007).

Gunderson and Holling (2002) viewed coupled human–natural systems as a ‘panarchy’: an interacting set of adaptive cycles that reflect the dynamic nature of human and natural structures across time and space. For example, the surprising result that found the extent of seagrass meadows have varied over the long-term due to the natural cycle of storm destruction and recovery, together with a natural periodicity of climate has motivated changes in which estuaries need to be managed (Jackson, 2001). Consequently, managers need simple evidence-based long-term landscape predictive models of ecosystem variance to protect ecological systems from human-scale anthropogenic impacts and to meet future social goals (Peters, 1991). Clearly, these predictive models must possess predictors that can be manipulated through engineering or environmental policy. They must either be of sufficient power to incorporate different regimes and their transition ecotones or be separate theories for different regimes that have previously been identified based on their ecosystem descriptors (*see* Scheffer and Carpenter, 2003).

1.2. Current theories of landscape-scale seagrass variance

1.2.1. Contiguous theories

There is no current unified theory that addresses all aspects of seagrass meadow variability at a landscape scale. In place of one unified theory, researchers and managers are forced to ascertain the functional state of the seagrass meadows regime in order apply one of two disparate theories based on meadow growth limited either by light or by nutrient supply (see Boer, 2007 for a review of examples and references). Light limitation is the result of excessive nutrient eutrophication, which leads to increased shading by net micro-/macro-phytal and calcareous epifaunal production within the water column and on seagrass leaves (Duarte, 1995; Borum and Sand-Jensen, 1996). Nutrient limitation is attributed to insufficient micro-/macro-phytal and epifaunal shading of seagrass leaves, which limits the availability of ambient light (*e.g.* Frankovich and Fourqurean, 1997).

Some long-term studies based on meadow coverage and water quality, however, have failed to account completely for the long-term continued decline of seagrass meadows (Jackson, 2001; Martin *et al.*, 2010) or variability (Nienhuis *et al.*, 1996; Morris and Virnstein, 2004; Frederiksen *et al.*, 2004a). There are many possible reasons behind the failure of current long-term studies: (1) the choice of predictive processes and components does not match the particular light or nutrient limited regime or combination of regimes along the time series; (2) missing blocks of data and different resolutions between processes and components (*e.g.* Frederiksen *et al.*, 2004a; Martin *et al.*, 2010) might lead to aliasing and either hide the underlying dynamics or produce aberrant correlations and long-term trends where there were none; (3) studies have not been designed to recognise or account for an emergent property, consequently models will probably lead to pseudo-prediction over the long-term (Wiens, 1989); and (4) the affects of external forcing factors may only emerge in the long term (*e.g.* Jackson, 2001).

Clearly, a neutral model[2] of ecosystem variance over a complete range of nutrient and light limited seagrass regime states[3] is needed as a basis to assess whether there has been an impact on seagrass systems today, through direct damage, catchment erosion, over fishing, over

[2] A neutral model is a minimum set of rules required to generate a spatial unit's complex deterministic patterns (Caswell, 1976; Gardner et al., 1987). In its temporal form the pattern can be expressed as an ecosystem attractor in phase space *e.g.* phytoplankton–zooplankton–nutrient supply as a 3−D manifold (Scheffer, 2004).

[3] Andersen *et al*. (2008) define regime change as a sudden shift in ecosystem status caused by passing a threshold at which core ecosystem functions, structures and processes are fundamentally changed.

grazing from anthropogenic ecosystem imbalance, eutrophication, aquaculture or disease (Jackson, 2001; Orth *et al.*, 2006). In addition, a general theory is needed to explain the mechanisms that stabilise/destabilise the light and nutrient limited regime states and the switch from one resource limitation to another.

Current research outside of direct animal grazing has focused on the potential of top-down control of the seagrass epiphyte community *via* predation of the meso-grazer community (Heck *et al.*, 2000; Heck and Valentine, 2006; Jorgensen *et al.*, 2007; Moksnes *et al.*, 2008). The argument is based on recognition that planktivore predation might play an important part in the buffer capacity of a nutrient limited regime state. Thus, any changes to planktivore numbers, natural or anthropogenic, will affect the stability of the seagrass regime through its buffer capacity. For example, a re-examination of Jorgensen *et al.'s* (2007) data suggest that oligotrophic seagrass meadows in San Quentin Bay (USA) are nutrient limited, while its mesotrophic and eutrophic seagrass meadows are light limited. This means that seagrass leaf growth at the oligotrophic sites is equal to or greater than at the eutrophic sites, and that a reduction in planktivore predation on seagrass meso-grazers appears to reduce the seagrass regimes buffer capacity for nutrient driven growth as increasing epibiont coverage eventually leads to light limitation.

Unfortunately, trophic cascade research is currently limited to the following areas: (1) simple modelling (Livingston, 1984) that recognises the non-linear responses of meso-grazer clearance rates for maintaining seagrass coverage at the patch scale, (2) experiments at the patch scale with exclusion from the remaining ecology (Heck *et al.*, 2000; Heck and Valenine, 2006; Moksnes *et al.*, 2008), (3) ecosystem correlations at the seasonal patch scale in an open ecology (Jorgensen *et al.*, 2007) or (4) over decadal periods of contiguous monitoring at the patch scale within an open ecology, but limited by the non-matching periods of some ecosystem components (Douglass *et al.*, 2010).

It is perhaps because of lack of attention to the configuration state and/or knowledge base of the researchers that the focus has been to regard any changes in planktivore predation as a surrogate external forcing factor and as implicitly independent of the physical state of the seagrass meadow. However, it is being increasingly realised that total planktivore predation within a seagrass meadow might vary out of proportion with coverage by the size, patch configuration and shoot density within the meadow. For example, Jelbart *et al.* (2007) found that planktivorous fish numbers were in higher densities and numbers in smaller patches.

Macreadie *et al.* (2009, 2010), using artificial seagrass, confirmed that increasing coverage was not synonymous with increasing planktivore abundance and that the corridors between patches might increase predation efficiency. Priyadarshana *et al.* (2001) found that shoot density can also affect planktivorous fish predation efficiency, although this might also be covariant with patch size. Consequently, the stability of both function regimes (light or nutrient limitation to growth) might vary as a function of meadow coverage, which in turn would affect the seagrass response to nutrient loading.

1.2.2. Effects from events

Implicit within the theories of long-term bottom-up or top-down control is the concept of ecosystem quasi-equilibrium with external forcing within a seagrass alternative regime state. Hence, consideration must be given to the effect of destructive events such as storms, floods and marine incursions. Destructive events, by their nature, remove the biome far from equilibrium within its continuous regime state, with recovery to an equilibria, potentially requiring more than a decade (*e.g.* Morris and Virnstein, 2004; Byron and Heck, 2006). In other words, the natural variance may include a significant proportion of dynamic transient regime states. Alternatively, the seagrass ecosystem might switch to an alternative discontinuous state, a path with hysteresis, dominated by micro-algal species (Scheffer, 2004; Bayley *et al.*, 2007). Consideration must also be given to an event's historical contingency. For example, hurricanes can destroy seagrass meadows (Byron and Heck, 2006), but they can also temporarily lead to the re-emergence of healthy seagrass meadows, a dynamic transient of several years after initially removing organic enriched, sulphidic sediments (Morris and Virnstein, 2004). It is currently unknown whether this situation also exists in relation to river floods. Depending on the frequency of events, estuarine ecosystems systems may never reach their stable end states, otherwise dictated by current rates of nutrient supply (*e.g.* Morris and Virnstein, 2004, uncommented). Thus understanding transient states driven by historical events in relation its alternative regime attractor may be more relevant in predicting long-term ecosystem variability than a choice between stable regime states (Knowlton, 2004).

1.3. Patterns of long-term ecosystem variance for a predictive ecology

The advantage of describing long-term variance at a landscape scale is the synergy that can be achieved between evidence-based results and the testing and/or formulation of theories from patterns and between components and processes through 'narrative knowing' (Mohr, 1982; Polkinghorne, 1988; Bruner, 1991). The great evolutionary biologist, Ernst Mayr (1982), credits the power of the temporal comparative method for 'nearly all of the revolutionary

advances in evolutionary biology'. Similarly, Deevy (1969), through a series of natural experiments (multi-chronic nested contrasts), illustrated how history has coaxed insights on ecosystem stability in ways not possible using spatial studies, while Coull (1985) illustrates how a contiguous time series of environmental data is currently one of the best and most practical means of formulating testable ecological hypotheses. Indeed, McGuinness (1988) 'demonstrated the dangers of drawing conclusions about processes based solely on spatial differences as natural experiments'; unrecognised factors can and do act to violate underlying assumptions.

New ecosystem theories based on long-term correlative studies, however, need not be restricted to the study's location, in this case the Little Swanport estuary. This is provided that the theory was developed in relation to a combination of experiments, natural history observations at the smallest level of abstraction common to all seagrass ecosystems (neutral model) that have been affected by common natural and anthropogenic pressures. That is, a detrital seagrass ecosystem system that can be explained with planktivores representing the highest significant trophic level (Valentine and Duffy, 2006) that may be affected by changes in nutrient supply (Duarte, 1995), increased flooding due to climate change (Milly et al, 2002) and the effects of global expansion of shellfish aquaculture along the coastal strip (Shumway, 2011). In this way, a scale independent narrative of processes and events can be applied at the minimum level of abstraction to other similar seagrass ecosystems around the world (excluding floods within the Mediterranean) or to judge the effects on the underlying ecology system by the presence of higher trophic levels (piscivores and seagrass grazers), pollution and other forms of direct damage

The disadvantage of long-term monitoring, and the condition of long-term monitoring data sets, is suggested by this method's failure to account for long-term variance in seagrass meadow coverage (see above). In brief, long-term records (decadal to inter-decadal) are rare (and without exception relatively short, incomplete and/or non-contiguous) for most estuary and coastal ecosystems with respect to the dynamics of the keystone predators or the meadow dynamics of vegetative foundation species. Reasons for this include that funding organisations are often reluctant to initiate long-term studies; studies are difficult to maintain; and studies are often limited in the range of processes and components they encompass, with a bias towards monitoring phytoplankton and serving the purpose of compliance with water quality standards, rather than being for hypothesis testing (Strayer *et al.*, 1986).

1.3.1. A solution: Recreating and augmenting ecological data sets

A traditional alternative to limited ecosystem long-term data sets is a palaeo-reconstruction of the ecosystem processes and components, integrated across its immediate surrounds from material deposited within the sump of the estuary's deep-water sediment column (*e.g.* Leavitt *et al.*, 1994). Of course, ecological reconstructions do not directly measure past events.[4] More usually, they use indirect proxies for evidence of an event as part of a holistic unit of events, evidence and explanation (Inkpen and Wilson, 2009). In this way, emergent ecosystem theories can be developed or tested from a pattern of correlations and constraints on hypotheses based on the sub-components of the ecosystem from previous experimental and correlative work (*e.g.* Carpenter and Leavitt, 1991; McGowan *et al.*, 2005).

Conflict arises when the ecosystem patterns have more than one set of holistic explanations. Either the proxy is related to a type of event or there is an alternative explanation for that event. For example, biogenic silica (BSi) is one of the more common proxies used to represent marine micro-algal populations (MOLTEN, 2004). However, this assumes that marine diatoms have always dominated the micro-algal population or that BSi is diatomaceous, which is not always the case. BSi is an operational definition that may overlap with other more dominant marine and non-marine siliceous forms, such as sponge spicules (*e.g.* Conley and Schelske, 1993) or inputs of catchment phytoliths transported by rivers (*e.g.* Carey *et al.*, 2005). Alternatively, explanations of patterns between different sedimentary signals might depend on those signals representing different proxies. For example, organic carbon stable isotope ratios can be a proxy for the primary productivity assemblages' inorganic carbon source, relative rates of production (Burkhardt *et al.*, 1999), different organic mixtures (*e.g.* Gonneea *et al.*, 2004; Turner *et al.*, 2006) and relatively early loss of materials from dissolution (Chen and Windom, 1997) or mineralisation (Zimmerman and Canuel, 2002).

To overcome the uncertainty in the choice of possible explanatory sets, there are currently four recognisable scientific justification methods within the time-series and palaeo-ecological literature: Robustness Analysis (RA), abductive inference to the best explanation (IBE), self-consistency (SC), and a re-analysis of an imputed and hindcasted time series. In practice, all

[4] The term event is used as an expansive term by Inkpen and Wilson (2009). In this context, it includes biological entities, external events such as marine incursions, floods and storms, as well as contiguous changes in external forcing factors such as river flows, tides, nutrient loading and in part internally generated physical forcing factors such as salinity, stratification, residence time and water temperature.

four of these methods of scientific justification are compatible and should be (Inkpen and Wilson, 2009), and were, used together in this study. The references in the following list refer to a well-considered example of each method:

- Coincident RA (Bycroft, 2009) by using the convergence of a cluster of direct proxies per unit, component or process, which can confirm the result and imply the truth and generality of the convergent proxies (*e.g.* Zong *et al.*, 2006);
- IBE (Lipton; 2000) uses the relationships between multiple component and process proxies to constrain multiple explanations (*e.g.* Zimmerman and Canuel, 2002);
- SC with current theories, together with a partial evaluation of the dynamics from a few examples of real data that span the dynamic range (*e.g.* McGowan *et al.*, 2005); and
- Re-analysis after statistical imputation of non-contiguous data sets (Kondrashov *et al.*, 2005; Kondrashov and Ghil, 2006; Golyandina and Osipov, 2007).

In this way, multiple proxies were evaluated from RA convergence clusters and hierarchical models (see Figure 1.1) and supported through SC with contemporary observations. Singular proxies were evaluated by IBE between new sets of ecosystem components and processes from all of the evaluated reconstructed proxies and available data sets after statistical imputation, towards a new ecological synthesis.

1.3.2. Robustness analysis

In RA, the problem of possible multiple hypotheses is solved through a cluster of independent proxies used for the target event or entity. This strategy was originally developed by Levins (1966) for evaluating the 'truth' of population modelling:

> [w]we attempt to treat the same problem with several alternative models each with different simplifications but with a common biological assumption. Then, if these models, despite their different assumptions, lead to similar results we have what we call a robust theorem, which is relatively free of the details of the model. Hence, our truth is at the intersection of independent lies (Levins, 1966, p.423).

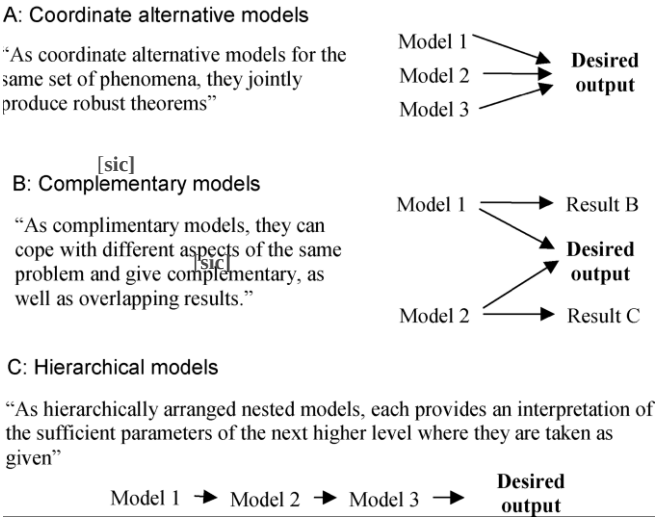

Figure 1.1. Levins satisfactory theory, showing the three types of model cluster. Copied from Nagy *et al.* (2007).

In Levins' original form, the clusters represent independent models rather than clusters of data sets from independent lines of evidence. Based on this and other formal logic considerations, philosophers of experimental science have analysed the merits of different forms of RA. However, it was Weisberg (2006) that convincingly argued that Levins' RA, based on a systems modelling architecture, could not confirm theorems but only identify them as robust (internal RA). Bycroft (2009) expanded the classification of RA from that of Weisberg to include coincident RA for data sets and mixed RA for models of proxies. The difference is that both forms of RA can confirm their theorems, formally for coincidence RA and in practice for a mixed RA, contingent on the models or proxies bring demonstrated to be independent.

Consequently, Bycroft (2009) argued for a two-step protocol to produce a successful and efficient coincident or mixed RA. The first step develops plausible proxies that have previously been independently tested, either taking the form of direct experiment or correlations between other proxies (IBE) or observed calibrations in contemporary space. Independence can then be ascertained by a transparent direct cause to effect (Weisberg, 2006; Bycroft, 2009). The second step tests for convergence to confirm the target event (*e.g.* with time) and in doing so infers the generality of the proxies in both space and time (Bycroft, 2009).

It is important to emphasise that the first step is necessary as an experimental control for a definitive interpretation because, if the proxies are not independent, then the convergence

towards a common result may be due to common features of the proxy's conceptual models and not the targeted event (Weisberg, 2006; Bycroft, 2009). For example, the micro-algal species assemblage for estuaries was found to be a function of salinity from its dependence on the freshwater residence time (Ferreira *et al.*, 2005), whereas calcareous epifaunal $\delta^{13}C_{inorg}$ can be a function of residence time from its dependence on salinity (Nelson and Smith, 1996). However, the convergence between the assemblage and $\delta^{13}C_{inorg}$ over time does not necessarily confirm the salinity or water residence time variance because the parameters that control the salinity and freshwater residence time (*i.e.* volume or tidal exchange) may change. In other words, the common feature between the proxies is the controlling parameter and not the salinity or water residence time.

1.3.3. Inference to the best explanation

Inference to the best (or elegant[5]) explanation (IBE; Lipton, 2000), does not rely on the convergence of available data or model clusters. Rather, it uses a number of single fallible but plausible proxies for processes and components within a web of axiomatic relationships. For example, 'when a detective infers that it was Moriarty who committed the crime, he does so because this hypothesis would best explain all of the evidence, the fingerprints, bloodstains and other forensic proxies' (Lipton, 2000). This method can not only be used to formulate new theories; it also has an inbuilt degree of testability of postulated relationships within the theory when there is a good mix of negative, positive and invariant relationships within the ecosystem. In this case, false proxies will result in a chain of inconsistencies across the other relationships that produce no current plausible explanation. In other words, for a coherent IBE, the truth is manifest from the consistency of relationships between sufficient independent lies.

1.3.4. Self-consistency

The third justification method, SC, differs from coherent IBE in that there is no internal test for inconsistency. At first, this may appear circular, as the data supports the theory and the theory supports the data. However, in defence of theory–proxy circularity, it is a matter of historical record that in the progress of scientific knowledge, data and theory are part of two moving targets that researchers try to overlay one upon the other (Fagerström, 1987). In other

[5] Elegant explanations, as argued by Lipton (2000) tend to be those that are judged likeliest and the best because they explain more types of phenomena, explain them with greater precision, provide more information about underlying mechanisms, unify apparently disparate phenomena, or simplify understanding of the world. In other words, simplicity laced with latent power.

words, ecological data sets can be fallible and most data is a fallible proxy for some concept (Ford, 2000) (*e.g.* chlorophyll as a measure of micro-algal biomass). Hence, in the case of a matching overlay between all proxies and a theory, there is no immediate need to reject any of the proxies. This is especially the case when the purpose is to test the persistence of the theory through time rather than to test it across the whole time series.

1.3.5. Re-analysis after statistical imputation of existing data sets

Many data sets are limited by their temporal resolution and length and missing blocks of data. Such short, non-contiguous, often non-stationary data sets were not amenable to the reconstruction of time-series dynamics until recent advances in time-series analysis. The recent parallel work of Kondrashov *et al.* (2005), Kondrashov and Ghil (2006) and Golyandina and Osipov (2007) developed a method of time-series data imputation for missing data based on singular spectrum analysis (SSAM). SSAM is unlike traditional Fourier models in that it is a model independent, principal components analysis within a time domain ideal for short non-stationary, non-contiguous time series (around 30 data points or more). Imputation of missing blocks of data is solved by an iteration procedure based on a best fit of significant components (non-linear trend and periodicity) extracted from the current information across the whole of the time series. The time series is then reconstructed from trend and periodic components for a re-analysis using the longer more powerful data set to statistically confirm periodic and trend components as significant (*e.g.* Kondrashov *et al.*, 2005).

1.4. Thesis aims

The aims of the palaeo-reconstruction were threefold:

- To describe the natural ecosystem intra and inter-regime variability during the late Anthropocene[6] of the upper and lower functional zones of the Little Swanport estuary, a shallow, dynamic bar-built water body on the east coast of Tasmania, in relation to flood and marine incursion events.
- To test whether the introduction of shellfish aquaculture has had a significant impact on the upper and lower estuary's health through divergence from the ecosystems natural variability, described by pattern and process over an appropriate period.

[6] The term Anthropocene has only recently become widely used in the global change research community as a new geological epoch in Earth history. Steffen *et al.* (2011) put forward a formal case for starting from the 1800's.

- To develop a neutral model as a temporal general theory behind the patterns and processes in an attempt to couple the three disparate theories of long-term seagrass meadow variance: light limitation, nutrient limitation and the implied stability imparted by planktivorous fish top-down control.

It is anticipated that the consequences of further pressure from land use, aquaculture or disturbance events can be assessed within this theoretical framework, which incorporates the underlying drivers of natural variability in relation to the current state of the ecosystem (historical contingency).

1.5. Thesis structure

The structure of the thesis uses a hierarchical sequence of inputs or tested postulates to achieve the aims. This includes (1) determining estuarine zones and boundaries; (2) testing plausible proxies for the paleo-reconstruction; (3) identification of sedimentary events within each estuarine zone for discrete and continuous chronology for correlating with reconstructed and imputated inorganic nitrogen data sets and ecosystem regime changes; and (4) application of the most plausible proxies for a synthesis of patterns and processes for the estuarine zones. The following list briefly describes the individual aims of each chapter.

Chapter 2. Materials and methods. This chapter discusses the criteria for sediment core-site selection and describes sampling and analytical methods used throughout the study.

Chapter 3. Evaluating proxies and processes along a transect within the Little Swanport estuary, towards a palaeo-ecological reconstruction. Traditional and newly proposed sedimentary signals for ecosystem proxies are evaluated along a surface transect—a subset of RA, IBE and SC—to determine: (1) estuarine zones and boundaries for the paleoreconstruction; (2) the plausibility of the proxy, more directly and specifically in space in order to be tested for generality in time, that is, by the convergence with other independent proxies (RA) that were both consistent with the living biome components and their organic and inorganic signals (SC), and the response of the proxy's signal to ecosystem processes within the framework of tested current theories (IBE); (3) plausible examples of changes to the estuary's ecosystem functional states (nutrient and light limited primary productivity), driven by the relative influence between coastal and river determinants, potentially disturbed by the presence of shell fish aquaculture and energetic environments (marine flood/tidal delta) as a surrogate for flood and marine incursive events, to be tested in time by an estuarine wide

paleo-reconstruction (IBE); and (4) the potential importance of proxies for top down and bottom up control for the stability of those ecosystem functional states (*i.e.* whether there was a sufficiently large component signal) to be tested in time by an estuarine wide paleo-reconstruction.

Chapter 4. Sediment column geochronologies for the upper and lower Little Swanport estuary. Depositional facies are marked and conceptually separated from baseline sediment horizons before the application of a range of ^{137}Cs and ^{210}Pb contiguous geochronological methods and models. The events are then identified as floods or various other marine incursions and matched with historic data and rainfall/river-flow models to evaluate the chronological approaches (mixed RA).

Chapter 5. A late Anthropocene palaeo-reconstruction of inorganic nitrogen availability in the Little Swanport estuary. The chapter reconstructs the net nitrogen supply to the estuary with a hierarchical cluster RA using the concept concentration of potential inorganic nitrogen (CPN). CPN was calculated from an imputated and hindcasted long-term coastal data set, a reconstruction of the 'average' estuary palaeo-salinity (surface and bottom waters) and from contemporary nutrient response curves coupled to a long-term rainfall/river-flow model.

Chapter 6. Natural and anthropogenic ecosystem regimes within the Upper Little Swanport estuary over the last 83 years: A palaeo-reconstruction. The estuary has previously been divided into two regime zones, with two different sets of historical events, for a separate consideration of natural and anthropogenic variability. This chapter reconstructs the biome variance within the Upper Middle Basin by using plausible proxies previously assessed in the transect study (Chapter 3). By using a mix of RA, IBE and SC, the biome proxies that could be generalised over time and space within the estuary are chosen for a synthesis, describing the patterns of ecosystem components and processes to suggest: (1) the reasons behind stability, (2) the causes of regime change in relation to flood events, a drought and the introduction of the lower estuary's shellfish aquaculture, (3) the type of regime, and (4) postulate reasons behind ecosystem change, and the conditions needed to test the postulate's hypotheses.

Chapter 7. Evidence of a neutral model for a general theory of seagrass meadow dynamics. This chapter tests Chapter 6's postulates of seagrass functional regime stability (light limitation or nutrient limitation) on an undisturbed late Anthropocene record of seagrass

ecosystem variance within the Lower Middle Basin. A complete temporal unit of pattern and process is constructed for testing impacts of the basin's shellfish aquaculture. From this, a neutral model of pattern and process is developed for a general theory of seagrass variance. The model is based the role of the top-down control (planktivorous trophic cascade) and bottom up control (inorganic nitrogen availability) within an evolving landscape configuration.

Chapter 8. Discussion and conclusions. This chapter summarises the findings of the study and discusses its implications for the study of other seagrass systems by formalising the general theory. Suggestions for future work are then based on the formal structure and predictions of future events and long-term changes of inorganic nitrogen supply.

Appendix. The Appendix contains the results from the diatom transfer function taken from a model developed by Saunders *et al.* (2007) with a laboratory report referred to in the text.

Chapter 2. Materials and methods

2.1. Study site

The Little Swanport estuary was chosen because for the study of major floods, pressed nutrient supply and shellfish aquaculture on a seagrass ecosystem because of its ideal geomorphology, history and availability of long-term data sets at its matching temporal and spatial landscape scale. That is, (1) its relative isolation from coastal waters and presence of a central muddy trench along the axis of the estuary (Figure 2.1), thus, restricting the loss of surrounding autochthonous production from the estuary towards deep water deposition (*c.f.* lake palaeo-reconstructions, *e.g.* McGowan *et al.*, 2005); (2) the knowledge that its seagrass *Zostera spp*. coverage has changed over the long-term (Rees, 1993); (3) the availability of a long-term rainfall–catchment river flow model (SKM, 2004), ongoing medium-term river nutrient monitoring and ongoing long-term coastal nutrient monitoring (Harris *et al.*, 1987; Thompson *et al.*, 2009), all of which illustrate the system has been subject to a range of pivotal flood events that has on occasion damaged its littoral benthic environment (Dyke, C., 2006, *pers. com.* Dykes Oyster Farm), together with long-term pressed variability in coastal and river nutrient supply both of which may lead to a change in seagrass coverage and structure (Eriksson *et al.*, 2002; Orth *et al.*, 2006); (4) the presence of an established shellfish aquaculture industry over the medium to long-term (*i.e.* over the last 20 years); (5) a recent survey that identifies the range of animal and plant species abundance, in order to determine and compare the structure of its ecosystem with other seagrass ecosystems around Australia and the rest of the world, and thereby borrow generic interpretations of experiments and pattern and process from those environments to construct a general theory of long-term seagrass meadow variance (see section 1.3).

The Little Swanport estuary (Figure 2.1) is located on the cool temperate east coast of Tasmania (42.33 °S, 147.98 °E). Its catchment (732 km^2) geology is primarily Jurassic dolerite, with land use divided into three broad categories: pasture 27 %, which is largely restricted to the upper catchment, clear felling forestry 8 %, which is scattered throughout the catchment and the remaining areas are native dry sclerophyll forest. The upper catchment pasture development has an influence on the upper Little Swanport River's water quality, leading to elevated total nitrogen concentrations (median 0.85 mg L^{-1}) above pristine levels as found for undisturbed parts of the upper catchment (median 0.2 mg L^{-1}) (DPIPWE, 2006). However, the lower sections of the river that enter Little Swanport estuary remained

relatively pristine with both total nitrogen and nitrate and total dissolved inorganic nitrogen concentration (DIN) below ANZECC guidelines for pristine waters (total nitrogen median 0.48 mg L^{-1}; DIN median 0.06 mg L^{-1}) due to the dilution by forested tributaries combined with a significant decline in land use activity in the lower catchment (DPIPWE, 2006).

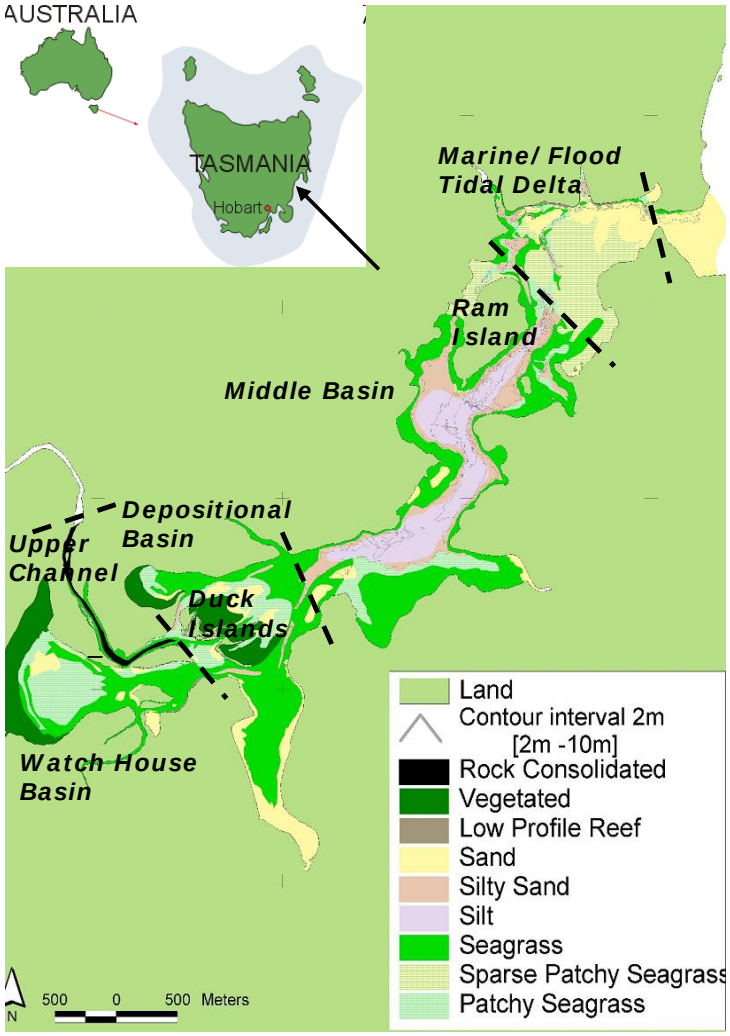

Figure 2.1. Benthic habitat description of Little Swanport estuary and its location in Tasmania (Australia).

Little Swanport River's catchment has a relatively small bar-built estuary (42.33 °S, 147.98 °E) (Figure 2.1). The estuary can be tentatively divided into five characteristic zones based on sedimentology, bathymetry and topography:

- The Upper Channel. A relatively deep (up to 10 m) narrow stony channel, the base of which is presently below mean sea level and is fed by the Little Swanport River.
- Watch House Basin. A relatively isolated shallow (<2m) water body that is set back from the entrance of the Upper Channel. The basin is fringed by salt marsh to its west and supports a lush meadow of the submerged aquatic rhizome macrophyte *Ruppia megacarpa*.

- The Depositional Basin. A relatively shallow water body (<3m) that encompasses the depositional levees (Duck Islands) and ends where a deeper muddy central basin begins. The basin presently supports a lush seagrass meadow of *Zostera tasmanica* and *Zostera muelleri.*
- The Middle Basin. The basin features a central muddy heterotrophic trench (Potts J, *pers. com.,* 2006) from 3 m to 10 m deep surrounded by a littoral zone that supports seagrass meadows dominated *Zostera tasmanica* and *Zostera muelleri.*
- The Marine/Flood/Tidal Delta. A relatively high-energy sandy shallow region with braided channels among inter-tidal sand flats. The narrow channels support extensive high densities of the seagrass *Zostera muelleri*.

Little Swanport estuary has been listed as a wave-dominated system (OzCoasts, 2006). This classification appeared to be based solely on its topography, bathymetry and surface sedimentology. However, on further examination of the data from Crawford *et al.*, (2005), it was found that tidal exchange was the dominant feature of its hydrodynamics. Readings from a tide gauge deployed within the centre of the estuary indicated a tidal prism for the whole estuary approximating 3.4 x 10^6 ML or 43 % of the high water volume of the estuary. In contrast, the median river flows of 9 ML/day and mean river flows of 34 ML/day, from published river-flow data over the previous 17 years (SKM, 2004), indicates that river flows would produce no significant contribution compared to the tidal prism.

Little Swanport estuary contains seagrass meadows that support a planktivore-dominated ecology, similar in species composition to Westernport and Port Philip Bay in Victoria (Australia) (*e.g.* Kimmerer and McKinnon, 1985, 1987). A list of animal and plant species collected over 10 years can be found in Crawford *et al.* (2005). Presently, most of the oyster aquaculture industry is spread throughout the Marine/Flood Tidal Delta, bordering the narrow deeper channels (approximately 2 m to 4 m deep). There is also a land-based oyster nursery that draws water from the upper Middle Basin.

2.2. Selection of sediment core sites

Estuaries are defined by an ecosystem gradient that has been generated by varying degrees of influence from its river and its immediate coastal environments. River and costal zones are defined by their integrity against the influence of the estuary, which in turn is influenced by the net balance between the river and coastal inputs. The net balance will also change at different temporal scales driven by tidal, seasonal and climate variability and interdecadal

flood frequency (Elwany *et al.*, 1998; Rustomji, 2007) as the estuary evolves over the millennia (Roy and Thom, 1981). The estuary can be divided into discrete zones that result, in part, from the estuary's tidal excursion (Dyer, 1973), which is influenced by discrete changes in volume along a complex estuarine topography.

For a palaeo-reconstruction there are additional practical sampling criteria to consider: (1) scaling up variance from small diameter sediment cores to a potentially heterogeneous surrounding landscape, (2) natural and anthropogenic disturbance of the sedimentary record, (3) different sensitivities of the sediment coring sites to coastal floods and marine incursions that may deposit material or affect the tidal exchange parameters (*e.g.* Morton and Donaldson, 1973; Roy *et al.*, 2001; Cooper, 2002; Rustomji, 2007). Traditionally, a central heterotrophic deep spot is selected that will integrate a well-preserved and undisturbed supply of particulate material from the surrounding littoral zone and the water column (Engstrom and Wright, 1984). The success of the reconstruction is contingent on the lack of anthropogenic or natural disturbances, for example, mixing or erosion of sediments during bottom dredging, floods (Cooper, 2002) or marine incursions. Unfortunately, disturbances at potential sediment core sites are not always known *a priori*.

Little Swanport estuary has a complex topography including an embayment set back from the main river channel (Watch House Basin), which may be ostensibly isolated from the direct influence of the river and coastal ecosystem gradient that defines the estuary. Similarly, coastal boundaries are not always clear. Rapid tidal exchange immediately inside the estuary's Marine Flood/Tidal Delta zone, in spite of the bar way, may result in an a disproportionate coastal influence over the estuary's function. In other words, the functional coastal boundary extends past the bar way into the estuary as currently classified from topography and sedimentology resulting from tidal dynamics. Furthermore, the tidal exchange parameters are subject to significant change. Available aerial photographs of the bar way indicated a more open system in 1948 than present, to a near closure of the bar in 1967 (see Chapter 4, Figure 4.18). The estuary also supports discrete ecosystem zones as a function of complex topography and changing bathymetry within the Middle Basin. Hence, a centennial scale palaeo-ecosystem reconstruction within Little Swanport estuary must account for ecosystem variability within estuary zones due to changes in both baseline river and coastal boundary conditions and their exchange parameters affected by flood and marine incursions. Furthermore, the functional boundaries may evolve over time, contracting or expanding with coastal and river-flow boundary conditions. Therefore, it is important to choose sampling sites

that maintain their integrity as part of the functional zones, to disentangle ecosystem changes on functional zones from a shift of the site to an adjacent functional zone.

Consequently, Little Swanport estuary's palaeo-reconstruction was centred on two distinct regions (see Chapter 3). The Depositional Basin, containing depositional levees (Duck Islands) to the Upper Middle Basin and the Lower Middle Basin (Figure 2.2) have been found to functionally define most of the estuary (see Chapter 3). Both zones support a heterotrophic central channel (3 m to 10 m deep). Sediment cores were extracted from both zones to reconstruct their respective palaeo-ecologies. The extraction sites were relatively protected from the effect of wind mixing. It was found that haline stratification was perennial during both baseline river flows and during drought conditions. During drought conditions bottom waters were found to be hyper-saline with respect to seawater and were formed from density currents after surface evaporation (see Chapter 3).

Within the lower estuary region two sediment cores were extracted from sites approximately 120 m apart (Figure 2.2) to: (1) select for both sensivity in the supply of macro-seagrass leaf detritus (LSPMB106, 8 m) and sediment brought in by marine incursions (LSPMB107**,** 9.9 m) and subsequently resources were focused on a single core (*e.g.* Turner *et al*., 2006) *i.e.* a shallower but closer site to the seagrass meadow and deeper site for the final resting place of a tsunamite and/or tempesite, (2) test for basin scale replication and to constrain individual sediment core stochasticity[7].

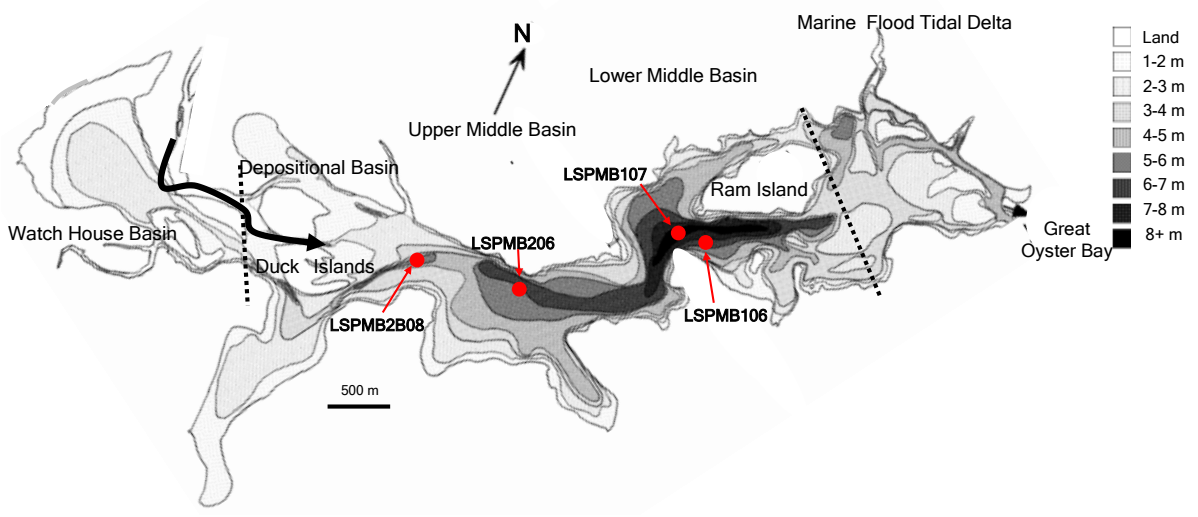

Figure 2.2. Sediment core sampling sites within the Little Swanport estuary's deep central basin.

[7] It is conceivable that an event that spans a sediment core horizon, such as the appearance of an animal or object, may give the impression of a basin wide event. However, without a comparison with another sediment core separated across the basin, it is equally likely that the deposition is just a localised incident.

Within the upper region (Figure 2.2 LSPMB206, 3.7m; LSPMB2B08, 3.2m), the sites were selected to: (1) constrain stochasticity within individual sediment cores, (2) balance a decision, not known *a priori* between the relative sensitivity to the magnitude of floods, though deposition (LSPMB2B08; see Figure 2.2) and relative insensitivity to flood erosion *i.e.* sites closer and further from the river respectively.

2.3. Sample collection for sediment cores

Sediment cores were collected using a sliding hammer Kajak corer (UWITEC, Austria) equipped with a 6 cm internal diameter polycarbonate core tube (Figure 2.3). The core tube had previously been washed with acid (10 % HCl, Analar grade), rinsed with distilled water, and then stored filled with distilled water until needed. After recovery, the sediment cores were kept vertical at all times and the sediment–water interface was stabilised for transport by pushing a porous polyurethane foam plug through the water head space to immediately above the surface of the sediment and the core was subsequently sealed at both ends. The sediment cores were packed in ice in an insulated box for transport and kept vertical at all times. On return to the laboratory, the cores were stored upright at 1 °C to 3 °C for up to one month before processing. The cores ranged from 0.8 m to 1.4 m long.

Figure 2.3. The sliding hammer Kajak corer used to extract the sediment cores.

2.4. Estuarine transect, water and catchment sites and sample collections

Surface sediment samples and their immediate sessile living biota were collected at 13 stations along a transect, within the littoral zones (Figure 2.4) during the summer (late February), to test the plausibility of chosen proxies (see Chapter 1) and to identify the estuary's boundaries and functional regions. At each of the 13 transect stations (Figure 2.4), three sediment samples were taken from sites within 10 m of each other (total 39) with an Ekman spring loaded grab (Figure 2.5). The grab was modified by attaching a 3 m long box section with a push button release rod running from the top to the spring release located at the top of the grab. In this way, a square section of seagrass and sediment could be taken from a boat by firmly pushing the grab past seagrass shoots and their rhizomes.

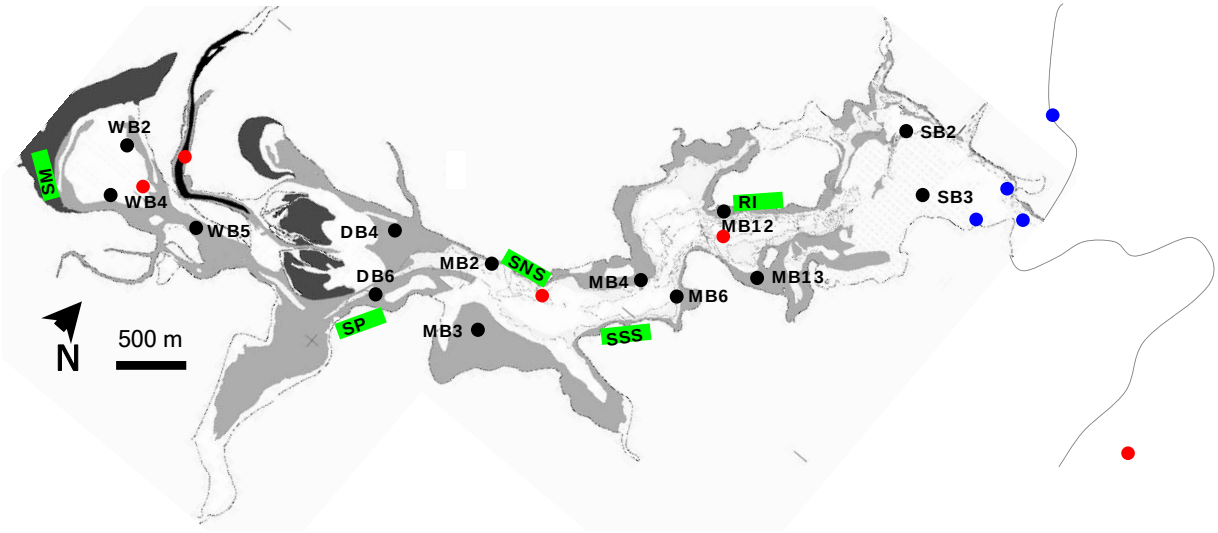

Figure 2.4. Position of the sampling stations for the transect, the surrounding catchment and the adjacent coastal waters of the Little Swanport estuary.
(●) Position of surface sediments stations within the littoral zones seagrass beds; (●) positions of surface water samples outside the seagrass meadows within deeper waters, (—) surface soil stations; (●) sampling stations for contemporary bivalve taphonomy. The grey areas are the sub-tidal littoral zones and the black areas are inter-tidal salt marsh.

Ten samples of seagrass shoots were then randomly selected from each site, along with their surface sediments (the rhizome horizon was around 1 cm to 2 cm thick). The samples were stored in the field, dark and under ice, in separate Whirlpak™ bags. After a few hours, they were frozen at around -4 °C for transport back to the laboratory and stored at -20 °C until needed.

Surface water samples together with temperature and salinity profiles (602 Yeokal Mk11 salinity/temperature bridge, ± 0.1 °C and ± 0.02 ‰) were collected at 4 estuarine sites and a coastal site, 3 km outside the estuary within Mercury Passage, well away from the immediate effects of the estuarine circulation. During sampling care was taken to minimise

contamination from any re-suspended sedimentary or floating material by collecting water immediately below the surface, during calm conditions, in at least 2.5 m of water. The samples were stored in the dark under ice for a few hours and then filtered onto pre-combusted (400°C) 47 mm diameter GF/F filters. The filters were then stored frozen, initially at -4 °C and subsequently at -20 °C, wrapped in a pre-combusted Al foil. The frozen samples were processed within 2 months prior to analysis of carbon and nitrogen content and their stable isotope ratios.

Figure 2.5. A seagrass–sediment sample taken by the Ekman grab.
The Ekman grab sampler modified by attaching a 3 m long box section used to drive the grab into the sediment, from which a long push bottom rod is pressed from the top of the section to release the grabs spring loaded jaws (right). The sample released from the grab (left).

Catchment soils at 10 random sites along a 250 m perimeter of a salt marsh (SM), eroded pasture (SP), steep and shallow slope dry sclerophyll forest (SNS and SSS respectively) and pasture with a history of recent fire (RI) were sampled (Figure 2.4). The samples were stored in the field in separate Whirlpak™ bags in the dark and under ice for transport back to the laboratory and subsequently stored at -20 °C until needed.

2.5. Sediment core sub-sampling

Within 4 weeks of collection, each core was sub-sampled for a range of analyses (Figure 2.6). Samples for water content, sediment wet bulk density, pore water salinity and loss on ignition at 550 °C and 950 °C were taken through the receiving liner with a 1 mL syringe with the tip cut off, resembling a piston corer (Livingston, 1984). In this way a sample was extruded across the diameter of the sediment core without any compression. Any voids and visible pieces of shell were expelled from the syringe and the process was repeated until a complete 1 mL was collected and then immediately placed into pre-weighted 2 mL Eppendorf™ tubes.

The remaining sediment was placed in either Whirlpak™ bags or pre-combusted glass jars. The residual mud clinging to the inside of the roughened receiving liner was discarded. The air from the glass jars and Whirlpak™ bags was removed *via* vacuum bagging and the samples were then kept in the dark, under ice, until needed (up to 2 months)[8]. Subsequently 2 mL to 3 mL of wet sample was sub-sampled for further processing for analysis of: particle size, macro-char counts, faecal pellet content, shell debris identification, bivalve taphonomy and their ^{14}C age, ^{210}Pb and ^{137}Cs radio-geochronologies, total and particulate organic carbon and nitrogen (TN, TOC, POC, PON) and stable isotope ratios ($\delta^{13}C_{org}$, $\delta^{15}N_{org}$), LOI 550 °C, stepwise thermogravimetry (Rp index) and labile BSi (Figure 2.6). Material that showed signs of surface oxidation, formed during the initial transfer and storage under vacuum was rejected for analysis of organic matter (OM) components.

2.6. Sub-sampling of the surface littoral zone sediment grabs

2.6.1. Seagrass leaves and their epibionts

Ten terminal live seagrass shoots, selected at random from the sediment grab from 3 sites at each transect station (Figure 2.4) were scraped between flat tweezers to separate the epiphyte community (using the edge of the tweezers) and then dried (<60 °C) for further processing and analysis. The scraped leaves were then soaked in 5 % HCl (Analar grade), rinsed in distilled water and dried for further processing and analysis.

The above procedure was repeated for detrital seagrass leaves, buried within the surface 1 cm to 2 cm of the surface sediments. Due to limited resources, seagrass leaves and their epiphyte communities at each station site were combined for analysis of carbon and nitrogen content and their stable isotope ratios, as equal dry weights for the epiphyte community and as equal wet leaf area for seagrass leaves. Only live seagrass shoots (Figure 2.7) were analysed for their N:P stoichiometry to constrain transect variance interpretations based on either nitrogen or phosphorus limitation (see Chapter 3).

[8] Freezing of samples was avoided so as not to influence the sediment size distribution by freeze/thaw fracture of delicate aggregates.

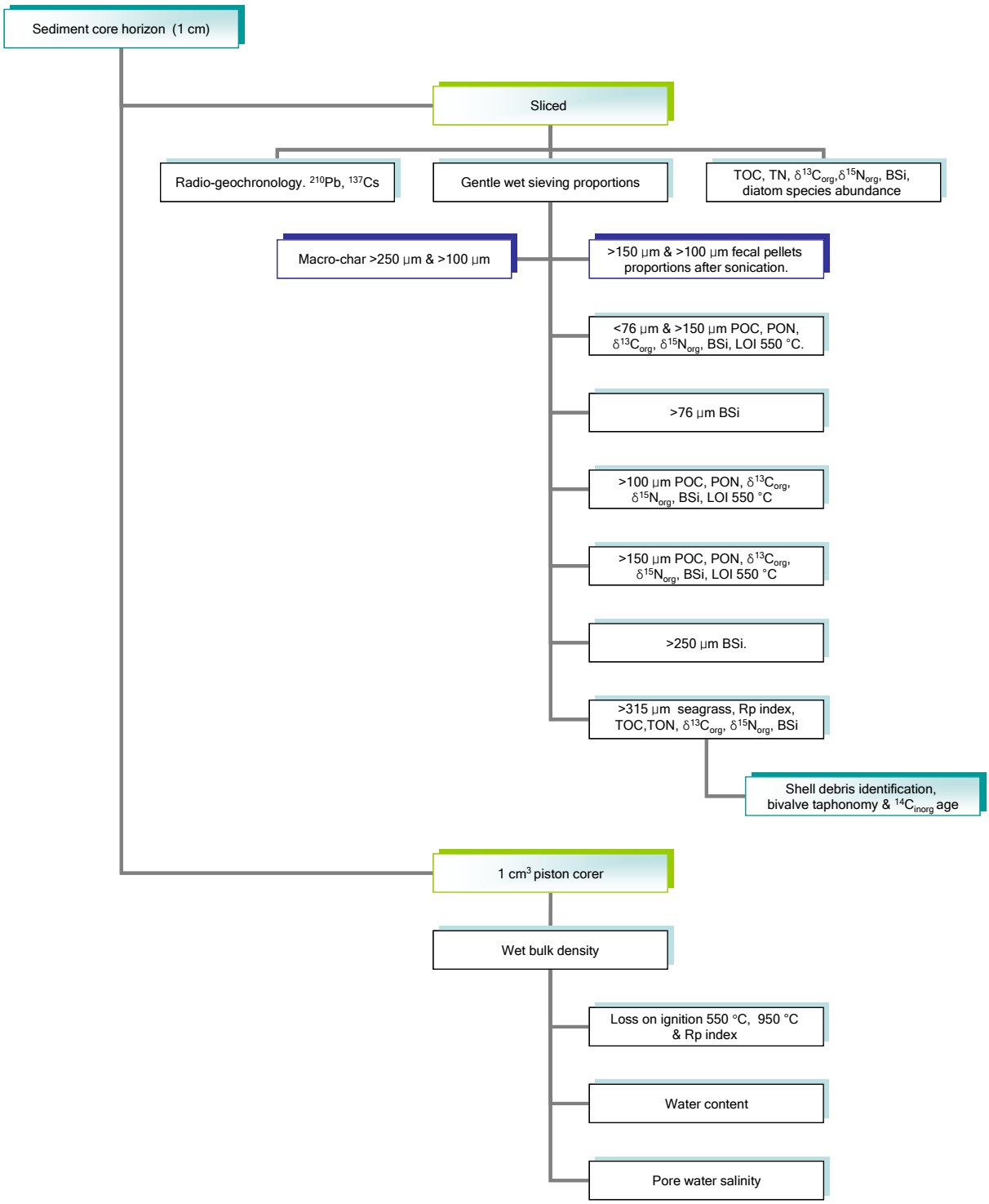

Figure 2.6. Sub-sampling protocols and subsequent analysis of sediment cores extracted from the deep, heterotrophic, central basin of the Little Swanport estuary.

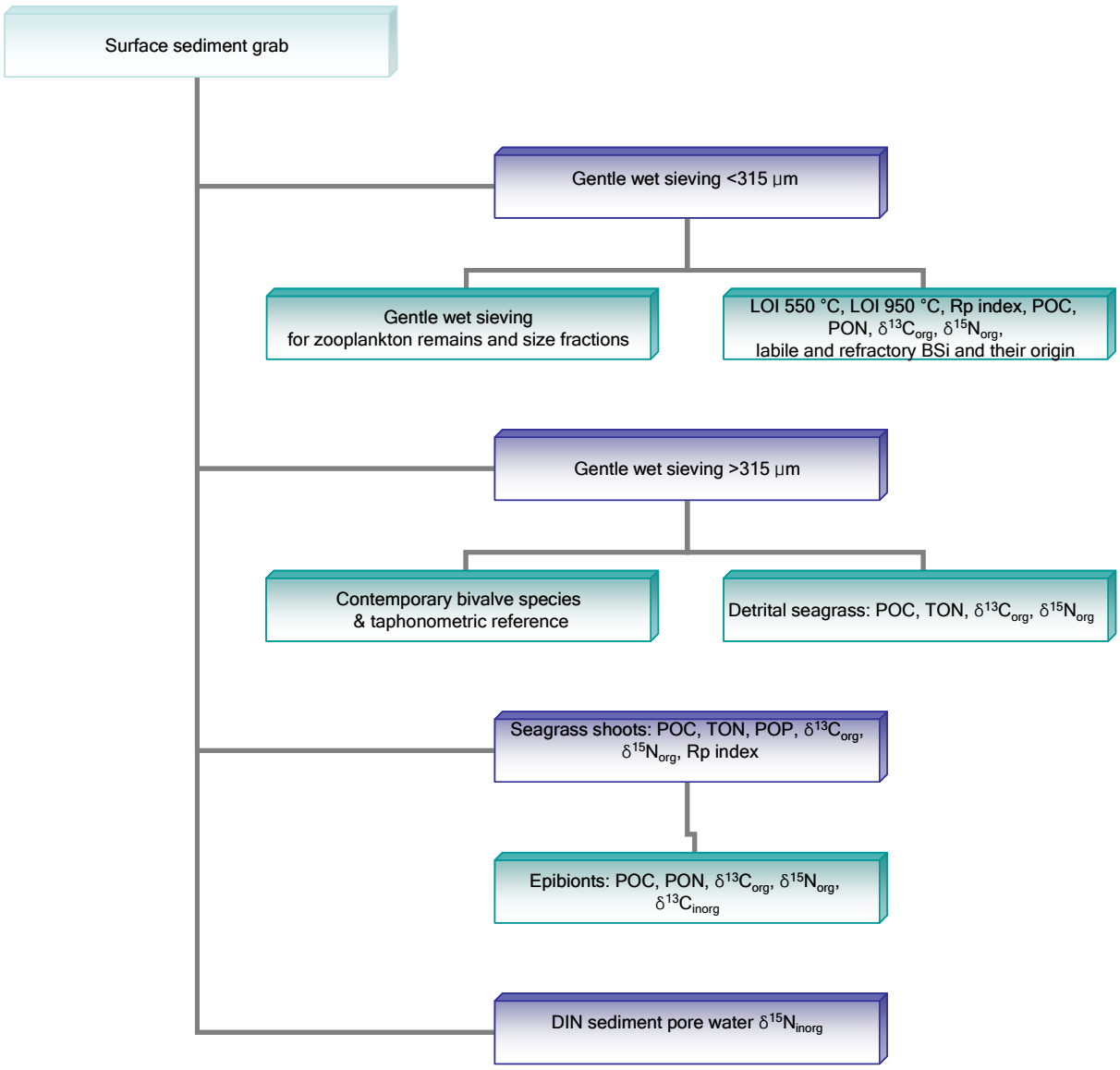

Figure 2.7. Sub-sampling protocols and subsequent analysis of the little Swanport estuary's littoral zone's surface sediment and surrounding catchment soils.

Serpulid worms and bryozoans attached to the seagrass leaves were picked off under a binocular microscope (x 20) and placed in 10 mL centrifuge tubes and stored at -20 °C until further processing and analysis of their $CaCO_3$ carbon stable isotope ratios ($\delta^{13}C_{inorg}$; see Figure 2.7).

2.6.2. Surface sediments

Approximately 5 mL of wet surface sediment collected using a cleaned metal spatula was first washed through a 315 µm stainless steel sieve with distilled water to separate live gastropod, mollusc, isopod and amphipod fauna from the detrital fraction. The distilled water washings

were aspirated from the sieved sediments after centrifugation (x 1000 g for 20 minutes). Again, due to limited resources, the sediments from 3 sites at each station were combined as equal dry weights for analysis of organic carbon and nitrogen content and their corresponding stable isotope ratios. Loss on ignition (Figure 2.7) and labile and refractory BSi samples were not combined.

In addition to processing for chemical analysis the sieved sediments from 3 sites at 4 stations were sub-sampled wet for identification of microscopic glassy components (*e.g.* diatoms, phytoliths, thecamoebians).

2.6.3. Catchment surface soils

The 10 sites along each of the 250 m sections (SM, SP, SNS, SSS, RI) were combined equally by weight. Visible stones were discarded and the samples were stored at -20 °C until further processing (Figure 2.7) for analysis of total carbon and nitrogen content, Rp index, loss on ignition and stable isotopes for dissolved inorganic nitrogen.

2.7. Chemical and physical analysis

2.7.1. Pore water salinity

Sediment pore water salinities from sediment core horizons were measured after centrifugation (x 1000 g) of 1 mL of wet sediment (Figure 2.6) by putting 50 μL of supernatant onto a hand-held refractometer. The precision of the refractometer was estimated to be approximately 0.5 ‰ (Lindberg and Harriss, 1973).

2.7.2. Water content

After centrifugation and pore water sub-sampling, the remaining wet sediment plug from the above sediment core sub-sample was dried in pre-weighed Eppendorf™ tubes at 60 °C for 24 hr, or until constant weight, and expressed as a percentage weight of dried solids. Correction was made for the small volume removed for determination of pore water salinity.

2.7.3. Loss on ignition (550 °C and 950 °C)

Sediments were dried overnight at 105 °C to constant weight and 0.1 g to 0.4 g was transferred to pre-dried and pre-combusted 5 mL porcelain crucibles then redried to constant weight at 105 °C (cooling in a desiccator). The crucibles were arranged in a grid on a porcelain tray, which could be placed reproducibly in the furnace. The samples were then heated in a muffle furnace to 550 °C for 4 hr, and cooled in a desiccator (Heiri *et al.*, 2001).

After weighing, the samples were further heated to 950 °C for 2 hr, cooled in a desiccator, and reweighed.

Samples of sediment working standards were positioned from the back to the front of the furnace as well as from left to right. In this way, intra-batch and inter-batch variance from either furnace inconsistencies and/or operator process bias could be removed by normalising ignition loss to the hot spots in the furnace. All contents for total sediment analysis were reported as dry weight after correction for pore water salt content according to Lavelle *et al.* (1985) and to a reference weight from a measured calibration curve (Equation 2.1)

Equation 2.1. $LOI550(0.3\ g) = -0.697*(sample)^2+0.657*(sample) +0.864*LOI550\ (sample)$

Calibration (r^2= 0.999, n=7) to correct LOI 550 °C weight dependent variance of the sample to a standard weight (0.3 g). Mixtures (50 %) from standard additions of muddy core sediments with pre-combusted residue (after 950 °C) gave no significant difference to the above LOI weight dependence, implying that it was a function of mass and not OM composition.

No correction was necessary for LOI 950 °C within the range 0.1 g to 0.5 g of sample provided the weight correction after LOI 550 °C had been applied. Where there was evidence of pyroxene clays, indicated by the formation of yellow residue after heating to 950 °C (See Appendix: Report from Mineral Resources Tasmania), the sample was acidified and the combustion repeated. The contribution from the loss of clay hydration above 550 °C was subtracted from the total combustion loss.

An estimate of the limit of detection of a series of sediment blanks (3 x standard error; n=5) was 0.1 % (for a 0.3 g sample) and 0.7 % for a 0.1 g sample and was based on analysis. These blanks were prepared by pre-combusting combined homogenised sediment samples at 1000 °C over 24 hr.

2.7.4. Wet bulk density

Wet bulk density of sediment core horizons was calculated in two ways: (1) weight of wet sediment and the volume measured within the syringe and (2) by the sum of calcium carbonate (as LOI 950 °C), water content and organic content multiplied by their respective particle densities (Binford, 1990). There was a strong correlation between the two methods (unpublished) but the calculated values were dependent on tabled values of sediment particle type from other environments that may have explained some of the residual variance. Therefore, the direct measurement of bulk density was preferred, with the latter method used

on the rare occasions when a mass of shell debris in depositional facies inhibited the collection of a smooth consolidated sample within the cut off syringe sampler.

2.7.5. Organic carbon and nitrogen content and stable isotope ratios

All manipulations were performed on a covered solvent cleaned, stainless steel tray after samples were dried at 60 °C. Individual samples of sediments, soils, previously treated seagrass leaves (live and detrital from the transect stations) and their live epiphyte community were ground to a fine powder with a stainless steel mortar and pestle previously cleaned with water and then methanol and acetone, and then transferred to acid-washed pre-combusted glass vials. After each sample was processed, the mortar and pestle was rinsed with distilled water and wiped out with lint-free wipes (Kimwipe™), re-rinsed in methanol, wiped once more, and then acetone rinsed. Before proceeding to the next sample, the pestle was checked with a magnifying glass for any lint contamination.

The powdered samples of soils, sediments and seagrass epiphytes were acidified within pre-combusted glass vials using 10 % HCl (Analar grade) to twice the volume necessary (previously estimated from LOI 950 °C) to remove carbonates. The samples were then left to evaporate at 60 °C overnight in a pre-cleaned stainless steel fan-forced oven fitted with a fine air filter. The tray of samples was loosely covered with a sheet of aluminium foil to prevent any dust contaminating the open vials. The next day the samples were wetted with distilled water then dried overnight at 60 °C to constant weight to drive off any excess HCl. For sediments with a high concentration of carbonate shell the sample was first treated with 30 % HCl (Analar grade) until no more reaction could be seen. It was then fumed for a further 24 hours within a desiccator over concentrated HCl and then dried for 48 hr.

While the samples were still warm, the vials were closed and vacuum bagged for later transport and analysis at the West Australian Biogeochemistry Centre (WABC), John de Laeter Centre of Mass Spectrometry, School of Plant Biology at the University of Western Australia. An automated elemental analyser interfaced to a continuous flow 20/20 mass spectrometer connected to an ANCA-S1 preparation system (Europa Scientific Ltd., Crewe, UK) quantified C, N, and $\delta^{13}C_{org}$ and $\delta^{15}N_{org}$. All $\delta^{13}C$ values were expressed as delta notation relative to Viennese Pee Dee Belemnite and $\delta^{15}N$ relative to atmospheric nitrogen. The standard deviations were 0.15 ‰ for $\delta^{13}C$; 0.35 ‰ for $\delta^{15}N$; 1.5 % for C; and 0.5 % for N for 5 replicates. All total carbon and nitrogen content from sediment cores were corrected for salt according to Lavelle *et al.* (1985) using the pore water salinity.

In addition, *Zostera* spp seagrass leaves from sediment cores (LSPMB2B08, and LSPMB106 and LSPMB107) were identified and removed from the 315 μm sieve under a binocular microscope (x10 to x15 magnification), washed in a bath of 5 % HCl within a disposable polycarbonate Petri-dish for several minutes, rinsed in bath of distilled water, followed by a stream of distilled water and subsequently dried below 60 °C.

The dried seagrass samples (approximately 1.0 mg to 2.5 mg) were weighed to ±0.001 mg as pieces (not ground) and placed into pre-weighed tin cups for analysis of carbon and nitrogen concentrations and their stable isotope ratios. The samples were stored in glass vials under vacuum for transport and later analysis at the Research School of Biological Sciences, Australian National University (Canberra). This research group had tuned their mass spectrometer, on request, to use a smaller sample size than usual. Standards, reporting and statistics were the same as the above WABC results.

Seagrass samples taken from the upper sediment core LSPMB206 were only analysed for organic carbon and nitrogen content. Owing to previous sub-sampling and analysis, there was insufficient seagrass material for stable isotope ratio analysis for many of the sediment horizons (1.0 mg to 0.02 mg) but sufficient material remained for carbon and nitrogen analysis *via* an Elemental Analyser at the Central Science laboratories, University of Tasmania (Thermo-Finnigan EA 1112 Series Flash). Samples of seagrass were from the rehydrated >315 μm fraction, previously dried at 60 °C and stored in evacuated plastic bags at 4°C from the previous year. However, it should be noted that separation from other amorphous particles was problematic. Amorphous particles, adhered to the rehydrated seagrass, were laboriously picked/scraped off the individual seagrass straps, under a binocular microscope (x10 to x20), using a needle and fine forceps. While every effort was made to make sure that no particles remained, it needs to be recognised that given the small quantity of seagrass, the apparent noise in organic content data for this sediment core may, in part, reflect amorphous particle contamination. Once separated from particles the seagrass pieces were immediately washed in 5 % HCl (Analar grade), gathered with forceps and rinsed in distilled water under a wash bottle stream, dried at 60 °C, and weighed intact to ±0.001 mg into tin capsules for subsequent analysis.

2.7.6. Inorganic carbon stable isotope ratios

The calcareous epibionts were treated to remove organic material with 3 mL of 30 % H_2O_2, with the reaction controlled under ice. During peroxide digestion, pH>8 was maintained by

the drop wise addition of 0.5M NaOH and the calcareous remains washed 5 times in distilled water and dried at 60 °C. Their stable inorganic carbon isotope ratios were determined at the Central Science Laboratories University of Tasmania by reacting the prepared sample with anhydrous concentrated phosphoric acid according to Swart *et al.* (1991).

2.7.7. Total iron analysis

Total iron analysis was performed on weighed, and ground (agate mortar and pestle) samples from the upper sediment core horizons that had been previously heated to 950 °C to remove water, organic material and carbonates. The samples were placed in acid-washed porcelain cups and reacted with 5.93M HCl (Analar grade) at sufficient volume to produce a yellow complex with an absorbance proportional to iron concentration (Box, 1984). All results were expressed as percentage of dry sediment, after correcting for the contribution from salt according to Lavelle *et al.* (1985).

2.7.8. Labile biogenic silica analysis

Sediment and surface soils for analysis of labile biogenic silica (BSi) were taken from the Whirlpak™ bags in which they were stored, dried at 60 °C, and broken up, in accordance with DeMaster (1981). The samples (0.30 g to 0.35 g) were digested in 40 mL of hot (85 °C) NaOH (Analar grade, 0.5 M), and the amount of silicate released measured by standard spectrophotometric methods (DeMaster, 1981) after digestion for 2, 3, 4 and 5 hours and extrapolation of the constant slope after 2 hours to zero time as a measure of labile BSi.

Paired samples for BSi analysis (n=12) taken from the same dried sediment stock (<315 μm size fraction; ≈ 9 % BSi) on different days and using different analytical stock solutions were highly normally correlated (r^2 0.85) leaving analytical variance BSi, in this study, of around 15 %. After removal of an anomalous pair the correlation coefficient increased to 0.92, a variance within the range reported by Conley (1988). All results reported as BSi content from sediment cores were corrected for salt according to Lavelle *et al.* (1985).

2.7.9. Refractory biogenic silica

Refractory BSi from surface sediments and soils were treated using the same procedures and reagents as for labile BSi but digested between 14 hr to 24 hr (Conley, 1988), and then calculated by extrapolating the released silicate back to zero time.

2.7.10. Rp index from stepwise thermogravimetry

Stepwise thermogravimetry measures the loss of mass from a sample as temperature is increased. Kristensen (1990) used stepwise thermogravimetry patterns for natural material to develop the Rp index, defined as:

Equation 2.2. $$Rp = \frac{PII}{(PI + PII)}$$

Where *PI* is weight loss from ignition between 130 °C to 280 °C and *PII* is the weight loss on ignition from 280 °C to 520 °C.

A low Rp index (around 0.2) is typical for materials rich in aliphatic compounds (lipids, carbohydrates), whereas high Rp (>0.5) represent aromatic compounds and materials rich in nitrogen (humates, proteins, nucleic acids).

The Rp index was determined using the method and protocols of Kristensen (1990), together with an additional correction of inter-batch and intra-batch variability using a sediment-working standard. The inter-batch standard deviation of the working standards was <3 % of the mean (0.586 ± 008, n=16).

2.7.11. Radioisotope-based geochronologies

Sediment samples from selected sediment core horizons were dried below 50 °C and several grams were ground to a power using an agate Retschmill automatic mortar and pestle with an adjustable tilling device for reproducible grinding.

Samples for ^{210}Pb dating were chemically processed by ANSTO at Lucas Heights, Sydney (Grant AINARA 07166 and private project number 2009rc11abc) by first removing iron using ether extraction, followed by acid leaching of ^{209}Po and, from which the ^{209}Po was plated onto silver disks by the addition of a reducing agent, hydroxylammonium chloride. Ra was co-precipitated with $BaSO_4$. The activities of the sample sources were determined by alpha spectrometry. ^{210}Pb activity was later corrected to sediment dry wet by accounting for contribution from pore water salt, according to Lavelle *et al.* (1985).

Samples for ^{137}Cs analysis, were pooled from groups of sampling horizons (3 or 4) to obtain the 12 g of material needed for analysis, came from a haphazard mixture and samples left over from previous sediment processes that had been previous dried (60 °C) and ground either in

agate or stainless steel mortars and pestles. The analysis was performed at the Marine Chemistry Department, Woods Hole Intuition for Oceanography (USA) using high–resolution gamma spectrometry.

2.7.12. Sediment size fraction classes

Unprocessed wet sediment (2 mL to 3 mL) from each horizon was gently washed with distilled water, through a stainless steel sieve stack (315 μm, 250 μm, 150 μm, 100 μm and 76 μm) and the effluent collected into a 500 mL polypropylene centrifuge container (Figure 2.8). For the more consolidated sediments, samples were initially soaked in 5 mL of distilled water for a few hours to assist in dispersal. When most of the sample appeared to have passed through the top sieve, a further oblique higher-pressure wash with a narrow bore wash bottle was used to clean the remnants of seagrass leaves and any aggregates on the top 315 μm sieve. Washing was considered sufficient when there was a noticeable absence of lumpy sediment aggregates and the seagrass straps and any pieces of shell debris appeared glossy. The sediment samples were completely rinsed from the sieves (from the top down) into pre-combusted and weighed aluminium dishes (500 °C), using a wide bore wash bottle. The <76 μm fraction was centrifuged at 1500 g for 20 minutes, the supernatant aspirated off and the sediment completely washed into weighed pre-combusted aluminium dishes. Large shells on the 315 μm sieve were picked off. The size fractions were expressed as proportions by dry weight (60 °C) of the sum of the fractions.

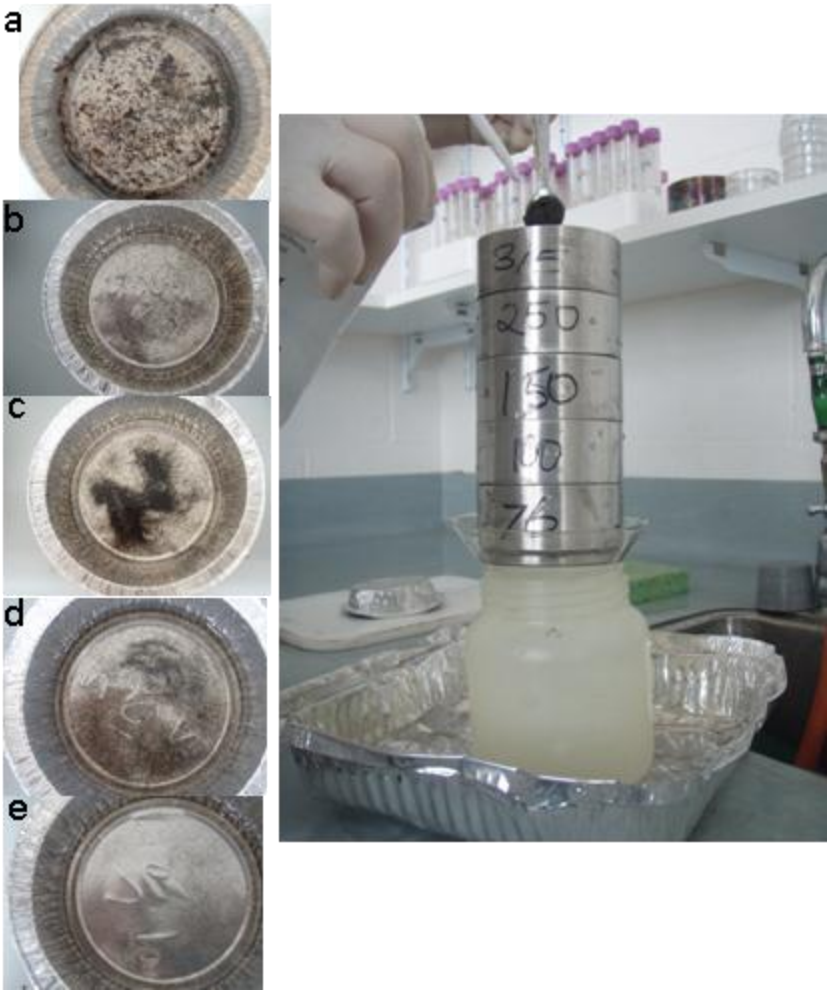

Figure 2.8. An example of a muddy baseline sediment sample gently washed through the sieve stack.
Note the relative proportions and nature of the material: (a) seagrass pieces >315 μm, (b) amorphous mineral and organic particles >250 μm, (c) faecal pellet aggregates >150 μm, (d) faecal pellet aggregates >100 μm, (e) amorphous particles with some faecal pellet aggregates >76 μm as minor contaminants to the fraction.

2.7.13. Diatom species abundance and biogenic glassy components

Sediment samples from the lower sediment core LSPMB106 were prepared for microscopic analysis of glassy biogenic components with 5 % H_2O_2, washed and mounted on microscope slides according to Saunders *et al.* (2007) for determining diatom species abundance. This data was applied to a local paleo-salinity transfer function (Saunders *et al.*, 2007). Diatom species were separated into environmental classes: epipelic, epiphytic, phytoplanktonic and facultative phytoplanktonic, according to Round *et al.* (1990) and Dr. K. Saunders performed the identification to a species level. However, the separation of diatom species into environmental classes: epipelic, epiphytic, phytoplanktonic and facultative phytoplanktonic, was performed by myself in accordance with Round *et al.* (1990).

Additionally, microscope slides were prepared in the above manner to assess the importance of other biogenic glassy components (phytoliths, thecamoebians) within the selected surface sediment stations (3 sites per station, WB4, MB2, MB13, SB4). The forms were identified as phytoliths and thecamoebians from examples illustrated in Carey *et al.* (2005) and Lu and Liu (2003).

2.7.14. Analysis of size classes: Macro-char particles

Two mL of sediment, measured by water displacement within a centrifuge tube, was taken from upper and lower sediment cores horizons (LSMB206 and LSPMB107) for macro-char counts on a 250 μm and 100 μm sieve stack. Preparation and clean up protocols were according to Carcaillet *et al.* (2002).

2.7.15. Analysis of size classes: Faecal pellets

All size fractions were examined at low magnification with a binocular microscope. Faecal pellets dominated the >150 μm and >100 μm fractions but no pellets could be found on the 250 μm sieve and were a minor component on the 76 μm sieve. Other materials, identified as pieces of seagrass leaf, occasional macro–char particles, foraminifera, quartzite particles, glassy sponge spicules, urchin spines and other shell debris were all minor components.

The quantity of faecal pellets associated, by weight, with the >150 μm and 100 μm fractions was estimated by dispersion and sieving of the faecal pellets after 5 mins to 10 mins of sonication. The material was then completely transferred and washed through a 76 μm sieve. The collected material, (dried at <60° C) was subtracted from the dry weight of the initial sieve fraction to calculate the proportion of faecal pellets within their size fractions.

2.7.16. Bivalve shell taphonomy

Bivalve taphonomy of shell deposits describes characteristic signatures of their transport conditions (floods, storms, tsunamis tides) through a bias in the physical condition and orientation of the shells type. Recently Donato *et al.* (2008) developed a relatively simple form of the analysis for distinguishing sediment deposits caused by storm surges (tempesite) and beach wash from those caused by tsunamis (tsunamites) that can also be used to distinguish between bivalve transport along the surface waters during tide excursions (Dent and Uhen, 1993).

A taphonometric analysis of bivalve shells was conducted through >37 cm thick shell deposit facies at the bottom of sediment core LSPMB107. Sub-samples (3 mL) were taken down the facies every 2 cm and were isolated on a 3.15 mm sieve, then separated into size classes, 3 mm to 6 mm, 6 mm to 10 mm, 11 mm to 20 mm and 21 mm to 30 mm. All the samples were then combined (483 bivalves, 981 recognised conditions) for a taphonometric analysis using the above classification from Staff *et al.* (2002). Bivalves were also collected using 15 cm x 15 cm surface grids from 4 sites along isolated and relatively inaccessible parts of beaches (Figure 2.4) for a baseline comparison. The samples were combined (500 bivalves, recognised 1399 taphonometric conditions) and treated as for the above shell facies. The spectrum of bivalve conditions was constructed as in Donato *et al.* (2008) by summing up the range of bivalve conditions from each individual bivalve.

2.7.17. Inorganic nitrogen stable isotope ratios of KCl soil extracts

Total dissolved inorganic nitrogen (ammonia, nitrite and nitrate) associated with soil was extracted and trapped, after the extract was made alkaline, onto acidified (2.0 M citric acid, according to Schleppil *et al.,* 2006) glass fibre filters wrapped in a floating polytetrafluoroethylene envelope (Sørensen *et al.,* 1991). Recovery of the inorganic nitrogen was always above 98 %.

The net inorganic nitrogen stable isotope ratios of the resultant trapped ammonium salt was analysed *via* combustion of the glass fibre filter using a Fisons NA1500 flash Elemental Analyser coupled via a Con-Flo II interface to a Thermo-Finnigan Delta S isotope ratio mass spectrometer at the Commonwealth Scientific Industrial Research Organisation (CSIRO) Marine and Atmospheric Research by D. M. Davies. CO_2 produced in the combustion was removed from the carrier gas with an inline sodium hydroxide scrubber to avoid isoptomer interference. Because of low sample weights, modified narrow bore furnace tubes were installed allowing for lower flow rates to the Conflo and a dynamic range of 5 μg to 50 μg N (Trull *et al.,* 2008). Percentage recovery of N within batches was measured using 168 μg N as KNO_3 working standard solutions and trapping on filters, then measurement on a CHNS Elemental Analyser at the Central Science Laboratories, University of Tasmania (performed by Dr. T. Rodemann). Further interpretation of the Rp index metric and Glyph Analysis within different surface sediment matrices, along a transect within Little Swanport estuary, was assessed in Chapter 3.

Chapter 3. Evaluating proxies and processes along a transect within the Little Swanport estuary, towards a palaeo-ecological reconstruction

3.1. Introduction

Deciphering and choosing estuarine sedimentary signals as proxies for appropriate components and processes needed for management and predicting changes to seagrass ecosystems, is a major challenge for its palaeo-reconstruction. For instance, for management it is necessary study the ecosystem at the appropriate landscape scale (Habeeb *et al.*, 2007; Nyqvist *et al.*, 2009) by including proxies for the components that compete with seagrass for light and nutrient resources (*i.e.* micro-algae) and the source of nutrients that can drive change (Duarte, 1995; Fourqurean and Zieman, 2002). Whereas, for prediction it is necessary to include proxies for the processes that link those components, for example, the trophic structure (top down control) than may ameliorate the micro-algal competition for light or nutrient resources for seagrass carbon fixation (*e.g.* Jorgensen *et al.*, 2007) or indeed, seagrass light mediated nitrogen fixation (Welsh, 2000). However, ecosystem signals are not necessarily specific and may act as proxies for a number of alternative components and/or processes. Furthermore, the original signal may have been modified or lost to the sediments, since deposition, to below analytical limits of detection.

To account for the above issues, it is often necessary to employ a number of scientific justification methods by using ecosystem diversity in space before they can be generalised over time. These include Robustness Analysis (RA), inference to the best explanation (IBE) and weak inference through self-consistency (SC) (see Chapter 1), and when used holistically it is possible to identify the importance from the relative magnitudes of their signals and their nexus to their components and process proxies. In other words, identifying the nature of the signals is dependent on both convergence with other lines of evidence provided they adhere to well tested current theories. Nevertheless, choosing and evaluating ecosystem proxies is a hierarchical procedure, in three steps:

1. Determine the plausible environmental context to select the appropriate range of proxies for theory and prediction, and identify the conditions that have generated and preserved the signal in the sedimentary record. This step requires a direct examination of the targeted water body's ecosystem processes and components, and the areas that can successfully record those processes and components. This may include examination of the species and trophic structure; external forcing factors from

catchment and coastal inputs, such as nutrient and sediment loading impacts on primary productivity; and an undisturbed central sump with little or no sediment column hypoxia, with the ability to integrate the whole of the water body's ecology.

2. List the plausible proxies consistent with the signal. This relies on a current understanding and assessment of the likely strengths and weaknesses of those proxies for the target environment. Consequently, the proxy may require further research and/or constraints to resolve any contradictions and underlying assumptions. The constraints are usually additional proxies to resolve assumptions.
3. Evaluate the independence of multiple proxies (RA) and/or test the nexus between a signal and a proxy (IBE, SC) within a plausible contemporary environment, such as a range of environments that reflect the type and the range of expected temporal changes (space for time). Traditionally, this step uses the environmental gradient represented by a range of water bodies (lakes and lagoons) at different stages of evolution and anthropogenic disturbance to evaluate or calibrate the sediment signal to the proxy and to establish the independence of multiple proxies. It is important to demonstrate independence; otherwise, convergence for an RA becomes a function of common features of the proxy's conceptual model with the signal and not the target process or component (*see* Chapter 1; Bycroft, 2009).

Using different water bodies to evaluate proxies can be potentially problematic. The proxy within the targeted water body might lie in one of the tails of the normal distribution, which describes the mean response between individual systems. In other words, the mean response represents the net effect of all uncontrolled variables between different water bodies and is not necessarily representative of the response within the targeted water body (Peters, 1986, 1991). The differences result primarily from:

- Different characteristic catchment signals. It is difficult to untangle the effect on a single estuarine water body from its catchment, if the theory is based on using the average response from different catchments. In other words, catchments have a range of different signals and event histories. Consequently, different water bodies might produce different regime states and different degrees of established equilibrium. For example, catchment $\delta^{13}C_{org}$ input signals, both particulate and dissolved, may differ because of varying proportions of C4 and C3 grasses (Fry, 2006). Agricultural fertilisers leaching into the catchment can enrich $\delta^{15}N_{org}$ signals (Ruiz-Fernandez *et al.*, 2002). The POC–PON ratios within catchment soils may be a function of different pre-Anthropocene aboriginal fire management practices (McIntosh *et al.*, 2005).

Catchments also have geological signals that might overlap the target estuary's signals, such as dolomite interference with epifaunal calcium carbonates proxy (LOI 950°C).

- Different degrees of established equilibrium. Cause and effect along an environmental gradient requires the presumption of equilibrium between variables (Carpenter and Kitchell, 1988). Disturbances and dynamic prey–predator interactions (limit cycles) are examples of processes that result in a state far from equilibrium. For example, polluted bottom sediments under fish cages require a number of years for benthic respiration to re-establish equilibrium and sediment hypoxia (15 months to 5 years; Woodward *et al.*, 1992). Storm damage of seagrass meadows requires a decade for ecosystem recovery (*e.g.* Bayley *et al.*, 1978). A five-year natural cycle in the zooplankton population is related to the life cycle of its stable planktivore population (Carpenter and Leavitt, 1991).
- Different historical contingencies between water bodies (*i.e.* different events at different times within different water bodies) may produce different regimes (Strayer *et al.*, 1986). For example, storm events can either destroy a seagrass regime and replace it with a micro-algal regime (*e.g.* Bayley *et al.*, 1978) or destroy a macrophyte/micro-algal regime and replace it with a seagrass regime (Morris and Virnstein, 2004). Even though the regimes are not stable, they do persist for up to 14 years (Morris and Virnstein, 2004) before returning to the original regime.

Unlike lakes and many lagoons, the competing influence of river inflows and coastal exchange defines the target estuary by generating an ecosystem gradient. The gradient may be continuous or divided into a set of discrete zones formed by irregularities in bathymetry and topography. Consequently, the zones or ecosystem gradient have a common event history, catchment geology, geomorphology and climate. A sampling transect along the estuary can thus be used to identify: (1) zones within the estuary that characterise the whole system and (2) a plausible range of past conditions for the individual estuarine zones. This is useful because past changes in nutrient supply will have produced an equivalent biome response to that which could be expected for a similar nutrient supply or condition change within today's estuary. Further, internal disturbances and functionally separate embayments (water bodies separated from the estuary) can be identified as outliers from the ecosystem gradient generated by river and coastal influences.

However, the single water body transect is not ideal. Most estuaries change in shape and volume towards the coast. This often leads to discrete estuarine zones that do not share a common bathymetry or topography (Roy *et al.,* 2001). Consequently, each zone will vary in its response to changing environmental river and coastal boundary conditions; any relationship formulated in space and applied over time may need an additional function to describe the varied response between zones. Nevertheless, there are more commonalities across a single transect than would be found using the alternative of sampling a number of individual but similar estuarine zones with different histories, catchment geologies, volumes and topographies.

A comparison between surface sediment signals and their immediate water body's biome cannot be used as a definitive evaluation of the sedimentary signal because there is a seasonal or inter-annual mismatch in comparing past conditions with present conditions. Hence, Zong *et al.* (2006) used previous knowledge of local surface sedimentation rates along transect zones within the Pearl River (China) to identify the years in which the surface sediments were deposited. In this way, they were able to match the period of available water quality data.

Detailed knowledge of local surface sedimentation rates or contiguous water quality data and biome signals are usually not available. Consequently, many contemporary transect evaluations and calibrations assume a short-term ecosystem steady state. For example, Saunders et al. (2007) produced a description of past salinity changes within Orielton Lagoon (Tasmania)using surface sediment diatom assemblage with spot water quality measurements, a variance that was self-consist with the history of the lagoon. Perry and Beavington-Penney (2005) found strong linear correlations between the immediate productions of the seagrass calcareous epibiont community with surface sediment $CaCO_3$ content. However, steady-state assumptions should be treated with caution for small, dynamic catchment/coastal estuary systems, such as the Little Swanport estuary, that is, estuaries that have a limited capacity to buffer changes in tidal exchange, rainfall (*see* Chapter 4), solar irradiance (Nunez and Li, 2008; Khalia *et al.,* 2009), and coastal nutrient boundary conditions (*see* Chapter 5).

The seasonal and inter-annual dynamics of an estuary ecosystem, thus, relegates contemporary observations and measurements to an environmental context; a context to support a spatial subset of RA and IBE (see Chapter 1) to the nature of the proxies that the surface sediment signals suggest. For example, the species responsible for the calcium carbonate signal is the likely source of the biomarker or likely reasons for a changing organic

stable isotope signal (*i.e.* relative supply between catchment and estuarine organic matter, productivity or its inorganic source; see Section 3.1.2.4).

3.1.1. Ecosystem processes and components for the Little Swanport estuary

The choice of ecosystem processes and components was based on a modified level of abstraction as used by the minimum models of Scheffer (2004) and van Nes *et al.* (2007). These models describe the competing effects of a planktivore/zooplankton/phytoplankton trophic cascade and external nutrient supply on a shallow lake's water quality and sub-aquatic vegetation coverage. For the Little Swanport estuary, nitrogen fixation *via* seagrass (Welsh, 2000), shading by seagrass leaf epibionts and water column seston (turbidity) were included with a consideration of using the ecosystem differences within the Marine Flood/Tidal Delta as the energy-energy proxy of flood and marine incursion affects.

3.1.2. Available common signals for ecosystem proxies

Among the choice of signals that are relatively easy to sample and process for a deliverable management tool (MOLTEN, 2004) are preserved plant and animal remains, stable isotope ratios, major elemental ratios, BSi content, organic carbon content, organic nitrogen content, organic matter (OM) content and calcium carbonate content from loss of weight on ignition as total content metrics. A little known development of loss on ignition, stepwise thermogravimetry (Rp index) has extended the relatively simple and cheap measurement of OM content to include the characterisation of organic sources and the fingerprinting of their mixtures within sediments (Kristensen, 1990; Kristensen *et al.*, 1994; Loh *et al.*, 2008).

3.1.2.1. Signal interpretations

With the exception of water column turbidity, the above range of signals has the potential to act as multiple or singular proxy for the conceptual model's processes and components. Nevertheless, like most if not all signals, there are alternative plausible interpretations that complement or add to the range of proxies that need to be considered.

3.1.2.2. Biogenic silica

Biogenic silica (BSi) is traditionally used to represent either diatoms or sponge spicules by altering the digestion times (Conley and Schelske, 1993) to remove interference from sands and clays. However, there may be some additional biogenic interference from siliceous phytoliths (*e.g.* Carey *et al.*, 2005), smaller labile sponge spicules (Conley and Schelske, 1993), relatively labile silicate minerals formed during the podzolisation of soils (Gibson,

1994) and interference of the analysis by the coating of the analyte with iron-laden clays (Michalopoulos and Aller, 2004).

3.1.2.3. Loss on ignition

Loss on ignition (LOI) from 105°C to 550°C and 550°C to 950°C is traditionally used as a proxy for OM and shell carbonate respectively (Heiri *et al.*, 2001). This analysis may be subject to significant interference from water loss due to clays (Mook and Hoskin, 1982; Santisteban *et al.*, 2004) and variance from different sample weights and furnace conditions (Heiri *et al.*, 2001).

Stepwise thermogravimetry is a LOI procedure that indexes weight lost (Rp index) over a number of temperature ranges. Rp index = PII/(PI +PII), where PII is the loss from ignition from 280°C to 520°C and PI is the loss from ignition from 130°C to 280°C. The Rp index has been used to fingerprint both living and detrital OM mixtures (Zimmerman *et al.*, 1987; Kristensen *et al.*, 1994, Loh *et al.*, 2008). Consequently, Kristensen *et al.* (1994) interpreted the Rp index to include ongoing humification to explain the origin and fate of organic sources down undated sediments (30 cm) within the mangroves of Ao Nam Bor (Thailand). However, experiments indicated that changes in the algal and seagrass Rp index appeared to reach an asymptote after only 50 days of mineralisation (Kristensen, 1994).

Kristensen (1990) warned that any thermogravimetry method used to characterise sedimentary organic mixtures might also be subject to interference from water loss within clays and a more efficient lower temperature combustion promoted by other organic compounds. The efficiency reduces the carryover of organic char formation for later combustion at higher temperatures (Kristensen, 1990) and thus affects the temperature index ratio. The combustion index modification is not restricted to organic compounds. Kok and Gundogar (2010) recently found that carbonates can also promote a more efficient combustion of organic mixtures (crude oil) at lower temperatures (<375 °C).

3.1.2.4. Stable isotope ratios and major elemental ratios

Particulate organic carbon stable isotope ratios ($\delta^{13}C_{org}$) have been used to measure changes in:

1) gross micro-algal productivity (*e.g.* Zimmerman and Canuel, 2002; Wu *et al.*, 2008), and when combined with changes to POC–PON ratios, as an indication of which resources (light or nutrients) limit productivity (Harris, 1999, 2001).

2) the proportions of different OM sources within simple two-component systems (*e.g.* Gonneea *et al.*, 2004; Turner *et al.*, 2006), and when combined with POC–PON ratios, to calculate the OM proportions within three component systems (*e.g.* Gonneea *et al.*, 2004).
3) water column salinity (indirectly), through its covariance with the proportions of catchment OM (*e.g.* Zong *et al.*, 2006).

However, an elemental ratio or mass ratio does not insulate their modification by organic mineralisation down the sedimentary record. Galman *et al.* (2009) found that the $\delta^{13}C_{org}$ signal changed markedly, but only over the medium term (within the first five years). In contrast, changes in POC–PON ratios across primary organic materials (*e.g.* seagrass, tree leaves, micro-algae and macrophytes) appeared to be confined to the first few months (*e.g.* Kristensen, 1994; Lehmann *et al.*, 2002; Fourqurean and Schrlau, 2003).

Organic nitrogen stable isotope ratios, expressed as $\delta^{15}N_{org}$, also respond to changes in primary productivity providing that inorganic nitrogen is not limiting to growth, such as within phosphorus-limited systems (Fry *et al.*, 2000). However, in nitrogen-limited systems, particulate's $\delta^{15}N_{org}$ value reflects the isotope of the dissolved inorganic nitrogen source. Consequently, increases in $\delta^{15}N_{org}$ in both sediment (Ruiz-Fernandez *et al.*, 2002) and seagrass macrofossils (Orem *et al.*, 1999) can be used to quantify nitrogen eutrophication. This is contingent on the value of the fertiliser and animal waste $\delta^{15}N_{inorg}$ being different to that of the previous catchment and estuary's primary productivity assemblage value.

3.1.2.5. Preserved plant and animal remains

The preserved diatom assemblage has been shown to respond to water quality. For example, Saunders *et al.* (2007) produced a salinity diatom assemblage transfer function constructed from sediment samples with estuaries and embayments along the east coast of Tasmania. However, such functions need to be carefully re-evaluated as its calibration may be affected during deposition. For example, Kashima (1990) found that the usually abundant diatom *Skeletonema costatum* was not present in surface sediments during times of euryhaline conditions, as it was quickly dissolved after deposition.

The relative abundance of preserved parts of or whole zooplankton species remains has been used to infer directly their presence within the water body and as an indirect indication of planktivore numbers. Planktivore predation selects for the persistence of smaller species (*e.g.*

McGowan *et al.*, 2005); that is, the largest species are preyed upon more efficiently. However, measurable numbers of preserved animal remains are usually contingent on a slow sediment accretion rate that is more typical of lakes, which can be orders of magnitude slower than for coastal waters (Burdige, 2006).

Though rarely reported, well-preserved copepod faecal pellets have been observed in both lake sediments (*e.g.* Smith and Syvitski, 1982; Haberyan, 1985; Dean *et al.*, 2001; Cromer *et al.*, 2005) and in the sediments of shallow estuaries (Roy *et al.*, 2001). It is important to note that the size of the sedimenting pellet found in estuaries, embayments and coastal waters is proportional to the size of the copepod (Uye and Kaname, 1994; Viitasalo *et al.*, 1999; Beaumont *et al.*, 2002) and the quantity of faecal pellets present represents their accumulation over the lifespan of the copepod. Hence, an assay of faecal pellets has potentially a greater sensitivity to copepod presence and the inferred planktivore presence based on the relative sizes of the copepods (*e.g.* McGowan *et al.* 2005). The Little Swanport estuary's copepod population is dominated by *Paracalanus indicus* (Crawford *et al.*, 2005) and the smaller morph of *Acartia tranteri* (Swadling, K., 2007, *pers. com.*). Indeed, Kimmerer and McKinnon (1985, 1987) found that the same planktivorous fish as found in the Little Swanport estuary (Hardy Head and Yellow Eyed mullet) controlled the relative abundance of same species of copepod in both Westernport and Port Philip Bay. This makes it reasonable to assert that the distribution of the smaller *Acartia tranteri* and larger *Paracalanus indicus* within Little Swanport is also the result of planktivore predation, given that the size selection mechanism is currently regarded as axiomatic across marine and lake ecosystems (Scheffer, 2004).

3.1.2.6. Water column turbidity

The only known water column light-level proxy is the presence or absence of bacterial photosynthetic pigments at the bottom anoxic hypolimnion of a shallow lake (Carpenter and Leavitt, 1991). However, shallow anoxic hypolimnion does not usually form within tide-dominated systems (Roy *et al.*, 2001) and the proxy requires specialised collection procedures (freeze coring), handling (in the dark, under nitrogen) and analytical equipment (HPLC). Clearly, there is a need for a more general and direct turbidity proxy. Water column light attenuation is a consequence of both external forcing factors (catchment erosion and wind induced littoral re-suspension) and net micro-algal productivity.

Light attenuation is primarily the result of turbidity from the suspended fine fraction (James *et al.*, 2004). Therefore, it is reasonable to suggest that the sediment's fine fraction content can

be used as the basis of a water column turbidity proxy for light attenuation. For example, Kozerski (1994) showed that within shallow wind mixed systems like Little Swanport estuary, the water column particle concentration could be calculated from the sediment trap accretion rate and the average sedimentation velocity. However, using the sediment's fine fraction content is contingent on the presence of copepod faecal pellets within undisturbed muddy sediments. This is because copepods are responsible for clearing the water column by packaging the sestonic fine fraction within lakes (Smith and Syvitski, 1982, Scheffer, 2004 and references therein) and represent a significant vector in the clearance of the estuarine sestonic fraction in shallow estuaries (Fulton, 1984; Sommer *et al.*, 2000). Should the sediments be composed mainly of larger sands, it cannot be discounted that the fine fraction was lost from winnowing (Smith, 1975). Sediment that contains no faecal pellets may indicate either that the total fine fraction represents the water turbidity, or that faecal pellets have spilled their contents from a damaged or degraded peritrophic membrane. For example, during floods, copepods are washed out (Crawford *et al.*, 2005), which can lead to a re-sorting of sestonic particle sizes and/or faecal pellet beak up.

3.1.2.7. High-energy events

Identification of depositional events is necessary for a sediment geochronology within shallow dynamic estuaries (*see* Chapter 4). Depositional events cannot be identified through an *a priori* knowledge of sediment accretion rates[9] calculated from a geochronology. Instead, a range of content markers is usually selected as weight of evidence to distinguish baseline sediments from event sediments (*e.g.* Thorndycraft *et al.*, 1998; Gilbert *et al.*, 2006; *see* Chapter 4). Consequently, for this study, three potential approaches synonymous with high-energy events were explored by using the sandy/shell debris-laden sediments of the Marine Flood/Tidal Delta as a high-energy environment model. These are (1) the effects of clays and shell carbonates on the Rp index (stepwise thermogravimetry); (2) the absence of faecal pellets within sediments, contingent on their presence within the quiescent muddy zones of the estuary; and (3) the development of a set of ideal neutral models (See section 1.2.1), which can distinguish the relative rates of lithogenic supply over autochthonous OM supply from the proportions of major sediment contents, named here as Glyph Analysis.

---

[9] A high sediment content of lithogenic material associated with some depositional events may be the result of either an increase in lithogenic supply or a fall in the supply of the remaining major estuarine sediment components. Rates of supply can only be directly calculated from knowledge of sediment wet bulk density and sedimentation velocities.

3.2. Goals and aims

The study's goal was to evaluate the nexus between the surface sediment signals and their assumed ecosystem process and component proxies through a sequence of hierarchical hypotheses, tested along a transect within the Little Swanport estuary. These hypotheses are contingent on the success of previous hypotheses and/or supported by contemporary observations and laboratory experiments. The following list gives the observations and hypotheses with their postulates:

1. A qualitative visual inspection revealed that the seagrass leaf epibiont community is dominated by sessile calcareous epifauna rather than plant epiphytes: The origin of sedimentary $CaCO_3$ (LOI 950 °C) comes from the remains of calcareous epibionts, which can both attenuate light to the seagrass leaves and reduce the area for nutrient absorption.
2. The calanoid copepod remains and/or their faecal pellets within the detrital sediment (<315 μm) represent a significant fraction of the remaining sediment contents: Fossil copepods/faecal pellet abundance is sufficient to represent the estuary's copepod population, their size distribution can be used to infer control through planktivore predation and the variance in sestonic turbidity is primarily controlled by copepod grazing.
3. Calanoid copepods and/or their faecal pellets are present within the upper muddy estuary sediments (<315 μm) and absent from the sandy sediments of the Marine Flood/Tidal Delta: High-energy environments and event deposition can be determined from the absence of copepod faecal pellets.
4. A visual search found no significant numbers of phytoliths and thecamoebians among microscopic glassy components (diatoms) within the surface sediments (<315 μm): Labile BSi content was dominated by diatoms and/or labile soil silicates.
5. Labile BSi content within salt marsh sediments and catchment soils are less than surface sediment contents of a dominant fine fraction: Soil and salt marsh labile silicate components do not control the variance of surface sediment labile BSi.
6. There is a distinctive step-like change in extraction times between the surface sediment's labile and refractory BSi: There was no contamination of labile BSi from smaller more labile refractory sponge spicules or interference from other sedimentary components.
7. There are high correlations between the surface sediment's labile BSi content, the OM content (LOI 550 °C) and $CaCO_3$ content (LOI 950 °C): Labile BSi and OM variances were proxies for micro-algae as prey for sessile epifaunal production. This is

contingent on the success of hypotheses 4 to 6, which suggest that labile BSi was dominated by diatoms, and on the hypothesis 1 observations, which suggest that the calcareous epibiont community is dominated by bryozoans.

8. The BSi:C sedimentary stoichiometry, normalised to zero lithogenic content and its associated organics, is typical of marine diatoms: The variance in OM content (<315 μm) is controlled by diatoms, contingent on previous hypotheses (4 to 7).
9. Separating the large mass of detrital seagrass leaves (>315 μm) from the detrital sediment fraction (<315 μm) does not affect the OM variance, as representing micro-algal variance: The large mass of detrital seagrass leaves, captured on a 315 μm sieve, represents the immediate live seagrass meadow (*e.g.* Davidson *et al.*, 1995). This is contingent on the success of the previous hypotheses (4 to 8) that hold that the surface sediment (<315 μm) OM represents micro-algae.
10. There is no covariance or overlap of $\delta^{15}N_{org}$ and $\delta^{13}C_{org}$ or $\delta^{13}C_{org}$ and PON–POC ratios for primary OM sources (epiphytes, soils/salt marsh sediments, suspended particulate matter [SPM] and seagrass leaves [live and detrital >315 μm]): Micro-algal and seagrass OM can be distinguished from soil/salt marsh OM with a triple-end point linear mixing model.
11. $\delta^{13}C_{inorg}$ variance of seagrass leaf sessile calcareous epifauna shell carbonate is not correlated with $\delta^{13}C_{org}$ variance for live and detrital seagrass leaves, SPM and surface sediments (<315 μm): $\delta^{13}C_{org}$ variance is a function of carbon fixation rather than of dissolved inorganic carbon isotopes. This is contingent on the success of previous hypotheses (4 to 8) that hold that surface sedimentary OM variance represents micro-algae.
12. Seagrass leaf N/P ratios are close to their optimum Atkinson ratios (Fourqurean and Zieman, 2002): The $\delta^{15}N_{org}$ for the primary productivity assemblage reflects its inorganic source.
13. There is a positive correlation between $\delta^{13}C_{org}$ and POC–PON for all primary biome and sediment ratios (Harrison, 1989): Inorganic nitrogen supply limits carbon fixation. This is contingent on the success of previous hypotheses (4 to 8 and 12) that hold that surface sedimentary OM variance represents micro-algae and not a significant change in the dissolved inorganic carbon source.
14. There is a positive correlation for $\delta^{15}N_{org}$ and $\delta^{13}C_{org}$ between the detrital and live primary productivity assemblage during early February transect sampling: There was a net annual to inter-annual steady state in production and no diagenetic parameter variance, and most of the sediment supply was during summer/spring growth.

15. The surface sediment Rp index/POC–PON ratio signature lies with a three-end point mixing model of detrital organic components (seagrass leaves, micro-algae and soils/salt marsh): The component proportions of OM and the sediment content, at the time of deposition, can be disentangled without the need of diagenetic corrections of Rp index and POC–PON ratios.
16. A significant correlation of the best sediment least squares linear regression for the Rp index requires both BSi content and LOI 950 °C as independent variables, contingent on the failure of hypothesis 15: The sediment Rp index has been affected by carbonates, contingent on the success of hypotheses (7 and 8) that hold that BSi is a proxy for the sediment OM variance as micro-algae.
17. The effects of standard additions and acid treatment of sediments comprising seagrass leaves, micro-algae, soils, organic free clays, fossil shells and their salts results in a linear or non-linear response of organic mixtures and elevated Rp index by $CaCO_3$ modification of lower temperature combustion. Rp index mixing models were linear or non-linear, and elevated Rp indexes outside the model's boundaries were the result of the components of high-energy events and environments.
18. There is a self-consistency between Glyph Analysis determination of the relative supply of lithogenic and OM with the estuary's geomorphology (lithogenic deposits, muddy deposits and sandy deposits), and changes in surface sediment $\delta^{13}C_{org}$ OM content. This is contingent on the success of the hypothesis (12) that the variance in $\delta^{13}C_{org}$ is a function of carbon fixation.

3.3. Data analysis methods

Details of sample collection, processing and analysis of detrital surface sediment (<315 μm), sediment particle size, detrital and living seagrass leaves, seagrass leaf epibionts, and soils and salt marsh sediments are described in Chapter 2. Below, the methods used to analyse the data are outlined.

3.3.1. Stepwise thermogravimetry experiment

The effects of organic matter and calcium carbonate sources on the Rp index was determined from a series of standard additions (see Chapter 2 for the analytical procedure) on the laboratory standard with an elevated Rp index (0.5), an Rp index not shared with the sources of organic matter. These additions included live seagrass leaves; a phytoplankton human dietary supplement (*Chlorella pyrenoidosa*), both fresh and aerobically mineralised over two months at 28 °C; catchment soils and salt marsh sediments; fossil shells; $CaCO_3$ (Analar) and

organic free clays. The clays were obtained from sediments after combustion at 950 °C for 2 hours. In addition, the sediment was also acidified (10 % HCl [Analar]) as a control for the above carbonate standard additions by removing any $CaCO_3$ content.

3.3.2. Neutral models for Glyph Analysis

Glyph Analysis was developed to determine the relative rates of lithogenic and autochthonous OM supply solely from changes in principal sediment proportions (by dry weight). Glyph Analysis compares the major content and ratio patterns, in space or time, to an ideal set of neutral models that have been solved for their supply of lithogenic and OM supply patterns. The model solution is contingent on a predator to prey relationship between the micro-algae (BSi and OM) and calcareous epifauna (LOI 950 °C), which is itself independent of the supply of lithogenic clays or sands from the catchment or coastal sediments. Content patterns that conform to any of the neutral models will therefore mark the transition to another type of environment or ecology; for example, high-energy events and Marine Flood/Tidal Delta environments are dominated by calcareous shell hash and sands (Roy *et al.*, 2001).

Glyph Analysis can be best understood by following the construction of the ideal Glyph neutral models that match the content variances and their ratios to each other and to their relative supply. The above conceptual model and its spatial boundaries was first determined, contingent on the success of the Glyph hypotheses expressed as synchronous correlations between the major biological components: BSi, LOI 550 °C (OM), LOI 950 °C as $CaCO_3$ (1.67 LOI 950 °C; see Figure 3.11). The remaining component residual detritus (RD) is the independent lithogenic fraction. Based on the above relationships, the construction of the content variability from relative changes in supply becomes straightforward. First, the relative fluxes of OM and RD are added together after varying OM and/or RD in all equivalent permutations (see Figure 3.1). The remaining fluxes of the BSi and $CaCO_3$ are then estimated from their proportional relationships to OM, as determined from the transect study. After each content flux permutation, the resulting relative proportions of the OM and RD and their ratios can then be calculated from proportion of total flux of all materials. The result is a set of unique variance combinations of OM content and RD content and their ratios to a unique set of relative RD and OM supply (see Figure 3.1).

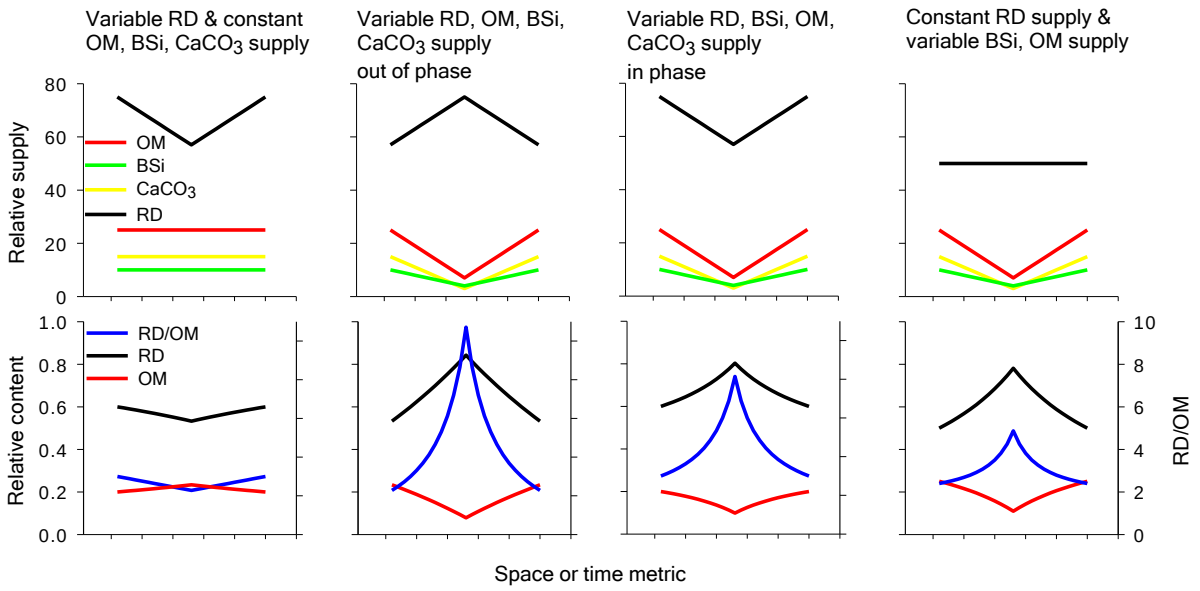

Figure 3.1. Glyph neutral models relating the BSi, OM and RD contents to their relative supply variance. The top row of figures is an idealised set of all equivalent supply variance scenarios between the major covariant biotic content variables—BSi, OM and $CaCO_3$—and the independent lithogenic fraction—RD. The bottom set of figures represents the calculated resulting relative supply variance with its matching RD and OM contents and ratios.

3.3.3. Data analysis

Relationships between proxies based on stated bi-variant hypotheses were tested using ordinary least squares regressions (Sigmaplot™). A stepwise regression procedure (Sigmaplot™) was used to test hypotheses that relied on multiple independent variables. In circumstances in which the regression residuals were not normally distributed, the portion of transect that was responsible for the outliers was separated from the best least squares model by using a novel application of a constrained two-way increasing window analysis. The analysis identifies the parameter transitions (slope and/or intercept) at the point of maximum correlation of the coastal and river influences. The analysis is generically similar to increasing the window size in univariate semi-variograms with time or space, for determining changes in scale (Habeeb *et al.*, 2007). The main point of difference between a univariate semi-variogram and a bi-variant moving window analysis is that the bi-variant data window does not directly measure space, but rather the zone the data stations represent; in this case, the obvious embayments and estuarine zones based on sedimentology and topography.

The size of the data windows were calculated by a constrained cluster analysis (PAST™) of all contiguous sedimentary and living biota variables along the estuary's transect. As a precaution, the best linear model boundaries were confirmed through an analysis of covariance (ANCOVA; PAST™) between two bi-variant relationships across the largest window size and the remaining section of the estuary, in the manner of Childers *et al.* (1994).

In this way, both internal disturbance and/or the functional boundaries of the estuary were tested along the estuary's transect.

Figure 3.2 illustrates the above reasoning behind the analysis by means of three ideal hypothetical examples. The assumed best linear relationship is overlain across a typical scenario of bi-variant data sets within the assumed window zones. Figure 3.2a clearly shows that the best linear model between proxies was influenced by the river until immediately before the lower estuary zone adjacent to coastal waters. In contrast, Figure 3.2b indicates that the functional state of the estuary remains constant, but varies in its response within a zone adjacent to the river input. The analysis also illustrates how to recognise internally generated anthropogenic disturbance through the interruption of the linear model from influence of the both river and coastal waters (see Figure 3.2c). In other words, such an interruption is inconsistent with the definition of an estuary as a spatially autoregressive water body between the coastal and river influence.

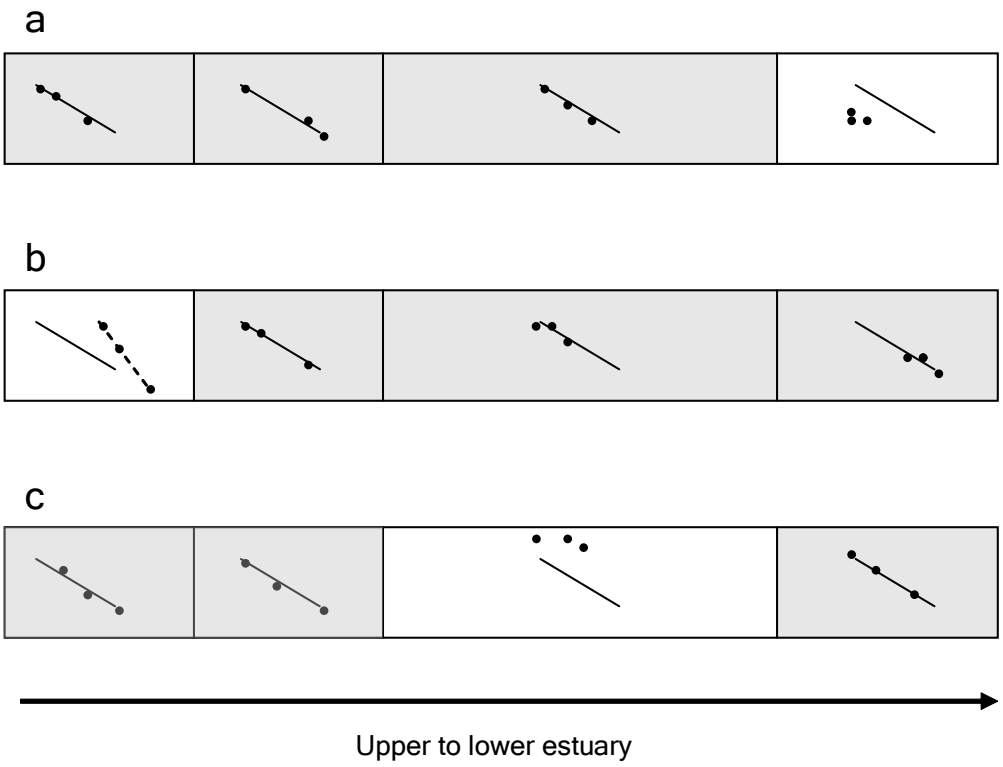

Figure 3.2. Three hypothetical spatial boundaries that mark the change in relationships between proxies.
(a) An example of a functional regime generated from the upper estuary and ending before the lower estuary zone, (b) an example of an isolated embayment that is functionally similar to the estuary, but with a different response parameter by virtue of its isolation, (c) an internal disturbance between the river and coastal boundaries that interrupts the estuary's functional regime.

3.4. Results

3.4.1. A description of content and quality metrics across the transect and surrounding catchment

Quality metric variables refer to indices (Rp index), elemental ratios and their stable isotopes. Content variables refer to the proportions as dry weight of the principal organic and inorganic sediment components. All of the proxy signals, with the exception of the live seagrass N:P ratios, clearly varied across the transect axis (see Figure 3.3) and between some of the axis pairs (*i.e.* the stations that straddled close to the north and south shores, WB2:WB4, DB4:DB6, MB4:MB6). However, the differences across the transect between the water body's north and south shores were not so numerous or large as to disrupt the overall appearance as a series of periodic non-linear trends or step transitions.

There was little correlation across the transect between sediment content and quality classes, with all significant correlations confined within classes (see Table 3.1). However, the residuals among the very strong content correlations (LOI 550 °C–POC; POC–labile BSi; PON–labile BSi) were not normally distributed (Durbin-Watson statistic <1.5 and >2.5; see Table 3.1). In contrast, the very weak correlations between the remaining content variables with the LOI 950 °C, and consequently the RD, appeared to be the result of two outliers from the Marine Flood/Tidal Delta (SB2 and SB3; see Figure 3.3). Conversely, refractory BSi across the transect appeared to be divided between a high concentration within the Middle Basin and absence outside the Middle Basin.

Similar to the LOI 950 °C and RD content, the weak correlations between the POC–PON ratios and sediment $\delta^{13}C_{org}$, seagrass $\delta^{13}C_{org}$ and SPM $\delta^{13}C_{org}$ appeared to result from Marine Flood/Tidal Delta outliers. In contrast to the content signals, the residuals for the very strong positive correlations (between Rp index and the sediment $\delta^{15}N_{org}$ and the seagrass $\delta^{15}N_{org}$; between the seagrass $\delta^{15}N_{org}$ and sediment $\delta^{15}N_{org}$; and between the $\delta^{13}C_{POC}$ and $\delta^{15}N_{PON}$) passed normality.

The non-contiguous quality signals across the transect more or less followed their coupled contiguous counterparts (*i.e.* SPM to sediments [<315 μm] and epibionts on seagrass leaves) (see Figure 3.3). However, particulate soil $\delta^{15}N_{org}$ and $\delta^{15}N_{DIN}$ from soil extracts and their refractory BSi and labile BSi contents appeared to be independent of each other (see Figure 3.3).

able 3.1. Linear regression correlations between content and quality variables across the estuarine transect.
The values in bold represent moderate to high correlations, with their residual Durbin-Watson statistics in brackets (PAST™).

	LOI 550 °C	$\delta^{13}C_{POC}$	LOI 950 °C	POC <315 µm	PON <315 µm	BSi	RD	Rp index	POC:PON	$\delta^{15}N_{PON}$	$C/N_{detrital\ seagrass}$
$\delta^{13}C_{POC}$	-0.01(1.4)										
LOI 950 °C	-0.05(1.25)	**-0.44**(**1.54**)									
POC<315 µm	**0.89**(2.64)	0.24(1.43)	-0.35(0.95)								
PON <315 µm	**0.87**(**2.34**)	0.37(**2.34**)	-0.30(0.91)	**0.98**(**1.52**)							
BSi	**0.82**(**1.53**)	**0.41**(**1.66**)	-0.35(0.95)	**0.87**(1.10)	**0.90**(1.41)						
RD	**-0.66**(0.57)	0.29(1.58)	**-0.71**(0.46)	-0.36(0.77)	-0.38(0.91)	-0.35(0.47)					
Rp index	-0.34(1.35)	**-0.66**(**2.01**)	**0.76**(0.96)	**-0.52**(1.09)	**-0.55**(1.23)	**-0.72**(1.17)	-0.28(1.13)				
POC:PON	**0.43**(**1.51**)	-0.33(1.08)	**-0.54**(1.13)	**0.46**(1.04)	0.29(1.32)	0.25(0.78)	0.14(1.36)	-0.30(0.47)			
$\delta^{15}N_{PON}$	-0.26(1.12)	**-0.84**(**2.02**)	**0.64**(1.20)	**-0.51**(0.79)	**-0.58**(0.80)	**-0.66**(0.88)	-0.26(1.43)	**0.88**(**1.65**)	-0.01(0.91)		
$C/N_{detrital\ seagrass}$	-0.20(1.13)	-0.09(1.53)	0.22(0.96)	-0.18(1.06)	-0.14(1.13)	-0.18(0.75)	-0.02(1.38)	0.39(0.68)	-0.37(0.91)	0.23(1.00)	
$\delta^{13}C_{detrital\ seagrass}$	0.20(1.15)	**-0.43**(**1.63**)	0.32(0.87)	0.12(1.38)	0.09(1.00)	-0.11(0.63)	-0.35(**1.67**)	**0.50**(0.57)	0.109(0.91)	**0.57**(1.16)	**0.46**(**1.96**)
$\delta^{15}N_{detrital\ seagrass}$	**-0.44**(0.91)	**-0.59**(**2.22**)	**0.42**(1.05)	**-0.52**(0.73)	**-0.55**(0.89)	**-0.71**(0.92)	0.05(1.25)	**0.84**(**1.71**)	-0.13(0.93)	**0.86**(**1.65**)	0.27(**1.80**)

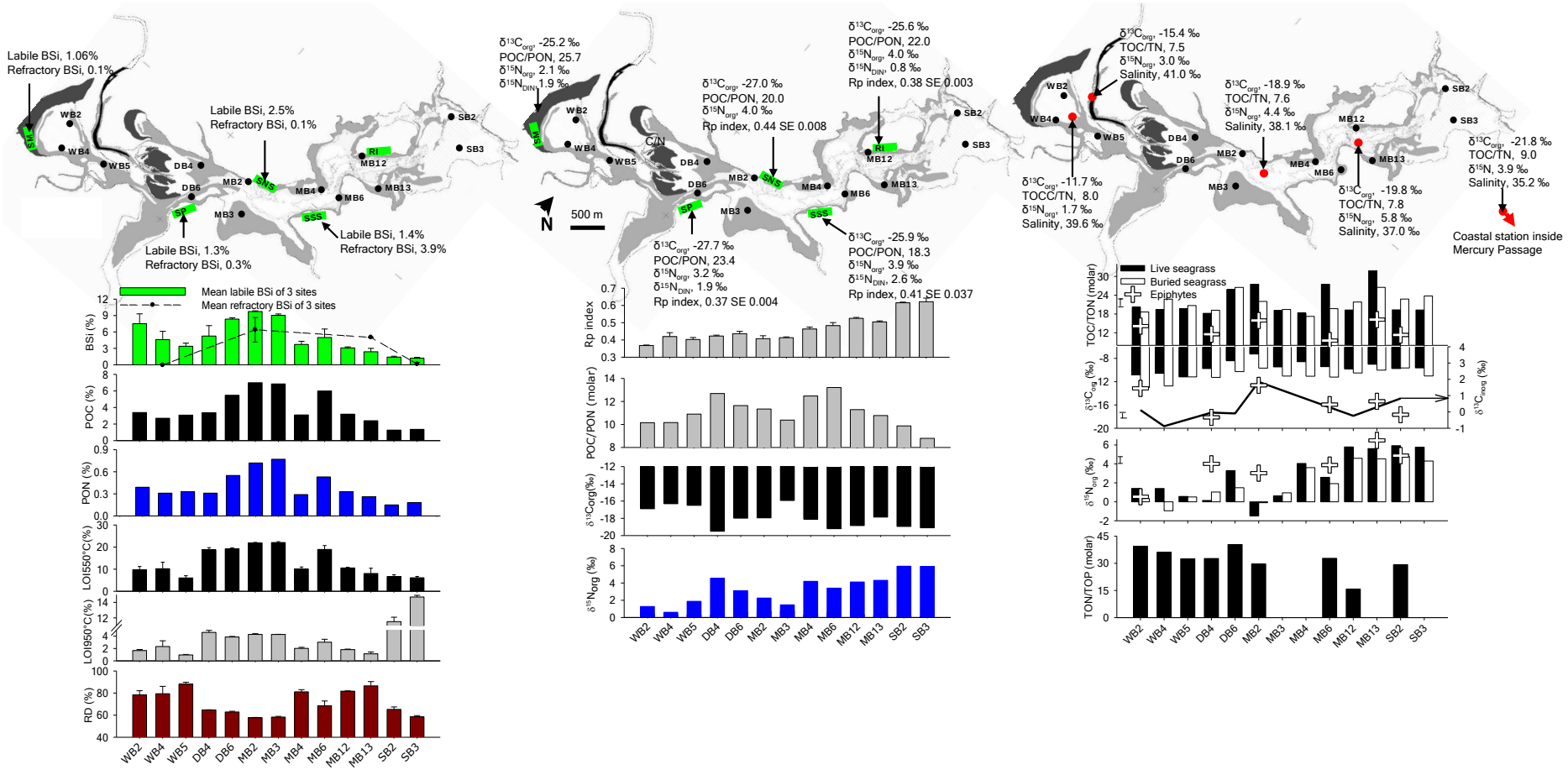

Figure 3.3. Content and quality variables across the estuarine transect and the surrounding catchment soils and coastal waters.
Littoral zone surface sediment (<315 µm) content variables (left), quality variables (middle) and signal variables and plant and epifauna quality variables (right) and selected soil particulate contents and dissolved inorganic nitrogen soil extract quality signals, along an axial transect of the Little Swanport estuary's main water body and adjacent soils. BSi, POC, PON, LOI between 105 and 550 °C (LOI 550 °C), LOI 550–950 °C (LOI 950 °C) and RD, the lithogenic fraction left after subtraction of LOI 550 °C, calcium carbonate (calculated from LOI 950 °C) and labile BSi and Rp index from stepwise thermogravimetry (see text). The error bars represent standard error for three sites at four representative transect stations (WB4, MB2, MB13, SB3).

3.4.1.1. Transect data windows

The constrained cluster analysis of the contiguous quality and content signals identified the data windows needed for the construction of best linear models (see Section 3.3) and for a descriptive context of signal variance (see Figure 3.4). The station data clusters were confined within four zones by assuming their boundaries could be delineated by the water body's topography and geomorphology (see Figure 3.4). The first data cluster was contained within the Watch House Basin, with its outer boundary chosen to exclude the depositional levees. The second station cluster zone was re-named the Upper Middle Basin by including the previous Depositional Basin classification (see Figure 3.3). The third zone was re-named the Lower Middle Basin by setting its upper boundary to the immediate expansion of the water body's surface area. The fourth data pair was clearly confined to the Marine Flood/Tidal Delta's sandy sediments and braided channels north of Ram Island.

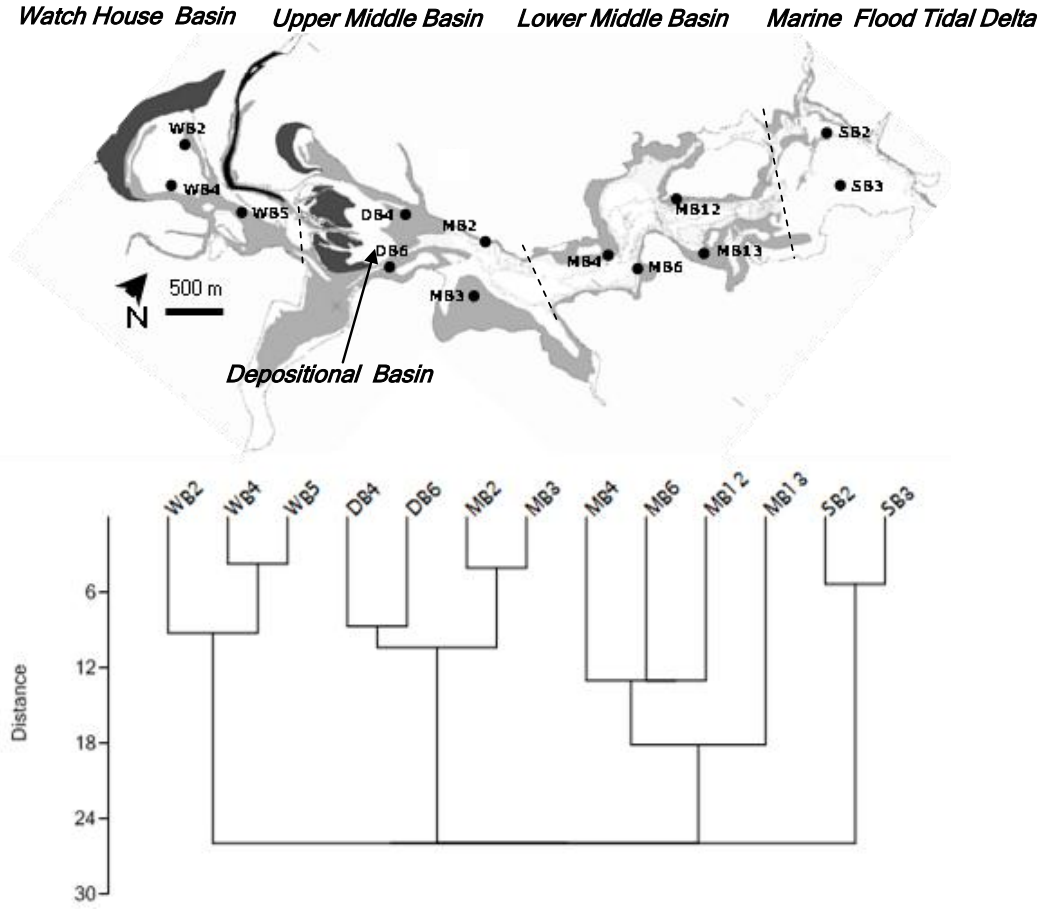

Figure 3.4. A constrained cluster analysis of all contiguous sediment and living analogue content and quality variables across the estuarine transect.
The cluster analysis used paired linkage Euclidean distance (PAST™); similarities were constrained within 95 per cent ellipses. The dotted lines (– – –) represent the tentative re-evaluation of spatial boundaries from the proximity of the four clustered stations.

3.4.2. Discussion: Descriptive postulates

3.4.2.1. A description of sub-aquatic vegetation and epibionts (postulates 1 to 3)

As in 2007, the sub-aquatic vegetation species distribution was in agreement with previous surveys conducted between 2004/2005 (Mount *et al.,* 2005). The shallow Watch House Basin supported a monoculture of the sub-aquatic macrophyte *Ruppia megacarpa*, the Middle Basin's littoral zones were dominated by *Zostera tasmanica* and the Marine Flood/Tidal Delta inter-tidal zone supported luxurious beds of *Zostera muelleri* bordering its braided channels.
The impression, during sampling, was that the Lower Middle Basin's seagrass coverage was patchier than that of the Upper Middle Basin. The impression was, in part, supported by randomly selected quadrant samples (0.25 m²) taken during the previous 2006 winter. The quadrants were placed immediately north of stations MB6 and MB4 and within 100 m of stations MB12 and MB13 (see Figure 3.4). The Upper Middle Basin seagrass density had a mean of 125 g dry wt m-^{2} and standard error 103 g dry wt m^{-2} (n=3) in comparison to a mean of 829 g dry wt m^{-2}, standard error 204 g dry wt m^{-2} (n=4) for the Lower Middle Basin.

The typology of the sub-aquatic macrophyte epibionts was divided between Watch House Basin, the Middle Basin and the Marine Flood/Tidal Delta (see Figure 3.5). Watch House Basin's coverage was associated with an ephemeral, heavy coating of clear mucilage over a low-density crust of white amorphous calcareous material. The mucilage was composed entirely of pennate diatoms (see Figure 3.5e). Within the main sections of the water body (Upper Middle Basin and Lower Middle Basin), coverage was dominated by variable densities of calcareous sessile epifauna, mainly serpulid worms and bryozoans (see Figures 3.6a, b and c). This contrasts with the thick covering of filamentous red algae with fine pieces of white calcareous hash (see Figure 3.5d) on seagrasses within the Marine Flood/Tidal Delta.

The origin of the calcareous hash on the Marine Flood/Tidal Delta seagrass leaves was not clear, but might have been re-suspended calcareous debris such as broken shells and urchin spines, as reflected by the high sediment LOI 950 °C (see Figure 3.3).

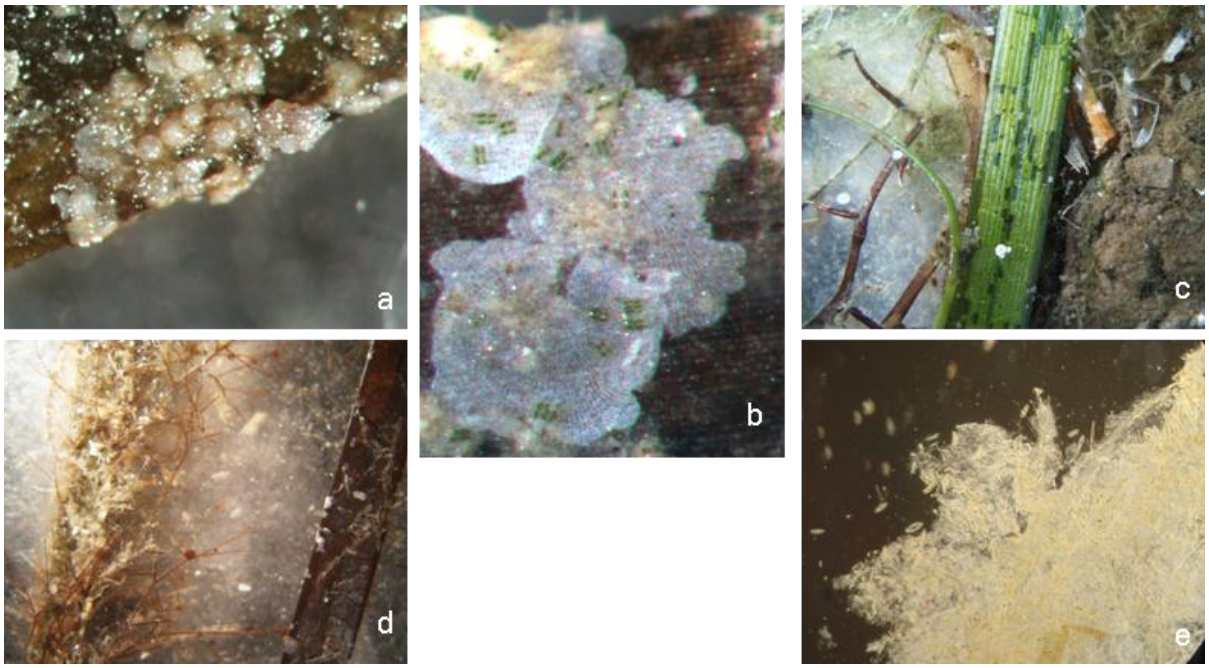

Figure 3.5. Examples of epibiont communities on seagrass leaves across the estuarine transect.
(a) Calcareous bryozoans at station DB4, (b) calcareous bryozoans at station SB2, (c) calcareous serpulid worms at station MB6, (d) trapped fine calcareous hash within a mass of filamentous red algae at station SB4, and (e) diatoms within a mucilaginous matrix at station WB4.

3.4.2.2. A description of sediment components (postulates 4 and 5)

Along the estuary's transect, sediment grain size peaked in content around phi 2.7 (<315 μm to >76 μm) and, with the exception of the Marine Flood/Tidal Delta sediments, the fine fraction content (phi 5.0, or <76 μm) represented the largest proportion by dry weight (see Figure 3.6). The character of the sediments around phi 2.7 within the Marine Flood/Tidal Delta was different, being composed mainly of shell hash in contrast to the organic aggregates found in the remaining zones. Preservation of the calcareous seagrass leaf epibiont community was not obvious, other than occasional remnants of bryozoans still attached to broken seagrass pieces (<315 μm). Nonetheless, outside the Marine Flood/Tidal Delta, both the origin of sedimentary $CaCO_3$, from seagrass epibiont production, and the lack of calcareous epibiont integrity was consistent with measurements and observations from sub-tropical to temperate systems around the world (Perry and Beavington-Penney, 2005; James *et al*., 2009).

Identical organic aggregates originating from the littoral zones, outside the Marine Flood/Tidal Delta, were also observed within sediment cores that were extracted from the heterotrophic central basin (see Figure 3.6). The organic aggregates were similar in size and shape to calanoid copepod faecal pellets (length:diameter ratio between 3:1 and 5:1; Hiromi *et al.*, 1988) and glistened as though packaged by a faecal pellet peritrophic membrane (see Figure 3).

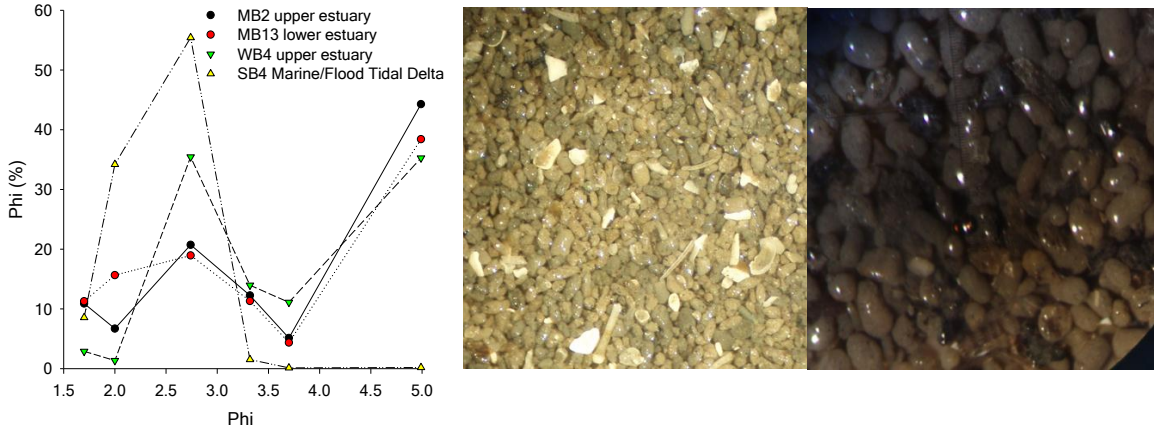

Figure 3.6. Sediment size fractions (<315 μm) across the estuarine transect and photographs of faecal pellets extracted from sediment cores.
The fractions were separated by gently sieving the sample through a sieve stack expressed as phi. The faecal pellet aggregates were separated on a 150 μm sieve taken from a muddy section of an upper estuary sediment core (right) and a lower estuary sediment core (left) at time of unrestricted tidal exchange entrance (see Chapter 4).

No zooplankton or fish remains were found within any of the sieved samples. Nevertheless, copepod egestion of the sestonic fine fraction by the Little Swanport estuary's smaller *Acartia tranteri* and larger *Paracalanus indicus* (Crawford *et al.*, 2005) might be used to determine a suite of proxies outside high-energy environments. For example, copepod egestion as their faecal pellet content, copepod predation by Little Swanport's Hardy head and Yellow-eyed mullet (Crawford et al., 2005) from their relative abundance (Kimmerer and McKinnon, 1985, 1987) as measured by faceal pellets sizes (Uye and Kaname, 1994) and the sestonic turbidity from the remaining fine fraction.

The sediment's microscopic glassy components were examined at all sites (three) of five stations that represented the zones across the transect (WB4, MB2 MB4, MB12, SB3). It was clear, after a peroxide digest (see Chapter 2) that the remains were composed of amorphous particulates and diatoms. Other siliceous forms (phytoliths and thecamoebians tests) were noted but were rare (see Figure 3.7). While soil contributions with diatomaceous BSi cannot be discounted, their contents were too low (1.52 %, standard error 0.32 %; see Figure 3.3) to explain the labile BSi variance across the transect (maximum >9 %; see Figure 3.3).

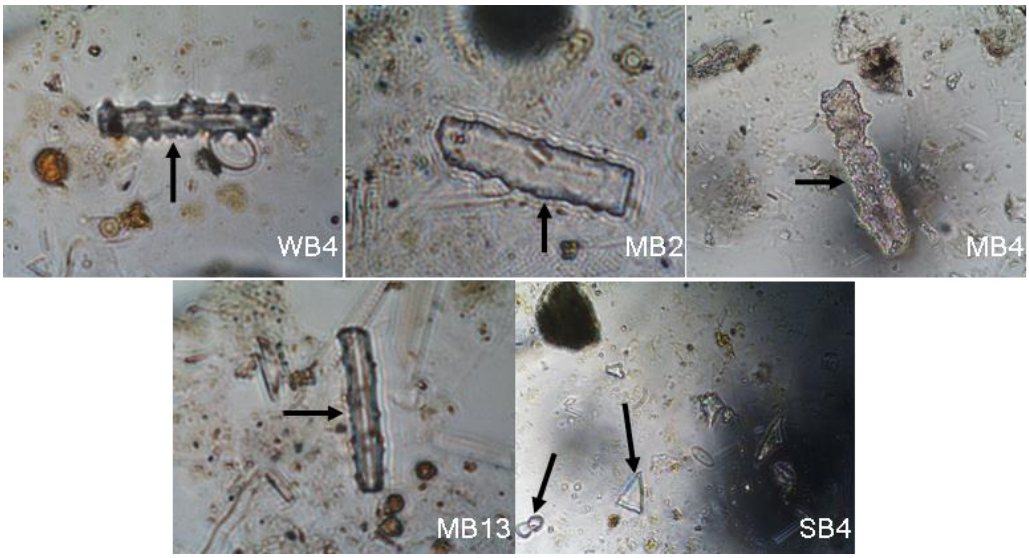

Figure 3.7. Examples (x1000) of phytoliths (WB4, MB2, MB4, MB13, SB4) and a thecameobian tests (SB4 triangular glassy form) found in surface sediments across the estuarine transect.

3.4.2.3. No interference of diatomaceous BSi (postulate 6)

The presence of refractory BSi in some of the surface sediments (see Figure 3.3) supported the contention that the choice of the alkali concentration was not sufficient to completely digest all refractory BSi forms. Nevertheless, the pronounced step-like digestion stages that delineated between labile and refractory forms were consistent with a clean digest that separated refractory from labile BSi, and without inference from a coating of iron-laden clays over the analyte (Michalopoulos and Aller, 2004). The rarity of other heavier, but potentially chemically labile catchment BSi forms (phytoliths, thecamoebians [see Figure 3.7]) and estuary BSi forms (*i.e.* no microscopic sponge spicules found) among the preserved diatom remains supports the latter contention.

3.4.3. Analytical postulates: Best least squares linear models

3.4.3.1. The relationship between organic matter variance and LOI 950 °C was consistent with the supply of diatoms for calcareous epibiont production (postulates 7 to 9)

There was a clear positive covariance outside the Marine Flood/Tidal Delta between all three biological content signals, LOI 950°C, LOI 550°C and labile BSi (see Figure 3.8a). The covariance was consistent with the prey–predator postulate 7; that diatoms represented the micro-algal population and supported calcareous epifaunal production (bryozoans). Interestingly, there was a stronger relationship between BSi and OM (LOI 550°C) across the Watch House Basin sites. The reasons are not clear, but probably reflect the conditions due to partial isolation of the basin from the Little Swanport River and main water body. For

example, it was noticed that the pH of the sedimentary pore waters from the Watch House Basin (6 to 6.5) was greater than for the rest of the estuary (7 to 7.5). This would enhance dissolution of BSi (Greenwood *et al.*, 2005).

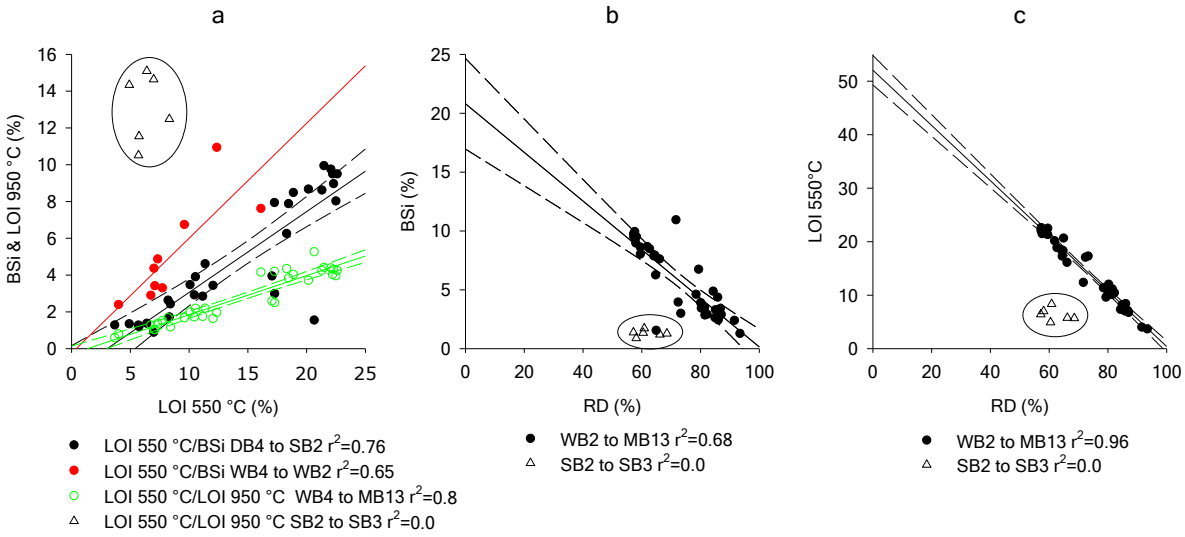

Figure 3.8. Best least squares models between the surface sediment (<315µm) major content variables across the estuarine transect.
(a) OM (as LOI 550 °C) and BSi; (b) BSi and RD; (c) OM (as LOI 550 °C) and RD. The RD regressions are extended to zero BSi content and LOI 550 °C for calculating the inferred diatomious molar BSi–POC ratio by excluding their proportions associated with the RD, as the remaining clay fraction. (see Footnote 9 for the conversion of LOI 550 °C to POC).

The support for labile BSi as a diatom proxy was tested by the autochthonous BSi–POC molar stoichiometry[10] by normalising the OM content and BSi content associated clays to zero (*i.e.* their intercepts; see Figures 3.9b,c). While the ratio (0.28) did not equal the 'Redfield' mean (0.12), it was well within the diatom's community range and resembled the ratios of heavily silicified benthic diatoms (Brzezinski, 1985; Chen and Windom, 1997; Sigmon and Cahoon, 1997). The different calcareous materials within the Marine Flood/Tidal Delta (*i.e.* shell hash and low OM marine sands) resulted in outliers and limited the above conclusion to the remaining transect zones. Nevertheless, the total BSi–POC ratio molar stoichiometry (0.22 to 0.18) within the Marine Flood/Tidal Delta was also typical of benthic diatoms assuming that this is ostensibly a marine environment with little contribution from the catchment.

[10] The percentage of carbon was calculated from LOI 550 °C from a least squares linear regression between the average of LOI 550 °C measured from three sites per station and POC from pooled samples from three sites per station. Pooled POC (%) = 0.147 + (0.281 * mean LOI 550 °C (%); (r = 0.91).

3.4.3.2. The proportion of organic sources was a function of carbon and/or nitrogen isotopes and their elemental ratios (postulate 10)

The position of the surface sediment's organic carbon and nitrogen stable isotopes and their elemental ratios is shown in relation to a range of plausible OM sources (see Figure 3.9); that is, OM sources identified from the descriptive postulates, SPM (micro-algae), epiphytes, soils and seagrass shoots. It was assumed that SPM represented micro-algae because samples were taken during the summer bloom period in dead calm conditions (see Chapter 2). The assumption is, in part, supported by the POC–PON ratios (7.5 to 9.0; see Figure 3.3c), which fall within the range for estuarine and coastal micro-algae (Cloern *et al*., 2002).

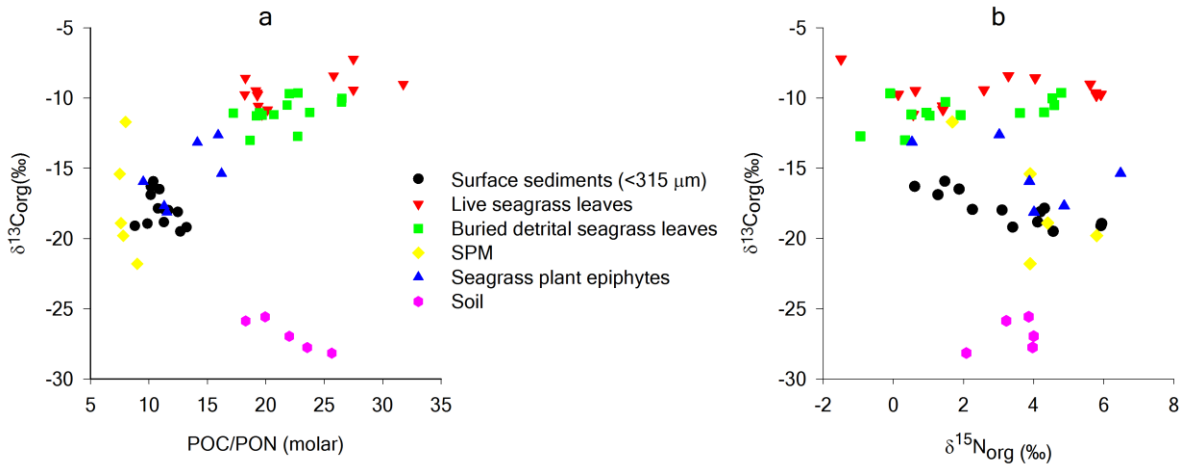

Figure 3.9. Particulate organic elemental and stable isotopes ratios ($\delta^{13}C_{org}$, $\delta^{15}N_{org}$, POC–PON) for detrital and live components across the estuarine transect, coastal waters and the immediate surrounding soils.

In comparison to the estuarine components, the soil's $\delta^{15}N_{org}$ signatures were relatively invariant and could not explain the $\delta^{15}N_{org}$ range found within surface sediments (see Figure 3.9b). Overall, SPM and epiphytes could explain most of the variability in sediment $\delta^{15}N_{org}$, but not its source. The model was incapable of untangling the contributions of organic sources of the sediment mixture, primarily because of the apparent $\delta^{15}N_{org}$ covariance of estuarine components.

In contrast, there appeared to be sufficient separation and little overlap between the $\delta^{13}C_{org}$ and POC–PON signatures of organic sources (see Figure 3.9a). However, the instability of both POC–PON and $\delta^{13}C_{org}$, particularly for estuarine components, suggests significant variability in their determinants; namely, the source and availability of inorganic carbon and light and inorganic nitrogen availability. This in turn limits the accuracy of the model. Furthermore, it was not clear which organic sources were the major contributors because the sediment signature was close to the junction between the two plausible binary mixing models (micro-algae and seagrass, detrital or live; or micro-algae and soil (see Figure 3.5a).

Nevertheless, irrespective of component signature instability, the most plausible choice lay with micro-algal and soil mixtures as: (1) seagrass and its epiphytes were ostensibly excluded from the sample on the >315 μm sieve, (2) the diatom BSi–POC stoichiometry was represented diatoms once normalised to a zero soil contribution (hypothesis 10) and (3) there was a clear need, outside the Marine Flood/Tidal Delta, to remove the soil contribution of OM to calculate the plausible BSi–POC stoichiometry.

3.4.3.3. The organic carbon isotope ratio primary productivity assemblage was a function of its inorganic carbon source (postulate 11)

The previous postulate identified the instability of the organic carbon isotope ratio among the components. To select the appropriate plausible proxy for the palaeo-reconstruction it is important to understand which of the two reasons (inorganic carbon source or carbon fixation) was responsible. The $\delta^{13}C_{inorg}$ signature of the calcareous epifaunal community is generally in equilibrium with $\delta^{13}C_{DIC}$ (Nelson and Smith, 1996) at similar time scales as its host leaf. Consequently, the broadly similar variance between live seagrass leaves $\delta^{13}C_{org}$ and the epifaunal $\delta^{13}C_{inorg}$ signatures should be robust test of the $\delta^{13}C_{DIC}$ contribution to seagrass $\delta^{13}C_{org}$ variance (see Figure 3.3). However, the absolute change in the epifaunal $\delta^{13}C_{inorg}$ was significantly smaller (1.8 ‰ to -0.9 ‰) than for the seagrass $\delta^{13}C_{org}$ signature (-7.2 ‰ to -11.2 ‰), implying a minor but covariant role in controlling the $\delta^{13}C_{org}$ of the primary productivity assemblage.

3.4.3.4. The primary productivity organic nitrogen isotope ratio was a function of its inorganic nitrogen source (postulate 12)

If the nitrogen is not in excess to demand, then its stable isotope signal will reflect its organic signature (Fry *et al.*, 2000). Fourqurean and Zieman (2002) recognised the limiting nutrient could be determined if the seagrass leaves' PON–POP ratios were significantly greater than the Atkinson ratio (30; Atkinson and Smith, 1983), provided a statistical sample was taken across the seagrass landscape. In other words, Fourqurean and Zieman (2002) found that the variability of the chemical analysis precluded the use of a thicket of individual shoots. Indeed, the PON–POP ratios of live seagrass shoots across the transect did vary (see Figure 3.3), but the variability was not significantly different from the Atkinson ratio (mean of 32.1, standard error 2.4). Hence, it appeared that phosphorus and nitrogen were not in excess to demand and consequently that the seagrass $\delta^{15}N_{org}$ transition between the Lower Middle Basin and the upper estuary (see Figure 3.3) reflected a change in the inorganic nitrogen source.

The results indicated that the transition for both sediments (<315 μm) and seagrass (detrital and live) $\delta^{15}N_{org}$ between the upper estuary (mean of 0.85 ‰; standard error 0.55 ‰) and a Lower Middle Basin (mean of 4.96 ‰; standard error 0.55 ‰) was the result of seagrass-mediated nitrogen fixation (Welsh, 2000). That is, the $\delta^{15}N_{org}$ signal was close to 0 ‰ (atmospheric nitrogen) compared with other sources that were often heavier such as inorganic nitrogen soil extracts (mean of 2.1 ‰; standard error 0.19 ‰) and the $\delta^{15}N_{DIN}$ of coastal waters (3.9 ‰ to 5.9 ‰ respectively; see Figure 3.3) and probably sediment pore waters. The $\delta^{15}N_{DIN}$ was inferred by the values of seasonally integrated particulate $\delta^{15}N_{org}$ (Francois *et al.*, 1997) of the Marine Flood/Tidal Delta surface sediments, adjacent to coastal waters, and supported by SPM's seasonal value for coastal waters and Marine Flood/Tidal Delta (3.9 ‰). However, the inorganic $\delta^{15}N_{DIN}$ of sediment pore water analysis was not reliable[11]. Nevertheless, Papadimitriou *et al.* (2005) found considerable $^{15}N_{DIN}$ enrichment of sediment pore waters from OM within *Zostera marina* seagrass beds. Thus, by assuming that Lower Middle Basin's seagrass $\delta^{15}N_{org}$ was purely from marine sources it appeared that on average, nitrogen fixation provided 86.3 % of the nitrgen requirments for the upper estuaries seagrass meadow (WB2 to MB3)

The reasons behind the transition to nitrogen fixation are difficult to determine without previous knowledge of system states and changes in forcing factors. Samples were taken during an extended period of drought, with no discernible freshwater inflow, and thus no catchment loading. This explains the seagrass dependence on nitrogen fixation within the upper estuary. However, the drought does not appear to completely explain the step like transition of seagrass $\delta^{15}N_{org}$ from light to heavy between the upper and lower estuary. In other words, a transition requires a non-linear response within the estuary, the result of something that is not shared between the two regions. It is proposed that such a transition may be associated with the presence of shellfish aquaculture (located adjacent to and in parts of the Lower Middle Basin), which can lead to significant removal of nitrogen resources after harvesting and from increased burial and denitrification (Dumbauld *et al.*, 2009), thus limiting the coastal supply of nitrogen to the upper estuary.

[11] It was found that pore waters had much buffer capacity to maintain the pH to >9.0 in order to convert inorganic nitrogen to its ammonia salt at the end of 5 days of incubation (see section 2.7.17).

3.4.3.5. The organic carbon isotope ratio of the primary productivity assemblage was a function of carbon fixation by either light attenuation or nutrient limitation (postulates 13 and 14)

Postulates 13 and 14 (Section 3.2) lead on from the finding that changes in carbon fixation rather than dissolved inorganic carbon sources is controlling the $\delta^{13}C_{org}$ signature of the major primary producers. Consequently, changes in the $\delta^{13}C_{org}$ signature will reflect changes in carbon fixation as either driven by light or nitrogen limitation (*i.e.* functional state of the regime). For example, increased nitrogen loading can either stimulate seagrass coverage (Fourqurean and Zieman, 2002; see Chapter 7) or reduce coverage *via* micro-algal production and shading (Duarte, 1995; Duarte *et al.*, 2006). Depending on the limiting resource, the changes in carbon fixation ($\delta^{13}C_{org}$) can lead to changes in the POC–PON stoichiometry away from its optimum, such as the production of carbohydrate under nitrogen limiting conditions (Burkhardt *et al.*, 1999).

Questions of nitrogen and light limitation can be addressed within the palaeo-reconstruction by assessing the long-term relationship between carbon fixation and carbon and nitrogen stoichiometry. Nonetheless, the transect analysis is used to define the functional boundaries of the estuary for its palaeo-reconstruction, and test the generality of the response for matching temporal and spatial scales (see Chapter 1). In doing so, the analysis also determines the previous conditions that led to the present state.

Functional boundaries were determined by using best least squares linear regressions of sedimentary $\delta^{13}C_{org}$ and POC–PON (<315 μm) ratios as representing the variance of micro-algae (molar ratio 7 to 9), together with $\delta^{15}N_{org}$ signatures to test the dependence of light or nutrient limitation with changes in light-driven nitrogen fixation (hypotheses 11 and 12 [Section 3.2]). A first examination indicated that there were two different sets of functional boundaries between all three modelled relationships (see Figure 3.10). $\delta^{13}C_{org}$ to POC–PON ratios were separated by Marine Flood/Tidal Delta (SB2 and SB3) and the remaining relationships were separated by the Lower Middle Basin and the Marine Flood/Tidal Delta (MB4 to SB3). However, a re-examination of the $\delta^{13}C_{org}$ to $\delta^{15}N_{org}$ and $\delta^{15}N_{org}$ to POC–PON models (see Figures 3.11a and b) indicated that the $\delta^{15}N_{org}$ and $\delta^{13}C_{org}$ signals within the Marine Flood/Tidal Delta might be outliers. That is, station SB2's and SB3's signatures only appeared to be a part of the upper estuary's linear model by virtue of their relative position to the trend (see Figure 3.10a) and in the formation of a trend (see Figure 3.10b), but they did not have a functional connection to the rest of the estuary, as indicated by Figure 3.10c.

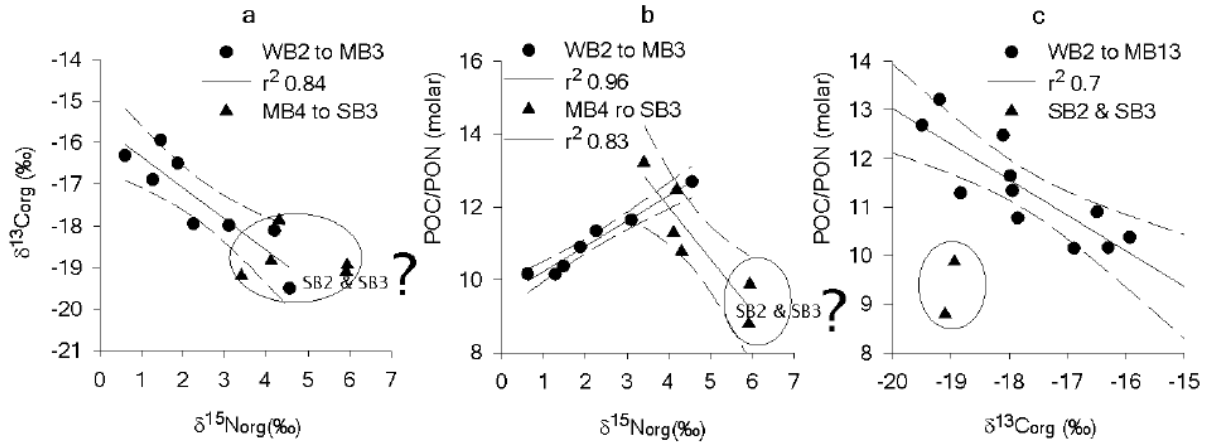

Figure 3.10. Best least squares models between surface sediment (<315 μm) organic nitrogen and carbon elemental and stable isotope ratios across the estuarine transect.
Each data point represents a weighted average of combined samples from the three station sampling sites within ≈10 m of each other (see Chapter 2).

The limitation of the analysis is best explained by the construction of a best linear model (see Figure 3.10b). The correlations increased as a consequence of both the number of data pairs and their adherence to proportional increases from the Watch House Basin (WB2) to the Upper Middle Basin (MB3; $r^2 = 0.96$). However, the strength of the correlation was partially reduced ($r^2 = 0.50$) by a subsequent inclusion of the Lower Middle Basin stations (MB4 to MB13) but significantly reduced when the Marine Flood/Tidal Delta were included ($r^2 = 0.0002$). The initial delineation between WB3 to MB3 and MB4 to SB3 can then be confirmed by the best linear model construction leading from the coastal boundary towards the upper estuary. However, a one-way ANCOVA between the two relatively strong models (WB2 to MB3 and WB2 to MB13) suggested a reasonable probability that their means ($p = 0.46$) and slope ($p = 0.35$) were the same, in spite of a fall in the correlative strength (type 1 error). Thus, the choice of which is the more significant correlation transition becomes a value judgment. Either, the transition was located immediately before the Lower Middle Basin stations (moderate fall in the correlation, but moderate similarity to the upper estuary) or it was located immediately before the Marine Flood/Tidal Delta stations (no correlation or similarity). The latter is supported by the best linear model of $\delta^{13}C_{org}$ and POC–PON (see Figure 3.10c). The $\delta^{13}C_{org}$ and POC–PON signatures were not only clearly separate from the lower estuary response curve; they were also typical of both coastal phytoplankton (*e.g.* Cloern *et al.*, 2007) and the adjacent coastal SPM (see Figure 3.3). It seems then, that the Marine Flood/Tidal Delta is part of the coastal boundary condition because the rate of coastal exchange of coastal waters was sufficient to 'dilute' the direct influence from the estuary.

Notwithstanding the delineation of the estuary boundary, the heavier $\delta^{13}C_{org}$ within surface sediments, including the SPM (see Figure 3.3) towards the upper estuary, was consistent with enhanced carbon fixation (Zimmerman and Canuel, 2002; Wu *et al.*, 2008) driven by nutrient supply. The heavier $\delta^{13}C_{org}$ was accompanied by an decrease in the POC–PON ratio (see Figure 3.10c) from a state of nitrogen depletion (see Figure 3.10b) towards the micro-algal Redfield ratio (molar ratio 6.6 [Redfield *et al.*, 1963]). Further, the increased productivity appeared to be coupled to an increased supply of fixed nitrogen (low $\delta^{15}N_{org}$ [see Figure 3.10a]).

The fall in seagrass carbon fixation towards the upper estuary (to a heavier seagrass leaf $\delta^{13}C_{org}$; see Figure 3.3) was accompanied by a fall in the seagrass POC–PON ratios towards the modal Duarte ratio ([24]; Duarte, 1990, 1992; see Figures 3.11a,b) and interestingly, inversely correlated micro-algal content with carbon fixation (towards a lighter $\delta^{13}C_{org}$ for SPM and sediments <315 μm [see Figure 3.3]). Such a pattern between seagrass carbon fixation and elemental ratios is consistent with the production of sugars for growth and reproduction other than just storage of sugars, expressed by the attempt to maintain elemental composition (homeostasis). In this case, evidence suggests homeostasis was maintained though an increasing dependence on nitrogen fixation because the POC–PON ratios were invariant with changes in $\delta^{15}N_{org}$ (Figures 3.11c,d). Further, it also appeared that nitrogen fixation by the seagrass' bacterial symbiont (Welsh, 2000) had leaked inorganic nitrogen into the micro-algal population (low $\delta^{15}N_{org}$ for SPM and sediments <315 μm [see Figure 3.3]).

Interestingly, such a state for a lush seagrass meadow is counter to the healthy evolution of an shallow estuary (see Section 1.1). Seagrass mediated nitrogen fixation is associated with oligotrophic systems that only support patchy seagrass meadows with low shoot densities. Consequently, the term juvenilisation is given here to describe the apparent re-oligotrophication of a seagrass meadow but in a mesotrophic context of the Little Swanport estuary (see Section 2.1).

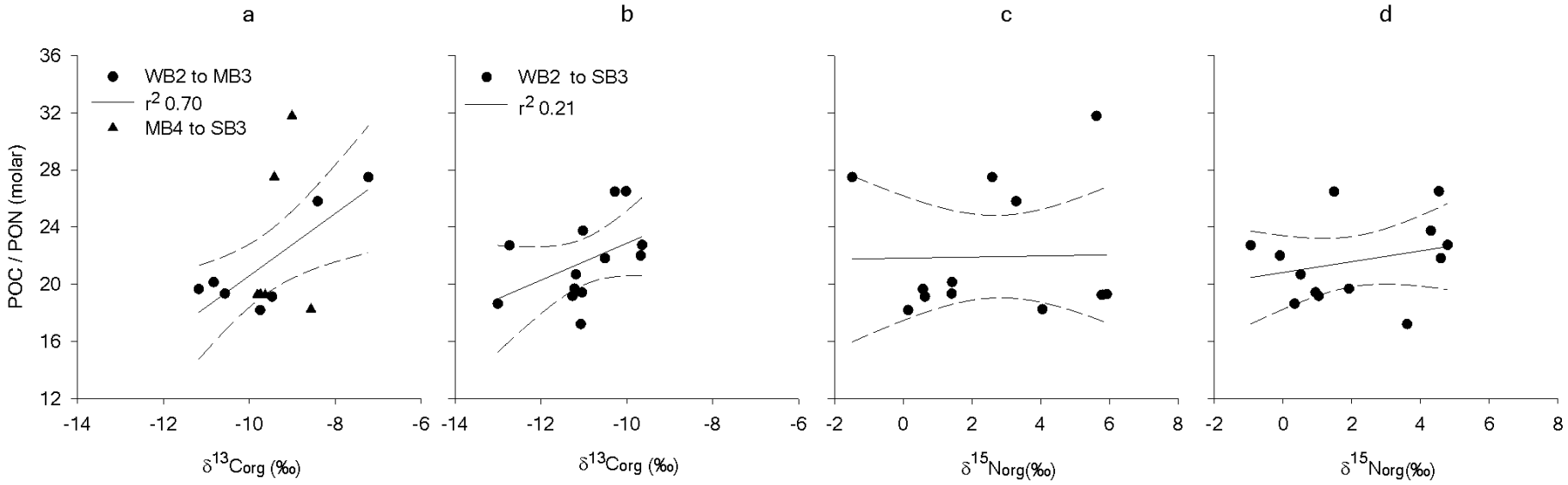

Figure 3.11. Best least squares models between organic carbon and nitrogen elemental and stable isotope ratios for living and detrital seagrass leaves across the estuarine transect

(a) and (c) Living seagrass leaves. (b) and (d) surface sediment detrital seagrass leaves. Each data point represents the analysis of an equally weighed combined sample of the three station sampling sites collected within ≈10 m of each other (see Chapter 2).

3.4.3.6. The proportions of sediment organic sources was a linear function of Rp index and POC–PON ratios (postulates 15 to 17)

In contrast to the $\delta^{13}C_{org}$ and POC–PON signatures, the stability of the Rp index and POC–PON ratios for soils, live seagrass leaves and micro-algae (SPM) was independent of changes in productivity and inorganic sources. There was good separation between the components, although there was a moderate degree of signature variability within each component, particularly for seagrass (see Figure 3.12). However, mineralised signatures from both micro-algae and particularly seagrass leaves were different to living components. Clearly then, in contrast to stable isotope analysis (*e.g.* Gonneea *et al.*, 2004; Turner *et al.*, 2006) any successful disentanglement of micro-algae and seagrass from a sediment mixture with soils require the use of mineralised OM signatures in place of their living components.

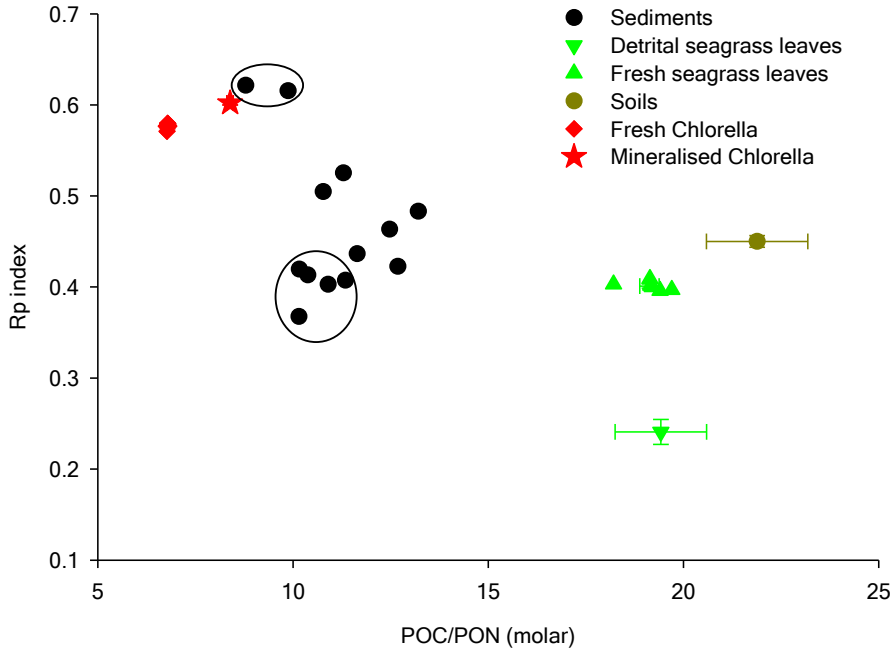

Figure 3.12. Cartesian coordinates for station's mean Rp index and POC–PON ratios for available detrital and live seagrass leaves across the transect, its immediate surrounding soils and fresh and mineralised micro-alga *Chlorella pyrenoidosa*.
The mean and standard error is calculated for all organic source end-points. Note that Rp index for sediment samples are represented by the mean of three sites per station and their POC–PON ratios from a sample pooled from the three station sites of which the standard errors were too small to register either side of the data points (*e.g.* see Figure 3.3). Due to an insufficient sample size, SPM as an organic source was replaced by micro-algae using *Chlorella pyrenoidosa* dietary supplement, both freshly freeze-dried and aerobically mineralised (see Chapter 2 for details of treatments).

Yet, some of the surface sediments (circled in Figure 3.12) lay outside a linear response to the mix of three organic sources from both their detrital or living analogues. The outliers with a low Rp index–POC:PON signature were primarily from sediments outside the Upper Middle

Basin (excluding stations MB2 and MB3), in contrast to the elevated Rp index outliers (up to 0.64) from the Marine Flood/Tidal Delta. Clearly, the position of the Marine Flood/Tidal Delta outliers suggests that other factors, other than a non-conservative mixing of OM, may be responsible. For example, high Rp indexes have only been recorded for pure alkali-extracted humic acids ([0.64] Kristensen, 1990), but the much higher POC–PON molar ratio ([19.6] Kristensen, 1990) excludes this as a possibility. Alternatively, an more efficient combustion due to the presence of $CaCO_3$ (see Section 3.1.2.3) of a large quantity of shell hash within the Marine Flood/Tidal Delta sediments and/or the proteaceous nacre with the shell matrix offers a plausible reason for the elevated Rp index, but not the low Rp index–POC:PON sediments of the upper estuary. It is more likely, the latter reflects a yet unidentified reason for a non-linear response of their signals to a mixture of OM sources (*e.g.* Kristensen, 1990, 1994).

To test the above hypotheses, acid was added to remove calcium carbonate effects from a sediment working standard (Rp index around 0.59). However, the result was inconclusive. The Rp index fell after the addition of acid, but the fall appeared not to be the result of removal of significant quantities of $CaCO_3$ salts, as there was no measurable fall in the LOI 950 °C after acidification. Instead, the fall in the Rp index resulted from an increased loss of material that was centred within the PI temperature range (130 °C to 280 °C), that is, the acid appeared to improve the low temperature combustion behaviour of an organic sediment component. The dilution from clays did not affect the combustion characteristics or the LOI 950 °C. However, clays such as montmorillonite, kaolinite and allophane can continue to dehydrate at temperatures higher than 550 °C (Jackson, 1975), thus the addition of acid may have been the cause of change, possibly in the electrochemical association of structural water with the clay's matrix. It was also unlikely that the fall in Rp index after acidification was due to the exposure of shell nacre as a mix of glycoproteins and celluloses. Shell nacre-like compounds burn at the lower temperature range (PI) to produce chars that burn at higher temperatures PII (280 °C to 520 °C). Thus, a more complete burn at low temperatures would result in an increased loss within the PI range and a fall in loss within the PII range.

Standard additions of bivalve shell debris and their Analar $CaCO_3$ salt to the sediment working standard led to an elevated Rp index (see Figure 3.13a) consistent with the lower temperature catalytic effect of the $CaCO_3$ on combustion, but not with the addition of other organic components (see Figure 3.13b). For both the shell and the $CaCO_3$ salt, the Rp index

increased (see Figure 3.13a) with a fall in their PI/PII ratios from 0.70±0.02 (n = 6) to 0.6±0.04 (n = 13) due to a more complete combustion at the PI.

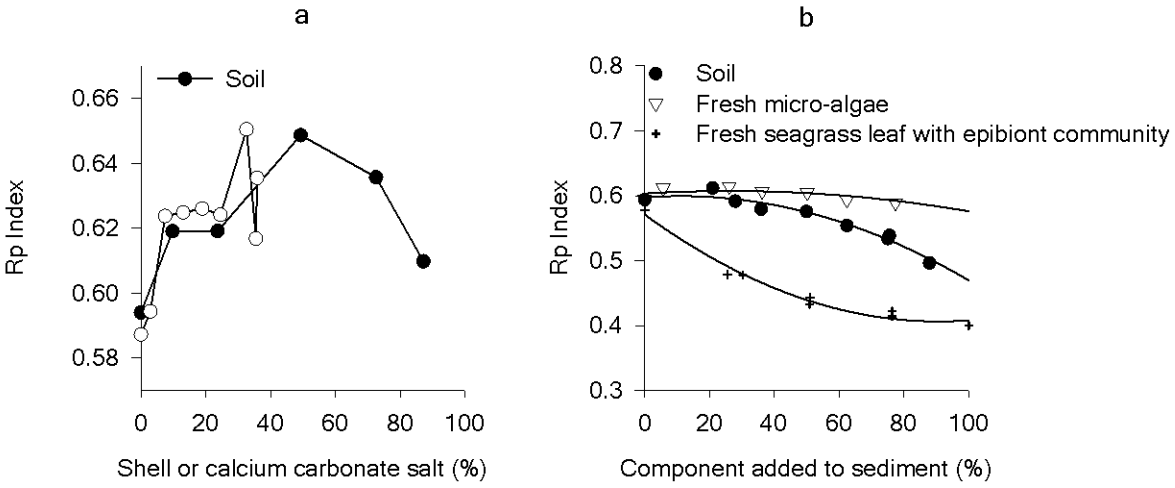

Figure 3.13. Standard additions effect on the sediments Rp index.
(a) Standard additions of pulverised fossil bivalve shell and calcium carbonate salts (Analar) to the working sediment standard (b) standard additions of OM sources to the working sediment standard.

It appears, that the usefulness of the Rp index as one variable for an organic mixing depends on the sensitivity of its response less than the asymptotic response from larger additions of CaCO3 (see Figure 3.13a), and possibly the loss of structural water from certain clays (Smith, 1975). contingent on normalising the results of non-linear mixing (see Figure 3.13b). In other words, the response before the asymptote is either a non-linear function or a step like threshold from a relatively low carbonate content (see Figure 3.13a). The type of response (i.e. Rp index to CaCO3 and clay dependence (RD)) was tested along the surface sediment transect using best fit multiple linear regression between the content components. It was found that only BSi content and LOI 950 °C were needed to produce a fair prediction of the Rp index (see Figure 3.14c; adjusted r^2 = 0.74) across the whole transect (see Figures 3.14b,c), albeit with variable degrees of fit across the transect. The model underestimated the data from the Lower Middle Basin stations (MB12 to MB13) and from the Watch House Basin (WB2 to WB5) to the Upper Middle Basin station (DB4). The underestimate may reflect the relatively larger contribution of RD as lithogenic clays within these station sediments (see Figure 3.3).

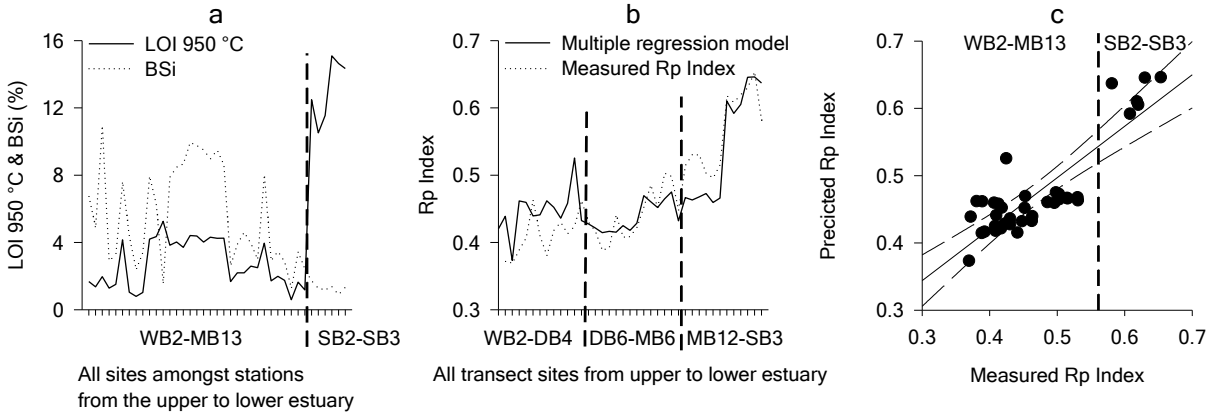

Figure 3.14. LOI 950 °C and BSi content for sampling sites across the transect for an Rp index multi-linear regression.
The vertical dashed lines (a and c) delineates the data boundary between the Marine Flood/Tidal Delta and the estuarine water body. The best fit of the model to the data is between DB6 and MB6 (see b; vertical dashed lines).

The only strong correlation was found between the remaining Upper Middle Basin stations (DB2 to MB6), where there was also a very high correlation between the Rp index and POC–PON ratios (r^2=0.86). The Rp index values of these stations were consistent with a simple mixing model of the major organic components (see Table 3.2) and had significant but relatively invariant LOI 950 °C and relatively low RD contents (see Figure 3.3). Thus, it appears that any application of an Rp index/POC–PON mixing model to calculate the components of organic mixtures should be restricted to sediments within this part of the Upper Middle Basin, after normalisation for the non-linear responses of the Rp index to component mixtures. Alternatively, an elevated Rp index might be used as a universal proxy for an extension of high-energy environments or events. Such environments and events include those that produce various combinations of fine shell hash, clays or possibly humic-acids, brought in by floods and precipitated at the seawater–freshwater interface (Sholkovitz and Copland, 1981).

Table 3.2. Loss on ignition and the Rp index and its temperature ratio for estuarine sediments and its postulated major components.
The statistics refer to standard deviation, with the number of replicates in brackets; <LD refers to less than the limit of detection for the method as three times the standard error of the blank.

Sample	Rp index	PI/PII	LOI 520 °C (%)	LOI 950 °C (%)
Sediment	0.59±0.01(6)	0.70±0.02(6)	17.51±0.08(6)	4.64 ±0.13(6)
Sediment+HCl	0.47±0.01(5)	1.13±0.04(5)	20.82±0.14(5)	4.89±0.12(5)
Sediment+50 % clay	0.58±0.01(5)	0.72±0.04(5)	8.60±0.44(5)	2.25±0.06(5)
North shore soil	0.46±0.01(4)	1.20±0.05(4)	8.32±0.03(4)	0.29±0.16(3,<LD)
Zostera spp. leaves	0.40±0.00(4)	1.5±0.02(4)	51.18±0.08(4)	10.7±1.20 (4)
Fresh *Chlorella*	0.57±0.00(3)	0.75±0.00(3)	93.6±0.07(3)	not determined
Mineralised *Chlorella*	0.60±0.00(3)	0.67±0.00(3)	84.3±0.08(3)	not determined
Fossil *Spisula* Shell	0.20(1)	4.08(1)	1.66(1)	42.85(1)

3.4.3.7. High-energy environments and changes in net productivity can be determined from content variance by Glyph Analysis (postulate 18)

A Glyph Analysis, based on the covariance of the major contents of BSi, LOI 550 °C, LOI 950 °C and RD (see Figure 3.8), was assessed by comparing changes in carbon fixation ($\delta^{13}C_{org}$, postulate 13) in relation to the best least squares linear models for surface sediment OM content (POC, as micro-algal variance, postulates 7 and 8). In this way, inferred changes in rates of OM supply from the Glyph neutral model[12] could be supported as self-consistent with: (1) the change in OM content with respect to net basin production, (2) expected basin losses from water advection and (3) its position with respect to lithogenic matter supply. For example, within isolated embayments, autochthonous micro-algal OM can be expected to dominate sediment control without significant contribution from fluvial or sandy sediments or loss from advection and so on.

Both the Glyph Analysis (see Figure 3.15) and the best linear models (see Figure 3.11) revealed marked changes between the Watch House Basin (WB2 to WB5), the Depositional Basin to Upper Middle Basin (DB4 to MB3), the Lower Middle Basin (MB4 to MB13) and the Marine Flood/Tidal Delta (SB2 & SB3). The matching Glyph neutral model (yellow) suggests that variance in the sedimentary OM content in the Watch House Basin was controlled by the supply of micro-algal OM. The relative invariant change in fluvial supply

[12] Caswell (1976) introduced the neutral model concept for landscape ecology as a determined null hypothesis on which to test differences in patterns to determine whether the studied process had an affect on the landscape.

was consistent with the isolation of the Watch House Basin from the Little Swanport estuary. Further, the fall in organic carbon content towards the Depositional Basin with an increase in micro-algal carbon fixation (towards a heavier $\delta^{13}C_{org}$) serves to highlight a plausible increase in advective loss to the Depositional Basin and an increased supply of nitrogen from coastal resources during the extended drought (see Chapter 4).

In contrast, the Glyph pattern model (green; see Figure 3.15) suggests that the increase in OM content from the Deposition Basin to the Upper Middle Basin was controlled by the falling supply of lithogenic material away from the influence of the fluvial levees (the Duck Islands [see Figure 2.1]). However, in spite of a relatively invariant change in net OM supply to the sediments, there was an increase in the rate of carbon fixation (heavier $\delta^{13}C_{org}$ [see Figure 3.15]). Such a productivity scenario is plausible when considering that there must be a significant net advective loss of micro-algal supply to the lower estuary, but an increase in individual micro-algal productivity towards the lower estuary due to an increasing availability of coastal nitrogen resources as the dominant supply (see Chapter 5).

The matching Glyph neutral model for the Lower Middle Basin was the same as found for the Watch House Basin (see Figure 3.15). The organic content was controlled by its rate of supply towards the Marine Flood/Tidal Delta with increases in individual productivity due to the supply of coastal nitrogen resources. Hence, this region appears to mark the end of the significant influence from the Little Swanport River.

In contrast, the content variance patterns within the sandier Marine/Flood Tidal Delta did not match any of the neutral models, suggesting that the functional limits of the estuary had been reached. In some ways, this contention was a trivial result. It was clear, from the presence of sediment shell hash and the elevated LOI 950 °C that this was a high-energy environment. Nevertheless, the transition away from possible neutral models has the potential to mark regime changes that do not rely on the covariance of calcareous epibionts and micro-algae.

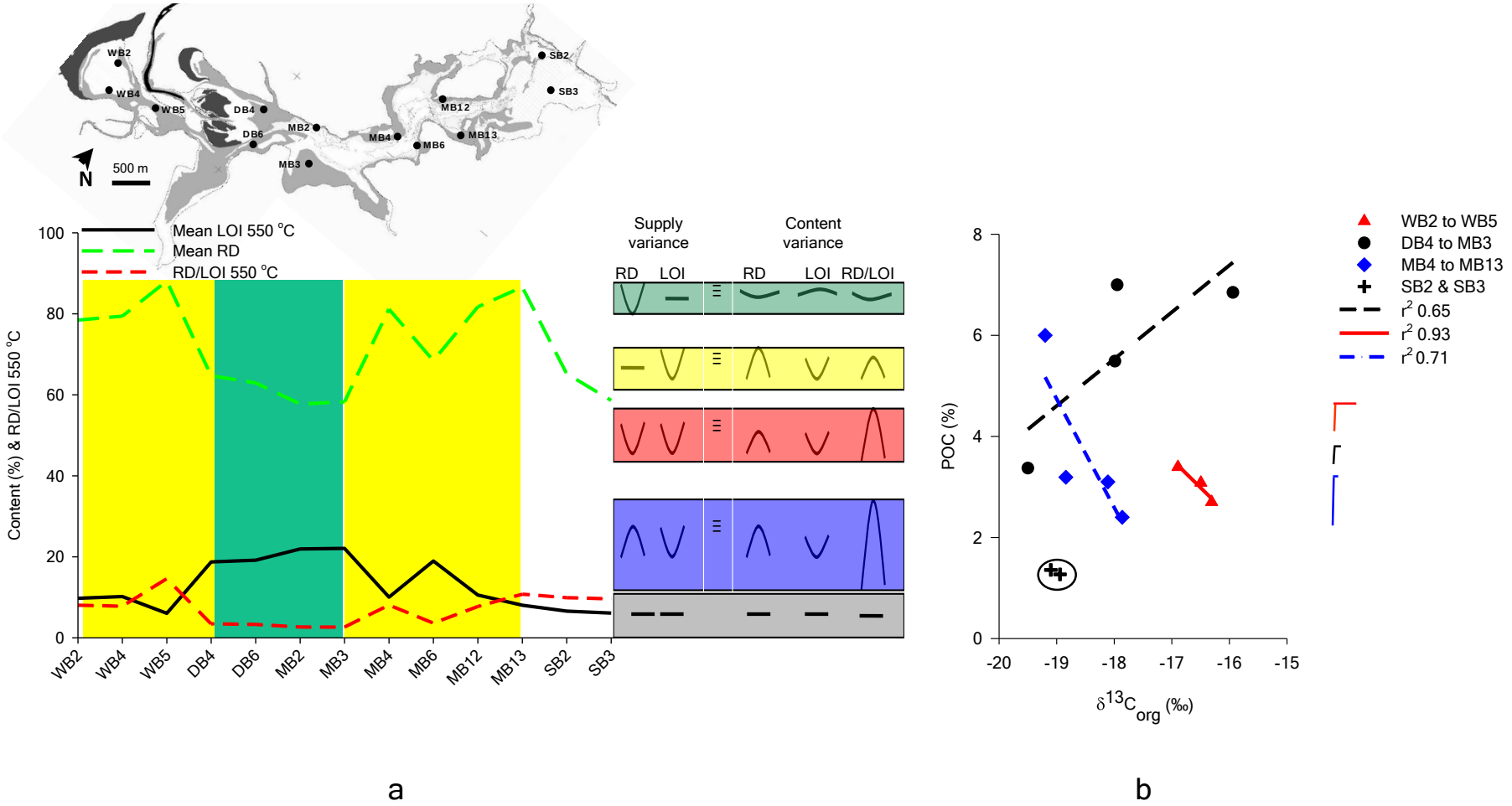

Figure 3.15. A Glyph Analysis of surface sediment (<315 µm) across the estuarine transect..
(a) The content patterns across transect were matched to the Glyph neutral model key as represented by its clour (to the right) in order to determine the relative supply of lithogenic RD and OM (LOI 550 °C). (b) Best least squares linear models running from the upper to lower estuary using the criteria of a maximum correlation coefficient to mark the regression boundaries. The models data points represent a combined equally weighted sample of three sites from each station (<10 m). The error bars (┌ ┌ ┌) are examples of the sum of analytical and site standard error (n=3), taken during the following winter (WB4, MB2, MB13).

3.5. Conclusions

The study indicated that a palaeo-reconstruction of ecosystem variability needs to be inclusive of the two distinct estuarine zones along an ecosystem gradient—Upper Middle Basin and Lower Middle Basin—that comprise the main body of the Little Swanport estuary. The Upper Middle Basin is inclusive of the region occupied by the alluvial depositional levees but exclusive of the relatively independent Watch House Basin. Hence, it is expected within the upper zone, close to the alluvial levees, that the direct affects of floods are more likely to affect its ecosystem regime state along with pressed changes in catchment nitrogen supply. While, the direct affects of floods and catchment supply on the upper zone can not be discounted, the proximity to the coastal boundary—Marine Flood/Tidal Delta—suggests that the direct affects of marine incursions and pressed changes in the coastal nitrate supply may be more important within the region.

Flood and marine incursions, then, have the potential to disrupt regime state continuity across the relatively long axis of the Little Swanport estuary. Whereas, the affects of pressed changes in the nitrogen supply from the two independent river and coastal boundary conditions (see Chapter 5) are restricted to effecting changes to the ecosystem gradient, which may potentially mitigate or enhance the differences between the upper and lower estuarine zones.

The nature of the estuary's spatial inorganic and organic sediment signals was also determined, as part of a multi-proxy and scientific justification and approach (*i.e.* RA, IBE, SC) for both spatial and temporal convergence (see Section 1.1.1) across the estuarine transect, and at an appropriate level of ecosystem abstraction for biome components and processes that was based on the strength on their sedimentary and biome signals. Namely, micro-algae, seagrass, calcareous epifauna, sestonic turbidity, copepod egestion, planktivore predation, carbon fixation (both nitrogen and light limited) and nitrogen fixation, together with high energy event (*c.f.* the Marine Flood/Tidal Delta sediments) and relative lithogenic supply markers:

- Labile BSi within surface sediments (<315 μm) was consistent with micro-algal organic carbon variance in spite of the presence of labile BSi from a minor soil component.
- Detrital seagrass leaves >315 μm represented a plausible proxy for the surrounding live meadow. However, it should be noted that to compare relative rates of carbon production with micro-algae the dry weight needs to be normalised for any variation in carbon content.

- Organic stable isotopes within detrital seagrass leaves was found to be a plausible proxy for carbon fixation and the sources of inorganic nitrogen (as either nitrogen fixation or external supply), in spite of apparent variability in salinity over the life time of the seagrass shoot.
- A linear organic component $\delta^{13}C_{org}$—PON/POC mixing model may be used to calculate the organic carbon contributions within sediments of seagrass, micro-algae and soils, provided the variations in seagrass and micro-algae signatures for that sediment horizon can be determined. For instance by separating detrital seagrass leaves >315 μm and using the remaining sediments or its fine fraction to calculate micro-algal POC–PON ratios (*e.g.* Wu *et al.*, 2008) and their $\delta^{13}C_{org}$ by constructing a Keeling plot[13] to separate the minor organic contribution from the catchment soils (*e.g.* Fry, 2006).
- The sedimentary organic source mixing model that uses Rp index and its POC–PON ratios, however was found to be limited to sediments restricted to central section of the Upper Middle Basin (*i.e.* free of the influence of high a $CaCO_3$ component and fluvial clays) after the response has been transformed to a linear function.
- The presence estuarine faecal pellets as proxy for copepod egestion of the sestonic fine fraction has the potential to be used for an addition suit of proxies. For example, sestonic turbidity from the remaining fine fraction and rates planktivorous fish predation, provided the smaller *Acartia tranteri* and larger *Paracalanus indicus* copepods remained the dominant species or predation size selection of other species continued to apply over time.
- An elevated Rp index was consistent with high shell carbonate and or fluvial clays, and thus, has the potential to be a universal depositional flood and marine incursion event marker.
- Glyph Analysis, however, as a means to discern changes between rates autochthonous and allochthonous supply to the sediments without previous knowledge of sedimentation accretion rates was not considered sufficiently robust to falsify hypotheses generated from other methods. Nevertheless, it was effective in providing another line of supporting evidence.

---

[13] A Keeling plot of $\delta^{13}C_{org}$ *vs* 1/C % is a special case of a two-component mixing model in which the contribution to the mixture $\delta^{13}C_{org}$ from the minor organic fraction is removed by extrapolating $\delta^{13}C_{org}$ to infinite addition of the major component content (micro-algae); that is, the intercept on the $\delta^{13}C_{org}$ y-axis when 1/C = 0.

Consequently, by using the above plausible suite of proxies, it is proposed that a palaeo-reconstruction of the two estuarine zones can be used to: (1) help identify depositional events down the sediment column as part of an evaluation through convergence with its ^{210}Pb geochronology; (2) describe a plausible range of pressed natural and anthropogenic intra-regime and inter-regime states (*i.e.* light limited nitrogen fixation and light limited carbon fixation for the upper and lower estuary respectively), possibly interrupted by high energy events; (3) determine if stabilising the stability of a regime state can be based on the balance between top down (*i.e.* planktivorous fish trophic cascade on calcareous epifaunal production); and bottom up control (nitrogen supply).

Finally, the transect variance indicated a possible role for historical contingency (see Section 1.1) as responsible for the current estuarine zone regime states due to either one particular event, that is, the timing of the postulated moderating effects on coastal nitrogen resources by the shell fish aquaculture, the start of current drought, or a narrative of unfolding events and/or pressed nitrogen supply variability. Consequently it is proposed that any ecosystem palaeo-reconstruction of regime change requires a matching reconstruction of the above events and variability. For the Little Swanport estuary this was achieved from rainfall/catchment models, an imputated time-series analysis of the long-term coastal nitrate data set and contemporary inorganic nitrogen river flow response curves (see Chapter 5).

Chapter 4. Sediment column geochronologies for the upper and lower Little Swanport estuary

4.1. Introduction

A sediment core paleoecological study that seeks to support adaptive management process requires an accurate and precise chronology of sediment deposition (Wolfe *et al.*, 1987; Groffman *et al.*, 2006). In this way: (1) an accurate mapping of reconstructed linear and non-linear trends can be used to statistically project robust medium to long-term changes to the ecosystem (Kondrashov *et al.*, 2005; Golyandina *et al.*, 2007), (2) an accurate and precise chronology can be used for testing recorded external forcing factors to their sedimentary proxies (von Gunten *et al.*, 2009), and (3) an accurate chronology is needed to disentangle delayed biome affects from external forcing factors or complex internally generated biome dynamics driven by external forcing factors (*e.g.* Sugihara *et al.*, 2012; see Chapter 7).

A variety of contiguous geochronological methods are available that can be applied to sediments deposited during the late Anthropocene (*i.e.* the last 100 to 150 years). The applicability of many of these methods, however, will depend on the existence of historical data that is not always available. Consequently, methods such as catchment quantitative process models (Paulsen *et al.*, 1999) or pollen stratigraphy (Brush, 1989) that rely on the history of the catchment, while potentially robust, cannot be applied to all water bodies.

In response, chronological methods that are ostensibly independent of site specific historical knowledge have been developed. These methods main requirement is a known rate of decay of a ubiquitous sedimentary particulate, for example, the deposition and decay of micro-algae (Chen and Windom, 1997) and natural radioactive isotopes such as ^{210}Pb. Yet, biomarker decay will vary for different estuaries and different estuarine sampling sites, as functions of salinity, temperature and redox conditions (Burdige, 2006). Consequently, the focus of late Anthropocene geochronologies has been on the supply and decay of unsupported ^{210}Pb (Robbins, 1978; Appleby, 2001).

Unsupported ^{210}Pb is formed from the disequilibrium between its parent isotope ^{226}Ra and total ^{210}Pb activity, through the diffusion of the gaseous intermediate daughter isotope ^{222}Rn from the catchment into the atmosphere and subsequently washed out onto the catchment and its receiving water body. At its simplest application, the sedimentation velocity is calculated by the radioactive decay curve of particulate unsupported ^{210}Pb with depth, contingent on

ideal conditions of deposition and supply. Namely, a constant supply of ^{210}Pb to the sediment–water interface, no differential sediment compaction, a constant rate of sedimentation and no internal remobilisation or redistribution of ^{210}Pb particulates. The rate of supply of unsupported ^{210}Pb to water bodies, however, varies around the globe, at the scale of its radioactive decay (22.3 years), with dry and wet precipitation (Krishnaswami *et al.*, 1971; Turekian *et al.*, 1977; Appleby, 2008) and the Little Swanport ctachment is no exception (Nunez and McGregor, 2007). Changes in rainfall can lead to both changes to the supply of unsupported ^{210}Pb from direct aerial precipitation and from the catchment to sediments adjacent to the river exit (Appleby, 2001) for example, the alluvial levees of shallow wave and tide dominated estuaries (Roy *et al.*, 2001).

In addition to unsupported ^{210}Pb supply variance, dynamic shallow marine systems similar to the Little Swanport estuary can add another set of changeable parameters to the simple ^{210}Pb radioactive decay model by:

- Changes to the rates of sedimentation due to changes in sediment focusing, driven by inter-decadal variability of westerly winds, as recorded across Tasmania (Harris *et al.*, 1987, 1988; Pooke, 1992).
- Changes to the rate of sedimentation due to changes in particulate catchment loading by changes in rainfall.
- Changes in water residence time due to changes in rainfall leading to loss of unsupported ^{210}Pb to coastal waters (Appleby, 2001).
- Sediment surface mixing of the ^{210}Pb decay profile by wind and animal reworking (Sharma *et al.*, 1987; Maire *et al.*, 2008) may be a problem within relatively shallow core extraction sites with little haline stratification.
- ^{210}Pb redox remobilisation affecting the ^{210}Pb decay profile within hypoxic sediments (Benoit and Hemond, 1990).
- Redistribution of old and/or newly deposited sediment within the estuary by floods onto exposed older sediments, which have been eroded by the same or previous floods (*e.g.* Eyre and Twigg, 1997).
- Inter-decadal changes in the supply of nutrients leading to changes in micro-algal primary production (see Chapters 6 and 7), which can affect the degree of unsupported ^{210}Pb particulate scavenging (Wan *et al.*, 2004).

With the exception of effects from flood erosion and deposition, there are processes, yet to be fully explored, which may buffer changes in the unsupported ^{210}Pb supply to the water body

by ameliorating the changes from the water body to the sediment–water interface. For example, changes in atmospheric supply should not affect the unsupported ^{210}Pb content at the sediment water interface if there is an excess of scavenging fine water particulates and thus irrespective of the extend of excess particulates. Conversely, an excess of supply of unsupported ^{210}Pb from the atmosphere over the supply of scavenging particulates would result in a constant flux of unsupported ^{210}Pb, irrespective of the supply of all particulate sizes. Indeed, it is the above hypothesised extremes that are consistent with the assumptions behind the two traditional methods for separating radioactive decay from changes in sedimentation rate, namely, a constant initial concentration (CIC) of unsupported ^{210}Pb, (Robins, 1978), which may be normalised to the fine fraction (Chanton *et al.*, 1983), and a constant rate of supply (CRS) of unsupported ^{210}Pb (Oldfield and Appleby, 1984).

CIC and CRS assumptions do not cover all combinations of relative sedimentation velocity and unsupported ^{210}Pb flux (see Carroll *et al.*, 1999a for modelled and real scenarios). Further, CIC and CRS geochronological calculations use curve fitting and mapping procedures on the ^{210}Pb depth decay curves.[14] The problem of curve fitting and mapping are that simple functions may not represent the data well, relevant processes may go unrecognised and inaccuracies may result (Robbins, *in* Hancock *et al.*, 2000). Consequently, the unsupported ^{210}Pb profile alone cannot be used to test their assumptions (Robins, *in* Hancock *et al.*, 2000). In other words, various combinations of flux and sedimentation can produce similar ^{210}Pb decay profiles. For example, a relatively invariant surface ^{210}Pb profile may be due to: (1) surface mixing, (2) rapid sedimentation rates in respect to ^{210}Pb flux, or (3) constant sedimentation with an increase in the flux of unsupported ^{210}Pb (*e.g.* Somayajulu *et al.*, 1999; Caroll and Lerche, 2003).

To overcome the above limitations, an inductive method has been developed, namely sediment isotope tomography (SIT) (Liu *et al.*, 1991). SIT uses signal theory to minimise the variance between the data and a physical equation. A physical equation that describes the dynamics of ^{210}Pb supply affecting its resultant depth profile, described by a source term and sedimentation term is Equation 4.1. The source term, represents contribution of ^{210}Pb variance

[14] CIC uses radioactive decay and the ratio of unsupported ^{210}Pb surface activity to the activity at a depth to calculate the age of horizons. For CRS, the total integrated unsupported ^{210}Pb inventory is equal to the ratio of its constant depositional flux to its rate of decay. Hence, knowledge of the total mass accumulation rate (MAR) over depth (age) can be gained through knowledge of the ^{210}Pb flux measured from the total inventory (see Appleby, 2001 for details of data processing).

due to geochemical processes at each depth, regardless of an increase or decrease in ^{210}Pb activity, and the sedimentation term records the loss of ^{210}Pb by radioactive decay. In this way, the changes to the rate of ^{210}Pb supply and rate of sedimentation can be inductively disentangled from the ^{210}Pb depth profile. This is done by describing each term with orthogonal sine (cosine) Fourier series, which can fit any shape. To help ensure the iteration scheme does not become stuck in a local minimum in parameter space, all except one of the parameters are held in turn at their best values and the remaining parameter is scanned to see if there is any improvement in the degree of fit[15].

Sedimentation term Source term

Equation 4.1. $$P(x) = P(0)\exp\left(\left[-Bx + \sum_{n=1}^{N}\frac{a(n)}{n\pi}\sin\left(\frac{n\pi x}{x_{\max}}\right)\right] + \sum_{n=1}^{N}\frac{b(n)}{n\pi}\left[1-\cos\left(\frac{n\pi x}{x_{\max}}\right)\right]\right)$$

Where $P(x)$ is the ^{210}Pb concentration at depth x, $P(0)$ the concentrations at the sediment–water interface, summations are for n=1,2,3…,N; $a(n)$ and $b(n)$ fitted sediment and source coefficients; $x_{\max}$ the greatest measurement depth; λ is the ^{210}Pb decay constant; .B is a trend coefficient related to average sediment velocity V where $B = \lambda / V$

The method is poorly known, but has been tested in a number of non-ideal dynamic environments of the Amazon delta (Liu *et al.*, 1991), lake systems disturbed by anthropogenic events, embayments affected by storms (Carroll *et al.*, 1999a and b; Carroll and Lerche, 2003) and a complete range of synthetic scenarios that covers the complete range of relative ^{210}Pb supply and sedimentation (Carroll *et al.*, 1995). However, in its present form, the SIT algorithm is not designed for systems that have undergone extensive mixing, nor can the method account for all possible unsupported ^{210}Pb decay profiles resulting from turbidites, tsunamites or flood deposits (Carroll and Lerche, 2003). Nonetheless, mixing and event deposition need not always interfere. For example, Lu and Matsumoto (2005) found that, like the CRS algorithm, the SIT chronology was not affected by surface mixing, provided the extent is within 15 % of the total unsupported ^{210}Pb inventory while von Gunten *et al.* (2009) managed to construct an accurate SIT geochronology despite the presence of turbidite slumps. Nevertheless, success is not always assured and it is prudent to determine the extent of surface mixing and the positions of depositional facies independently in order to apply any ^{210}Pb

[15] The algorithm was designed to maximise disentanglement between the source and sedimentation terms away from local minima in phase space for the least number of terms source and sedimentation terms (*N*) by This is adjusting the equation's terms in a strict hierarchy (see Liu et al., 1991; Carroll and Lerche, 2003 for details of the protocol).

method (SIT, CRS or CIC) to the baseline sediments (*e.g.* Robbins, 1978; Arnaud *et al.*, 2002; Garces *et al.*, 2008).

Identification of sediment erosion or mixing hiatuses from the unsupported ^{210}Pb decay profile is more problematic. Suess (1978) gave a series of hypothetical scenarios of unsupported ^{210}Pb decay profiles for a range of different mixing, erosion and rapid deposition conditions for normal and abnormal source material. Suess's (1978) examples, however, were restricted within the framework of a constant sedimentation rate, from which Suess proposed that a 'hole' or depositional facies can be identified by the disturbance of its unsupported ^{210}Pb profile, provided the expected variance in the profile was known beforehand, such as through a simple logarithmic decay with depth.

It would be dangerous to assume that the ideal conditions necessary to interpret complex ^{210}Pb profiles as ascribed by Suess (1978) will apply to all systems. For example, aside from a different rate of baseline sedimentation, floods within shallow estuaries can both erode and remobilise contemporary littoral sediments and old catchment soils and redeposit them further down the estuary (Eyre and Twigg, 1997). An example can be seen in the case of the Rhone River (France), where the unsupported ^{210}Pb within the fine fraction was diluted during floods near the mouth of the river (Drexler and Nittrouer, 2008). Drexler and Nittrouer (2008) suggested that a dilution signature was the result of flood sediments (presumably old) restricting the contact between particles and dissolved ^{210}Pb forms.

4.1.1. A potential solution for erosion

By identifying the position of flood deposition facies, it then becomes feasible to both identify the position and the amount of sediment erosion, provided unsupported ^{210}Pb is supplied by atmospheric deposition, for example, by choosing sampling sites that are remote from the immediate effects of river deposition (Appleby, 2001, 2008). The amount of erosion can then be calculated from the difference between the measured total unsupported ^{210}Pb inventories within baseline sediments and the known inventory from atmospheric deposition (Turekian *et al.*, 1977). Each erosion horizon is assumed to be located immediately below the depositional facies after the flood peak. The amount of material lost is then proportional to amount lost from the calculated total unsupported ^{210}Pb inventory and in proportion to the relative strength of the flood. The appropriate metric of flood strength (*i.e.* height, maximum flow, duration, or strength) is uncertain, but can be assumed to be related to the depositional facies signal or the thickness of the depositional facies.

Depositional facies have been distinguished from baseline sediments by a combination of fluvial sedimentary markers and major sediment content variables (Chanton *et al.,* 1983; Drexler and Nittrouer, 2008; Moreno *et al.,* 2008). In contrast to long-term particle tracer experiments (Wheatcroft, 1992) or short half-life radioactive elements (*e.g*. Lecroart *et al*., 2005), the depth of surface mixing due to wind-current and activity of sediment infauna is often assessed from a weight of evidence. This is: (1) a relatively invariant surface unsupported ^{210}Pb decay profile, indirectly evaluated from the convergence of horizons date from another geochronological marker; (2) modelling of the unsupported ^{210}Pb decay profile from deposition and bioturbation (*e.g.* Gardner *et al.*, 1987); (3) assuming no significant mixing layer from the presence surface anoxia and varving (*e.g.* Zimmerman and Canuel, 2002); and (4) the depth of surface anoxia (*e.g.* Carroll and Lerche, 2003), with the absence of extensive surface worm tubes (Gardner and Bohn, 1980).

In the final analysis, the choice of methods will depend on the specific circumstances and history of the deposition site. For example, Ruddiman *et al.* (1980) used the older spread of volcanic tephra below the mixed layer to calculate the rate of surface mixing. Indeed, the more common char deposits from larger fire events, typical of the local landscape, could also be used as a natural pulse marker from either relatively recent fires, distributed through the surface mixed layer, or previous deposits below the mixed layer. Alternatively, the depth of surface mixing may be judged by changes to an uninterrupted expected profile common to most sediment columns such as sediment compression. Surface mixing would be expected to interrupt the normal bulk density/porosity or water content logarithmic change with depth that accompanies accumulated sediment compression (Burdige, 2006). The effect is contingent on other factors that affect the profile, such as grain type and size, remaining relatively constant.

4.1.2. Evaluation of ^{210}Pb chronologies: An imperative

Notwithstanding the assumptions of the ^{210}Pb geochronological methods, the accuracy of the chronology is dependent on identification of all deposition facies, the extent of the surface mixed layer, the appropriate flood metric (height, duration, maximum flow or some combination), or whether some flood deposits have themselves been eroded. Therefore, all ^{210}Pb geochronologies within dynamic environments that are based on the ^{210}Pb profile shape (CRS and CIC mapping methods) require evaluation (Smith, 2001) as do apparent model fits to data such as SIT that still have underlying assumptions that need to be evaluated (Abril, 2004).

Traditionally, the convergence of a horizon date with that of an independent signal or event facies has been used to evaluate a contiguous ^{210}Pb geochronology. It should be noted however, that a convergence of dates between an event(s) and a ^{210}Pb geochronology cannot be used to evaluate the assumptions behind a model, or the date of the formation of an event signal in relation to the time of deposition, as well as the dates of the remaining horizons. Therefore, it is dangerous to assume the accuracy of the chronology between temporally well-spaced events markers or horizons older than the event markers. For example, the CIC method depends on a calculation that compares the surface ^{210}Pb activity with each individual horizon that leaves each horizon date independent of its neighbours. The CRS method's independence is not as easily defined, as the calculation is dependent on the ratio between the total unsupported ^{210}Pb inventory to the inventory below the sample horizon (Appleby, 2001). The result is a reduced dependence with increasing depth in a non-linear manner as a function of ^{210}Pb decay profile, which can become increasingly subject to error bias in deeper and older sediments (Binford, 1990). In contrast, the SIT algorithm can use the position of a known event to reduce the number of probable minimal solutions (Carroll and Lerche, 2003). However, Abril (2004) argued that not even SIT could be excluded from the uncertainty in the timing of an event. Abril's argument can be summarised as incorporating a biased event date within an inductive modelled structure that will also conceivably bias the range of probable SIT solutions.

The most commonly used marker is a ^{137}Cs particulate signal peak or horizon, principally because of it ubiquitous distribution around the globe (Smith, 2001). ^{137}Cs originated from fallout during the period of atmospheric atomic bomb testing (1958 and 1963), or more recently for northern Europe, from its accidental release from the Chernobyl atomic reactor (1986). In the southern hemisphere, the level of ^{137}Cs activity is relatively low and the major 1963 peak is not easily resolved (Brunskil *et al., in* Hancock *et al.*, 2000). Further, it should be stressed that such a ^{137}Cs peak or horizon need not be synonymous with the depositional position or the date(s) of its release to the atmosphere and thus cannot be used to falsify the correspondingly ^{210}Pb geochronological date or the assumptions behind its conceptual model (Abril, 2004). There are associated delays in transport of ^{137}Cs fallout from the catchment particulate ^{137}Cs peak translocation by surface mixing (Guinasso and Schink, 1975; Ruddiman *et al.*, 1980; Wheatcroft, 1992) and remobilisation. ^{137}Cs activity in Western Port (Victoria, Australia), a similar system to the Little Swanport estuary, has been detected in sediments prior to the atomic bomb input (Hancock *et al.*, 2001). Longmore *et al.* (1983) measured the

presence of ^{137}Cs within Hidden Lake (Fraser Island, Australia) in sediment dated by ^{14}C organic carbon fraction to 430-year BP and attributed this to desorption and diffusion. Foster *et al.* (2006) explained the advective ^{137}Cs mobilisation within a coastal lagoon through salt replacement and hydrostatic pressure, driven by its adjacent higher sea level.

If there is no convergence of dates between geochronological methods, then correcting for the translocation, remobilisation and mixing is neither simple nor always possible. Current models of ^{137}Cs remobilisation are contingent on constant sedimentation rates (Abril, 2004). Corrections for surface mixing translocation of an event signal may be solved through deconvolution procedures but require *a priori* knowledge of the process to construct the appropriate deconvolution filter (Ruddiman *et al.*, 1980; Schiffelbein, 1985; Bard *et al.*, 1987). Clearly, for a successful ^{210}Pb geochronology a site should be chosen for a minimal surface disturbance with known event signals that are robust enough not to be affected by remobilisation or translocation.

4.1.3. A solution for evaluating ^{210}Pb geochronologies for shallow dynamic estuaries

Less ubiquitous, but more stable than the ^{137}Cs particulate signals are the dates of distinct particulate signals and depositional facies that are likely to be characteristic of the Tasmanian and Australian catchment and marine landscape. These include fire char inputs (McIntosh *et al.*, 2005), flood deposits (Eyre and Twigg, 1997), marine-derived sediments from local storms, tsunamis (Dominey-Howes, 2007) and conceivably 'pressed' changes to baseline lithology resulting from long-term transitions in flood frequency during entrance exposure (Rustomji, 2007). Further, there is a synergy in identifying the type, date and frequency of events powerful enough to have affected the sedimentary record for testing the event historical contingency on ecological variance (see Chapter 1), and for the application and evaluation of contiguous radio-geochronological models that need to be restricted to baseline sediments.

For an event chronology, the challenge is to match the date of the event and type of event to the depositional facies or signal. For example, without a dating context, the number of events to consider will depend on *a priori* knowledge of the maximum age of the sediment core. It may be difficult to distinguish the dates of small relatively common events (*e.g.* floods, fires), which may not have disturbed the sediments, from large rare events that have disturbed the sediments. Consequently, it may be necessary to identify two types of event impacts to constrain the position of sediment depths to the chronological scale. That is, large rare events

that are likely to have had an impact with a high degree of chronological certainty but low resolution (*e.g.* tsunamis and large pivotal fires) together with relatively common events that produce high chronological resolution but have a low degree of chronological uncertainty (*e.g.* floods).

Identifying the type of events, however, may not be straightforward. Some baseline sedimentary signals are specific to an event (*e.g.* ^{137}Cs, fire char), but the depositional facies, formed by different events, may share a range of similar characteristics. For example, Donato *et al.* (2008) and Switzer and Jones (2008) used a number of lines of evidence to distinguish shell-laden storm surge deposits from tsunami deposits within coastal lagoons based on origin of identifiable contents (terrestrial material/marine shells) and particle sorting, and arguably, frequency. It is also conceivable that flood facies within estuaries may share a number of similar characteristics with marine incursions and that there may be other marine incursions that have yet to be generally recognised as important. For example, shell debris from inter-tidal sand flats are re-floated and transported by flood tides (Dent and Uhen, 1993). This would have relevance for the Upper Middle Basin Little Swanport estuary because floating shell debris has been observed by oyster farmers during king tides (Dyke, C., 2006, *pers. com.* Dykes Oyster Farm). Clearly, this supply of floating shell debris will be amplified during times of extreme king tides that appear at interdecadal frequencies ('emperor tides' [Ray, 2007]).

4.2. Goals and aims

The goal of this study is to produce a robust geochronology for sediment cores extracted from the central trench that represent the two functional zones, which define the Little Swanport estuary (Upper Middle Basin and Lower Middle Basin; see Chapter 3). The study aims to achieve robustness by constructing an event geochronology matched to a contiguous ^{210}Pb geochronology (mixed Robustness Analysis (RA), Section 1.3.2) by a series of hierarchical analyses to: (1) identify event signals (fire as macro-char, and ^{137}Cs fallout) and depositional facies, (2) identify the types of events as either storm surges, tsunamis, emperor tides, floods or baseline sedimentation changes, (3) correlate the events with historical information on major fires, marine incursions, the largest of the floods and baseline changes *via* flood frequency using a 101 year-long rainfall/river-flow model (SKM, 2004) and (4) produce a contiguous ^{210}Pb geochronology (SIT, CRS, CIC) down the predetermined baseline sediments, contingent on an independent assessment of a small surface mixing depth and erosion hiatuses. In this, the events, the extent of erosion, and the appropriate contiguous

^{210}Pb geochronology can be evaluated through mixed RA convergence of their matching dates.

4.2.1. Distinguishing event depositional facies from baseline sediments

Depositional facies were identified by the weight of evidence using a suite of non-tautological content and quality variables, signal markers and conceptual models previously tested or recommended for their most plausible explanation (see Chapter 3). These included elemental and isotope ratios to identify catchment signals, organic matter (OM) and water content, and baseline calcium carbonate contents to postulate changes in fluvial supply, Glyph Analysis, elevated Rp indexes and faecal pellet content to test the latter postulates' catchment markers, together with the occurrence of iron-laden pyroxene clays and the age of shell debris. The age of shells was used to ascertain the degree of inundation based on the elevation of mid-Holocene sea levels (Mazebar, C., 2007, *pers. com.*, unpublished data, Dept of Mines, Tasmania). The analysis was done on a case-by-case basis, recognise that the type of event signal (as a discontinuity) may vary with catchment historical contingency and remobilisation of the upper or lower littoral zone sediments (floods and marine incursions)[16]. In this way, provided there was a convergence of more than one line of evidence, all of the plausible depositional facies and fire event signals within the sediment core were identified and evaluated by convergence with the subsequent event and ^{210}Pb chronologies.

4.2.2. Changes in baseline sedimentation

Baseline changes in sedimentology were only identified for the Lower Middle Basin sediment cores through a conceptual model that recognises that a more open bar way results in a migration of the sandy Marine Flood/Tidal Delta zone up the estuary (Morton and Donaldson, 1973).

4.2.3. Surface mixing depth

The extent of surface mixing was determined as suitable for a baseline ^{210}Pb geochronology, by: (1) examining sediment colour for the extent of anoxia, (2) using divergence from an ideal model of sediment compression (power law), based on the assumption that the particle size spectrum had remained constant (Burdige, 2006), and (3) using the extent of translocation of

[16] Trials with principal components and constrained cluster analysis did not compress the data in any meaningful way, as there were more dissimilarities than similarities within baseline sediments (due to regime shifts; see Chapter 6) and between event facies.

recently deposited macro-char down the Lower Middle Basin sediment cores from a fire (2005) on adjacent Ram Island (Dyke, C., 2006, *pers. com.* Dykes Oyster Farm).

4.2.4. Event identification

It is assumed that all depositional facies within the Upper Middle Basin were the result of a flood, contingent on shell debris within the facies being typically estuarine in origin. Within the Lower Middle Basin, the type of depositional facies was identified by using a weight of evidence score from a number of plausible alternatives including largest of king tides, storm surges, tsunamis and floods. The scores were set at 1 for consistent with the evidence, 0 for uncertain and -1 for not consistent with the evidence, based on current knowledge of historical frequency, sedimentological particle spectrum, sediment contents and shell taphonomy and fidelity. Once the events were identified they were then correlated to historical accounts based on the oldest plausible horizon, taken from the limit of detection of ^{210}Pb activity (100 years to 150 years). Fire events were identified from peaks in macro-char content, providing that the peaks did not reside within the event facies.

4.2.5. Identifying sediment column erosion

The position and extent of the erosion was solved for CRS and SIT methods[17], contingent on the total unsupported ^{210}Pb inventory down the sediment core being less than expected from local atmospheric supply. For the CRS method, the position of the hiatus and the quantity of material eroded was solved down baseline sediments by first consecutively increasing the total amount of sediment lost as accumulative mass[18] within the limits of measurable ^{210}Pb activity. This loss of accumulated mass was then distributed from the base of each event facies in proportion to the strength of its corresponding event. The strength of the event was measured by either the thickness of the discrete facies or the magnitude of the signal. After each addition, the total unsupported ^{210}Pb inventory was recalculated in the usual manner through ^{210}Pb profile integration and smoothing across the additional cumulative mass from the adjacent ^{210}Pb horizons (Appleby, 2001). The solution to the amount of erosion was reached, as accumulative mass, when the recalculated total unsupported ^{210}Pb inventory was equal to the local aerial depositional inventory as measured by Turekian *et al.* (1977).

---

[17] The CIC method baseline horizons are independent of erosion and event facies; that is, the algorithm only requires decay rate and the difference in activity between the surface and the particular horizon when calculated in the usual manner according to Robbins and Herche (1993).

[18] For CRS and CIC, model depths are expressed as accumulated mass depth to normalise for sediment compaction (Appleby, 2001).

The same iterative protocol used for CRS was applied to SIT solutions, but in place of accumulated mass, the depth of baseline sediments was used[19]. The model depths (*i.e.* the resultant profile after removal of depositional facies and inclusion of baseline sediment erosion) for each of the measured baseline sediment's unsupported ^{210}Pb activity were then recalculated using an estimated sediment bulk density of the eroded horizon, taken from the average of four adjacent horizons immediately below the erosional hiatus.

4.3. Materials and methods

Positions of the core extraction sites and references sites for bivalve taphonomy are illustrated in Figure 4.1. For details of sample collection, processing and analysis of sediment signals see Section 2.7. For the construction of Glyph neutral models see Section 3.3.2.

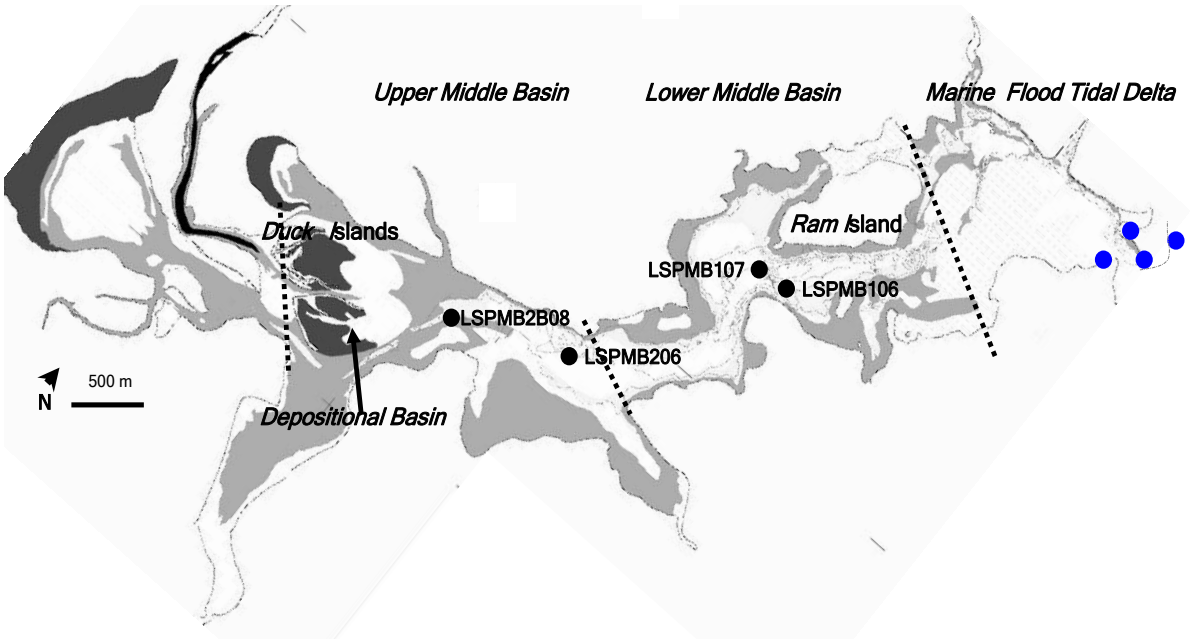

Figure 4.1. Sediment core and bivalve sampling sites within the Little Swanport estuary.
(●) Sediment core sites; (●) bivalve shell inter-tidal sampling sites. The grey shading represents the seagrass meadows located within the littoral zones. Depth contours are spaced every 2 m.

4.3.1. Data analysis

The changes in baseline sedimentology, as represented by LOI 550 °C and POC content, within the Lower Middle Basin sediment cores and change in annual flood frequency were identified by a cumulative sum of the mean within an ordered series (CUSUM) change point

[19] The SIT algorithm incorporates bulk density at a latter stage in its source and sediment term disentanglement procedure. As a result, the hiatus position and amount of erosion as mass was able to be iteratively estimated from the above procedure.

analysis (Pettit, 1980; Taylor, 2000) within the software package Variance™. Flood frequency was expressed as the number of flood days for a year, which were defined as those modelled daily averaged river flows (SKM, 2004) from 1900 to 2001 that resulted in a catastrophic fall in the river nutrient concentrations (>226 ML day^{-1}; see Chapter 5).

4.3.2. Radio-geochronology

For details of ^{210}Pb and ^{137}Cs sampling, processing and analysis see Chapter 2. For details of SIT protocols see Liu *et al.* (1991), and see Appleby (2001) for CIC and CRS. The chronological bias for individual Upper Middle Basin sediment cores was addressed in the manner of Cooper *et al.* (2004) by rationalising differences in mean dates between contiguous geochronological methods and discrete events based on their individual strengths and weaknesses. For Lower Middle Basin sediment cores, a cross-validation procedure was included to identify any chronological bias in the optimum SIT simulation caused by an uneven sampling distribution and the weakness of constraints of other lines of evidence. That is, weakness from the uncertainty of CUSUM baseline sediment core transitions with the uncertainty of flood frequency transitions, postulated from only anecdotal evidence of an entrance restriction and untested postulates on the effects of oyster cage placement. Further, to overcome zone pseudo-replication of a chronology based on an individual sediment core, the mean sediment core chronology was calculated from its basin replicate pair, assessed as identical to the changes in major organic content variance in the manner of Turner *et al.* (2006).

4.4. Results and discussion

4.4.1. Recorded and recalled historical accounts of local events

A number of events were identified which may have left a depositional signal or deposition facies within the Little Swanport estuary's sediment column during the late Anthropocene (see Figure 4.2). The accounts were divided between those recorded formally or informally (*i.e.* recollections from locals that had lived continuously within the area) and those inferred from modelled river flows taken from rainfall data on catchment topography, geomorphology and farm dam lease records (SKM, 2004).

There were only two floods (1986 and 1960) that resulted in damage sufficient to be noted by local recollections and newspaper accounts. The 1986 flood resulted in the destruction of the Little Swanport estuary's shellfish aquaculture leases, which had been granted and subsequently located within the upper estuary after 1980 (Dyke, C., 2006, *pers. com*. Dykes

Oyster Farm). The 1960 flood was the second largest of the twentieth century, after the largest in 1923, and according to informal accounts, affected waters bodies around southeast Tasmania, but not identified specifically with the Little Swanport estuary. In addition to the 1960 and 1986 floods, it is probable that other pivotal flood events directly affected the estuary's ecosystem, as suggested by relative the strengths of the above two noted events to other floods (see Figure 4.2). For example, the largest flood of the twentieth century was in 1923 (37 000 ML day^{-1}) and the third largest flood, in 1969 (25 000 ML day^{-1}), was equal to the 1986 flood.

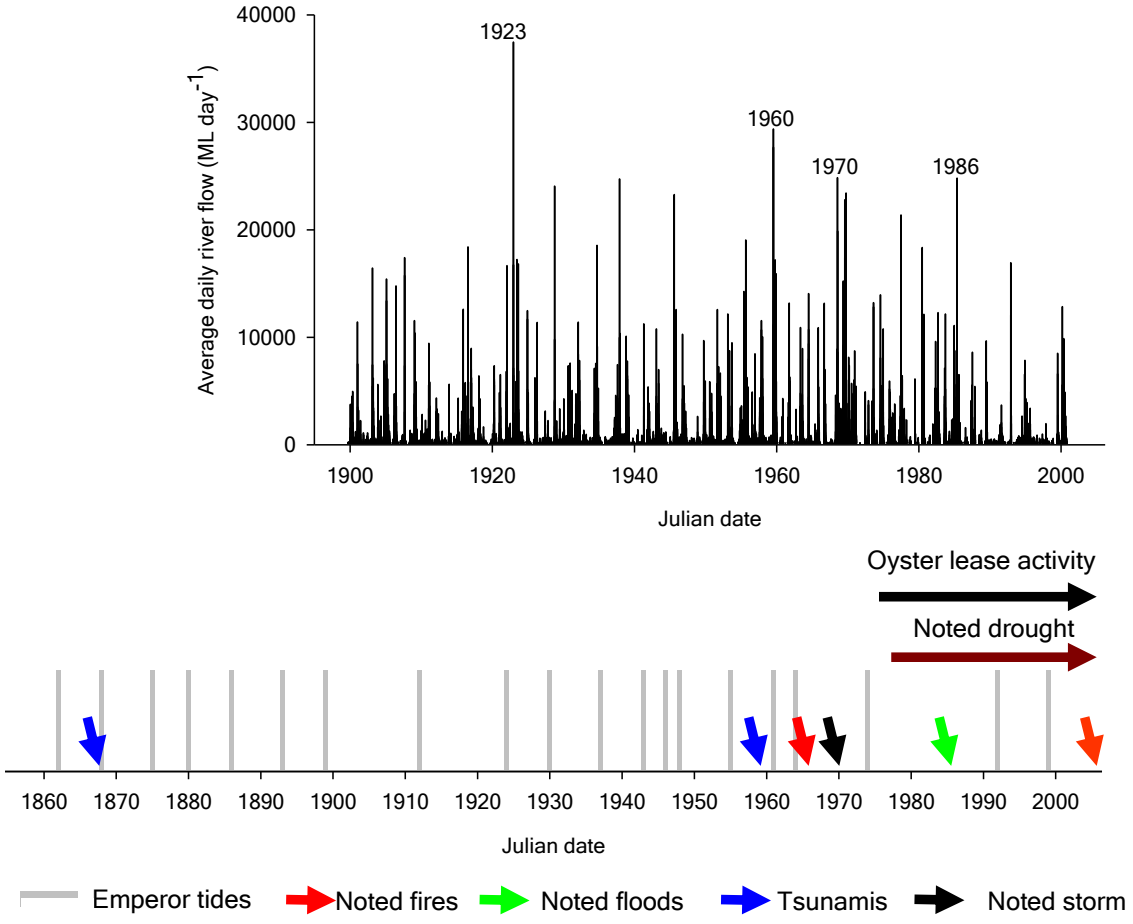

Figure 4.2. Recorded and modelled historical events over the late Anthropocene that were observed or likely to have affected the Little Swanport estuary.
(top) Modelled average daily river flow taken (SKM, 2000) illustrating the magnitude and frequency of flood events. (bottom) A summary of recorded events that may have affected the Little Swanport estuary. The timing extreme tides was taken from Ray (2007).

Other events, such as small local forest and grass fires within catchments are a consistent feature throughout Tasmania (McIntosh *et al.*, 2005). Consequently, the topsoil maintains a significant load of char that constantly washes into its receiving water body as erosion occurs. Nevertheless, some fires have been of such intensity that they have over-shadowed the usual course of a summer fire season, resulting in peaks in char deposition above the background

inter-annual variability. For example, the fire of February 1967, known as 'Black Tuesday', was the largest recorded fire of either the twentieth or twenty-first centuries. The fire extended across the southeast of Tasmania, including the lower Little Swanport catchment (Marsden-Smedley, 1997). More recently (2005), a smaller fire occurred on Ram Island (see Figure 4.1) but directly adjacent to the lower estuary sediment coring sites (Ram Island, Dyke C. *pers. com.*, 2006, Dykes Oyster Farm). Such close proximity, even with a relatively small fire, could explain the noticeable presence of char particles observed within the nearby surface sediments of the littoral during the transect study (unpublished data; see Chapter 3).

In 1868 and 1960, the two largest tsunamis of the nineteenth and twentieth centuries were generated off the coast of Chile and arrived along the southeast coast of Tasmania (Dominey-Howes, 2007). Figure 4.3 shows the trajectory of the 1960 event as it impacted from the south onto the Tasmanian coast and the Australian mainland states of Victoria and New South Wales (Mader, 2008). There is no official record of the effects of the tsunamis on the Little Swanport estuary. Nevertheless, recorded personal accounts give a rhetorical feel of the tsunami's power. For example, the 1868 tsunami produced a wave within a southern Tasmanian bay of up to 10 ft in amplitude (Launceston Examiner 1868, Tasmania) and destroyed the Bay's local jetty, together with the remaining natural oyster beds on the Tasmanian east coast (Report of the Commissioners, 1883). The 1960 tsunami was reported to have damaged boats and moorings off the east coast of Tasmania. However, the potential of the 1960 tsunami to remobilise sediment into and/or within a water body came from aerial observations around Port Albert (Victoria, directly north of Tasmania). A pilot of an aircraft recounted that seiches generated by the tsunami were of sufficient size and power to empty and refill local lagoons up to a mile long in the space of 20 minutes (The Mercury news paper, 1960, State library, Hobart, Tasmania).

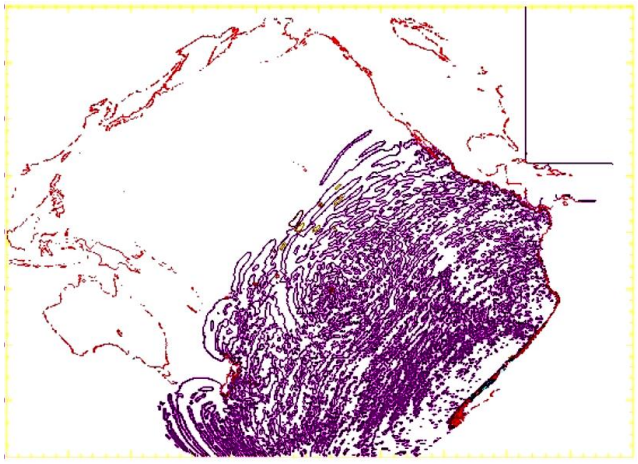

Figure 4.3. A numerical simulation of the 1960 Chilean tsunami's progression across the Pacific.

The simulation was taken from the CD accompanying Mader (2008). The simulation was halted just before the tsunami's arrival off the southeast Tasmanian coast.

Other normal extreme events, such as storms and king-tides, have been observed within the area. In 1972, a large onshore storm along the Tasmanian east coast was observed by local Cray fishermen as the biggest in 50 years. However, effects of the storm on the Little Swanport estuary were not reported. It is during king tides that notable masses of floating shell debris are brought into the Little Swanport estuary from Oyster Bay and subsequently deposited onto the oyster racks located within the Marine Flood/Tidal Delta (Dyke, C., 2006, *pers. com.* Dykes Oyster Farm).

4.4.2. Sediment core descriptions

The upper estuary sediment core (LSPMB206) was extracted from the central heterotrophic trench within the Lower Middle Basin in 4 m of water (see Figure 4.1). However, the length of the core (75 cm) was restricted by a mass of well-consolidated shell debris. The top 2 cm of the sediment core had the consistency and colour of an olive green to black anoxic mud with a faint smell of sulphide. Below 2 cm, black mud, with a pungent sulphide smell, was prevalent throughout the core. Dispersed throughout the core were well-preserved pieces of leaves of the seagrass *Zostera* spp. The length of the leaf debris ranged from a few mm to around 2 cm. From around 28 cm to 35 cm and 62 cm to the 75 cm base of the core there were two notable masses of shells and shell debris within a black sandier matrix.

The shells within the intrusive masses consisted of gastropods, molluscs and (notably) the bivalve *Spisula trigonella*, up to 4 cm in length (see Figure 4.4). Outside the masses, occasional small whole or pieces of gastropod and mollusc shells a few mm in diameter were found dispersed throughout most of the sediment core. All of the shell species' habitats were typical of sub-tidal to inter-tidal regions of a muddy estuary and not characteristic of the deep extraction site habitat (see Table 4.1).

Figure 4.4. The base of sediment core LSPMB206, showing the layering of the bivalve *Spisula trigonella* inter-dispersed with small pieces of shell hash and small gastropod shells (see Table 4.1).

Table 4.1. Gastropods, molluscs and their habitats, identified within sediment cores of the Upper Middle Basin and Lower Middle Basin of the Little Swanport estuary.

LSPMB206, LSPMB2B08, LSPMB106 and LSPMB108; (×) indicates the presence of the species.

Gastropods and Molluscs	HABITAT	LSPMB107	LSPMB206	LSPMB2B08
Limatula strangei	Moderately and sub maximally exposed reef, 2-15 m			X
Anodontia perplexa	Sheltered sand: 0-5 m depth	X		X
Mactra pusilla	Marine sand, low intertidal zone	X		
Spisula trigonella	Sheltered sand, mud: 0-1 m depth		X	X
Tellina margaritina	Sheltered sand and mud: 0-15 m	X		
Tellina deltiodalis	Sheltered sand, mud, seagrass, low intertidal zone		X	X
Soletelllina biradiata	Sheltered sand, mud, 0-3m	X		
Gari lividia	Moderately exposed sand, 0-70 m	X		
Kalysia scalarina	Sheltered sand, low intertidal zone	X		
Olividae	Common on ocean beaches, sandy Inter-tidal to sub tidal zone	X		
Leiopyrga octona	Sand shallow, sub-tidal zone. Beaches?- improbable	X	X	X
Cabestana spengleri	Sheltered and moderately exposed reef, 0-20 m		X	
Astralium squamiferum	Sheltered seagrass, 0-5 m			X
Bembicium melanostrom	Sheltered mud/sand, mid to high Intertidal zone			X
Autrocochlea brevis	Sheltered rock, seagrass and sand , upper to mid Intertidal zone			X
Limatula strangei	Moderately and sub maximally exposed reef, 2-15 m			X
Agnewia sp	Moderately sub maximally exposed reef:			X
Limatula strangei	Moderately and sub maximally exposed reef, 2-15 m			X
Foraminifera Ammonia bercari	Upper muddy estuarine oxia/anoxia sediment t zones		X	X
Foraminifera Cribononium oceanicus	Marine to lower estuarine sediments	X		
Siliceous sponge spicules	Marine and estuarine zones	X		
Echinoderm plates	Marine and estuarine zones	X		

The remaining Upper Middle Basin sediment core (LSPMB2B08) was extracted closer to the depositional levees (Duck Islands; see Figure 4.1) in 3 m of water, where it was noticed that the upper zone had the greatest amount of littoral sediment disturbance, from boats returning to oyster lease shore facilities. An additional effort was made without success to core past the mass of shells encountered at around 80 cm down the sediment column and coring was abandoned at a depth of 134 cm. The top 4 cm of the core was of a similar olive green colour to sediment core LSPMB206. However, a faint smell of sulphide was detected deeper down the core from around 5 cm to 12 cm. Below 12 cm, the sulphide was quite pungent and the sediment became black and gelatinous. Small voids, a few mm in diameter, were ubiquitous within the black gelatinous sediment down around 50 cm to 53 cm. Similar to core LSPMB206, well-preserved pieces of *Zostera* spp. seagrass leaves were dispersed throughout the sediment core, but in obvious greater abundance. Whole gastropod and mollusc shells and their debris were found intermittently throughout the core, including a piece of a well-preserved red to orange freshwater tunicate, at around 2 cm in diameter. There were two notable intrusive sandy masses containing gastropods and molluscs, but at different depths and closer to each other (around 59 cm to 75 cm and 80 cm to >134 cm) than in sediment core LSPMB206.

The shell masses were dominated by relatively large numbers of the bivalves *Spisula trigonella* (up to 3 cm long) and *Tellina deltoidalis* (up to 5 cm long) and a more diverse mix of gastropods and molluscs than in sediment core LSPMB206 (see Table 4.1). This is despite the fact that these species' habitats lay within the same sub-tidal to inter-tidal zones as those evidenced in sediment core LSPMB206.

The Lower Middle Basin sediment core (LSPMB106) was extracted from 8 m of water on the southern side of the deep central basin (see Figure 4.1). The coring was halted at 82.5 cm after it was noticed that there was little progress in extending the length of the core despite continued hammering. The top 20 cm to 21 cm was composed of olive green mud, which became increasingly more gelatinous down the core. A void around 0.5 cm across was observed around 5 cm to 6 cm from the top of the sediment core. Below 21 cm to around 80 cm, the sediment core was composed of black gelatinous mud extended to the base of the core with a pungent sulphide smell. Below 80 cm, the sediment contained pieces of terrestrial grass, a tree twig and some shell debris. Inter-dispersed down the core were pieces of well-preserved *Zostera* spp seagrass from a few mm to 4 cm long.

The remaining lower estuary sediment core (LSPMB107) was extracted further up the Lower Middle Basin at the deep centre of the estuary (9.9 m). An additional effort was made to core past the restrictive sandier mass encountered at around 80 cm. However, the coring remained difficult and it was abandoned when the length of the core reached 137 cm. From the surface to 78 cm, the sediment core was similar in appearance and smell to LSPMB106. Below 78 cm, it was again similar to sediment core LSPMB106; there were occasional remnants of terrestrial grasses that sat above gastropod and mollusc debris that extended to 100 cm.

From 100 cm to the base of the core (137 cm), there was an obvious well-consolidated shell layer. The layer was composed of gastropods and molluscs and articulated valves and single valves of the bivalve *Mactra pusilla* 0.3 cm to 0.6 cm long were noted (see Table 4.1). However, the size of the shells and shell debris was not restricted to the >315 μm fraction. All of the examined sieve fractions down the sieve stack (>315 μm, >250 μm, >150 μm, >100 μm and >76 μm) consisted mainly of juvenile bivalves and gastropods, foraminifera, sponge spicules, broken echinoderm plates and spines, all interspersed with a relatively minor fraction of quartzite particles. The quartz particles were noticeably less sharp and angular than the upper fluvial sands in the sediment cores from the Upper Middle Basin, but were not as rounded or smooth as beach sand. Again, most of the bivalve and gastropod habitats were more typical of shallower, lower estuarine and marine environments (see Table 4.1) than the deeper extraction site would suggest.

4.5. Relative stratigraphic variance between the Upper Middle Basin sediment cores

The two extraction sites from which the sediment cores were obtained did not share the same net sediment accretion but may have shared a common event history. That is, the different OM content stratigraphy was consistent with a different net accretion rate (see Figure 4.5), yet the presence of two similar notable masses containing shells/shell debris and a relatively low LOI 550 °C (≤15 %) suggested that the masses were caused by the same events. Further, assuming the same event history, the deeper but closer positions of the two notable masses down core LSPMB208 than LSPMB206 suggested a greater rate of baseline sedimentation and a greater level of flood erosion at the extraction site. Indeed, the relative rates of accretion and erosion were consistent with their relative positions within the estuary; the closer the site to the Little Swanport River, depositional levees (Duck Islands; see Figure 4.1) and boat traffic, the greater rate of flood erosion and sediment remobilisation.

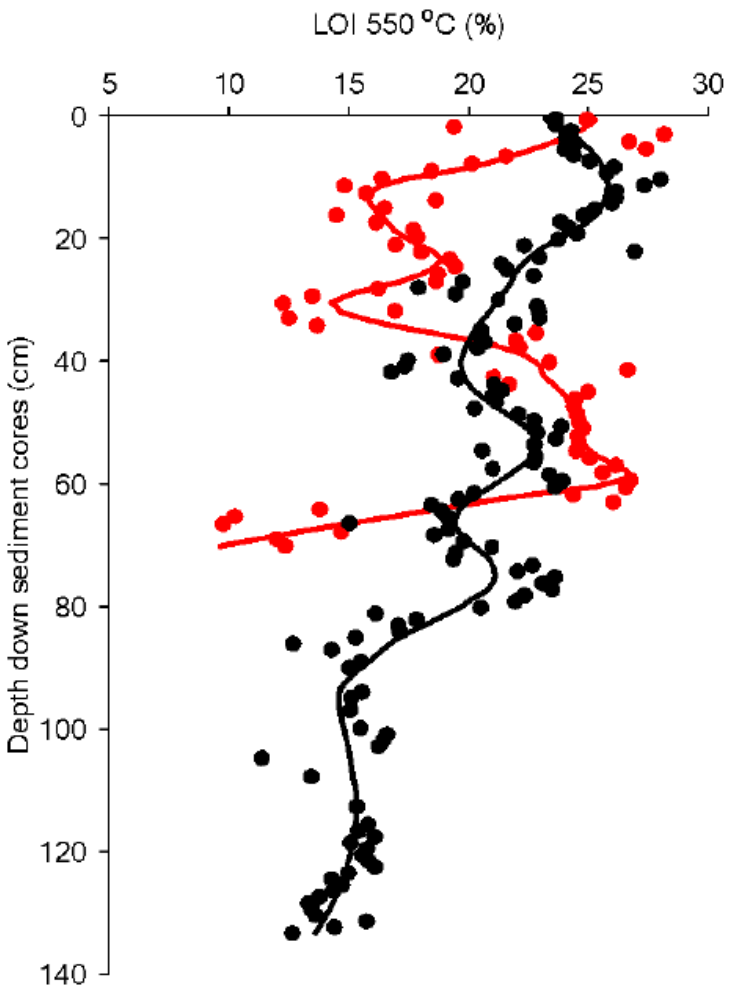

Figure 4.5. OM as LOI 550 °C down the Upper Middle Basin sediment cores.
Sediment cores LSPMB2B08 (─) and LSPMB206 (─). The non-linear trend was generated by a LOESS smoothing function that extrapolates data *via* a second order polynomial from an adjacent 0.3 % of the data set.

The analyses of each Upper Middle Basin sediment core were treated separately but in sequence starting with core LSPMB206 because sediment core LSPMB206 has a similar event history and in which there was evidently little, or at least less, erosion. In this way, the conclusions from the lower station (LSPMB206) acted as an interpretative 'anchor' for any erosional loss of flood signals and baseline sediments from the upper station (LSPMB2B08) that could have affected its event-based chronology and radio-geochronology.

4.5.1. Upper Middle Basin sediment core LSPMB206

4.5.1.1. Content, quality and marker signals

Figure 4.6 illustrates the stratigraphic variance of content and quality variables in relation to the sediment size fraction spectrum. All of the sediment horizons down the two Upper Middle Basin cores had a bimodal fraction size distribution, with a peak in content in the fine fraction

<76 µm (phi 5.0) and a peak in content within a larger fraction centred around the 150 µm to 100 um sieve sizes (phi 2.7). The larger faction was composed primarily of either low organic quartzite sands or faecal pellet aggregates. The pellet aggregates were composed of a conglomerate of fine fraction particulates contained within a peritrichous membrane (see Chapter 7). The water content, LOI 550 °C and LOI 950 °C as $CaCO_3$ content values were typical of low carbonate muddy and sandy sediments (Burdige, 2006) and ranged from 52.8 % to 84.4 %, 9.8 % to 18.4 % and 4.3 % to 10.1 % respectively. The range of Rp indexes down the sediment core (0.45 to 0.69) was within the range measured along the surface sediment transect (see Chapter 3). The lower value was typical of muddy environments and the higher value was typical of the shell debris-laden Marine Flood/Tidal Delta sediments. $\delta^{13}C_{org}$ and PON–POC ratios ranged from -15.0 ‰ to -23.2 ‰ and 0.055 to 0.076, respectively. When taken as a Cartesian duplet, the above range of isotope and elemental ratios suggested that the OM source was primarily micro-algae, with significantly smaller contributions from seagrass and catchment soils (see Chapter 6).

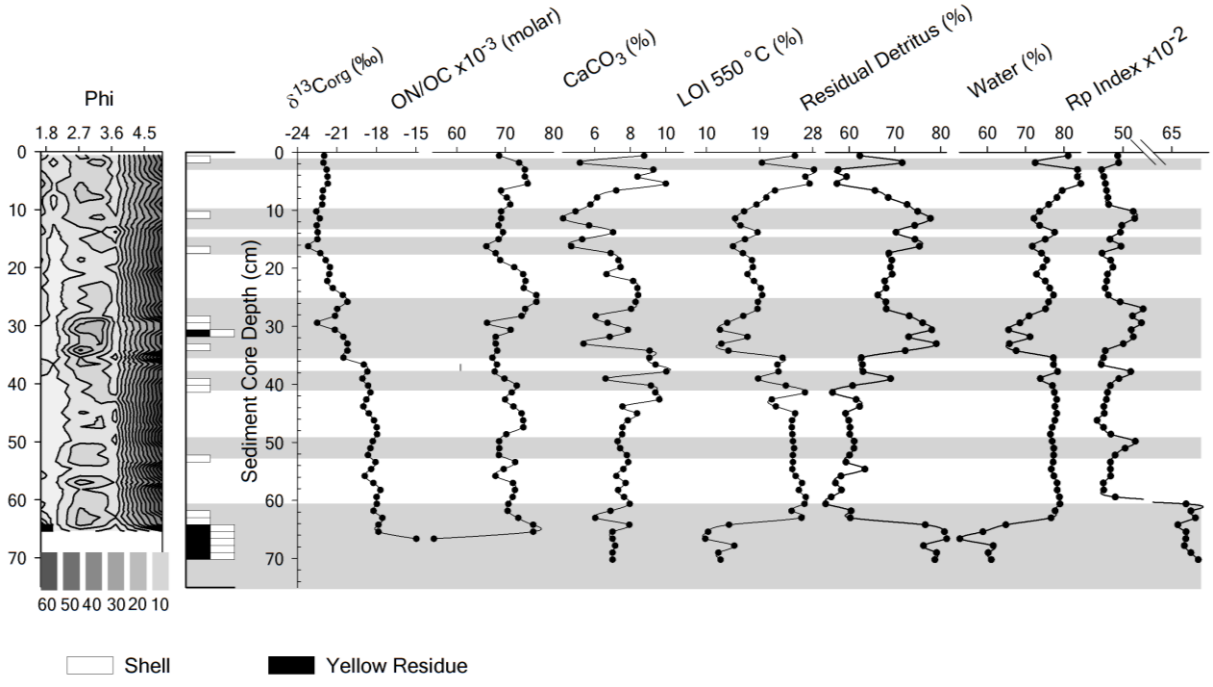

Figure 4.6. Content variables, shells and pyroxene clays (yellow residue) down the Upper Middle Basin sediment core LSPMB206.
The yellow residue appeared after LOI 950 °C and was identified as due to the interaction of calcium carbonate and pyroxene clays (see text). The particle size distribution was measured as phi from the size of the sieve stacks (see Chapter 2). The key shows the percentage of size categories as phi.

4.5.1.2. Stratigraphy

The grey bars (see Figure 4.6) represent the positions and extent of discontinuities from baseline trends, analysed after the fact, to assist in the comparison between the variance of content and quality variables. This suggests the premature conclusion that the total number of

peaks and troughs (with the exception of the Rp index) was not represented by any one content or quality variable, and baseline trends between discontinuities ranged from non-linear to stationary.

Overall, it was found for the content variables LOI 550 °C, RD and water content, non-linear baseline trends, and peaks or troughs followed each other relatively closely, but not in constant proportions (see Figure 4.6). Baseline trends differed down the core for the above variables and for $CaCO_3$. The trends fell (or rose in the case of RD) down the sediment core from around 3 cm, and by 46 cm the baseline trend had reversed (see Figure 4.6). With the exception of $CaCO_3$, which remained relatively constant below 61 cm, the peaks in the discontinuities from the remaining content variances converged at the same depths down the sediment core (see Figure 4.6). In contrast, the Rp index peaks were on a stationary baseline trend and, with the exception of an extra peak at around 49 cm to 53 cm, arguably followed the content discontinuities, although not always their shallower upper boundaries (*e.g.* 25 cm; see Figure 4.6). During combustion (LOI 950 °C), a distinct yellow residue formed within some of the horizons instead of the usual brick red associated with sediment residue. Subsequent X-ray analysis indicated that the yellow residue had formed in the presence of calcium carbonates and iron-laden pyroxene clays (see Appendix A).

The $\delta^{13}C_{org}$ and ON/OC profiles showed little correlation with each other or to the rest of the signals. Both depth profiles had generically different baseline trends and/or deviations from their baselines (see Figure 4.6). The $\delta^{13}C_{org}$ profile remained relatively invariant down the sediment core to around 46 cm, and was significantly heavier below 46 cm (see Figure 4.6). The ON/OC profile displayed an apparent periodicity about a relatively invariant trend down the length of the core (see Figure 4.6). Indeed, the capacity of $\delta^{13}C_{org}$:ON/OC duplet variance for detecting flood events was surprisingly poor and probably reflects importance of flood remobilisation and re-deposition of littoral sediments over the deposition of catchment OM.

Sub-tidal to inter-tidal gastropod and mollusc shells and shell debris appeared to occupy all discontinuities as a group (see Figure 4.6). However, it should be noted that the shells might have come from an inter-tidal tidal habitat belonging to an elevated mid-Holocene shoreline. The ^{14}C age of the *Spisula trigonella* shells (503 years BP to 791 years BP; see Table 4.2) was much older than the presence of unsupported ^{210}Pb activity would suggest (<150 years, see Section 4.8) and closer to the age of the elevated mid-Holocene shorelines (Mazebar, C., 2007, unpublished data, Dept of Mines, Tasmania).

Table 4.2. ^{14}C dates of inorganic carbonate of shells from the Upper Middle Basin and Lower Middle Basin sediment cores.
The corrections for reservoir effects are from data taken from Bass Straight marine reservoir effects (between Tasmania and the Australian mainland [Reimer and Reimer, 2006]), with the caveat that coastal water masses may also be influenced by three other possible sources: the Leeuwin Current (Western Australia), the East Australian Current, and the Southern Ocean.

Sample Core and Facies	Lab Code	Sample Species	Radio Carbon Age yrs	Standard deviation 1σ	ΔR (14C yrs)	Lower calibration 1σ	Upper calibration 1σ	Median Probability
LSPMB206;36.6cm	OZK961	Bivalve Spisula trigonella	503	38	-13 ± 120	0	384	167
LSPMB206;70.2cm	OZK962	Bivalve Spisula trigonella	791	41	-13 ± 120	146	644	421
LSPMB107;99cm	OZK963	Bivalve Mactra pusilla	2353	44	-13 ± 120	1700	2307	1999
LSPMB107:44.8cm		Shell Fragment	Modern (post bomb)		-13 ± 120			

However, the shells and shell debris did not occupy all of the content or Rp index discontinuities, nor were their distributions always contiguous within those discontinuities (see Figure 4.6). There was a similar non-contiguous depth profile for the appearance of the yellow residue (see Figure 4.7), which was particularly prevalent within the largest of the two shell masses (around 28 cm to 35 cm and >61 cm).

Figure 4.7. Sediment residues after combustion at 950 °C (2 hr).
The stratigraphic variance down the sediment core can be followed from the bottom to the top, then right to left of the photograph. Note the speckled appearance in the yellow residue found in the presence of carbonate salts and iron-laden pyroxene clays (see Appendix A). The capped cups mark the positions of in-house sediment standards for inter-batch and intra-batch calibrations (see Chapter 2).

The discontinuities in the Rp index were the only examples of an overlap between content and quality discontinuities and shell residue markers. However, the peaks in the Rp index stratigraphy were not always clear, such as in the case of the relatively small Rp index peak (0.5) at 16 cm (see Figure 4.6), which could arguably be the result of a stochastic outlier. Further, the Rp index discontinuity boundaries were not always the same as other content variables and the extra Rp index peak (at around 53 cm) was only coincident with one weak signal, namely, the presence of a single gastropod shell near the border of its deeper boundary (see Figure 4.6).

Clearly, before the Rp index peaks can be used as a universal event marker, there is a need to include other more obvious convergent peaks or troughs from other signals with a robust explanation to support the presence of less distinctive Rp index peaks. The following hypotheses represent the extremes of two alternative sets of postulates but does not discount a different mixture of postulates as plausible complete explanations:

- Hypotheses 1. The elevated Rp index resulted from the deposition of low organic sediments with relatively high fluvial clay content (RD) and/or fine shell debris (see Chapter 3). The incomplete convergence of content component peaks and boundaries and the non-contiguous nature of biomarker profiles with the Rp index reflected the variability of flood signals due to variability in flood magnitude and temporal structure. The extra Rp index peak (at 53 cm) was the result of a yet unrecognised flood event signal.
- Hypotheses 2. The troughs in content variables (LOI 550 °C, $CaCO_3$) and matching peaks in RD content were the result of flood deposition and/or the net effects of post-depositional changes. For example, the surface discontinuity was result of a loss of water by surface sediment compaction and early loss of OM and $CaCO_3$ (from mineralisation and dissolution) after a previous (deeper) increased supply of autochthonous OM (net basin primary productivity). The remaining content variance down the sediment column was not the result of a depositional event but the result of relative changes in the supply of autochthonous OM. The shell debris and clays markers (yellow residue and total iron) were a set of non-contiguous false event positives that elevated the Rp index.

4.5.1.3. Evidence for Hypotheses 1

The Little Swanport estuary has experienced a number of larger pivotal flood events (see Figure 4.2) that exhibited a range of different temporal structures, ranging from a simple rapid rise and slower decay (*e.g.* 1923; see Figure 4.8) to a number of successive rises and decay

sequences (*e.g.* 1960; see Figure 4.8) all of which is consistent with a layered structure down a depositional facies. Further, the ages and intertidal habitat of the fossil bivalve *Spisula trigonella* (see Table 4.1) are consistent with the age and current position of mid-Holocene sea levels, suggesting they entered the estuary through large flood inundations. Mid-Holocene sea levels were measured between 1 m to 2 m above present sea level around southeast Australia (Sloss *et al.*, 2007). For southeast Tasmania, mid-Holocene net isostatic rebound is considered to have been smaller, yet still greater than present day sea-levels (Mazebar, C., 2007, *pers. com.*, unpublished data, Dept of Mines, Tasmania). Indeed, support for flood inundation (up to 2 m above sea level) was observed from a recent flood in 2009.

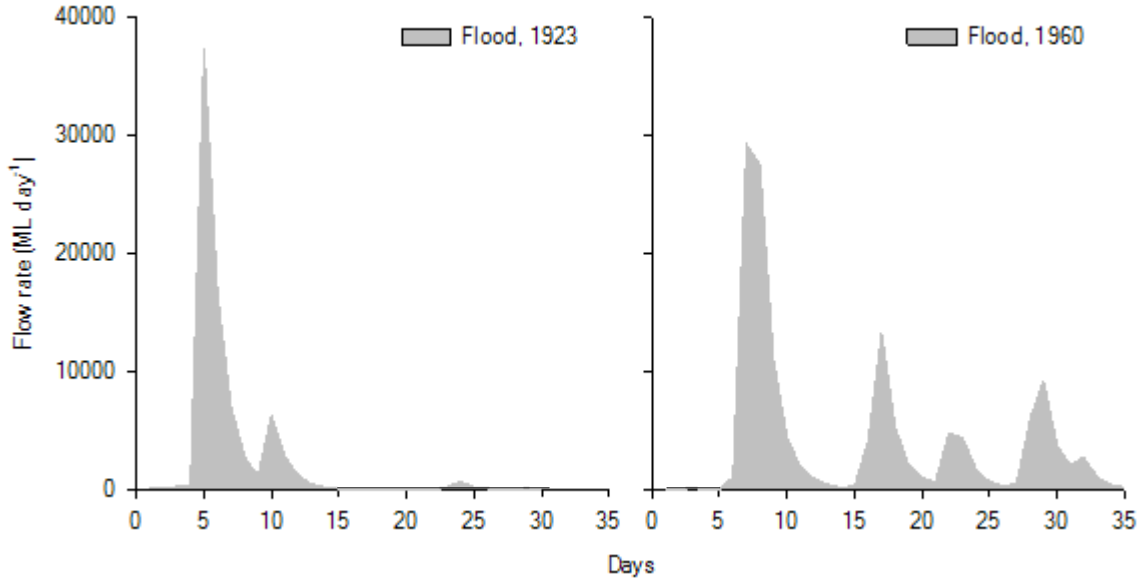

Figure 4.8. The daily average river flows of the Little Swanport River during the two largest floods of the twentieth century.
The river flows were calculated from local rainfall data and catchment/dam modelling (SKM, 2004).

The mechanisms by which the elevated values in the Rp index changes became manifest has already been attested to within the transect study (see Chapter 3). An Rp index above 0.5 was found to be due to significant proportions of both pyroxene clays and shell carbonate hash, associated with high-energy environments. Thus, with the exception of the extra peak centred around 49 cm to 53 cm, the Rp index peaks are consistent with the origin of other convergent content peak and trough discontinuities. Namely, a decrease in supply of OM (LOI 550 °C) was associated with high fluvial sands (RD) content and the remobilisation of shells from the inter-tidal zone and supra-tidal zones during peak flood times.

A high freshwater particulate humic-acid content is the most likely explanation for the additional Rp index peak (49 cm to 53 cm), given that the peak was coincident with the fall in

the ON/OC ratio (see Figure 4.6). Humic-acids have a characteristic elevated Rp index (0.63) coupled with a low ON/OC ratio (0.051). The above duplet is not shared by any other living or detrital organic source (Kristensen, 1990). Further, significant inputs of humic-acids to lower estuarine sediments can conceivably be associated with strong flows and floods as they flocculate near the freshwater–seawater interface, located at the base of the deep-water salt wedge (Sholkovitz and Copland, 1981; Karbassi *et al.*, 2008).

4.5.1.4. Evidence for Hypotheses 2

Theory 1 would seem the more plausible choice given the current weight of evidence. However, the surface variance due to compaction and early organic and inorganic mineralisation and dissolution cannot be discounted. In particular, when delineating the upper boundary of the second depositional facies from baseline variance as somewhere between 3.5 cm to immediately after 11 cm (see Figure 4.6). Indeed, the boundary positions of the remaining facies, as marked by discontinuities in content and quality variables, did not completely converge. Under these circumstances, it was tempting to use the maximum facies thickness selected from a group of signals. However, such an approach assumes that the borders of a deposition facies could be represented by the selection. Consequently, there was a need to apply the convergence of two, arguably less sensitive but robust cause and effect conceptual models, namely, the absence/presence of faecal pellets and Glyph Analysis (see Chapter 3) for a more direct assessment of baseline trends and facies boundaries.

4.5.1.5. Copepod faecal pellet presence/absence

It was postulated (see Chapter 3) that a significant presence of copepod faecal pellets could be quantified by a parallel variance between the OM content of the pellet's size fraction and the OM content from the remains of the unpackaged fine fraction. In other words, the organic content of the faecal pellets should closely reflect the egested fine fraction in a way that similarly sized sand/shell fraction would not (see Chapter 3). Consequently, absence of copepods and their faecal pellets, recorded during flood events (Crawford *et al.*, 2005), would result in a change from a positive correlation or no/inverse correlation between faecal pellet fractions, and fine fraction OM content.

The clearest decoupling of OM content between the total and fine fraction was from 25 cm to 35 cm and below 59 cm to the base of the core (see Figure 4.9). The decoupling is consistent with the absence of faecal pellets and supports the contention that the largest of discontinuities were the result of flood deposition and not the result of falls in autochthonous

OM supply. The boundaries that marked the decoupling of the sand/faecal pellet fraction from the total and fine fraction were not as clear down the rest of the core. The reasons for lack of clarity were twofold: (1) the influence of additional OM variance from seagrass pieces (>315 µm), and (2) the relatively low signal to noise ratio and sample resolution across the narrower discontinuities.

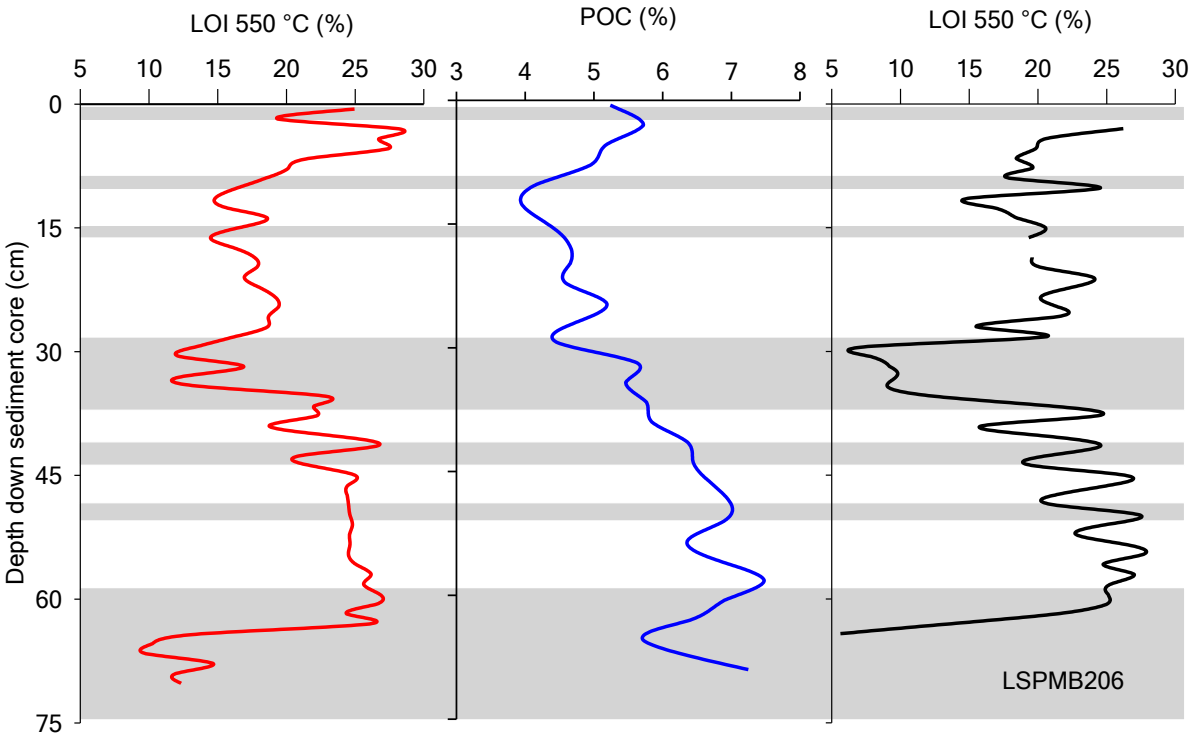

Figure 4.9. The OM content of sediment size fractions as either POC or LOI 550 °C used to infer the presence of faecal pellets down the Upper Middle Basin sediment core LSPMB206.
Total sediment (—);the faecal pellet or quartzite fraction (<250 µm to >100 µm) (—);the fine fraction (<76 µm) (—). The shaded areas represent deposits from high-energy events such as floods (see text for their assignments).

Despite the lack of sensitivity, the decoupling of the OM content of the fine fraction from the sand/faecal pellet fraction content can be discerned within horizons of the total water content and Rp index troughs and peaks. This included the extra Rp index peak not shared by the other total content variables (49 cm to 53 cm; see Figure 4.9) but shared by the LOI 550 °C within the fine fraction. Further, it was clear that the fall in total LOI 550 °C from around 3 cm to 9 cm (see Figure 4.9) was not the result of flood deposition, but rather of baseline variance. There was no decoupling of the OM variance between the sand/faecal pellet fraction and the fine fraction until immediately below 9 cm. The 9 cm upper boundary for the second discontinuity from the surface was in agreement with the upper boundary of the corresponding Rp index peak (see Figure 4.6).

Glyph Analysis

A convergence between a plausible Glyph Analysis (Chapter 3) with the conclusions of the faecal pellet model was used to evaluate the robustness of event identification and the underlying assumptions behind both models (a mixed RA). Glyph analysis attempts to determine cause and effect using neutral models of relative rate of supply of the lithogenic fraction (RD) to the rate of supply of autochthonous OM (LOI 550 °C). The analysis is based on a coupling of major biogenic content variables (BSi $CaCO_3$, LOI 550 °C) to an independent RD supply to construct all equivalent neutral models (see Chapter 3 for the details of construction of Glyph neutral models).

Similar to the faecal pellet model, the resolution between Glyph patterns was relatively coarse and assigning the sediment content and content ratio variance to a set of possible Glyphs was not always clear, such as between 12 cm and 17 cm (see Figure 4.10). Nevertheless, the Glyph within the largest of the two discontinuities (25 cm to 35 cm and >61 cm) clearly shows that a fall in OM content was controlled by both a fall in the OM supply and an increase in lithogenic supply (see Figure 4.10). The supply variance was consistent with the deposition of sediments with a high content of fluvial sands and low content of OM from the fluvial deposition zones (Roy *et al.*, 2001).

The set of Glyph neutral models was not able to resolve the remaining discontinuities but was able to distinguish four types of baseline variance. In particular, the transition around 4 cm to 11 cm (red) largely agreed with the faecal pellet model (see Figure 4.6) and appeared to be the result of an increase in supply of both lithogenic and OM sources. The reasons behind the above supply variance were not immediately clear, but it did suggest a period of greater baseline net accretion, possibly by re-suspended littoral sediments with a higher fluvial sand and OM content. The remaining baseline Glyphs suggested a dynamic environment. The major yellow Glyphs below 36 cm, which bordered an invariant lithogenic and OM supply (grey), indicated that there were two periods of increasing OM supply from increases in net basin micro-algal productivity. The timing of the increased productivity appeared to be immediately after the oldest flood event and *circa* a younger flood event marked by the extra Rp index peak (49 cm to 53 cm; see Figure 4.6). In contrast, the green Glyph, between 16 cm to 25 cm, implied that the fall in OM content was controlled by an increase in lithogenic supply rather than being synonymous with flood events. However, the source of the lithogenic material was not clear. The material could conceivably be supplied from either fluvial or marine sands; that is, from an increase in fluvial deposition during an inter-decadal period of

relatively wet weather, or from an increased supply of marine sands as a result of a larger entrance exposure by an increase in flood frequency (Rustomji, 2007).

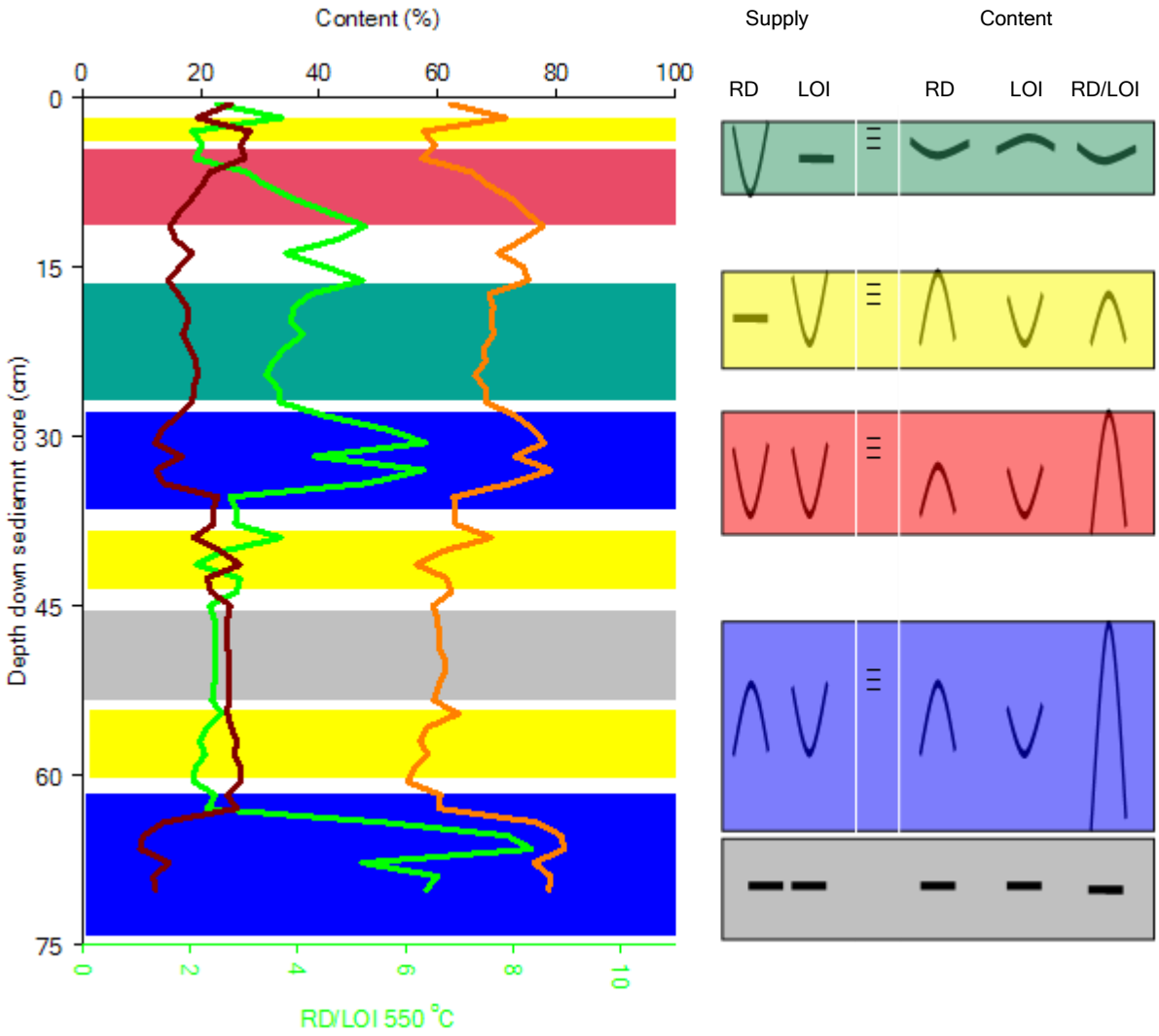

Figure 4.10. Glyph Analysis for the Upper Middle Basin sediment core LSPMB206.
(—) RD, (—) total OM as LOI 550°C and (—) RD/LOI 550 °C.

4.5.2. Upper Middle Basin sediment core LSPMB2B08

4.5.2.1. Content and quality signals

BSi (needed for RD calculation) organic stable isotopes and elemental ratios were not available for sediment core LSPMB2B08 due to slow analytical turnaround times and material resources. In response, a relatively simple total iron analysis was added to the suite of variables for a more sensitive quantifiable measure of iron associated with pyroxene clays (yellow residue) or 'dissolved iron' supplied from the river that may have co-precipitated with any humic-acid floccs (Sholkovitz and Copland, 1981; Karbassi *et al.*, 2008) postulated as present within Upper Middle Basin sediment core LSPMB206.

The major sediment contents and Rp index depth profiles for core LSPMB2B08 in relation to their size fraction spectrum are illustrated in Figure 4.11. The grey bars locate the positions of flood facies after the fact, to assist in comparison between signals. Similarly, to core LSPMB206 there was bimodal size fraction distribution within all the core horizons that peaked at the sand/faecal pellet size fraction (phi 2.7) and towards the fine fraction (phi 5.0). Consequently, the origin of the peak at phi 2.7 cannot be determined by size distribution alone. Both Upper Middle Basin cores (LSPMB2B08 and LSPMB206) had a similar range of $CaCO_3$, LOI 550 °C and water content: 4.4 % to 8.7 %, 11.3 % to 28.0 % and 48.3 % to 85.8 %, respectively. However, the baseline Rp indexes found down core LSPMB2B08 (around 0.53) were significantly larger than were those found down core LSPMB206 (around 0.45), despite the fact that both sediment cores had similar maximum values located within their deepest discontinuities (0.68 and 0.69 for sediment core LSPMB2B08 and LSPMB206, respectively). For the most part, the major content profiles and the Rp index profile for LSPMB2B08 were nosier than for LSPMB206. In particular, for LSPMB2B08, the depth profile of the $CaCO_3$ content noise to signal ratio was too large for any definitive identification of peaks or troughs.

4.5.2.2. Stratigraphy

The peaks in iron content and the Rp index, with the exception of the surface-elevated iron content, converged down the sediment core. It is probable that the surface iron content was the result of iron redox remobilisation and precipitation immediately above the anoxic–oxic interface (Davison and Heaney, 1978; Burdige, 2006). The peaks in iron content within the largest intrusive shell mass (>80 cm) were more variable than the Rp index and were always accompanied by the appearance the yellow residue (formed after combustion at 950 °C [see Figure 4.11]). Interestingly, the iron content peaks around 28 cm, 40 cm and within the shallower large shell mass (around 56 cm to 78 cm) were not accompanied by the presence of a yellow residue (see Figure 4.11). The reasons for the lack of consistency are not clear. Perhaps the shell debris was larger than the diameter of its 1 mL sampling syringe (see Chapter 2) and thus the shell carbonate was not available in sufficient proportions with pyroxene clays in the production of the yellow residue during combustion (>550 °C). Alternatively, the iron might have been associated with freshwater humic-acid floccs and not with pyroxene clays.

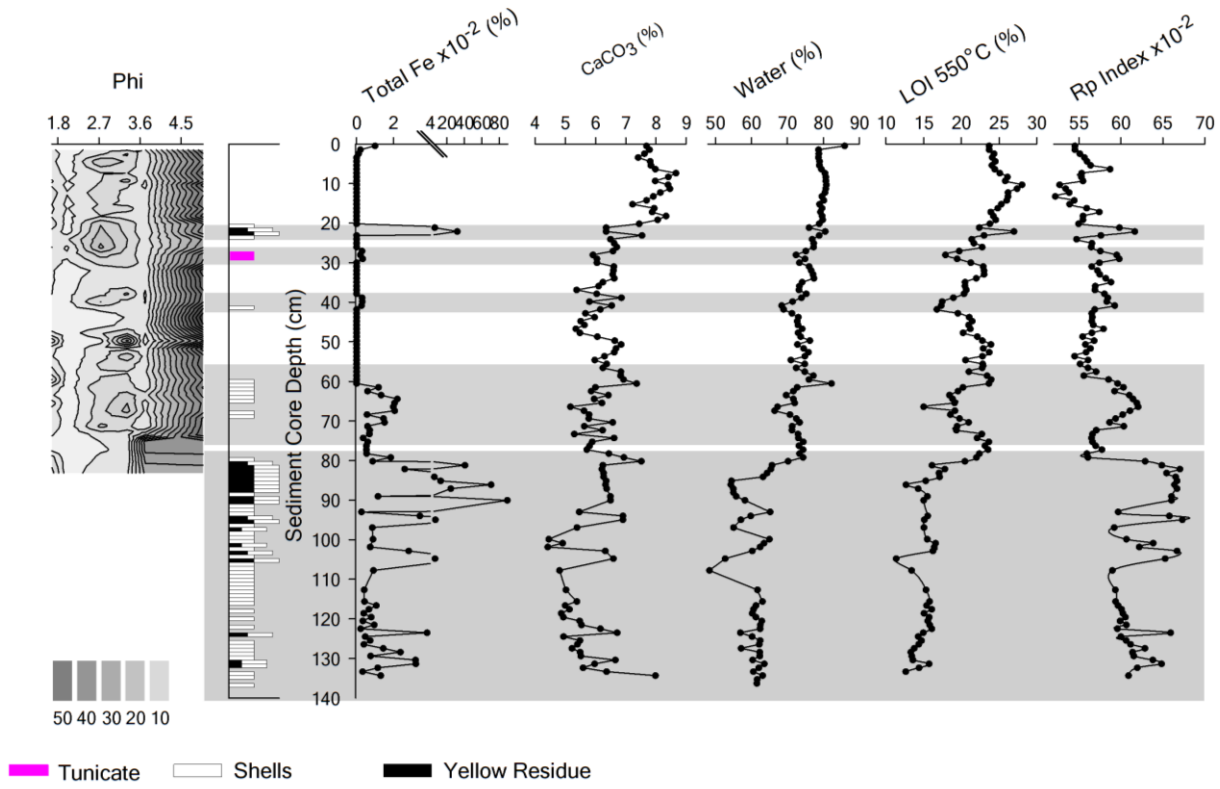

Figure 4.11. Content variables, shells and total iron down the Upper Middle Basin sediment core LSPMB2B08. Yellow residue refers to the sediment appearance after LOI 950 °C in the presence of $CaCO_3$ and iron-laden pyroxene clays. Carbonate refers to LOI 950 °C as $CaCO_3$ confirmed only after acid addition and re-analysis (see Chapter 2). The contours represent particle size distribution as phi. The key gives the percentage of size categories as phi. The grey bars are the suggested positions of flood facies.

Largely, troughs in water content and LOI 550 °C also followed the Rp index peaks, and at times had a clearer signal to noise ratio. Indeed, the larger distinct LOI 550 °C trough at 40 cm, together with the elevated iron content, confirmed the presence of a relatively small Rp index peak at that depth. In contrast, the clearer Rp index peak and iron peak around 24 cm supported evidence for an event deposition where there was water content or a LOI 550 °C trough (see Figure 4.11). The reasons for such a decoupling from LOI 550 °C and water content is, again, unclear. Nevertheless, the pattern is consistent with two plausible exceptions to an implicit rule that considers most of the content variance is associated with supply of finer biogenic and lithogenic material; namely, additional contribution to the sediment water and OM from juicy seagrass leaf fossils and/or relatively high freshwater humic-acid floccs content and its associated iron.

4.5.2.3. Discontinuity boundaries for sediment core LSPMB2B08

The boundaries of many of the discontinuities in sediment core LSPMB2B08 were not as clear as those within the sediment core LSPMB206. The lack of clarity may have been due to a number of factors that includes (1) nosier content variables and Rp index profiles; (2) the

proximate nature of iron, shell and animal markers under the umbrella of content and Rp index troughs and peaks; (3) incomplete convergence between shells and iron markers; and (4) incomplete convergence of boundaries between content and Rp index peaks and troughs (see Figure 4.11). For example, based on the total iron or water content, the deeper boundary of the shallower notable mass arguably ranged from 70 cm to 72 cm (see Figure 4.11). Based on LOI 550 °C profiles, the boundary appeared to sit close to 80 cm, which was immediately adjacent to the shallower boundary of the noted mass at the base of core (see Figure 4.11).

4.5.2.4. Event boundaries: Faecal pellet presence/absence

As in sediment core LSPMB206, the boundaries were best discerned from the divergence between the fine fraction's OM and the OM within the sand/faecal pellet fractions (see Figure 4.12). The figure clearly shows a divergence between the fine fraction and the faecal pellet/sand fraction down the two bottom notable masses from around 56 cm to 74 cm and >78 cm, separated by 3 cm to 4 cm of baseline sediment. The sampling resolution was not sufficient to separate the two discontinuities between 22 cm and 31 cm (see Figure 4.11), but was sufficient to resolve the remaining discontinuity (around 40 cm; see Figure 4.11) as a notable switch to an inverse correlation, with both the total LOI 550 °C and the fine fraction LOI 550 °C.

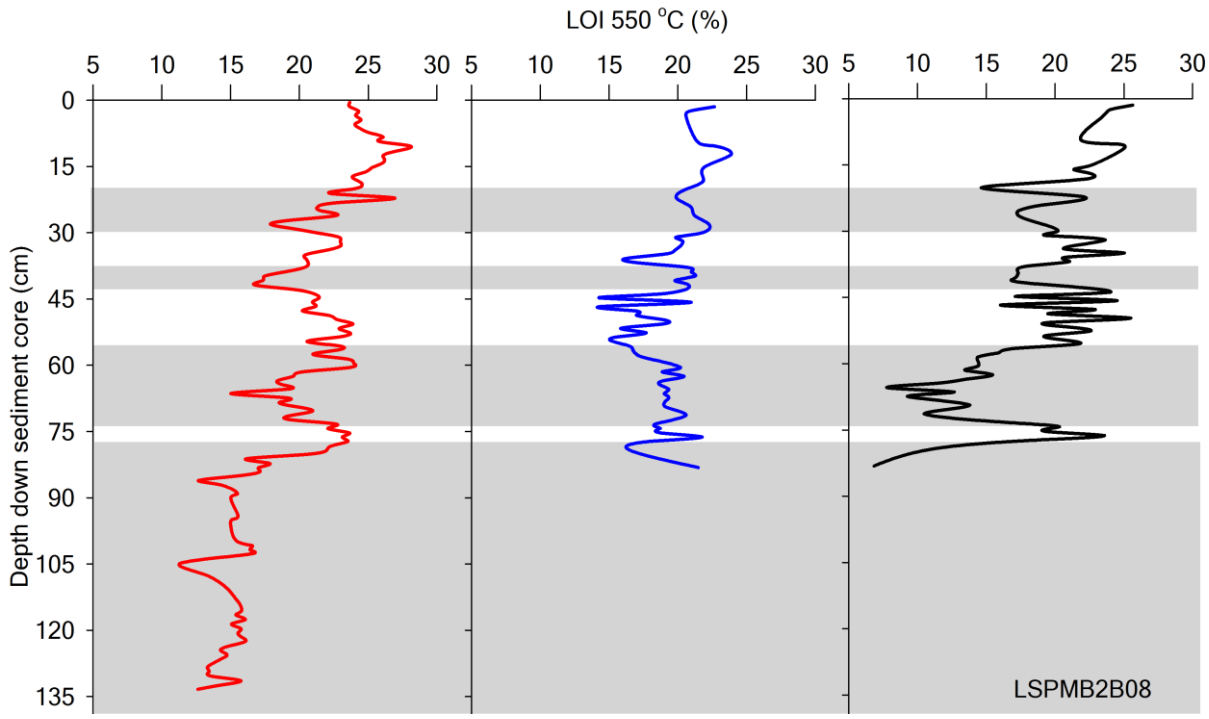

Figure 4.12. Organic matter content of sediment size fractions used to infer the presence of faecal pellets down the Upper Middle Basin sediment core LSPMB2B08.
The OM content within three fraction sizes as either POC or LOI 550 °C. (—) Total sediment; (—) <250 µm to >100 µm faecal pellet or sand fraction; (—) <76 µm fine fraction. The grey shaded areas represent the suggested deposits from high-energy events, such as floods (see text for their assignments).

4.5.2.5. A false positive?

There is always the possibility that the choice of signals was not sufficient to identify and confirm all types of flood signals. For example, notwithstanding noise among content variables and the Rp index, a small but significant contiguous asymmetrical peak in the Rp index centred at 37 cm could be identified (see Figure 4.11). However, the peak was not coincident with any accompanying fall in LOI 550° C, $CaCO_3$, water content or appearance of event markers. Instead, the accompanying LOI 550 °C and $CaCO_3$ variances were counter to what was correlated within the rest of the core. Hence, a value judgment was made, based on the weak inference and parsimony, that the apparent Rp index peak at 37 cm was nothing more than baseline noise.

4.6. Relative stratigraphic variance between the Lower Middle Basin sediment cores

The absence of features distinguishing the organic content with depth among the Lower Middle Basin sediment cores supports the conclusion that the cores were under the influence of similar depositional environments (see Figure 4.13). However, there were some small absolute differences. Within the top 44 cm the LOI 550 °C for core LSPMB106 was 9.7 % greater than core LSPMB107 but with a near identical total organic carbon (TOC) content. The larger LOI 550 °C might reflect the core's closer position to the littoral zone and its particular lithogenic material's water content (Mook and Hoskin, 1982).

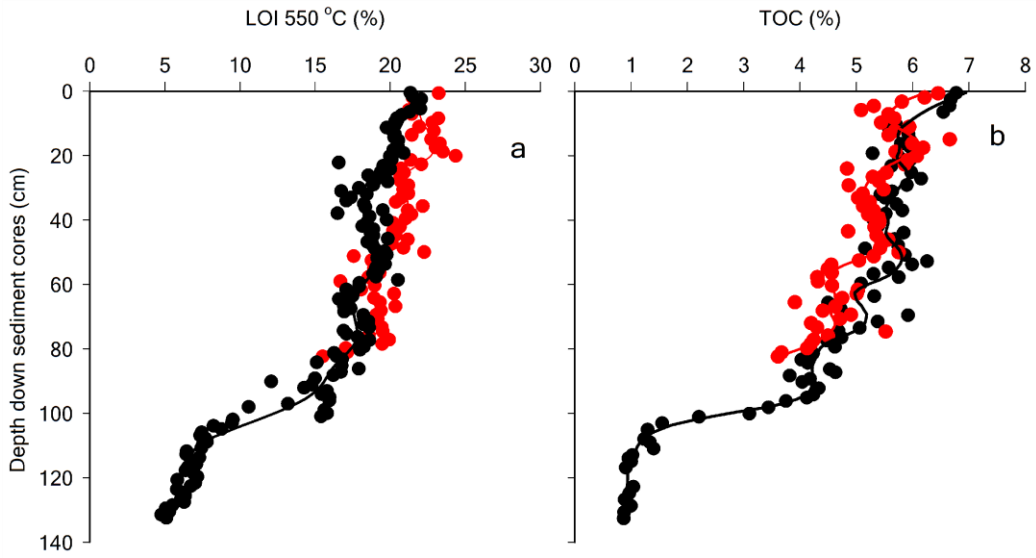

Figure 4.13. LOI 550 °C and TOC down the Lower Middle Basin sediment cores..
(●) Sediment core LSPMB107, (●) sediment core LSPMB106. Profile trends were calculated using a LOESS smoothing function that extrapolates with a β-spline second order polynomial from an adjacent 0.3 % of the data set.

4.6.1. Lower Middle Basin sediment cores LSPMB107 and LSPMB106

4.6.1.1. Content, quality and marker signals

Similar to the Upper Middle Basin cores, the Lower Middle Basin cores had a bimodal size fraction distribution throughout the sediment core (see Figure 4.14). However, below 100 cm, the bimodal structure was particularly intense and dominated by the larger fraction (phi 2.7). The similarity between the OM signals, RD and water content down as far as 78 cm was not always reflected in the absolute values and/or stratigraphic variance of other quality and content signals[20]. The range of $\delta^{13}C_{org}$ between the two sediment cores was similar, -21.6 ‰ to -18.6 ‰ and -21.3 ‰ to -18.8 ‰ for sediment core LSPMB107 and LSPMB106, respectively, but there was a distinctive peak of heavier $\delta^{13}C_{org}$ centred around 19 cm down the sediment core LSPMB106 that was not recorded down sediment core LSPMB107 (see Figure 4.14). Relative stratigraphic variance between the ON/OC down the two sediment cores was similar, but their ranges over comparable depths were significantly different, 0.09 to 0.078 and 0.094 to 0.119 for LSPMB106 and LSPMB107, respectively. The above differences reflected an additional contribution from fossil seagrass leaf pieces within sediment core LSPMB106 due to its closer proximity to the adjacent seagrass meadow (see Chapter 7).

There was a similar range of values for the remaining minor content variable (LOI 950 °C) between the two cores, 8.5 % to 4.3 % and 8.9 % to 5.5 % for LSPMB107 and LSPMB106, respectively. There was a notable difference, however, down one strata (10 cm to 36 cm; see Figure 4.14). Again, the generally larger values and difference within sediment core LSPMB106 probably reflected an additional contribution from calcareous epifauna associated with an increase in supply of seagrass pieces (see Chapter 7).

4.6.1.2. Event depositional facies

The only strong evidence of a depositional event was the appearance of terrestrial grasses and some shell debris (see Section 4.4.2) immediately below 78 cm to 80 cm for cores LSPMB106 and LSMB107, respectively. The appearance of debris was followed by a relatively complex falling trend in RD content and LOI 550 °C down core LSPMB107 to around 100 cm (see Figure 4.14b). In contrast, there was relatively little variance in LOI 950

[20] The Rp index results for LSPMB107 were considered unreliable. During the analysis, the working standards had an unacceptable range of values due to the deterioration of the furnace at this time (a difference of 22 % at LOI 520 °C and up to 49 % at LOI 280 °C). Insufficient material remained to repeat the analysis.

°C between 78 cm and 80 cm for core LSPMB106 until the rapid increase from around 100 cm (see Figure 4.14b).

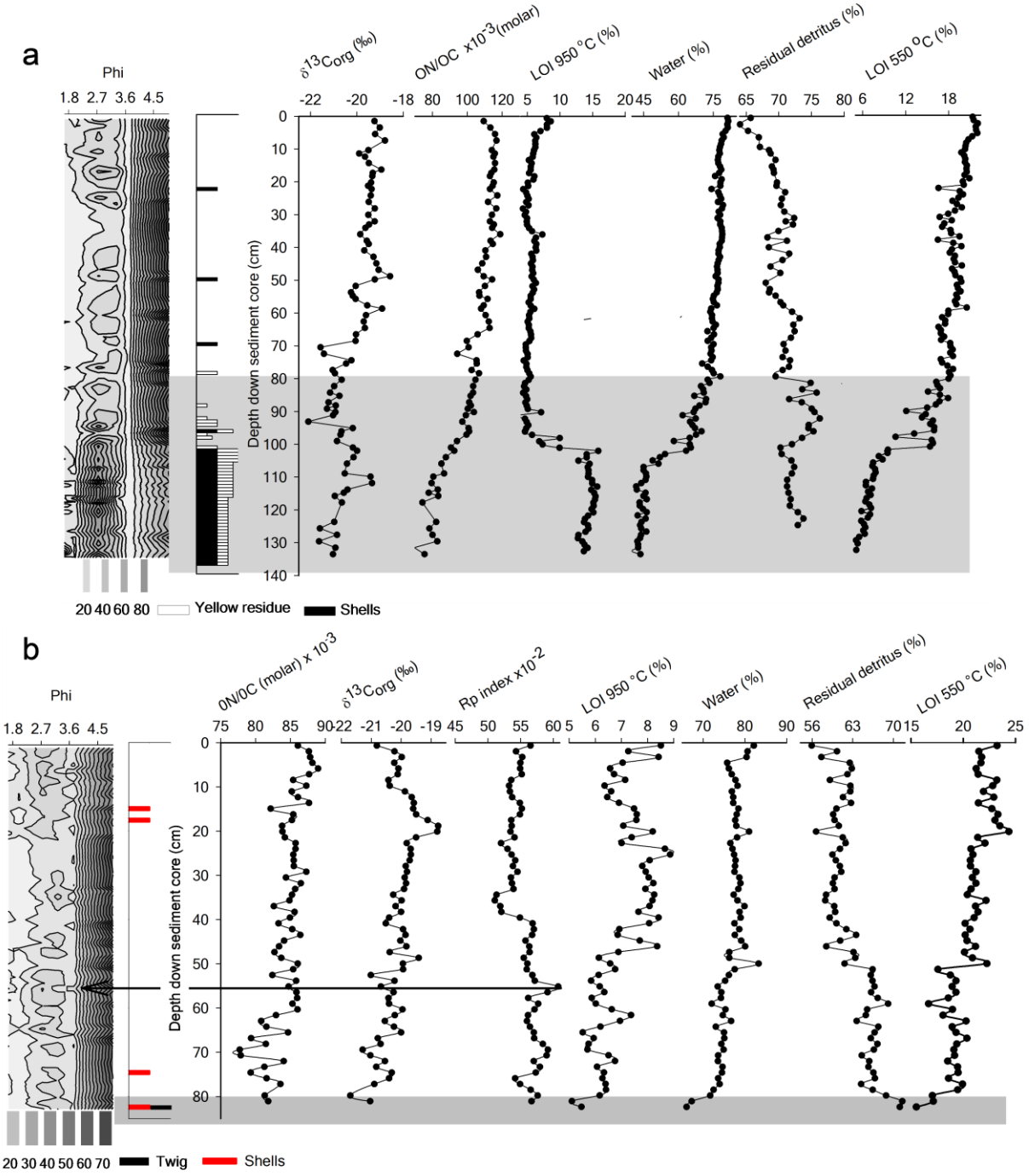

Figure 4.14. Sediment size fractions, shell and pyroxene clay markers with available content and quality variables down the Lower Middle Basin sediment cores.
(a) LSPMB107 and (b) LSPMB106. The grey bar marks the suggested position of intrusive tsunamite facies (see text for analysis).

The above differences were reflected in the proximate appearance of shell fragments and pyroxene clays (yellow residue) from 78 cm to a large mass of shells and shell debris from below 100 cm. The shell debris was a mixture of fragments and whole valves of inter-tidal

and sub-tidal marine and upper estuary species (see Table 4.1) and was not typical of the deeper extraction sites depth or age. The age of the bivalve shell was around 2350 years BP (see Table 4.2), at a depth (80 cm) which is not consistent with the rate of sedimentation for similar water bodies (0.07 cm yr^{-1} to 0.6 cm yr^{-1}[OzCoasts, 2006])

Above 80 cm, there was some evidence suggesting other event disturbances. Occasional small pieces of shell debris (2 mm to 3 mm) were found scattered through the core (see Figure 4.14b) and there was a peak in the Rp index between 55 cm to 56 cm (LSPMB106). The peak was also accompanied by a small shift in the particle size from a peak centred around the usual phi 2.7 to phi 3.74. However, the Rp index peak, and the presence of shell debris, was not marked by peaks or troughs in other variables (see Figure 4.14b) and the significance of the shift in particle size was not clear.

4.6.1.3. The event boundary position: Faecal pellet presence/absence

The above content signals and markers show two plausible event boundaries, from either 78 cm or 100 cm (see Figure 4.14a). Choosing the 100 cm as the facies boundary could imply a dynamic period of shell and pyroxene clay false positives on rising muddy baseline sedimentation. Conversely, a boundary at 78 cm suggests a high-energy event deposition with a layered internal structure, such as the result of particle sorting during the formation of distal turbidites (Middleton, 1993), tsunamis or storm deposits (Dawson and Shi, 2000).

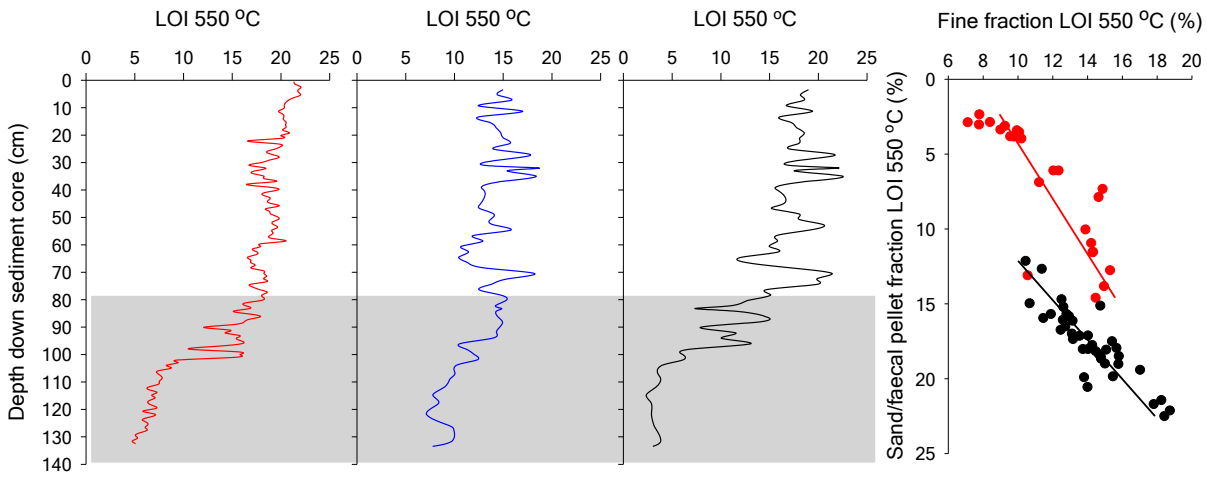

Figure 4.15. LOI 550 °C of sediment size fractions used to infer the presence of faecal pellets down the Lower Middle Basin sediment core LSPMB107.
(—) Total sediment, (—) sand/faecal pellet fraction (<250 µm to >100 µm), and (—) the fine fraction (<76 µm). The grey bar represents depositional facies (see text). The chart to the right shows the results of least squares linear models between the LOI 550 °C (OM) of the fine and sand/faecal pellet fractions for: (●) baseline sediments, and (●) the bottom depositional facies.

.

The divergence of profile variance of the OM content of the sand/faecal pellet fraction from and the profile variance of the OM content of the fine fraction marks the absence of pellets at the 78 cm (see Figure 4.15). This is consistent with the former contention that 78 cm marks the top of a depositional event that contains a layered internal structure. Further, the evenly distributed residuals around a least squares regression above 78 cm, between the fine fraction and the faecal pellet/sand fraction, are consistent baseline sedimentation that reflect the dynamics of water column sestonic supply, egestion and clearance.

4.6.1.4. Cause or effect of lithogenic and organic content: Glyph Analysis

In contrast to the faecal pellet model, the Glyph Analysis marked both the bottom event facies transition zone, between 97 cm and 80 cm, and the consolidated shell zone below 97 cm (see Figure 4.16). The Glyph model that marked the 97 cm to 80 cm transition zone (blue; see Figure 4.16) was consistent with fall in lithogenic supply and a rise in OM supply. Such a transition does discount the position of the facies at 78 cm as suggested by faecal pellet model as it is also consistent with patterns of settlement from distal turbidites (Middleton, 1993) and some tsunamites (Donato *et al.*, 2009). That is, the more buoyant terrestrial grasses and high organic fine fraction settled on top of the denser and larger low organic sand fraction. Below 97 cm, there was no matching Glyph. However, it was identical to the Glyph along the surface sediment into the high-energy Marine Flood/Tidal Delta (see Chapter 3).

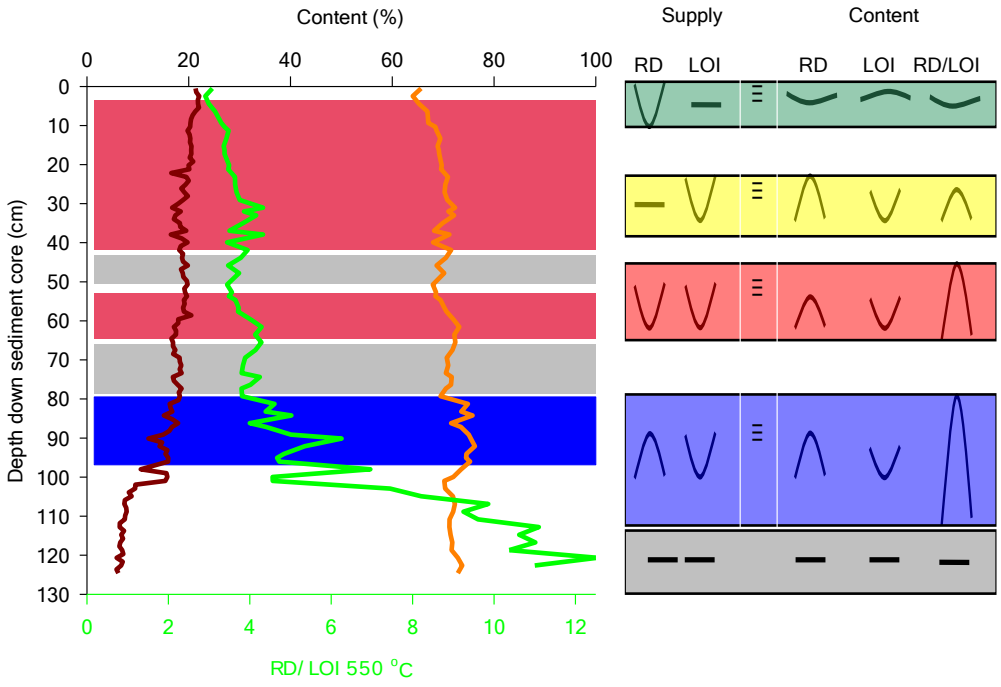

Figure 4.16. Glyph Analysis for the Lower Middle Basin sediment core LSPMB107.
(—) LOI 550°C as a proxy for OM, (—) RD and (—) RD/LOI 550 °C. The Glyph below 97 cm has no example from the conceptual neutral model (Glyph coloured reference table) and represents a period of high-energy dominated by $CaCO_3$ supply (see text).

Above 80 cm, the Glyph did not suggest any other significant depositional event. Interestingly, from around 65 cm to the surface, the content patterns suggested a time dominated by increased lithogenic supply and OM supply (red Glyph; see Figure 4.15). Such a pattern was found in sediment core LSPMB206 as possibly resulting from a recent increase in net accretion due to the re-suspension of littoral zone sediments.

4.6.2. Origin of the event

Clearly, there was strong evidence for a large depositional event from 78 cm to 80 cm down both of the Lower Middle Basin cores. There are a number of plausible possibilities, arguably a tsunami, storm surge, flood or a large king tide (see Section 4.1). By using a scored weight of evidence approach (see below) it was found the most probable event was more consistent with a tsunami (see Table 4.3).

4.6.2.1. Tsunami evidence

Bimodal particle structure: score 1. Studies of tsunami deposits indicate that these deposits are often bimodal (Dawson and Shi, 2000; Goff *et al.*, 2004; Switzer and Jones 2008), provided the sources of the material from entrainment and gathering reflect such a structure (Switzer and Jones, 2008). Indeed, the bimodal particle size structure was a strong feature of the shell facies (see Figure 4.14a). However, the particle structure of nearby contemporary surface sediments (marine tidal delta) had a uni-modal particle size distribution, with no significant clay or silt size fractions (see Chapter 3). Nonetheless, the sediments outside the estuary were sandy within the shallows with a significant silt clay fraction in deeper waters (DPIW, 1998). It is therefore conceivable that the bimodal structure in the shell layer arose from the entrainment of deeper, finer sediments from the tsunami backwash followed by the subsequent flood that gathered up the shell rich beaches of the shallow marine tidal delta.

Sum of all shell categories: score 5. The shell deposit's foraminifera, gastropods, bivalves and sea urchins were predominantly inter-tidal, sub-tidal marine and lower estuarine species (see Table 4.1). Such low spatial fidelity of marine shell species are common to tsunamite deposits (Donato *et al.*, 2008; Morales *et al.*, 2008).

Table 4.3. Weight of evidence for different events in relation to the bottom deposition facies of the Lower Middle Basin sediment core LSPMB107. A score of 1 is consistent with the evidence, 0 is uncertain and -1 is counter. The weight of evidence is the sum of the scores.

Shell presence low fidelity	Terrestrial plant material only on top of facies	Abundant whole, fragmented and articulated bivalves	Marine shells	Mainly lower estuarine shells	Sediment bimodal size structure	Shells older than facies	Centennial rare event	Event dated *circa* recorded	Weight of evidence score	Event description
1	1	1	1	1	1	1	1	1	9	**Tsunami**
1	0	-1	1	1	-1	1	0	0	2	**Storm surge**
1	0	1	-1	-1	1	1	-1	0	1	**Flood**
0	1	-1	1	1	-1	1	1	1	4	**Emperor tide**

The age of the shell *Mactra pullisa* (2353 yrs ^{14}C [see Table 4.2]), taken from the sediment core's bottom shell layer, suggested that the inundation was consistent with supra-tidal beach wash in close proximity to local shell middens at the entrance of the estuary (Sloss *et al.*, 2007). A recent relatively simple bivalve taphonometric analysis (see Donato *et al.*, 2008), found that storm deposits have no articulated valves and that a high proportion of valves are encrusted, worn away or have a dissolved pitted surface, in contrast to tsunami deposits that contain articulated valves, which are fragmented with stress fractures. It is the latter distribution that most closely resembled the modification of bivalves taphonomy as indicated by samples collected around storm and wave affected intertidal zones (see Figure 4.17). It should be noted that there was a change to a smaller modal size class of shells sampled from the coastal entrance and estuarine littoral zones not found during the original development of the proxy within Sur Lagoon (Donato *et al.*, 2008). The reasons for these differences between size classes are unclear but it may be due to the smaller size of tsunami waves arriving at Little Swanport, making them unable to lift the larger marine shell deposits from their position.

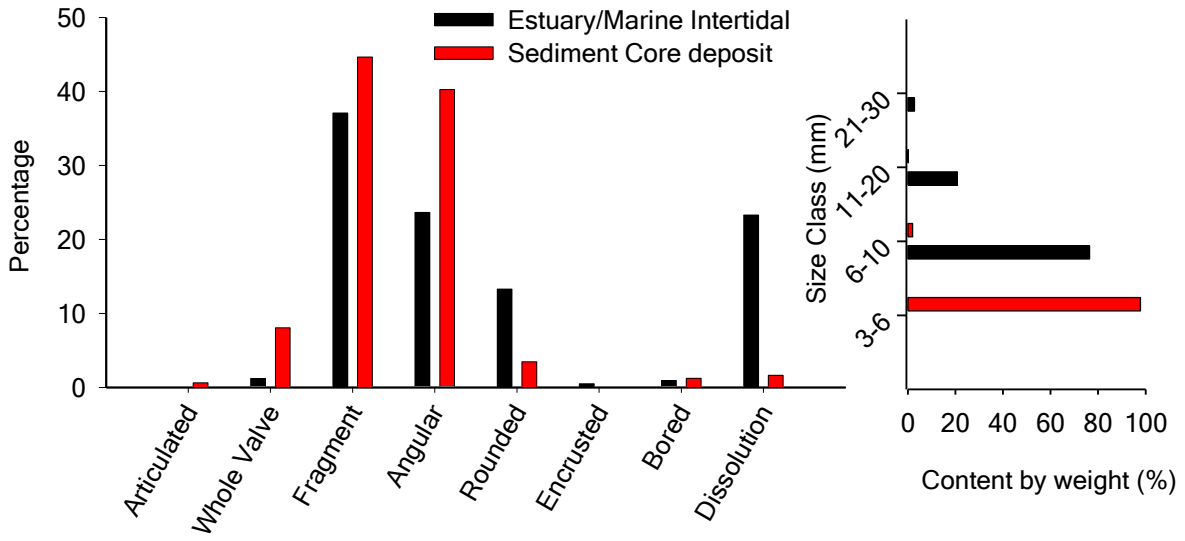

Figure 4.17. Bivalve shell taphonometric character and size classes down the Lower Middle Basin sediment core LSPMB107 and the surrounding contemporary inter tidal zones.
Samples were taken from the bottom facies of the Upper Middle Basin sediment core LSPMB107 and from the inter-tidal regions of the Little Swanport estuary's Marine Flood/Tidal Delta and immediate coastal beaches.

Historical accounts: score 2. Assessing the rarity of the deposition event will depend on *a priori* age of the sediment core. Hence, in a strict sense, the rarity of the event that this analysis was designed to determine cannot be assessed. Nevertheless, the presence of a small but measureable unsupported ^{210}Pb activity towards the base of the core (see Figure 4.22) indicated a maximum age of no more than 100 to 150 years. Only two significant tsunamis

have been recorded over the last 140 years, in 1868 and 1960, both of them generated from Chile (Dominey-Howes, 2007; see Section 4.2).

4.6.2.2. Storm surge evidence

Bimodal particle structure: score -1. Switzer and Jones (2008) showed that storm deposits have a uni-modal structure that reflects the beach face and near shore sediments as found for surface sediments of the Marine/Flood/Tidal Delta (see Chapter 3 and Figure 3.10), and would not be expected to draw up the deeper bimodal sediments from the coastal zone to produce the bimodality found throughout the shell facies.

Sum of all shell categories: score 3. In the same manner as a tsunami, storm surges can rework shell deposits within the marine and upper estuarine inter-, sub- and supra-tidal zones and redeposit them into the estuary (Staff *et al.*, 2002). On the whole, it has been found that storm surges do not carry its depositional shell load far inland (Goff *et al.*, 2004), and in the process their bivalves fragmentation patterns do not change (Callender *et al.*, 2002).

Historical accounts: score 0. Other than recalled accounts of pivotally large storms in 1970 (see Figure 4.1), there was no record of storm surges that would suggest the possibility of estuarine inundation. Although extreme weather events could be expected to be more frequent than once or twice a century, it is uncertain what proportion of storms would be sufficiently large enough to breach the entrance.

4.6.2.3. River flood evidence

Bimodal particle structure: score 1. The flood deposited shell facies down the Upper Middle Basin sediment cores showed a similar strong bimodal structure as the LSPMB107 bottom facies (see Figures 4.6 and 4.11).

Sum of all shell categories: score 3. Shell species within this depositional facies have both marine and upper estuarine inter-, sub- and supra-tidal sources (see Table 4.1). Floods within the main body of the estuary have been observed above mean sea level. Hence, it is conceivable that the remobilisation and redistribution of fossil shells, recorded within the upper cores, were transported to the lower estuary.

Historical accounts: score 0. The river-flow data indicated that floods were not centennially rare events (see Figure 4.2). Nevertheless, it is conceivable that two of the outstanding floods

of the century (in 1923 and 1960; see Figure 4.2) were sufficiently intense in both magnitude and duration to deposit a significant amount of material to the lower estuary (see Figure 4.8). By inference, the bottom layer would have to be the earlier 1960 flood. However, this is unlikely because the low excess ^{210}Pb activity towards the top of the depositional facies suggests a significantly older date than 1960.

4.6.2.4. Emperor tide evidence (the larger of king tides)

Sum of all shell categories: score 2. The mechanics and extent of bivalve shell transport from tidal flooding has been studied by Dent and Uhen (1993). They found that single valves of bivalves shells, re-floated from a sand bar and convex down, were transported as far as 119 m shoreward before sinking, irrespective of their size or species. Indeed, observations of shell debris re-floated by the smaller king tides have been observed as travelling as far as the oyster racks of the Little Swanport estuary's Marine Flood/Tidal Delta. However, this was not consistent with the presence of articulated bivalve shells or those valves with holes, such as found within the bottom depositional facies (see Figure 4.17), as Dent and Uhen, (1993) found that these forms sank within <1 m after they were re-floated.

Bimodal shell particle structure: score -1. Shell flotation as described by Dent and Uhen (1993) did not result in a bimodal structure nor was there any evidence to suggest any form of bimodal size dependence during transport and deposition.

Historical accounts: score 1. Generally, Emperor tides are not rare centennial events and can be calculated; typically appearing every 15 years to 19 years (see Figure 4.2). However, their magnitude, within their class, varies at different times around the world. For the east coast of Australia, the largest Emperor tides appear as relatively rare events at a supra-decadal scale (around 59 years).

To summarise, the weight of evidence was clearly in favour of a tsunami event (weight of evidence score 9). Furthermore, this conclusion is robust. For example, should future studies transform any uncertainty (a score of 0) to support their event categories, then this would result in a rival score of only 5 that is still not sufficient to equal or exceed the tsunami weight of evidence (score of 9).

4.7. An event geochronology for the Little Swanport estuary

4.7.1. The Lower Middle Basin

There have been two significant tsunamis over the late Anthropocene (1868 and 1960), the earlier of which is considered larger. Based on a general assessment of the sedimentation velocities from similar water bodies of the east Australian coast (0.07 cm yr^{-1} to 0.6 cm yr^{-1}; OzCoasts, 2006), it would suggest that the older tsunami (1868) was responsible for the bottom depositional facies. However, without supporting evidence or a plausible explanation, reliance on a theory based on similar separate water bodies is not a robust test of an individual water body (Peters, 1991). For example, Sydney Harbour[21] was a notable exception, in which its sedimentation velocity (1.7 cm $year^{-1}$; OzCoasts, 2006) was significantly greater than the mean.

Unfortunately, there are no accounts of the effects of 1960 tsunami on the Little Swanport estuary. The closest impacts reported by local newspapers (The Mercury, 1960) were 20 km south at Spring Bay. There, the tsunami wave caused damage to fishing boats and moorings, and made scallop dredging within the area difficult throughout the day. Nevertheless, a strong anecdotal argument can be made of why there was no apparent 1960 tsunami signal by matching rare exceptions to known expected patterns to an exceptionally rare set of circumstances. That is, an unusual closure of the estuary after an improbable circumstance comprising one of the largest floods of the twentieth century (1960) amid the arrival of one of the strongest tsunamis of the twentieth century (Dominey-Howes, 2007). In other words, it will be argued through a simple narrative that the clash between the flood and the tsunami could have conceivably blocked off the estuary's entrance.

Over a period of a month, the three distinct flood peaks (29 000 ML day^{-1}, 15 500 ML day^{-1} and 11 000 ML day^{-1}; see Figure 4.8) deposited estuarine sediments immediately outside the shallow entrance (*e.g.* Cooper, 2002). By the time the tsunami arrived, the river was still flowing strongly (140 ML day^{-1} *c.f.* to a 100-year median flow of 35 ML day^{-1}) and with sufficient momentum to partially counter the sediment-laden tsunami wave. Consequently, the previously deposited sediments were picked up by the tsunami wave and dumped into the relatively deep channel of the bar-built entrance.

Aerial photographs indicate that the entrance was closed and that the outside beach appeared to be scoured away sometime between 1948 and 1967 (see Figure 4.18). Further, entrance closure appears to be unusual (see Figure 4.18). All other available photographs show the

[21] Sydney Harbour is a busy and disturbed water way with a well-developed surrounding catchment and a large perimeter edge to volume which results in increase rates of sediment accretion (1.5 cm yr^{-1} to 1.7 cm yr^{-1}).

entrance as open to navigation, and the entrance is known to have been continuously open from 1980 to the present (2007) (Dykes, C., 2007, *pers. com.* Dykes Oyster Farm).

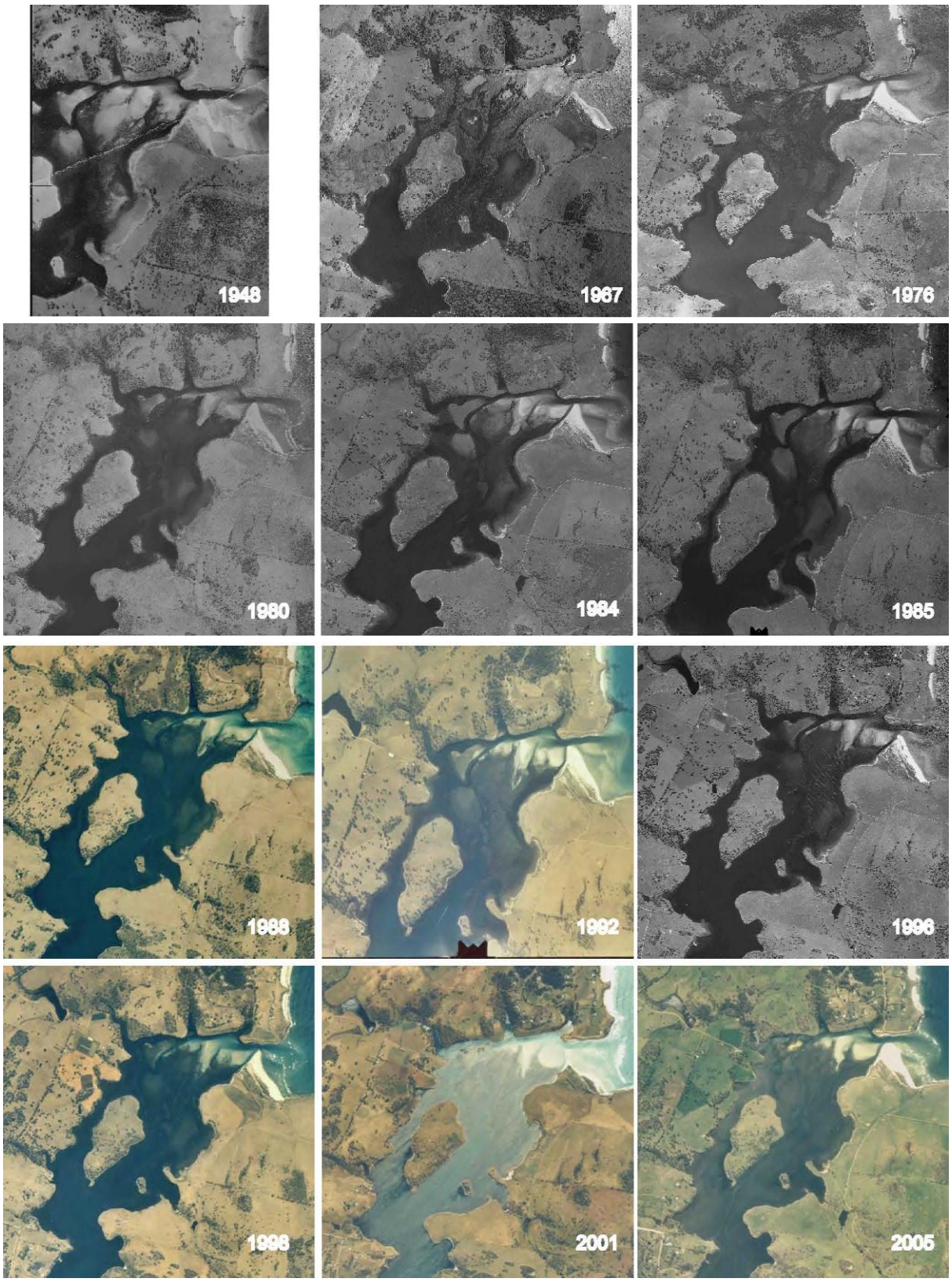

Figure 4.18. Aerial photographs of the entrance of the Little Swanport estuary (top right of each photograph), illustrating the range of entrance exposures from 1948 to 2005.
Note the near complete blockage of the entrance channel in 1967 and the apparent disappearance of the beaches to the north and south of the entrance.

4.7.1.1. Discrete changes to baseline sedimentology

The composition of the Lower Middle Basin sediment is potentially sensitive to the effects of discrete changes in long-term tidal exchange. For example, increases in the rate of coastal exchange will increase the proportion of coastal, relatively coarse low organic sand to high organic mud content in the Lower Middle Basin or Marine Flood/Tidal Delta sediments (Morton and Donaldson, 1973).

For the Little Swanport estuary, there were three potential candidates affecting a relatively sudden long-term tidal exchange: (1) the period of near entrance closure after the 1960 flood and tsunami event; (2) flood frequency (Rustomji, 2007), which can exhibit inter-decadal transitions with changes in baseline flow rates (Franks, 2002; Franks and Kuczera, 2002); and (3) the 'choking' of the Marine Flood/Tidal Delta with oyster long lines (Plew, 2011) and inter-tidal oyster racks.

*4.7.1.2. The period of oyster rack influence (***circa** *1990 to 2007)*

The period of oyster cage influence on tidal exchange can be deduced from both historical accounts and confirmed from the more frequent aerial photographs of the time. The oyster industry moved into the Marine Flood/Tidal Delta after 1986 and by 1988 to 1992, the density of oyster racks had reached close to its present day maximum (Dyke, C., 2006, *pers. com.* Dykes Oyster Farm).

4.7.1.3. The period of near entrance closure (1960 to 1969/1970)

It has been argued that the closure of the entrance from 1960 to 1967/1970 was probably the result of the 1960 flood/tsunami event. However, the timing of the reopening is not immediately clear. There are no annual collections of aerial photographs or accounts to mark the years from 1967 to before the first evidence of reopening of the entrance in 1976 (see Figure 4.18). However, entrance blockages, in wave-dominated systems, are only cleared by pivotal floods events (Rustomji, 2007).

Thus, the relative flood magnitudes from entrance closure in 1960 to the first evidence of usual entrance exposure in 1976 (from Figure 4.1) could indicate when the estuary was reopened. It is likely that the 1969/1970 floods reopened the estuary, as these floods were the first floods greater in magnitude than were those observed during 1960 to 1967. The reasoning is that, as smaller floods than those between 1960 and 1967 (which closed the entrance) were shown to be insufficient to remobilise entrance sediments, the floods to reopen

the entrance had to be equal or greater than were those that closed the entrance. Pre-1976, the 1969/1970 floods were the only ones to satisfy this magnitude requirement (see Figures 4.2). Indeed, the 1969/1970 floods were the third largest of the twentieth century.

4.7.1.4. Changes in flood frequency (1979 to 2007)

A CUSUM analysis of modelled annual flood days and the average annual daily river flows over the twentieth century marks the start of the drought from 1979 with a fall in flood frequency. The change was immediately before the 1986 flood, an event that forced the re-location of the oyster industry to the Marine Flood/Tidal Delta.

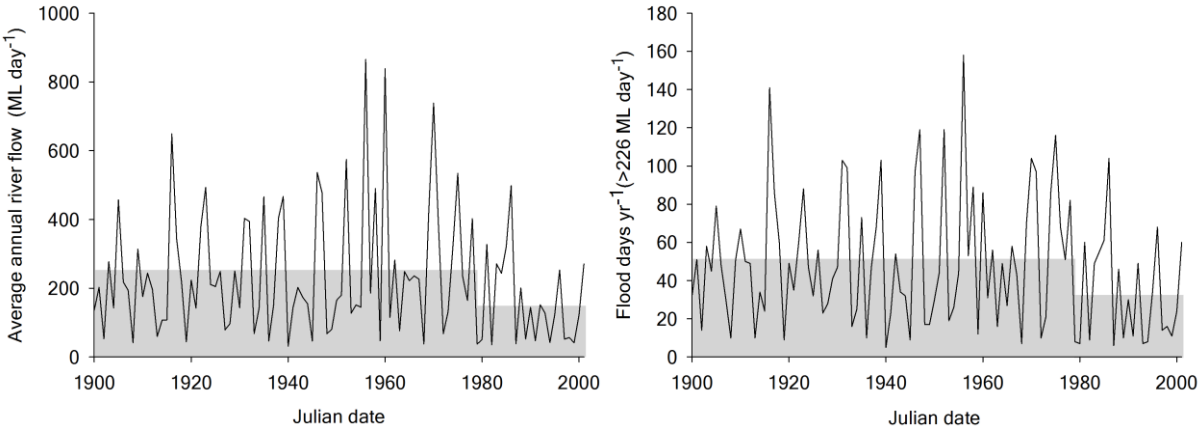

Figure 4.19. The average annual daily river flows and the annual number of flood days for the Little Swanport River.
Floods were defined as average daily river flows >226 ML day^{-1} and were calculated from the rainfall/catchment/dam model (SKM, 2004), along with the average annual river flow. The top of the grey bar marks the CUSUM mean of the river flow and flood metrics.

4.7.1.5. Correlations with changes in tidal exchange and sediment core OM content

Figure 4.20 shows the CUSUM positions, magnitudes and probability ranges of OM transitions (LOI 550 °C). The surface change point was consistent with a typical depth and variance found in most estuarine sediment core profiles as due to a combination of surface bioturbation and an early rapid diagenetic loss (Zimmerman and Canuel, 2002). Thus, by ignoring the surface change point the number of transitions identified in sequence after the 1868 tsunami could be fitted to above external forcing factors (see Figure 4.20) to the following self-consistent narrative.

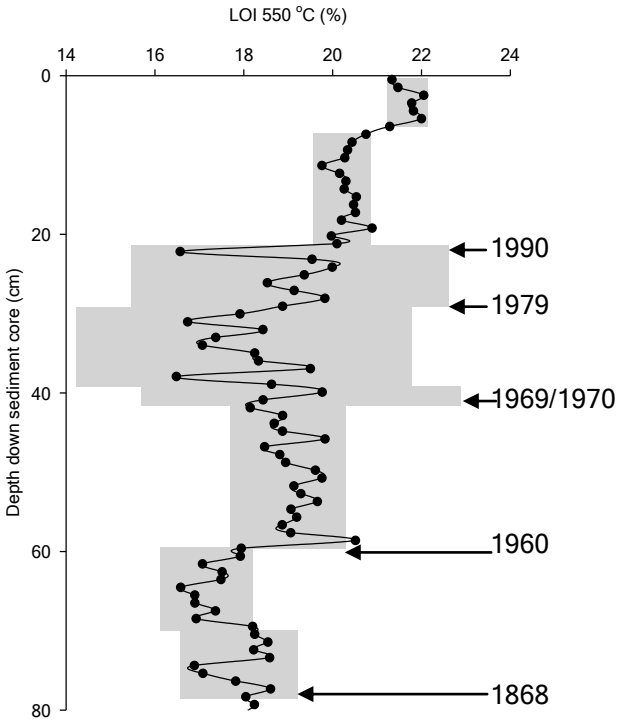

Figure 4.20. LOI 550 °C change point stratigraphy down the Lower Middle Basin sediment core LSPMB107. The grey bars represent CUSUM standard deviation about the mean of LOI 550 °C, calculated in sequence from the bottom to the top of the sediment core.

The transition immediately after the 1868 tsunami (69.4 cm) appears to be the result of a larger pre-1900 baseline river flow (von Platen, 2008). From 1960 to 1969/1970, the entrance restriction resulted in a muddier higher organic sediment at the core extraction sites (see Figure 4.20), as influenced by the sandy Marine Flood/Tidal Delta migrating towards the entrance due to a reduction in tidal exchange. After the entrance reopened between 1969/1970, the OM content returned towards its pre-1960 values together with the sandy Marine Flood/Tidal Delta (see Figure 4.20). By 1979/1980, the fall in flood frequency resulted in more restrictive entrance equilibrium leading to a reduction in tidal exchange and a remigration of the sandy Marine Flood/Tidal Delta. After 1986, the shellfish aquaculture industry re-located to the Marine Flood/Tidal Delta, and by 1988 to 1992, the quantity of newly located oyster racks reached a maximum (see Figure 4.18). The oyster racks affected a further buffer in tidal exchange to the Lower Middle Basin, which was marked by a higher OM content with significantly less variability than in previous transitions (see Figure 4.20).

4.7.2. The Upper Middle Basin

The magnitudes of the modelled flood events (SKM, 2004) down sediment core LSPMB206 were successfully matched to the magnitude of the Rp index signal/thickness, in sequence from the top core, where the date is known, towards the bottom (see Figure 4.21). The correlation was considered robust, as it identified: (1) the two significantly larger floods of the

twentieth century (1923 and 1960) with the two clearly identifiable major facies down the sediment core; and (2) the relative position of the largest fire recorded within southeast Tasmania (Black Tuesday in 1967) (see Section 4.4.1). Further, between the 1960 and 1969/1970 flood events, the net accretion rates between the flood facies were roughly proportional to the amount of erosion expected from the average daily peak flood strength, assuming a relatively constant sedimentation velocity (see Equation 4.2)

Equation 4.2 Flood (ML day $^{-1}$x10^3) = -0.34 (cm) + 27.7 (ML day $^{-1}$x10^3)
(r^2 = 0.25)

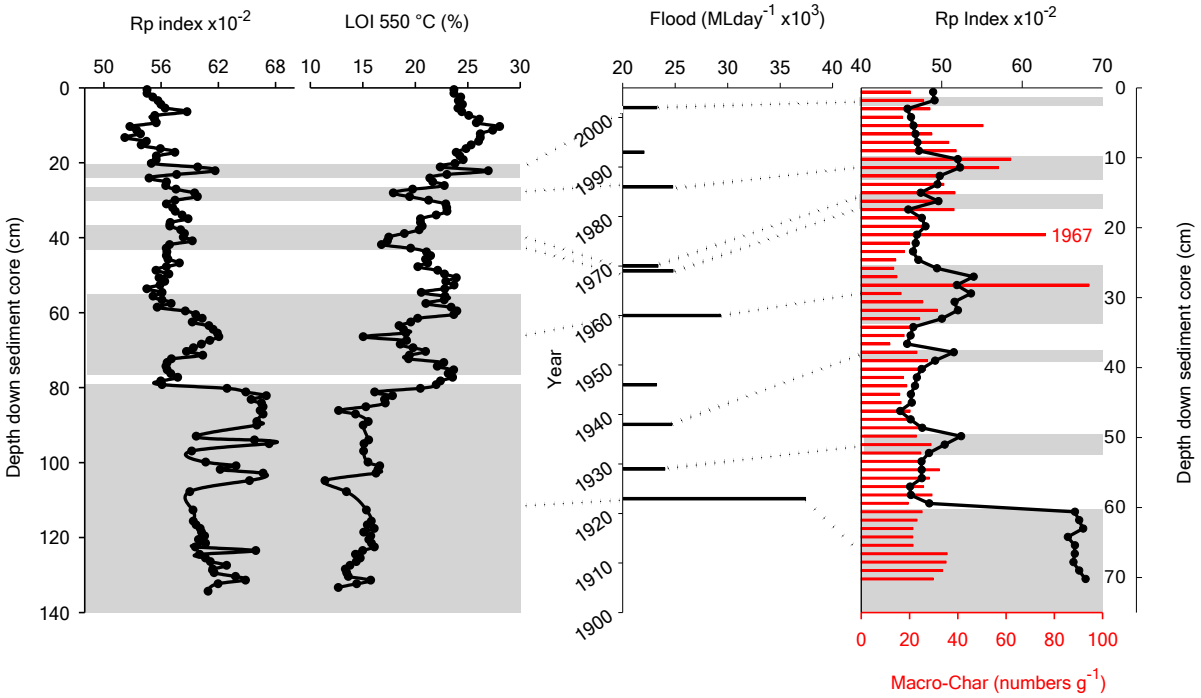

Figure 4.21. Event-based geochronologies of the Upper Middle Basin sediment cores.
(left) Sediment core LSPMB2B08, (right) sediment core LSPMB206. The relative event magnitudes, within the sediment core are represented by the event facies thicknesses and the magnitude of the Rp index for sediment core LSPMB206, and in combination with LOI 550 °C for sediment core LSPMB2B08.

The correlation between flood events and event facies down sediment core LSPMB2B08 was not clear because neither the magnitude of the Rp index signal, nor the other content variables, reflected the thickness of all the facies. However, using the Rp index in combination with LOI 550 °C, there was sufficient commonality and overlap between all three metrics (facies thickness, LOI550°C and Rp index) to match flood events to their facies. Nevertheless, a solution was only possible by assuming that the two larger intrusive masses represented the 1960 and 1923 flood events, and that the flood facies between these points had been eroded by the 1960 flood. That the LSPMB2B08 station was further up the estuary towards the Little Swanport River is consistent with this assumption.

4.8. Radio-geochronologies of the Upper and Lower Middle Basins

4.8.1. Surface mixing depths

None of the sediment cores showed an immediate exponential decay of ^{210}Pb activity from the surface (see Figure 4.22). However, it would be a mistake to attribute the relative invariance in the surface ^{210}Pb activity to extensive surface mixing. The rapid increases in bulk densities in the presence of surface sediment anoxia (see Section 4.4.2) indicated that surface mixing by animal reworking and wind mixing down the Upper Middle Basin cores (LSPMB2B08 and LSPMB206) was <1.24 cm (see Figure 4.22).

In contrast, anoxic surface sediments down the Lower Middle Basin sediment cores (LSPMB107 and LSPMB106) showed some evidence of previous macro-benthic activity, including the presence of a void near the top of the core (5 cm to 6 cm). However, any sediment reworking attributable to this void was not evident. Bulk densities were invariant below the surface 2 cm to 3 cm (see Figure 4.22). Further, the recent deposition of macro-char from a fire on adjacent Ram Island had not mixed beyond the second sampling horizon (2.54 cm) in the eight months following the fire (see Figure 4.22).

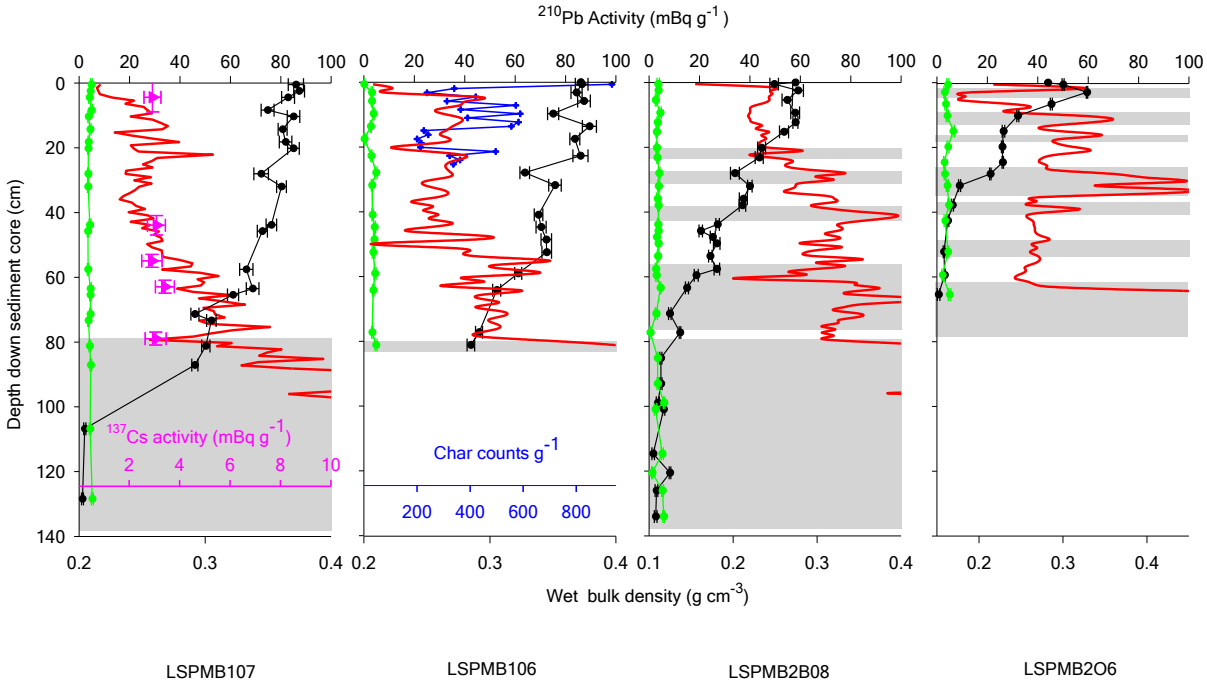

Figure 4.22. ^{210}Pb and ^{137}Cs profiles down sediments cores extracted from the Little Swanport estuary. (●) Unsupported ^{210}Pb activity, (●) ^{210}Pb supported fraction, (●)^{137}Cs activity, (—) wet bulk densities, and (●) surface sediment macro-char counts. The error bars are standard deviations of decay counts. The grey bars mark the suggested positions of intrusive masses (see Figure 4.1 for the position of the sediment core sampling sites).

It appears that none of the shallow surface mixed layers across any of the four sediment cores were sufficient to affect the results of a full baseline CRS and SIT ^{210}Pb geochronology (Appleby, 2001; Lu and Matsumoto, 2005). It can also be argued that these shallow mixing zones (less than or equal to sampling resolution) may not significantly affect the CIC result, if the shallow surface layer formed relatively quickly and always to the same extent. Under these conditions, a direct comparison with depth can still be approximated by referencing the average age of the first sample (a young and shallower mixed layer) to the deeper baseline horizons.

^{137}Cs activity down through Lower Middle Basin sediment core LSPMB107 (see Figure 4.22) was very low and the resolution was not sufficient to mark a horizon or peak period of atomic bomb testing.

4.8.2. Geochronological methods and models for the Upper and Lower Middle Basin

SIT, CIC and CRS models were applied to the unsupported ^{210}Pb profiles within previously identified baseline sediment horizons, assuming that event deposition was effectively instantaneous. However, erosion corrections between events for the Upper Middle Basin cores could only be applied to sediment core LSPMB206 and not LSPMB2B08. The unsupported ^{210}Pb baseline inventory for the sediment column within sediment core LSPMB2B08 (4990 Bq m^{-2}) was considerably larger than local aerial deposition (3363 Bq m^{-2}; Turekian *et al.*, 1977) commensurate with the southeast climate of Tasmania. The excess may reflect a high degree of sediment focusing and/or fluvial deposition at and close by the Duck Islands. In contrast, the unsupported ^{210}Pb baseline inventory of sediment core LSPMB206 was considerably less than local aerial deposition (2260 Bq m^{-2}; Turekian *et al.*, 1977). Of course, the deficiency may represent only a net loss between flood erosion and supply from river and remobilised sediments of the littoral zones, nevertheless, the approach can be evaluated through a convergence with its event chronology (mixed RA).

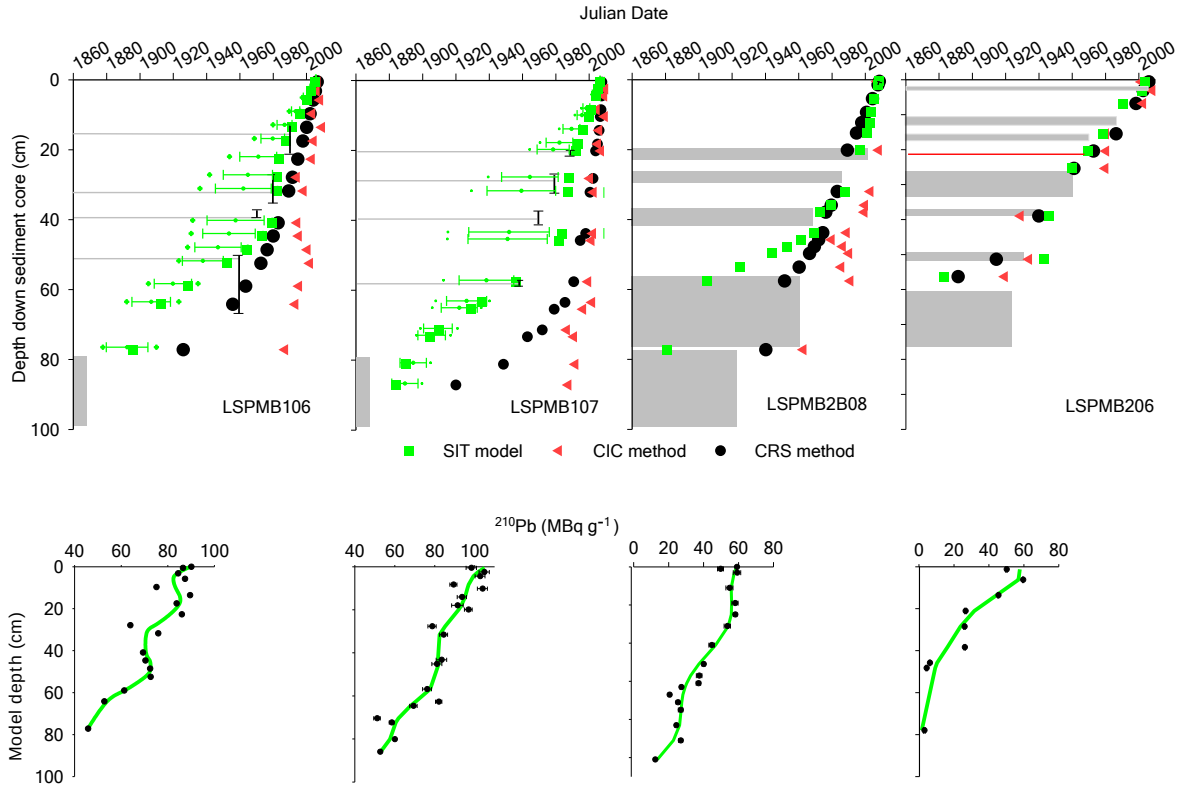

Figure 4.23. Event and ^{210}Pb geochronologies for the Upper Middle Basin and Lower Middle Basin bottom sediments.
The red bar marks the 1967 fire and the grey bars mark the positions and age of river flood depositional facies and the tops of 1868 tsunami event facies. The black error bars are the CUSUM 90 % confidence limits for baseline sedimentological changes (10 000 bootstrap runs without replacement). The green error bars represent SIT standard deviation and green squares either side of the errors bar are maximum and maximum dates. The lower charts are the SIT solutions to the unsupported ^{210}Pb profiles down baseline horizons (model depths).

Figure 4.23 shows the results of all of the Middle Basin ^{210}Pb geochronological models and methods. Only for one Upper Middle Basin sediment core (LSPMB206) did all models and methods converge towards a common chronology. Consequently, the assumptions, such as the extent of erosion, flood facies identification, their extent through the sediment column and the common assumptions that bind all ^{210}Pb methods (constant sedimentation rate and constant flux of unsupported ^{210}Pb) are evaluated as robust (mixed RA; see Chapter 1). Nevertheless, each method had its own inaccuracies and accuracies down through the sediment core, although the SIT model remained the most accurate, with the possible exception of the 1923 flood event. This was in contrast to the CIC horizon, which closely matched the 1923 flood event, but exhibited greater divergence within the upper and middle core sections. Conversely, the CRS method underestimated the event age towards the top of the sediment core, but diverged towards an older estimation of the remaining flood events towards the bottom of the sediment core (*c.f.* SIT). Despite the above relative bias, the general agreement between all models supports the assumptions behind each of the methods; that there was little

sediment focusing around the LSPMB206 extraction site, a correct assessment of where baseline horizons lay and the extent of erosion.

In contrast to sediment core LSPMB206, for sediment core LSPMB2B08 there was no convergence between any of the radio-geochronological methods and events, despite an increased sampling resolution (see Figure 4.23). The inability to correct for erosion, however, was only partly responsible for the divergence between the separate geochronologies. The CIC baseline horizons (independent of erosion) did not match any of the events dates, including the most likely events to leave a signal, namely, the pivotal 1923 and 1960 flood events, thus indicating a complex relationship between the rate of sedimentation and the supply of unsupported ^{210}Pb. A relationship that does not conform with suggested reasons behind the assumptions of CIC and a CRS geochronology, that is, an excess of scavenging particles (see section 4.1) or no sediment erosion, respectively.

Similarly to core LSPMB2B08, all of the radio-geochronological methods that were applied to the Lower Middle Basin sediment cores (LSPMB106 and LSPMB107) diverged from the surface (see Figure 4.23). However, in contrast to LSMB2B08, the SIT solutions did converge *circa* the postulated baseline transitions and the top of the tsunami facies.

Based on the above evidence, it would seem that the SIT model was sufficiently robust to capture the changes in base line sedimentation and the 1868 tsunami event. However, in truth, the event model did not strictly conform to conditions embedded within a mixed RA (see Chapter 1). That is, the event model was arguably not fully tested as plausible (*i.e*. there was only anecdotal evidence for reasons behind a reduction tidal exchange between 1960 to 1969/1970). The models were not completely independent, as the event chronology relied on the context of the 1868 tsunami. Further, the dichotomy between the low but measurable presence of ^{137}Cs older at a depth older than suggested by all the ^{210}Pb methods (late 1950s atomic bomb testing), suggested a rate of sedimentation much greater than is usual for these water bodies.

The presence of low ^{137}Cs activities below the atomic bomb horizon, however, is not uncommon. Furthermore, ^{137}Cs horizons cannot be used to falsify ^{210}Pb geochronological models (Abril, 2004). Indeed, it is conceivable a water level greater than the mean sea level resulted during floods and/or over the period of entrance restriction (1960 to 1969/1970) (*e.g*.

Rustomji, 2007), which was responsible for remobilising the ^{137}Cs down through the sediment column (*e.g.* Foster *et al.*, 2006).

4.8.2.1. Cross-validation of the lower middle basin SIT model

It would then appear that the first step in explaining the Lower Middle Basin's geochronology lies in accepting the SIT result as other evidence suggests that sedimentary conditions were ideal for the model (*i.e.* no erosion and a small surface mixing depth) and that there maybe some doubt to plausibility baseline event changes other than the tsunami. Thus, the reconstruction of the post tsunami events should not be used to confirm the chronology though convergence of a common result (mixed Robustness Analysis) but only used as weak supporting evidence for the post tsunami SIT chronology. Hence, it is prudent to cross-validate the SIT model, particularly as the rapid changes in sediment velocity in combination with an uneven sampling distribution resulted in a large probability distribution (Carroll and Lerche, 2003 [see Figure 4.23]). Consequently, a series of 11 SIT cross-validation runs was used to determine whether the solution was the result of sampling bias. Each run was carried by first randomly removing 27 % of the baseline ^{210}Pb samples from the larger data set within sediment core LSPMB107 (see Figure 4.24a). It was found that that all of the cross validation SIT solutions converged to around the early 1880s, *circa* Chilean tsunami of 1868.

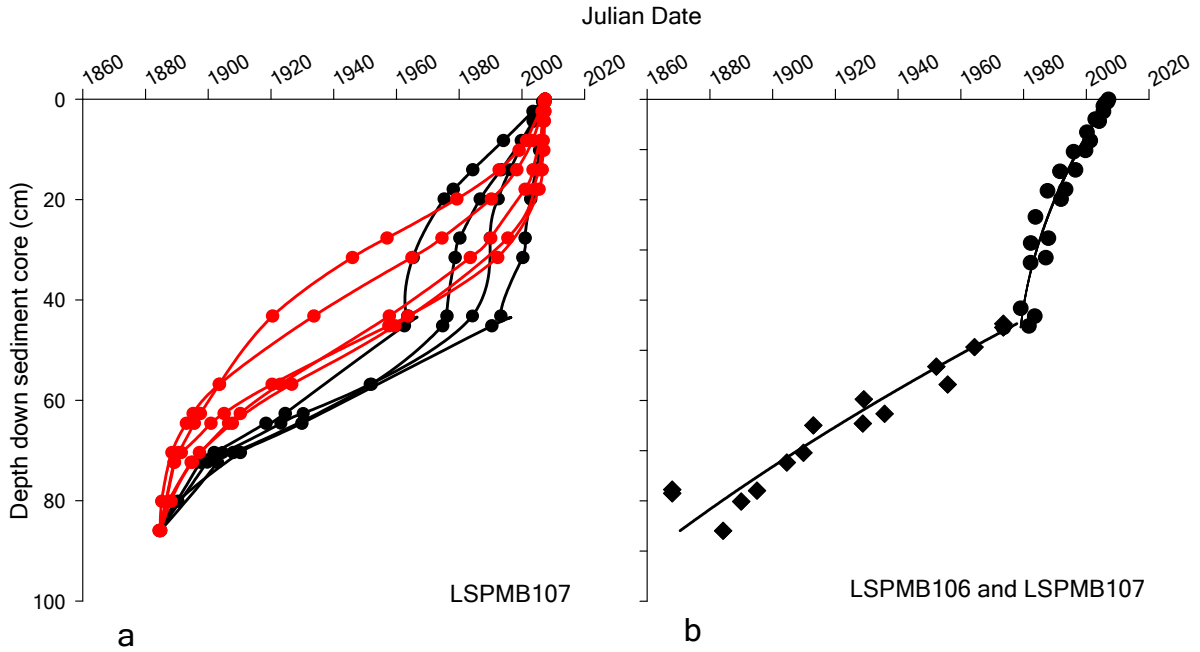

Figure 4.24. Cross validation of the SIT model and the Lower Middle Basin's resultant geochronology.
(a) SIT solutions after 27 % of the data points were randomly removed down through sections of the sediment core LSPMB107; (b) a combined geochronology for the Lower Middle Basin using the full SIT runs for the Upper Middle Basin sediment cores LSPMB107 and LSPMB106 with of their 1868 tsunami facies. The curve fits were based on two separate second order polynomial linear regressions after identifying the position of the CUSUM change point at 1979/1980 (Variance™).

In addition to the convergence with the 1868 tsunami, however, there was a broad range of chronological variance down the sediment core. For the purpose of description, the variance can be divided into two generically different forms: series X (black lines; see Figure 4.24) and series Y (red lines; see Figure 4. 24). The full SIT simulation was clearly within the series X category (*c.f.* Figure 4.23), in which the transition to high rates of sediment accretion was much earlier than for series Y. The differences between series Y and X appear to be the result of sample clumping of series Y near the top and bottom of the profile. Overall, the profiles with the least data clumping and the most even horizon distributions most closely resembled the full SIT solutions, typical of series X. The cross validations also indicated two forms of bias within series X: a younger accretion transition to greater values around 40 cm for profiles deficient in samples between 42 cm and 63 cm, and an older transition around 40 cm for profiles deficient in samples from 63 cm towards the bottom. The latter categories also broadly describes the differences in total sampling distribution between the upper sediment cores LSPMB107 and LSPMB106 (see Figure 4.23). Hence, to increase the SIT minimal model's chronological accuracy for the Lower Middle Basin, the two sediment core's SIT minimal solutions were combined with the position of their tsunami facies to represent the optimum sample distribution for the least bias (see Figure 4.24b).

4.9. Discussion and conclusions

Seven major depositional flood events >23 200 ML day^{-1} affecting the Upper Middle Basin of the Little Swanport estuary (core LSPMB206) were recorded, dated and evaluated with a suite of ^{210}Pb models (SIT) and methods (CRS and CIC). All the re-constructed events and geochronological models and methods converged and thus supported the assumptions behind the construction of events, models and methods (mix Robustness Analysis; Bycroft, 2009), namely: (1) the LSPMB206 core's extraction site recorded all the floods that affected the surrounding environment's baseline deposition, (>33 cm) and erosion (*calc*. 25 cm) over the last 83 years; (2) there was no significant long-term sediment focusing, as indicated by the broad agreement between the CIC and CRS methods (Appleby, 2001), (3) there was a relatively constant supply of unsupported ^{210}Pb only from atmospheric deposition; and (4) there was no significant surface mixing (<15 % of the ^{210}Pb inventory). In contrast, within the upper region of the Upper Middle Basin (core LSPMB2B08) none of the events and geochronological models and methods agreed with each other. This was due to a mix of variable rates of sedimentary parameters and unaccounted loss of baseline sediments and some depositional flood facies, probably through erosion during the pivotal 1960 flood event.

Within the deeper central trench of the Lower Middle Basin (water depth 8 m to 9.9 m), a resilient weight of evidence suggested that the shell and terrestrial material found within the deposits near the base of both sediment cores (LPMB107 and LSPMB106) was a result of gathering and deposition by the 1868 Chilean tsunami. Overall, there was good evidence, from reconstructed changes in baseline deposition, to support the SIT geochronology down both of the Lower Middle Basin sediment cores. Furthermore, it was found from a series of cross-validation runs that any small differences between the SIT chronologies down the two Lower Middle Basin sediment cores were more a function of sampling resolution and distribution than real differences in sedimentation. Consequently, the two SIT chronologies were combined for a more considered Upper Middle Basin average and identified a transition to a greater rate of sedimentation from around the early 1980s. The cause of the change was not clear, other than it is was *circa* the start the lower estuary's oyster aquaculture development and may be due to the disturbance of littoral zone sediments by aquaculture activities.

However, support did not extend to the CIC or the CRS methods. Given the limitations of the CIC and CRS models, the reasons were self-evident, in that the relative changes of sedimentation and supply of ^{210}Pb led to conditions that were outside the parameters of the two methods. For example, the failure of the CIC method during pre-disturbance times (1980) suggests that the natural supply of unsupported ^{210}Pb may have been in excess of scavenging particles (see Section 4.1). This contention is, in part, supported by both the sediment core's ^{210}Pb inventories (*calc.* 17 446 to 14 300 Bq m $^{-2}$ for core LSPMB107 and core LSPMB106, respectively) that were well excess to aerial deposition (2260 Bq m $^{-2}$; Turekian *et al.*, 1977). The reasons behind such an excess are not clear but unlikely to be due to the proximity of the river and more likely because of internal processes. For example, it is conceivable that sedentary epipelics and seagrass epiphytes would have been exposed to aerial ^{210}Pb deposition over longer periods than waterborne particles such a phytoplankton or washed in clays. Under the circumstances unsupported ^{210}Pb may be expected not only to adsorb but also to be absorbed (Robbins, 1978) before natural disturbance eventually transported the epiphytes and epipelics into the deep spot.

Chapter 5. A late Anthropocene palaeo-reconstruction of inorganic nitrogen availability in the Little Swanport estuary

5.1. Introduction

Currently, outside of direct grazing by animals, changes to the inorganic nutrient supply is recognised as the major factor affecting the seagrass ecosystem at the meadow–landscape scale (Orth *et al.*, 2006 and references therein), particularly within the confines of lagoons or estuaries (Burkholder *et al.*, 2007). Of course, Livingston (1984) indicated that other periodic 'catastrophic' events such as river flooding of estuaries can affect the standing crop biomass and productivity of seagrass beds for years, but argued that such periodic natural events have not had a long-lasting influence on population distribution or food web structure in contrast to slight changes in water quality.

Consequently, in order to study nutrient–meadow dynamics the rate of change in nutrient supply needs to be measured close to the same temporal response of the whole seagrass meadow. If only a proportion of the meadow is chosen, we may not detect its actual ecosystem dynamics and patterns but may instead identify patterns that are artefacts of scale such as the relationship between the greater temporal variations between patch clusters and the entire bed (Habeeb *et al.*, 2007; Nyqvist *et al.*, 2009 Yamakita *et al.*, 2010). The scale of the meadow response is determined primarily by the seagrass species, nevertheless, with the exception of the slow growing *Posidonia* spp the recovery time scales of seagrass meadows can range from intra-decadal to decadal (*e.g.* Livingston, 1984; Morris and Virnstein, 2004, Duarte *et al.*, 2006). Indeed, such scales are similar to industrial and agricultural development, economic cycles and human generations and thus directly relevant to society from a standpoint of changes to seagrass meadow ecosystem services.

Traditionally, long-term changes in nitrogen supply in estuaries and lagoons have been attributed to trends in catchment loading. Changes in catchment loadings are often the result of land development or contemporary catchment remediation projects (*e.g.* Zimmerman and Canuel, 2002; Martin *et al.*, 2010). However, for the Little Swanport estuary, upper catchment development or remediation was unlikely to be an important factor (see Chapter 3). Decadal changes to the river flows with rainfall patterns (Nunez and McGregor, 2007; see Chapter 4) affect nitrogen loading irrespective of the state of the catchment, a variance which is likely to match the spatial response of a *Zostera* spp. meadow to changes in its limiting nitrogen supply (see Chapter 3). However, it would be a mistake to ignore the variability of the coastal nitrate

boundary condition. For example, a higher but invariant concentration of DIN within a river that mixes with lower but variable coastal nitrate waters over the long term will control the mean response of the seagrass meadow but not the long-term variability, should seawater be of a significantly greater proportion than freshwater. Conversely, a higher but variable concentration of river DIN that mixes with lower but invariant coastal nitrate waters will control the mean seagrass response and its variance about the mean.

Indeed, near contiguous monthly salinity and temperature data from nearby coastal waters (from a site offshore from Maria Island; see Figure 5.2) since 1944 showed a decadal periodicity in the extent of relative influence between the oligotrophic warm East Australian Current and the more nutrient rich, colder, southern waters (Harris *et al.*, 1987, 1988; Hill *et al.*, 2008). The long-term nitrate data set that accompanied the salinity and temperature measurements was not as complete (27 % of data missing). Nevertheless, a compilation of all of the depth profile values over time resulted in periodic residuals about a stationary series (Thompson *et al.*, 2009). However, the analysis of Thompson *et al.*, (2009) was not powerful enough to confidently infer a relationship between nitrate concentrations and salinity or temperature data because of the way the annual average nitrate was calculated. That is, the averages were calculated from a mix of incomplete seasonal data sets.

5.2. Reconstructing estuarine inorganic nitrogen availability

Traditionally, transfer functions based on diatom assemblage distributions down sediment cores are used to reconstruct the changes in nutrient status of a water body. Typically, the function is constructed by relating changes in contemporary nutrient concentrations to that of the diatom assemblage preserved in the surface sediment diatom (Smol *et al.*, 2001). However, there are two issues that limit the interpretation of this singular approach: (1) an independent model is needed to evaluate the generality from its construction in space to its application in time (mixed Robustness Analysis [RA], see Section 1.3.2); see Chapter 1); and (2) spot measurements of nutrient concentration as proxy for nutrient loading are only appropriate for highly eutrophic systems (NRC, 2000; Lee *et al.*, 2004; Scanes *et al.*, 2007). In other words, inorganic nutrients are efficiently utilised within oligotrophic and mesotrophic systems, which results in little or no variance in concentration with loading. Consequently, any relationship between the diatom assemblages becomes a function of more than one competing process, for example, nitrogen availability, nitrogen utilisation and competition between the estuary's micro-phyta and macro-phyta.

The non-conservative nature of nutrient concentrations can be addressed by using the concept concentration of potential inorganic nitrogen (CPN) (NRC, 2000). The CPN is the resultant annual average DIN concentration before it has been utilised by the assemblage of primary producers. CPN is calculated from the nitrogen loading, the estuary volume and the freshwater flushing time, but it can also be calculated from the annual average river DIN and coastal water nitrate concentrations, itself arguably a conservative metric (Ferreira *et al.*, 2000; Dettmann, 2001), and the average salinity. The salinity is used to calculate the proportions of river and coastal waters to weight their contributions. CPN assumes no significant internal net loss or gain of nitrogen within the estuary. Indeed, Dettmann (2001) found that for a range of individual estuaries with residence times of less than a month, such as the Little Swanport estuary (Crawford and Mitchell, 1999), net loss of nitrogen (denitrification) was not significant (<5 %,). However, it remains conceivable that an estuary with an extensive littoral zone occupied by a lush seagrass meadow, such as the Little Swanport estuary, may obtain a significant fraction of its inorganic nitrogen from nitrogen fixation to supplement nitrogen supply during times of low external supply (Welsh, 2000). Nevertheless, any divergence between CPN and the effect on the assemblage of primary producers can be constrained by changes in its organic nitrogen stable isotope ratios (see Chapter 6).

5.3. Aims

The aim of the study described in this Chapter was to reconstruct a late Anthropocene contiguous time series of CPN by: (1) using contemporary river-flow–DIN response curves with 101 years of modelled daily average river flows between 1900 and 2001 (SKM, 2004), (2) imputation and hind casting of the incomplete long-term nitrate coastal data set (CSIRO national reference station) from 1944 to 2004; and (3) using a diatom transfer function for surface waters down the Lower Middle Basin sediment core and an inverse model of pore water salinities (see Figure 5.1) to calculate bottom salinities, to estimate the average estuarine salinity.

Evaluation of CPN time series was carried out by testing the river flow, salinity and inorganic nitrogen inputs by calibration from available data, independent models or constraints on possible solutions from previously evaluated reconstructions. Figure 5.1 illustrates the inputs, evaluation, constraints and calibration hierarchy. The white boxes represent the reconstructed input data CPN calculation (blue box), the green boxes represent the other lines of evidence and solution constraints, and the turquoise boxes are the inputs for the other lines of evidence.

In this way, the diatom-derived surface salinity was evaluated over time by a multiple linear regression model by matching the fit with proxies of three independent controlling variables, namely, modelled river flows (SKM, 2004), previously calibrated by 17 years of data; westerly wind strength and frequency and resulting fetch from high altitude pressure changes (Pook, 1992); and tidal exchange from reconstructed bottom water salinities, normalised for long-term changes in river flow (see Chapter 4). The regression model, as representing the annual average variance was tested using a re-analysis of 101 years of modelled summer/spring and winter river flows.

Figure 5.1. Flow diagram for the palaeo-reconstruction of CPN for the Little Swanport estuary (blue box). The white boxes represent the data inputs and model outputs and the green boxes were the constraints on model solutions, verification data and models from independent lines of evidence.

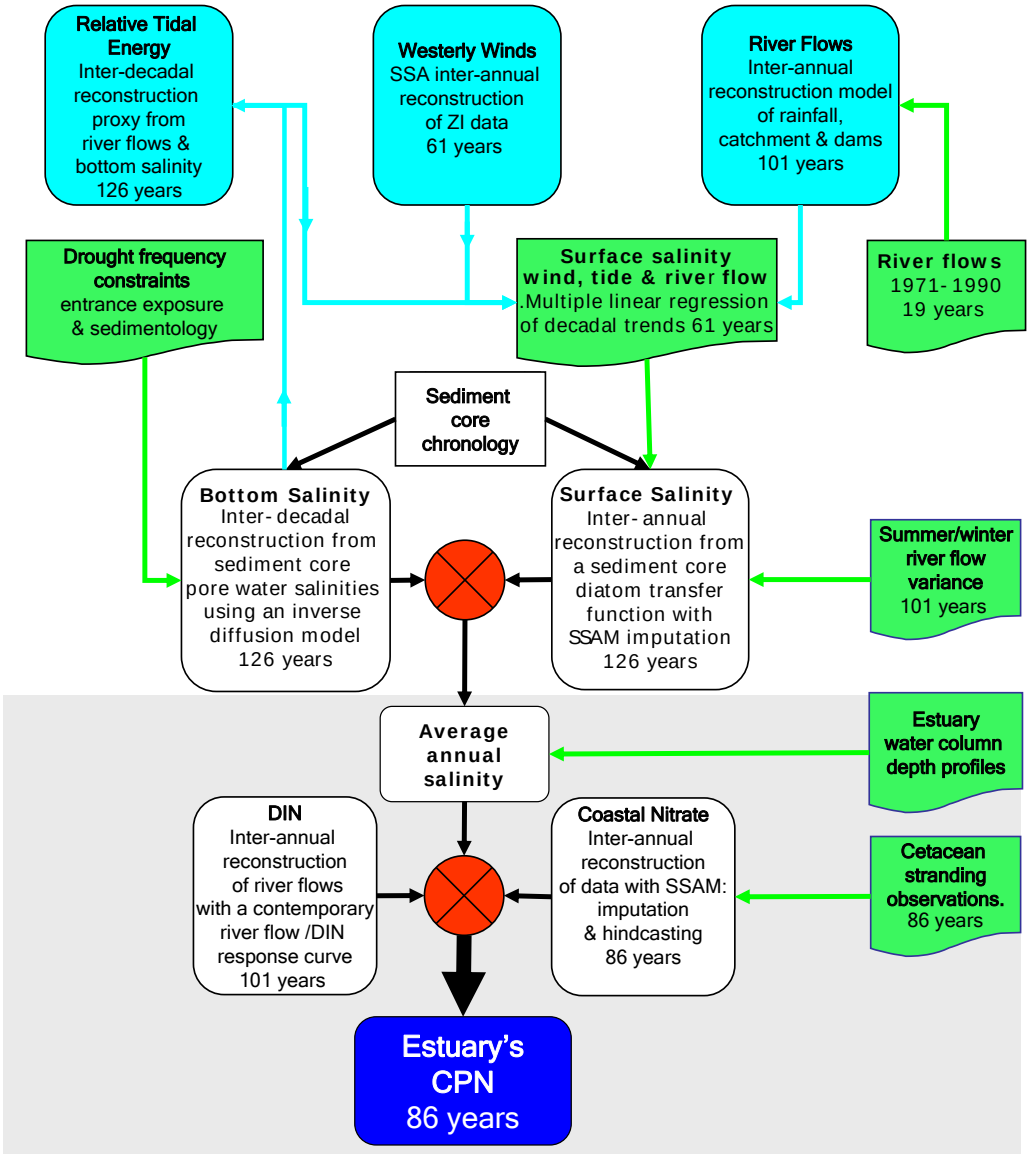

The bottom salinities were reconstructed by inverse modelling of pore water salinities (Stiller *et al.*, 1983; Adkins and Schrag, 2003; Soulet *et al.*, 2010), contraining solutions by

referencing contemporary salinities to long-term relative changes in tidal exchange and river flows (see Chapter 4). The averages of the reconstructed bottom salinities and the diatom-derived surface salinities from the Lower Middle Basin were evaluated as approximating average salinity using water column salinity profiles over the range of median flows to small floods. Finally, the periodicity of the hindcast coastal nitrate data set (from the Maria Island reference station), expanded from 1944 to 1920, was evaluated by the convergence with an overlapping longer data set of cetacean stranding (1920 to 2004), previously related to changes to coastal productivity (Evans *et al.*, 2005).

5.4. Materials and methods

5.4.1. Site description

The Lower Middle Basin sediment cores (LSPMB107 and LSPMB106; see Figure 5.2) were chosen for their representation of: (1) the late Anthropocene record (1868 to 2006; see Chapter 4), (2) the maximum bottom salinity at the estuary's deep spot (9.9 m; LSPMB107); (3) the availability surface salinities calculated from the diatom assemblage data down to the adjacent shallower core (LSPMB106); and (4) the core sites being a zone of the estuary at which the average salinity between the surface and bottom waters was expected to converge towards the estuarine weighted average. The Lower Middle Basin's volume (3 268 000 m^3) is currently twice the volume of the remaining zones (1 642 000 m^3; *calc.* from Crawford and Mitchell, 1999). Hence, the difference in average salinity between the upper and lower estuary zones is buffered by a smaller quantity of salt within a smaller volume to a larger quantity of salt within a larger volume. Further, the larger volume and amount of salt within the Lower Middle Basin will weigh its average salinity towards the estuary's average. See Chapter 2 for details of sediment core collection and processing for pore salinity analysis and for salinity and temperature profiles.

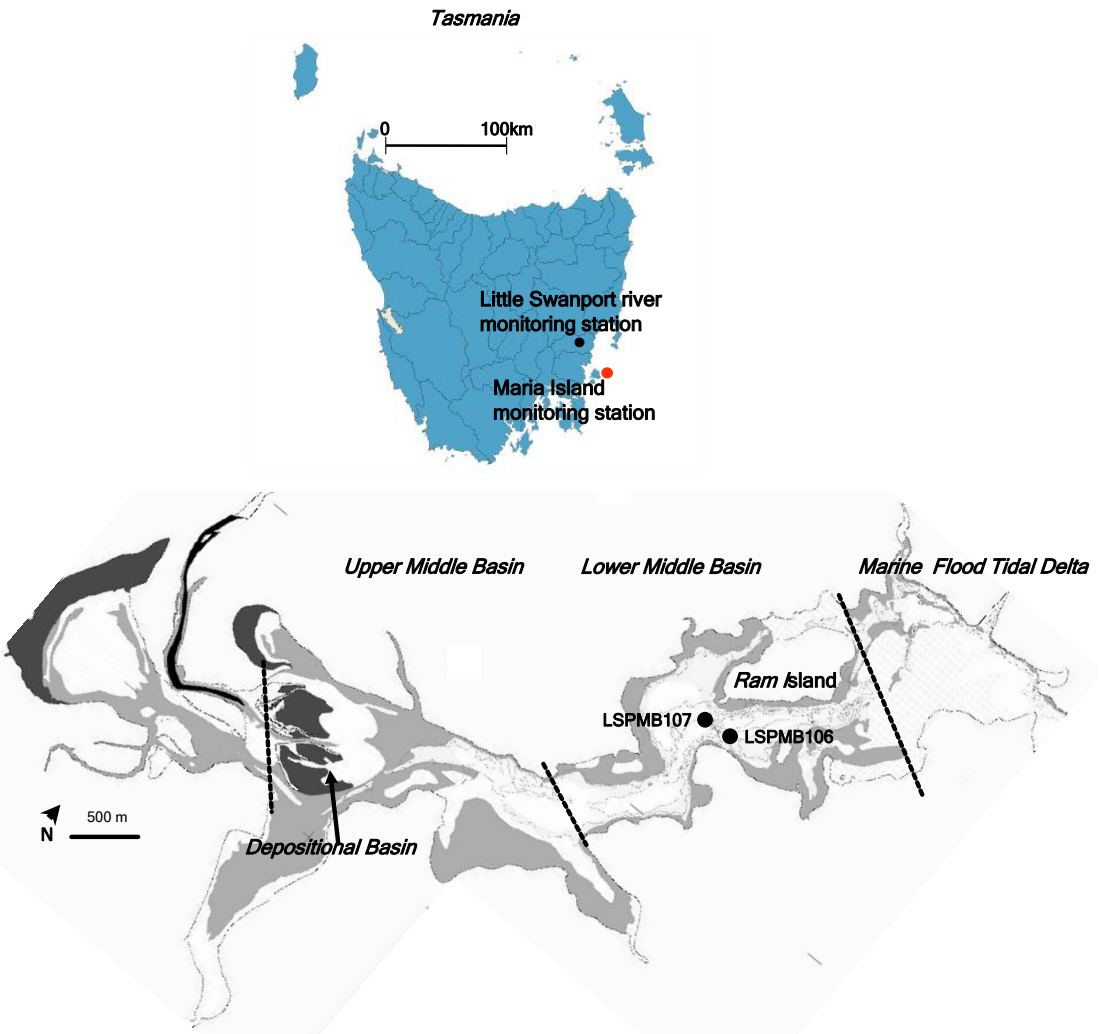

Figure 5.2. Positions of inorganic nitrogen monitoring sites and the Lower Middle Basin's sediment core extraction sites used for reconstructing bottom and surface salinities.

5.4.2. Data sources

Contemporary DIN for the lower Little Swanport River, immediately above the maximum tidal excursion, along with daily average river-flow rates, were obtained from the Tasmanian state government (DPIW, 1998). Coastal surface water nitrate concentrations (1944 to 2004) came from ongoing long-term monthly monitoring program data collected immediately east of Maria Island (see Figure 5.2) by CSIRO.[22] The zonal atmospheric pressure index (around 500 hPa; 1945 to 2004) over the surrounding Tasmanian sector of the Southern Ocean was supplied by Dr M. Pook (CSIRO, Tasmania) as monthly averages. River-flow data between 1900 and 2001 were taken from a simulation of daily average flow rates generated using a rainfall/river-flow/dam model (SKM, 2004).

[22] The national reference station, offshore from Maria Island, was started in 1944 by CSIRO Marine and Atmospheric Research Australia to measure coastal water quality off the east coast Tasmania and the Australian mainland (see Thompson *et al.*, 2005)

5.4.3. Salinity models

The bottom water salinity of the estuary was calculated over the last 126 years by solving Ficks second law advective/diffusion equation (Equation 5.1) for measured pore water salinities (Stiller *et al.*, 1983; Adkins and Schrag, 2003; Soulet *et al.*, 2010). The equation was solved numerically and constrained by expected relative changes in salinity by river flows and net tidal exchange (see Chapter 4), between a choice of two alternative pre-1868 boundary conditions; a fixed boundary condition of coastal salinities, or on an effectively infinite column of coastal seawater. The latter simulated by extending the sediment column depth to a point (20 m) where there is no significant feedback with depth over the simulation time.

Equation 5.1. $$\partial S/\partial t = \partial/\partial z(\partial Db \partial S/\partial z) - \partial(US)/\partial z$$

Where S is the salinity at depth z at time t, Db is the effective diffusion coefficient for a seawater salinity composition down a muddy sediment core (Matisoff, 1980) and U is the sedimentation velocity.

During the numerical simulation, the diffusion coefficient (Db) was fixed at $5x10^{-6}$ cm^2 yr^{-1}, which was calculated by Matisoff (1980) as optimal, irrespective of effects from surface bioturbation and compaction (Stiller *et al.*, 1983) and for a similar muddy sediment, age and temperature range as the Lower Middle Basin cores (14.5°C, DIPW, 1998). The sedimentation rate was also held constant as the average over the simulation period (1880 to 2007) because Adkins and Schrag (2003) found that the solution was not sensitive to large changes in sedimentation rate, algorithmic simplicity and significantly shorter simulation times. The numerical solution constraints on relative bottom salinities were based on relative changes in tidal exchange per unit change in inter-decadal river flow (see Chapter 4) and were kept coarse as step-like transitions.

5.4.4. Numerical algorithm

The diffusion/advection equation (Equation 5.1) was solved numerically in an Excel™ spread-sheet. Towards the top of the spread-sheet, the bottom water salinities were kept constant (fixed boundary condition) over their transition periods above a sediment column of pore water salinity set initially at a lower estimate of past bottom water salinities and a maximum salinity represented by the first 20 cm of pore water data (annual average; Matisoff, 1980) for the only extended drought period from the late nineteenth century to early twenty-first century (see Chapter 4). The number of spread-sheet rows was set to represent the thickness of the sediment horizons formed after a unit simulation accretion time. The bottom pore water boundary condition (before 1880) was set either as a constant coastal seawater

salinity or as a 20 m column (effectively infinite) of coastal salinities. It was found that 20 m was a sufficient length to remove effectively the 'feel' of any diffusive salt accumulation from the bottom of the column during the simulation. The accretion of the sediment column was simulated by inserting a row into the spread-sheet at the top of the pore water sediment column. After each period of accretion, the resultant salinities were calculated from the flux of salt across all of the horizons (Equation 5.1). In this way, the column grew in length down the spread-sheet from a fixed surface above fixed bottom water salinity over each transition period.

The time and depth flux calculations were based on 2 cm weekly iterations, which were similar in scale to those used by Stiller *et al*. (1983) for the Dead Sea (5 days and 5 cm). Like Stiller *et al*. (1983), the iterative resolution produced a modulus of less than 0.5, necessary to satisfy numerical analysis stability requirements (Carslow and Jaeger, 1959). The solution was considered optimal after the convergence of two metrics, a minimum mean square error and a minimum sum of the differences between the bottom water salinity transitions. In this way, the solution was considered to represent the most conservative of choices in salinity variance and in turn to be a more robust test of the significance of nutrient dilution by coastal waters. However, in practice, it was found that only the mean square error was necessary.

5.4.5. Surface salinities

Surface salinities down sediment core LSPMB106 were determined using a local diatom assemblage transfer function (Saunders *et al.,* 2007). The transfer function was constructed using the relative abundance data for preserved diatom remains from the surface sediments of Tasmanian east coast estuaries and lagoons, including the Marine Flood/Tidal Delta sediments of the Little Swanport estuary (Saunders *et al.,* 2007). For reasons of specialist expertise and consistency, Dr K. Saunders was requested to identify the diatoms to species level. The non-contiguous time series was then reconstructed by using the average annual geochronology for the Lower Middle Basin central trench from 1880 and 2006 (see Chapter 4).

5.4.6. Surface salinity evaluation

The long-term non-linear trends of diatom inferred annual average surface salinities (see data analysis) were evaluated using a multiple linear regression model of nondimensionalised external variables (Equation 5.2; Sigmaplot™) that control surface salinity: wind (zonal index [ZI]), tidal exchange (bottom salinities per unit river flow) and median river flow (SKM,

2004) after a ladder of powers transformation of the river flow as its cubic root (Tukey, 1977). This nondimensionilisation then allows: (1) a comparison of the relative size or importance of terms in a linear equation, (2) the number of equations that link flow to salinity is reduced by the number of original dimensions, and (3) it allows semi-empirical formulas to be derived from observations of non-linear complex phenomena, especially those that deal with factors that induce turbulence (Tober *et al.*, 2008).

Equation 5.2. $S = aR^{0.3} + bR^{0.2} + cR + dZI + eT$

Where a, b, c, d, e are coefficients, S is diatom based reconstructed salinity, R is the non-linear inter-annual trend of median annual river flows, ZI is the non-linear inter-annual trend of westerly winds and fetch and T is the inter-decadal changes in bottom salinity normalised for pre- and post-drought conditions.

The annual median river flow was chosen over the average because the annual average salinity distributions more closely matched the less skewed annual median river-flow distributions than did the highly skewed annual averages (Alber and Sheldon, 1999). The median removes the non-linear response of salinity to strong flows and floods as the estuary moves towards a freshwater body.

5.4.7. Data analysis

Contiguous temporal data sets (river flows, ZI) were re-analysed for inter-decadal non-linear trends using singular spectrum analysis (SSA) within the architecture of Kspectra™. The method is a data-adaptive, model independent spectral analysis that is ideal for non-stationary short time series (>30 points), which has been described as a principal components analysis within a time domain (Vautard *et al.*, 1992).

A modification of the method, singular spectrum analysis of missing data (SSAM), has been used for reconstructed annual average surface salinities and monthly coastal nitrate data sets. SSAM was developed primarily for imputation of a time series with missing blocks of data and arguably for hindcasting. The extended imputed time series can then be re-analysed for a more powerful statistical assessment of trends and periodicity (Kondrashov and Ghil, 2006). SSAM works by using all of the information within the time series by first iteratively producing estimates of missing data points to compute a self-consistent lag-covariance matrix and empirical orthogonal functions based not on extrapolation but an underlying periodicity. The result is then cross-validated to optimise the window length for long-term non-linear trends (12 years for all data sets) described by the dominant SSA components (four for all

data sets). It should be noted that before SSAM, the coastal nitrate data were rounded up to their nearest monthly time slots and any duplicates or triplicates were averaged. Further, the noted aberrant data sets were removed and constraints were added within the Kspectra™ program's 'preferences' by setting the maximum and minimum nitrate concentrations to 6.0 μM and 0.0 μM, respectively. This was to remove large outliers and diminish possible reconstruction of negative nitrate concentrations.

5.5. Results and discussion

5.5.1. Bottom water salinities

5.5.1.1. Solution constraints

The bottom salinity's solution constraints were based on changes in tidal exchange (see Chapter 4) in relation to two river-flow regimes during the post- and pre-drought conditions (1979/1980). Hence, from 1980 to 2007, it was assumed that the average bottom water salinity was equal to the 2007/2006 annual average; that is, the average of 20 pore water salinities measured within the surface 20 cm (Matisoff, 1980; see Figures 5.3a and b). For the time period between 1970 and 1980 it was assumed that the bottom water salinities were no longer hyper-saline but were greater than salinities during the pre-entrance restriction times (1911 to 1960) by the relatively greater tidal exchange (see Chapter 4). During the period of entrance restriction (1960 and 1970; Chapter 4), the estuary can be expected to have had the lowest bottom salinities since the late nineteenth century. The period from 1911 to 1960 was the period of greatest tidal exchange (see Chapter 4) and a time when the bottom waters were less than, but the closest to, coastal water salinities.

5.5.1.2. Iterations

Figure 5.3b shows examples of various sub-optimal iterations to illustrate the form and sensitivity of the model simulations. The blue iteration clearly over-estimates the salinity depth profile (see Figure 5.3) and it was based on a period of hyper-saline water conditions over the drought period (1980 to 2007) on an infinite column of coastal seawater. The iteration serves to illustrate the necessity of a relatively low pre-drought salinity and relatively high fixed bottom salinity boundary condition to 'flatten' and reduce the simulation's salinity depth profile.

The remaining simulations illustrate the sensitivity of the analysis to relative change in salinity for different bottom boundary conditions. For example, it was found that the two different bottom boundary conditions gave the same optimal solutions but the mean square

errors for the fixed bottom coastal salinity boundary condition (black line Figure 5.3a) were clearly significantly less than the alternative; that is, an infinite column of coastal seawater (red line Figure 5.3a). The green iteration illustrates that the sensitivity of the simulation is of the same order as the changes in pore water salinity down the sediment core.

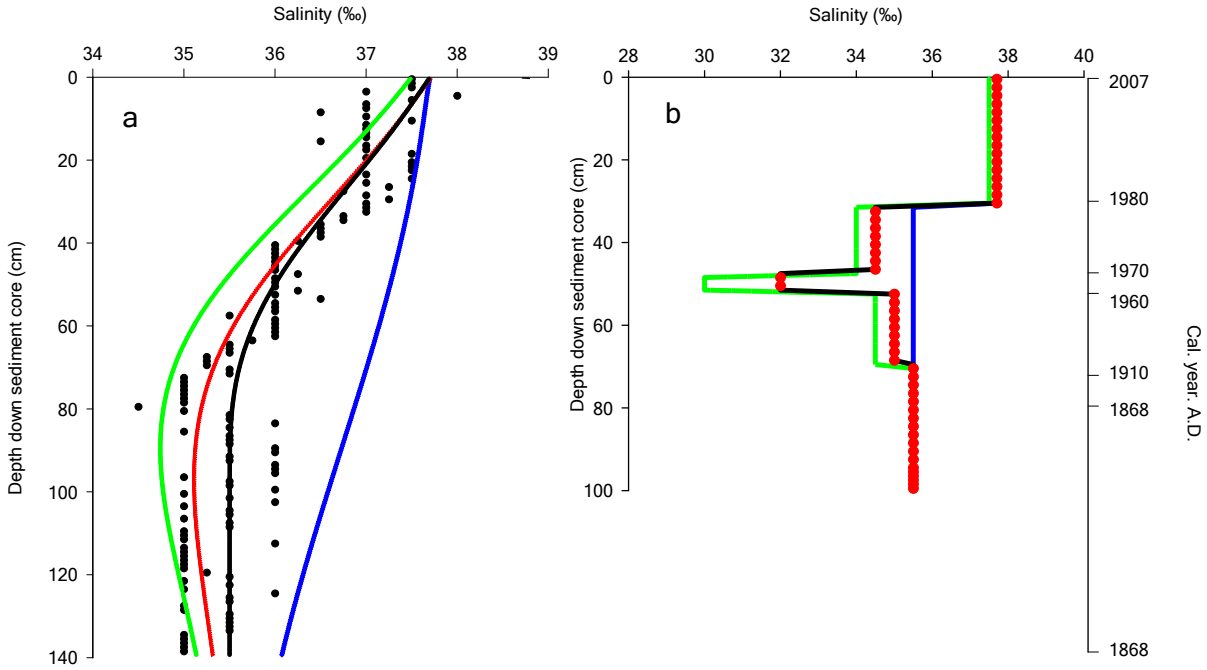

Figure 5.3. Reconstructed bottom water salinities modelled from contemporary pore water values down the Lower Middle Basin sediment core LSPMB107.
(a) Examples of bottom water palaeo-salinity optimal fits of post-diffusion simulations in relation to the measured pore water salinities (●). The colours of the simulations refer to their respective bottom water temporal salinity variability scenarios, illustrated in (b).

Despite being coarse, the evaluation of the model is dependent on the robustness of the timing and the magnitude of the event constraints. The events appeared to be consistent with the SIT ^{210}Pb geochronology (see Chapter 4). Nevertheless, it should be noted that there might have been some model bias by overestimating the period of drought. The drought period was based on cumulative sum of the mean within an ordered series (CUSUM) changes in annual average baseline river flows (see Chapter 4) and CUSUM analysis is sensitive to the length of the data set after the final change point. That is, no change point in the mean river flow could be determined when the last 10 years of data were removed from the time series (1991). In contrast, the change to a lower mean river flow was extended to 1987 when the last 10 years was added to the time series (2011).[23] Indeed, it is possible that 1987 may be a more appropriate date for the beginning of the drought as the original change point analysis also

[23] It was noted that the drought along the east coast of Tasmania had ended by 2009.

suggested a reduction in the series standard deviation from 1987 (unpublished expression of the analysis), which can be clearly seen in Figure 4.19 (see Chapter 4).

5.5.2. Surface salinities

With the exception of the low salinities between 1960 and 1970, the surface salinities were not positively correlated with the bottom salinity (*c.f.* Figure 5.4 with Figure 5.3). In particular, there was a counter intuitive fall in surface salinity during the onset of a fall in mean river flow over the drought. However, this was not inconsistent with the behaviour surface salinities at low river flows, neither should the temporal variance between surface and bottom necessarily follow one another (*e.g.* Schröder *et al.*, 1990). For example, Tully (1949) first observed that surface salinities fell then rose with increasing river flow within the fjord Alberni Inlet (USA). The reason for the different salinity response is a transition from laminar to turbulent flow within increasing river flow and shear. After an initial fall in surface salinity with increasing river flow, the surface layer depth remains relatively constant but becomes increasingly fresher as it is stabilised by tidally driven bottom water entrainment. Eventually, the increasing velocity shear within the freshwater layer results in turbulence (Froude Number >1; Dyer, 1973), which drives entrainment of salt into the surface layer, thereby increasing both the depth and salinity of the layer.

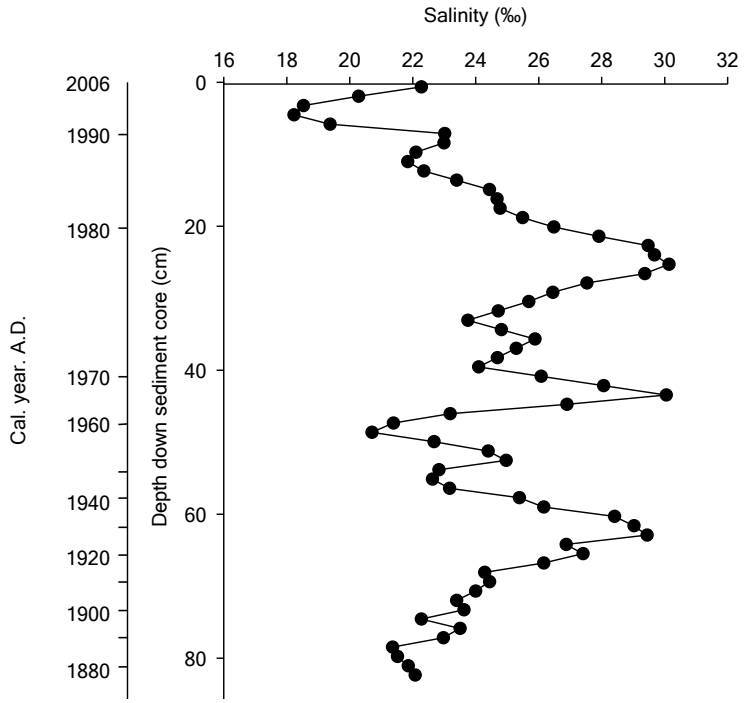

Figure 5.4. Diatom-derived surface salinities down the Lower Middle Basin sediment core LSPMB106.

Irrespective of the fall in surface salinities over the drought, the surface salinity variance remained more complex than could be ascribed to the step-like character of the inter-decadal river-flow regime (see Chapter 4) or the changes in tidal exchange, such as the peaks in surface salinity around 1925 and 1965 (see Figure 5.4). Either the spatial transfer function was not sufficiently general in time, the CUSUM analysis was too crude a metric to disseminate the changes in river-flow and tidal exchange through the core's organic content (see Chapter 4), or other external forcing factors, such as wind, contributed to the surface salinity variance.

5.5.3. Evaluation of surface salinities by long-term wind, river-flow and tidal variance

The bottom water salinities, normalised to remove the effects of the drought, were used as a scalar proxy for tidal exchange (see Figure 5.5a) with the ZI for increasing fetch from stronger westerly winds and river flow, deconstructed as the sum of its dimensions as a scalar metric (Equation 5.2). A SSA found that the westerly wind and river flow had strong decadal quasi periodicities (around 13 years and 10 years respectively) and trends. However, neither wind, nor river-flow periodicities or tidal exchange variance were in phase with each other. All three forcing factors were needed for the best correlation with annual average surface salinities (adj. r 0.68; see Figure 5.5b). Indeed, such a strong to moderate correlation from all three independent variables was remarkable when considering the undoubtable errors in the sediment columns chronology and gives further support for a complex sediment column geochronology (see Chapter 4).

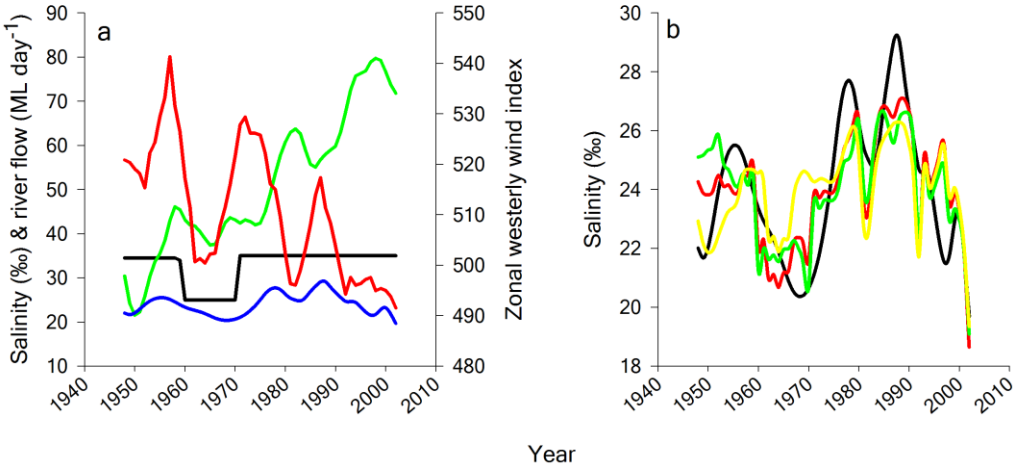

Figure 5.5. Reconstructed long-term non-linear trends of river flows, wind and tidal proxies for a multiple linear regression with the reconstructed surface salinities of the Lower Middle Basin sediment core LSPMB106.
(a) Non-linear trends westerly winds as ZI (—); annual median river flow (SSA) (—); diatom-derived surface salinity (—); tidal variance as bottom salinity (—). (b) Diatom-derived surface salinity multiple linear regression model: diatom-derived surface salinity (—); salinity fit from a model using ZI, tidal exchange and annual median river flows (—); salinity fit from a model using tidal exchange and annual median river flows (—); salinity fit from a model using westerly wind and annual median river flows (—).

All three forcing factors made significant contributions to the surface salinity prediction but at different times, and this was reflected in the moderate correlations between paired combinations (adj. r =0.53) for river flow and westerly winds, and adj. r =0.62 for tidal exchange and river flow. For ZI, the manner of salinity dependence was seen in the pre-1960 divergence of the ZI–river-flow model from the complete model. There was a pre-1970 divergence of bottom salinity/river model from a complete model fit for tidal exchange during the entrance restriction (1960 to 1970; see Figure 5.5b).

Further, the diatom-derived surface salinity was consistent with the annual average and not the result of an assemblage formed during the drier spring/summer growing period (see Figure 5.6a). The surface salinity multi-linear regression was based on a SSA of monthly averages. There was a strong correlation between annual average river flow (total amount salt) and average winter river flow (see Figure 5.6b), where most of the long-term variance was located (see Figure 5.6a).

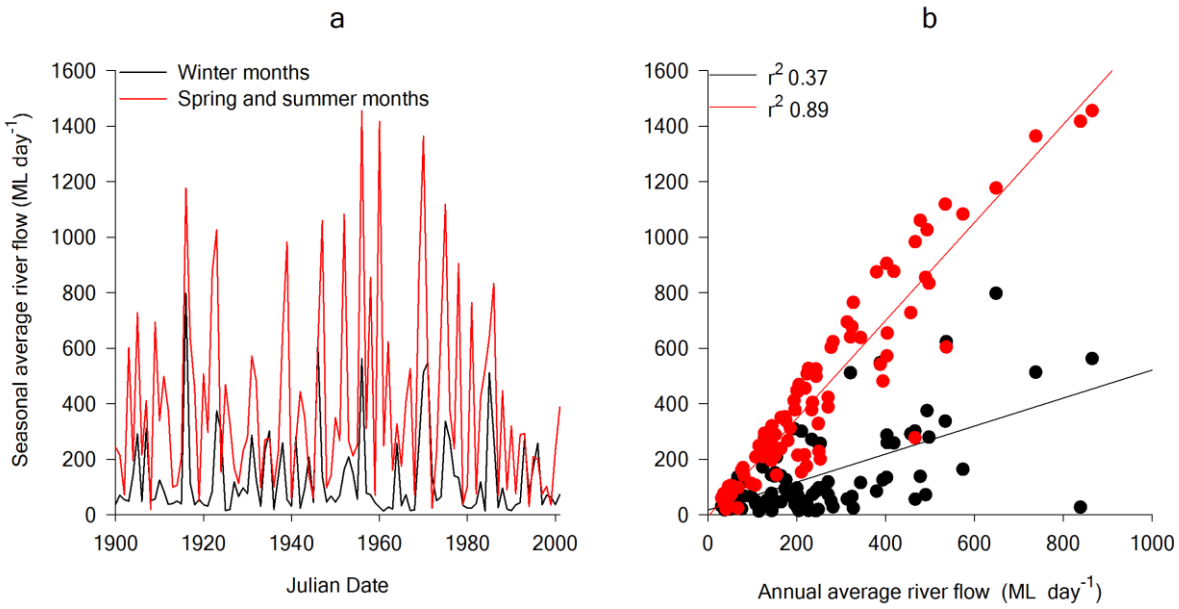

Figure 5.6. A re-analysis of 101 years of modelled seasonal river flows for the lower Little Swanport River. (a) Time series of winter and spring/summer average river flows from the river/catchment/dam model (SKM, 2004). (b) Correlations between the average annual winter flows with annual average river flows (●);correlations between the spring/summer average river flows with the annual average river flows (●).

5.5.4. Evaluation of the average estuarine salinity

The average salinities for the CPN calculation were estimated from the average of the bottom and the surface salinities down the Lower Middle Basin sediment cores. The estimate did not take into account the weighted differences in salt content down the water column, or across

the estuary. Nonetheless, it was found that the concept did approximate the estuary's weighted average salinity.

Figure 5.7 shows the salinity depth profiles across the three functional zones (see Chapter 3), determined by their baseline river flow history (Alber and Sheldon, 1999) 40 ML day^{-1} to 82 ML day^{-1}, values that were close to the 100-year median (35 ML day^{-1}), and river flows from 205 ML day^{-1} to 383 ML day^{-1}, more typical of a strong flow or small flood. It was found that despite of the difference in the fraction of freshwater, 0.07 and 0.25 between the median river flows and the flood, the calculated volume weighted and average salinities ratios between the Upper Middle Basin and Lower Middle Basin were not vastly different (0.7). Further, the volume weighted average salinities across the whole Middle Basin closely approximated the average salinity within the Lower Middle Basin when this was calculated for the palaeo-reconstruction (the average of surface and bottom salinities): 22.2 ‰ *c.f.* 23.6 ‰ and 29.6 ‰ *c.f.* 32.1 ‰ for the floods and baseline river flow, respectively.

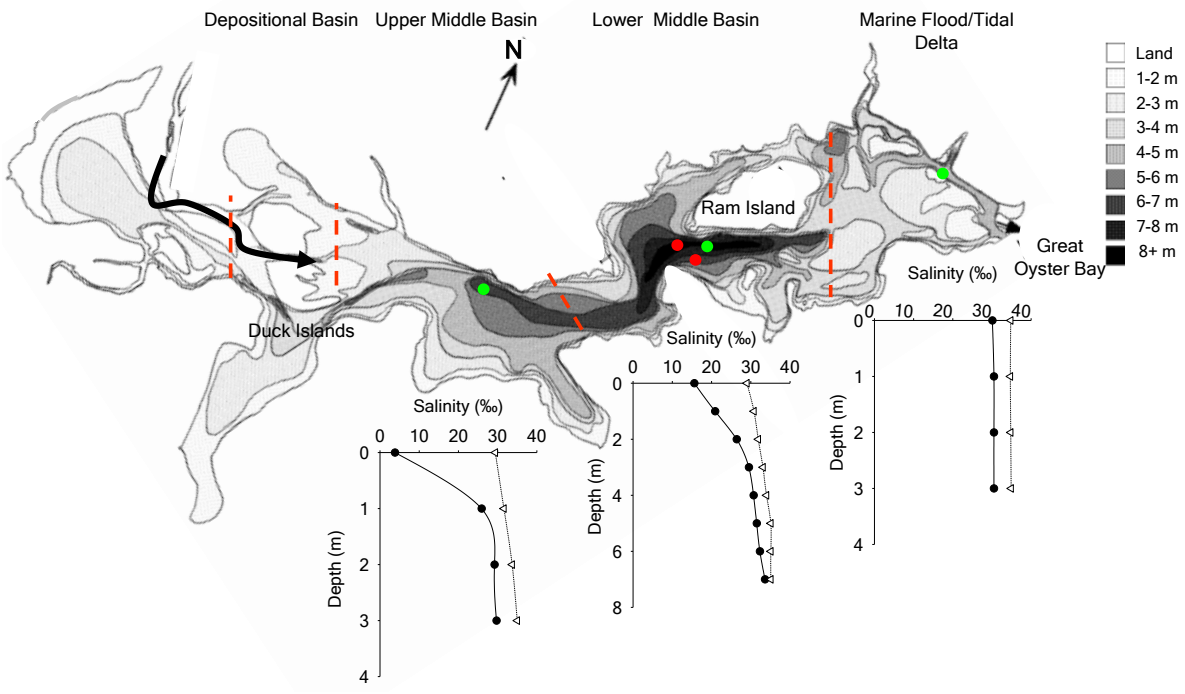

Figure 5.7. Bathymetry, sampling sites and salinity profiles down the Little Swanport estuary.
Sediment core extraction sites (●);salinity profile stations (●).Salinity profiles taken during a small flood averaging 205 ML day^{-1} (●);salinity profiles taken during a river flow close to the *calc.* 100-year median (50 ML day^{-1}) (Δ). The thicker black arrow shows the major direction of river flows into the main body of the estuary.

5.5.5. River-flow/DIN response curves

It is clear from the data distribution between river flow and DIN concentrations (see Figure 5.8) that a simple curve fit would not produce a set of normally distributed residuals (*e.g.* a traditional second order polynomial or hyperbolic relationship). Other than one complex empirical curve, a series of four curves, which had been statistically separated by their CUSUM change points, were fitted to the river-flow and DIN concentrations (see Figure 5.8) and with a variance that was consistent with a set of plausible postulates that appeared to explain the evolution of the curve transitions:

1. A stagnation phase (green zone) where there was a build-up of the DIN concentrations from internal mineralisation of OM.
2. A dilution phase (red zone) where dilution by river flows overwhelmed the catchment DIN loading and internal recycling and resulted in a smaller but invariant mean DIN concentration than the above stagnation phase.
3. A proportionate response of DIN catchment loading with increasing river flow (yellow zone).
4. Flood dilution (grey zone) where most of the DIN associated with soil extracts had been previously washed out, resulting in a fall in DIN but at equilibrium with a high concentration of soil particulates.

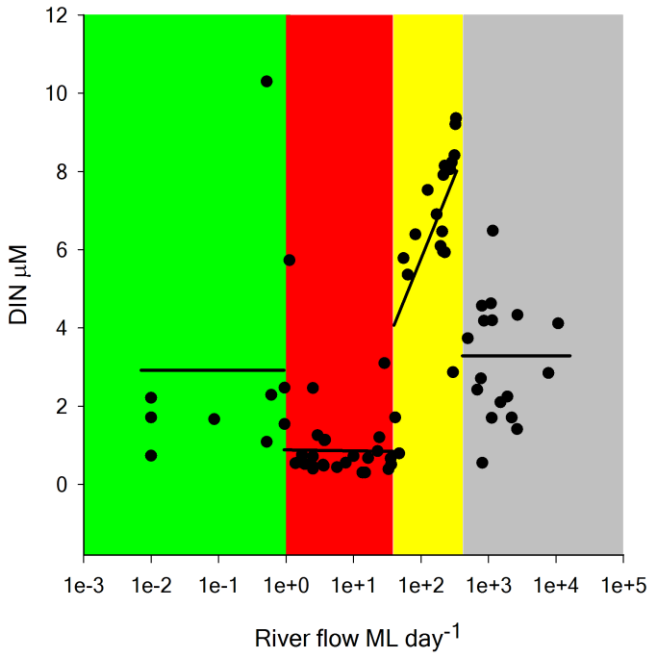

Figure 5.8. The CUSUM change points for the Little Swanport River's DIN concentrations (DPIPWE, 1998) in relation to measured daily average river flows.
The horizontal lines are CUSUM means of DIN and the sloping line a least squares regression (yellow bar; r^2 = 0.36).

5.5.6. Surface coastal nitrate variance: Maria Island data, SSAM imputation and hind casting

It was fortunate that the long-term Maria Island coastal monitoring station near the Little Swanport estuary provided over 60 years of data. However, it was found that 27 % of the monthly surface nitrate data was either missing or in error (see Figure 5.9a). Consequently, SSAM was applied to the current data set to imputate the variance within the data gaps and to extend the data set back to 1920. Otherwise, analysis-based simple extrapolation techniques (*e.g.* running averages and LOESS) would lead to errors in both non-linear trends (periodicities) and the global trend along the series (Kondrashov and Ghil, 2006) and not provide a sufficiently long time series for the late Anthropocene palaeo-reconstruction or a good test of any periodicity with biome variance over coincidence (see Chapter 7).

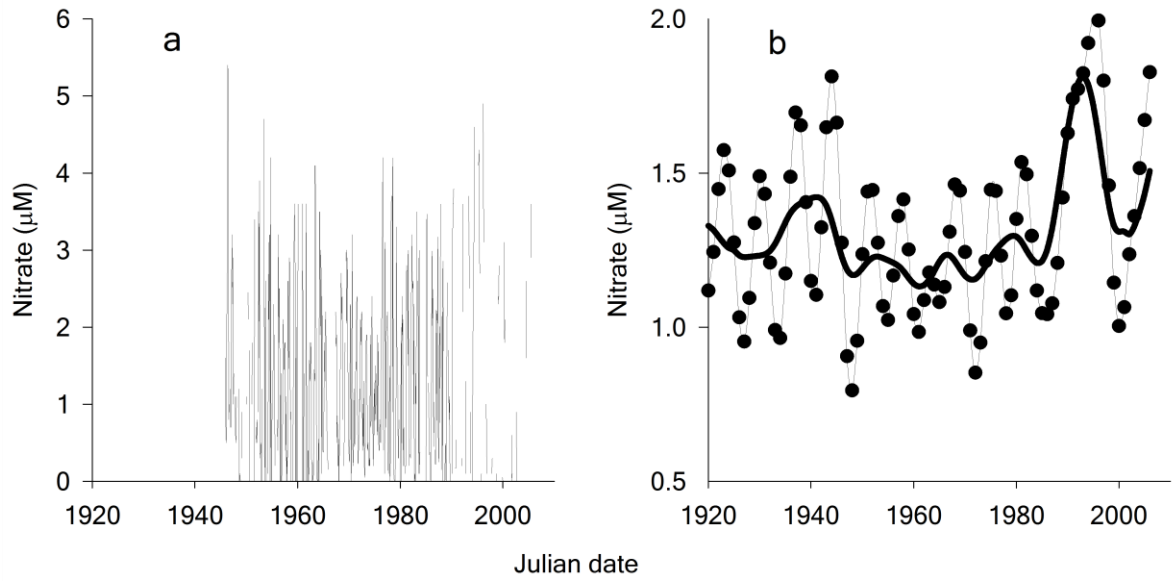

Figure 5.9. Long-term coastal nitrate data and its imputed time series
(a) A scatter plot of available and verified monthly surface nitrate data taken from the CSIRO coastal monitoring station offshore from Maria Island; (b) SSAM imputation and hind casting: annual average coastal nitrate concentrations after white noise was removed (●), and its long-term non-linear trend (▬).

The SSAM analysis identified two significant periodicities at both inter-annual and decadal scales: 6.83 years and 12.91 years, respectively. The longer frequency component correlated with both the contiguous SSA re-analysis of the ZI from 1948 to 2004 (see Figure 5.3a). It was the periodic changes towards westerly winds that appeared to increase coastal nitrate concentrations (Harris *et al.* 1988; Evans *et al.*, 2005) and was used to explain the periodicity of cetacean stranding around Tasmania from 1920 to 2004 (*i.e.* feeding in more productive waters). Indeed, the convergence of the imputed nitrate time series extended with the stranding data to 1920. This then confirms both Evans *et al.*'s (2005) plausible explanation

and the plausible SSAM imputation analysis (*i.e.* a coincident RA; see Chapter 1) that was based on information across the whole time series.

5.5.7. Potential concentrations of dissolved inorganic nitrogen

The average annual river DIN concentrations were calculated by matching the daily average modelled river flows (SKM, 2004) between 1900 and 2001 (see Figure 5.10a) to the contemporary river flow (see the DIN response curves in Figure 5.8). Annual CPN was then calculated from the annual average SSAM coastal nitrate as DIN (Riley and Chester, 1971) and the average annual river DIN, in proportion dictated by annual average estuarine salinity (see Figure 5.10a).

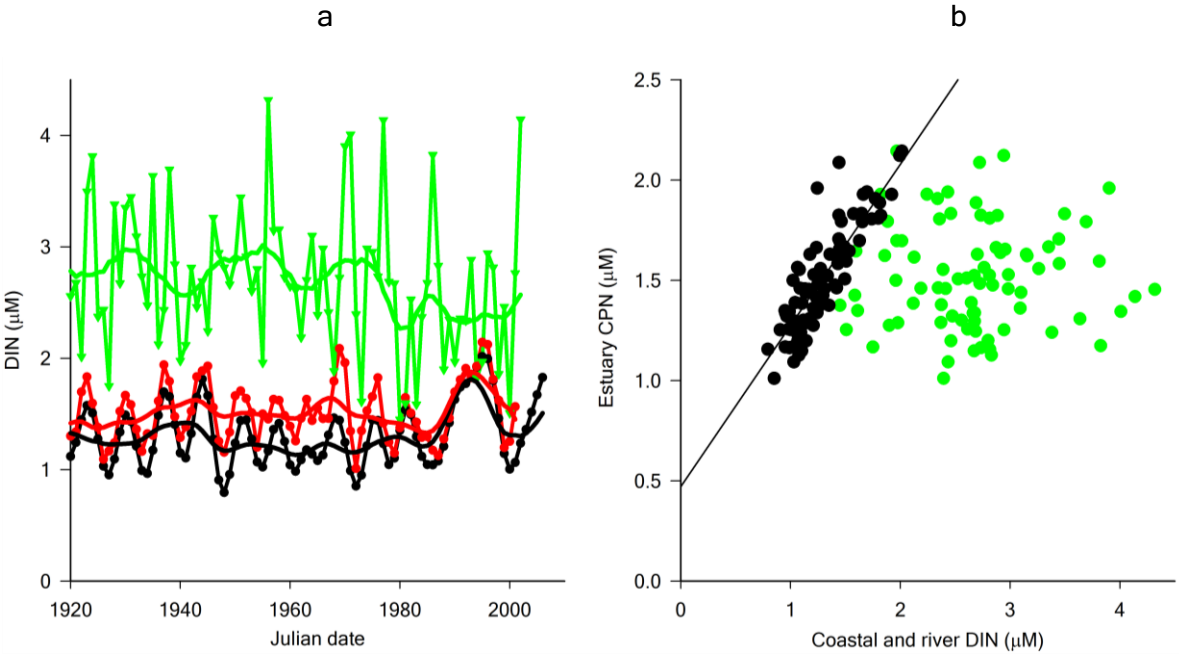

Figure 5.10. Reconstructed time-series and correlations between river and coastal dissolved inorganic nitrogen and the resultant estuarine CPN.
(a) Annual average DIN concentrations with their SSA non-linear trends for the Little Swanport River (—), adjacent coastal waters (—), and the CPN (—); (b) correlations between the annual average river (●), coastal nitrate time series, and the estuary's CPN (●),.

As expected, the river DIN concentrations (mean 2.7 µM, standard deviation 0.64 µM) were significantly larger than for the coastal DIN (mean 1.3 µM, standard deviation 0.28 µM). However, the river concentrations were not large enough to compensate for the relatively small proportions of freshwater within the estuary. Consequently, the variance in estuarine DIN could not be predicted from changes in river DIN but was well correlated from the coastal DIN (see Figure 5.10b). The only significant deviation between CPN and coastal nitrate variance appeared to result from the time of a significant change in tidal exchange during the entrance restriction between 1960 and 1970 (see Chapter 4), At this time there was a somewhat improbable set of circumstances of tsunami and flood confluence (see Chapter 4) that is unlikely to be repeated over centennial time scales.

5.6. Summary and conclusions

The new inorganic nitrogen availability (CPN) for the primary productivity assemblage in the Little Swanport estuary was reconstructed for the last 81 years. The calculation depended on a palaeo-reconstruction of both surface and bottom salinities to estimate the contribution of modelled river DIN and coastal DIN concentrations using SSAM time series analysis. It was found that the both the average salinity and coastal nitrate reconstruction was robust with respect to other of lines of evidence. The argued assumption of little change to contemporary inorganic nitrogen response curve (i.e. no significant changes from upper catchment pastoral development) could not be directly evaluated. Nevertheless, the assumption was insensitive to the CPN variance because the CPN variance was controlled primarily by the periodic intra-annual to inter-decadal variance in coastal nitrate concentrations. In other words, if there were significant contributions from the catchment development, then removing this bias would further strengthen the dependence of the estuary's CPN on coastal variance. Furthermore, the dependence of the CPN on coastal nitrate can also be considered robust because the reconstruction was based on an evaluated 80-year time series of salinity and river and coastal nitrate that represented a wide range of local river flows, flood strengths and frequencies with elevated river DIN concentrations over different times of the year.

The resultant CPN dependence on variance in the coastal nitrate boundary condition, also highlight the limitations of predictive models based only on catchment loading by not testing for changes in the nitrate coastal boundary conditions over the medium (inter-annual) and long-term (inter-decadal). Consequently, future concerns regarding changes to ecosystem services that depend on DIN supply should first be addressed from the standpoint of medium to long-term sustainability based on changes in coastal supply and not necessarily from changes to the catchment. This of course, would make any potential engineering solution, outside global climate change, focus on changes in coastal tidal exchange (entrance modification) to directly influence coastal supply of nitrate to the estuary and other than regulating nitrogen loading through managing water catchment allocation.

Chapter 6. Natural and anthropogenic ecosystem regimes within the Upper Little Swanport estuary over the last 83 years: A palaeo-reconstruction

6.1. Introduction

The contemporary transect study (see Chapter 3) indicated that the upper estuary's seagrass and micro-algae were nitrogen-impoverished, and only maintained in their current regime state of healthy seagrass coverage and shoot density by seagrass-mediated nitrogen fixation. Users of the upper estuary rely on ecosystem services it provides, namely, aesthetics, biodiversity, fish habitat and a robust net micro-algal production to support the upper estuary's shore-based juvenile oyster aquaculture. Hence, the reasons behind the nitrogen impoverishment and the feedbacks that maintain and destabilise primary production are of concern for users of the seagrass ecosystem.

There are a number of plausible causes, both natural and anthropogenic, for the current upper estuary regime state, and a number of plausible factors than can stabilise the regime state. It has been argued in Chapter 1 (see Section 1.1) that the current regime is either the result of the history of natural and anthropogenic external forcing factors (*i.e.* historical contingency) or it may be a naturally stable and persistent regime that is resilient to events or changes in nutrient supply.

A number of natural and anthropogenic events have been identified as directly or indirectly affecting the Upper Middle Basin of the Little Swanport estuary, namely, floods, the drought (Chapter 4), including inter-decadal variance of the coastal inorganic nitrogen supply as the major source of limiting nutrients (see Chapter 5). It was suggested that the lower estuary's shell fish aquaculture (Chapter 3) may have been responsible for the present state of the upper estuary's nitrogen impoverishment by moderating its supply of coastal nitrate resources. However, it was unclear if nitrogen impoverishment was also contingent on the effects of the long-term drought and a reduction in supply of catchment resources or a natural response to times of low costal supply. Furthermore, the extent of light mediated nitrogen fixation, of nutrient impoverished systems, may vary should the estuary's postulated planktivorous fish trophic cascade (i.e. fish–copepods–diatoms–epifaunal coverage [Chapter 3]) significantly affect the seagrass leaf light attenuation by effecting changes in epifaunal coverage.

Cleary, there is a need to account for the historical contingency on regime change together with a general theory that can describe the factors that led to regime change. In this way, predictions based on different combinations of regime state, events and anthropogenic pressure can be made to manage the ecosystem services in a manner that maintains biodiversity in an equitable way (see section 1.1). Such a general theory would need to address the causes of regime change, the structural (seagrass and micro-algae abundance) and functional nature of the regime (light or nutrient limited), and the factors that stabilise its function (see Section 1.1). In brief, a nutrient limited micro-algal stable regime state maintains its function through light attenuation and thereby inhibiting seagrass recruitment and growth (Duarte, 1995; Scheffer and Carpenter, 2003; Duarte *et al.*, 2006). A stable seagrass state's response of light limited growth is maintained through net micro-algal eutrophication that leads to significant light attenuation of the seagrass (bottom up control). Attenuation, however, may be ameliorated by a planktivorous fish trophic cascade on net micro-algal growth and maintain the seagrass meadow stable state's dependence on nitrogen (Frankovich and Fourqurean, 1997; Heck *et al.*, 2000; Heck and Valentine, 2006; Jorgensen *et al.*, 2007; Moksnes *et al.*, 2008). Alternatively, for nitrogen-impoverished systems, a strong planktivorous fish trophic cascade can potentially maintain the seagrass–micro-algal system by light mediated nitrogen fixation (see Chapter 3).

The above descriptions of regime structure and function are based on the states that persist at equilibrium with external inorganic nitrogen supply or, in the case of nitrogen fixation determined by external nitrogen impoverishment. However, there are regimes that are not at equilibrium but may still persist over a number of years. These states are the dynamic transient regimes between two stable states (micro-algal or seagrass [Scheffer and Carpenter, 2003; Knowlton, 2004]). Indeed, micro-algal transients may be maintained by the previous store sediment nutrient resources or conversley the time it takes for a benthic macrophyte such as a seagrass meadow to collapse (Scheffer and Carpenter, 2003; Knowlton, 2004).

Nevertheless, by following a sequence of events within a disturbed dynamic system, at the appropriate level of ecosystem abstraction, is arguably the best means to both assess the importance of historical contingency and produce a general theory of intra-regime and inter-regime variance (see Section 1.3.1).

6.1.1. Aims

The aim of the study was to determine the reasons behind the Upper Middle Basin's current juvenile state, as either a natural process or one affected by the timing of the lower estuary's shellfish aquaculture, and to postulate a general theory of seagrass variance that can be used to predict the future affects on the estuary(s) by anthropogenic pressures from aquaculture and on going natural changes in coastal nitrate supply for different historical contingencies. This was achieved by a late Anthropocene palaeo-reconstruction of the Upper Middle Basin's ecosystem variance that enabled identification of the sequence of events that led to regime change, the functional and structural nature of the regime (i.e. any micro-algal or seagrass stables states and their dynamic transients) together with factors that control the regime's stability type of regime change.

The level of abstraction used in the palaeo-reconstruction was chosen to reflect the probable causes and stability of regime change to nitrogen supply. The cause of any regime change was postulated as being due to the pivotal floods recorded within the Upper Middle Basin sediment cores (see Chapter 4), drought (1980 to >2007 [see Chapter 4]) and the replacement of the lower estuary's shellfish aquaculture (1986 [see Chapter 3]). The mechanism behind stability of the resultant regime is determined by comparing temporal patterns, in relation to current theories, of seagrass and micro-algal proxies, external inorganic nitrogen availability (CPN [see Chapter 5]), proxies for the extent of nitrogen fixation and organic nitrogen mineralisation, and proxies for the strength of the planktivorous fish trophic cascade.

6.2. Materials and methods

In order to evaluate the biome variance, the paleo-reconstruction relied on the convergence and plausibility of multiple lines of evidence—plausible models and proxies recommended by the estuary's transect study (see Chapter 3)—for the temporal element of a mixed Robustness Analysis (RA), inference towards the best explanation (IBE) and self-consistency (see Section 1.3.2 and Section 3.1). The following section lists the types of mixing models, their primary organic source end-points, other singular proxies for primary organic sources, inorganic nitrogen sources, together with turbidity and representatives of trophic levels and processes (i.e. calcareous epifauna and copepod and planktivorous fish predation rates).

6.2.1. Proxies and models

- The application of two organic ternary mixing models to calculate the proportions of seagrass, micro-algae and soils down the Upper Middle Basin's two sediment cores

(*i.e.* organic carbon stable isotope ratios ($\delta^{13}C_{org}$) and their particulate organic nitrogen (PON) to total organic carbon ratios (TOC)[24] and a stepwise thermogravimetry Rp index and their total nitrogen to organic carbon ratios (TN/TOC [see Chapter 3]).

- Seagrass pieces (>315 μm) and diatomaceous biogenic silica (BSi) for the primary producers (see Chapter 3).
- The ratio of total organic carbon (TOC) to BSi content, as an index of seagrass carbon for sediments with minor soil variance or content (Chen and Windom, 1997).
- Particulate organic carbon content (POC) within the fine fraction (<76 μm), as micro-algal variance (see Chapter 3).
- LOI between 550 °C and 950 °C (LOI 950 °C), as seagrass calcareous epifauna (*e.g.* bryozoans [see Chapter 3]).
- Sediment size fractions that represent: sestonic turbidity (<76 μm), copepods based on the presence of their faecal pellets (150 μm and 100 μm) and an index of inferred planktivorous fish predation based on the ratio of the two copepod faecal pellet size fractions (see Chapter 3).
- Organic nitrogen stable isotopes ($\delta^{15}N_{org}$) of seagrass pieces and the sedimentary fine fraction (<76 μm) to distinguish between internally generated and externally supplied inorganic nitrogen to the primary productivity assemblage respectively (see Chapter 3).

6.2.2. Study sites and sample collection

Sediment cores were extracted from two sites within the deeper central trench of the Upper Middle Basin (see Figure 6.1). The focus of the study was on sediment core LSPMB206, which had been shown to record all of the major floods since 1923 that had directly affected the upper estuary, but with the least amount of flood erosion (25 cm [see Chapter 4]). The remaining sediment core (LSPMB2B08), from a site further up the Upper Middle Basin, was used to augment the resolution of the LSPMB206 seagrass pieces profile over matching years. This was because the amount of seagrass material in the LSPMB206 sediment core was sufficient for elemental analysis (μg dry weight) but not always sufficient for isotope analysis (mg dry weight).

[24] Perdue and Koprivnjak (2007) showed that organic mixing models must be expressed as PON/TOC and not TOC/PON for linear solutions of organic component mixtures.

See Chapter 2 for details of sediment core collection, sub-sampling, size fractionation and analysis of proxies for sedimentary and seagrass TOC, POC, BSi, isotopes of organic carbon ($\delta^{13}C_{org}$) and nitrogen ($\delta^{15}N_{org}$), $CaCO_3$ (LOI 950 °C) and processing for faecal pellet content. See Chapter 4 for details of the sediments cores geochronology and Chapter 5 for details of external nutrient supply variance, as the concentration of potential inorganic nitrogen (CPN).

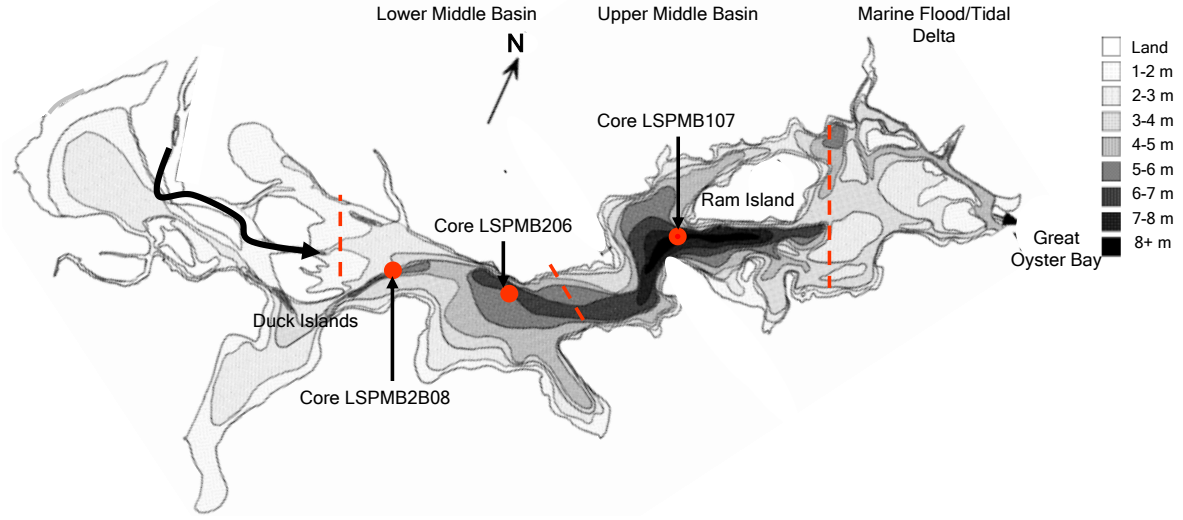

Figure 6.1. Bathymetry of the Little Swanport estuary and the position of sediment cores within the Upper Middle Basin and Lower Middle Basin.
The thick black arrow to the left represents the major direction of the river flow into the estuary's main body.

6.2.3. Diagenetic models

6.2.3.1. Organic matter and biogenic silica

It is particularly important when using organic geochemical indicators for reconstructing the recent past (Anthropocene) to consider the role of diagenesis in altering the geochemical record of the dynamics of environmental change (Chen and Windom, 1997; Zimmerman and Canuel, 2002; Khalil *et al.*, 2007; Wu *et al.*, 2008). To address this problem, Zimmerman and Canuel (2002) calculated the amount of organic carbon lost to mineralisation by using the robust TOC diagenetic model of Middelburg (1989). Middelburg's model incorporates a time-dependent apparent degradation rate parameter ($k = 0.16^{t-0.95}$) into the more familiar 2-G decay models of Berner by which any sample deposited 't' years ago ($C_{lost\text{-}t}$) be estimated using Equation 6.1.

Equation 6.1. $$C_{lost\text{-}t} = C_{mo} - C_{mo}e^{-kt}$$

Where C_{mo} is the original depositional organic matter's carbon content, k is Middleburg's time-dependent decay coefficient ($k= 0.16.t^{-0.95}$) and t is the time since deposition (years).

The apparent age 't' used in the Middleburg model is a concept that links the age of organic matter (OM) since deposition, to an equivalent contemporary form of OM. For example, fresh micro-algae have an apparent age of a few hours, while the apparent age of fresh lignocelluloses may be as great as a few months. The choice of the initial apparent age for TOC near the top of the sediment core was referenced to the average age of the first horizon using examples of similar surface sedimentary environments taken from Middleburg (1989).

Khalil *et al.* (2007) successfully matched deep sea sediment core BSi profiles by using a similar time-dependent dissolution rate constant to Middleburg's (1989) organic carbon mineralisation model. However, the model used by Khali's *et al.,* (2007) was expressed as a function of depth rather than time. Nevertheless, Chen and Windom (1997) found that down late Anthropocene salt marsh and estuarine sediment cores the dissolution of BSi was coupled to the mineralisation of TOC resulting in similar decay constants. Thus, it was assumed that losses of BSi over time could be calculated from the same TOC time-dependent function and initial apparent age as used by Middleburg (1989).

The equation was solved numerically by simulations that calculated the horizon's content from the past to the present for various estimates of POC or BSi content at the time of the original surface deposition (see Chapter 4 for the geochronology). A solution was reached when the starting estimate matched the measured horizon content down the core. The simulation was performed within the architecture of an Excel™ spreadsheet by incorporating Solver™ in the iteration choices to match the profile's horizons to those of the simulation. The simulation time intervals and the decay constants were set at every seven days from 1923 to the present (2006). It was found that the difference in the diagenetically corrected values between monthly and weekly estimates was less than 10 %, thus, further iterative resolution was considered both unnecessary and costly in simulation time, as each horizon simulation was run individually.

6.2.3.2. Preserved seagrass pieces

Evaluation of medium to long-term diagenetic loss of seagrass leaf pieces (>1year) down the sediment cores was assumed to be unnecessary because: (1) it was observed that the broken edges of pieces remained sharp and square with their epidermises intact, irrespective of abundance or depth down the core, (2) most long-term (up to 1 year) litter bag studies found that after the first few months, the loss of carbon and nitrogen, as well as changes in stable isotopes approached an asymptote that reflected the original composition (Harrison, 1989;

Holmer and Olsen, 2002; Fourqurean and Schrlau, 2003), and (3) there was parallel compositional variance between buried seagrass pieces and their living analogues (*e.g.* Orem *et al.*, 1999; see Figure 3.11).

6.2.3.3. Calcium carbonate (LOI 950 °C)

In contrast to TOC and BSi, it was assumed that there was no diagenetic loss of particulate calcium carbonate. This was in part a pragmatic decision based on recent research, which found that within seagrass bed sediments, dissolution of metastable carbonate phases occurs in conjunction with re-precipitation of more stable carbonate phases (Xinping and Burdige, 2007). In addition, it is generally considered that the preservation of calcium carbonate shells within sediments is an order of magnitude greater than for TOC or BSi (Berner, 1980; Green and Aller, 2001), which was supported by observations from surfaces of shell pieces and benthic foraminifera, taken from the bottom of the core. All the shell fossils were smooth and firm with a well-defined and sharp architecture (no pitting or thinning).

6.2.4. Ternary mixing models of organic components

The proportions of three sedimentary OM sources (seagrass, micro-algae, and soils) were calculated from a $\delta^{13}C_{org}$ and PON–POC ratio ternary mixing model by solving for proportions with respect to $\delta^{13}C_{org,}$ and PON–POC ratios (*i.e.* three simultaneous linear equations [*e.g.* Gonneea *et al.*, 2004]). Before the organic proportions were calculated all $\delta^{13}C_{org}$ were corrected for the 'Suess effect', with the exception of naturally older soils, using the polynomial of Schelske and Hodell (1995). The Suess effect describes the increase of atmospheric $^{12}CO_2$ caused by fossil fuel burning since 1840 with respect to the Viennese Pee Dee belemnite standard. The sedimentary TON converted from the TN analysis by removing the contribution from ammonia as the value of the intercept taken from the relationship between TN and TOC along the surface sediment transect (see Chapter 3).

The isotope and elemental ratio signatures of seagrass pieces varied systematically down the sediment core (see Section 6.3.1.1), over a similar range found across the estuarine transect (see Chapter 3). Consequently, multiple average seagrass and micro-algal end-points were used. Average seagrass end-points were determined by a CUSUM change point analysis (see below Section 6.2.6). Average micro-algal signatures were calculated from the fine fraction PON–POC ratio for baseline best least squares linear model depth profiles (see Section 3.3.3),

together with Keeling plots[25] for their respective $\delta^{13}C_{org}$ (Fry, 2006), but only after a correction for loss of carbon (DTOC [see Section 6.2.3.1]). Isotopic and elemental ratio parameters for soils were taken from the average of the estuary's immediate surrounding surface soils (see Chapter 3). Finally, the model's end point signatures were optimised by adjusting the micro-algal PON–POC ratios within the fine fraction, in proportion to differences between regimes, to match the BSi content variance, after first correcting for loss from dissolution (DBSi [see Section 6.2.3.1]).

The non-linear Rp index–TN/TOC ternary mixing model (see Chapter 3) was $\log_{10}$ transformed to approximate a linear mixing response for the solution of its three linear simultaneous equations. The combined average signature of preserved seagrass leaf pieces down sediment cores, soils and laboratory-mineralised micro-algae (*Chlorella pyrenoidosa*; see Chapter 3) were used as the organic component end-points, contingent on their organic carbon content remaining constant.

6.2.5. Absolute water column turbidity and light levels

The median annual absolute water column turbidity was estimated from the gently sieved fine fraction content (<76 μm), after it had been corrected for mineralisation of OM and dissolution of BSi, by division of the fine fraction's sedimentation velocity into its median mass accumulation rate (MAR [see Figure 6.2]) according to Kozerski (1994). The mineralisation of OM was calculated from the loss of POC within the fine fraction and converting the loss to LOI 550°C from the sediment core's relationship between TOC and LOI 550°C. The fine fractions average sedimentation velocity was incorporated into the calculation by calibrating median MAR of surface sediments spanning the last 3 to 4 years (see Figure 6.2) with the median baseline surface water turbidity over a similar period from June 2003 to December 2007 (median NTU 9.2; 25 % quartile 1.7; 75 % quartile 16.6; n=105).

For the purpose of MAR calculations the sedimentation velocity was divided between its pre-1960 median, its median between 1960 and 1970, during the period of entrance restriction (see Chapter 4), and its post-1970 median. The larger and more uncertain sedimentation rate in 2001 was not included in the calculations, as it was probably the result of the sediment

[25] Keeling plots of 1/C *vs* $\delta^{13}C_{org}$ are a special case of a two-component mixing model between a variance in a major organic carbon component 'contaminated' by a minor organic component, in which the major organic component's $\delta^{13}C_{org}$ can be calculated by extrapolating the carbon content to infinite addition (Fry, 2006).

sample contaminated by the 2002 depositional flood facies. The resultant baseline fine fraction MAR was then corrected to give the sediment load according to Almroth *et al.* (2009 [Equation 6.2]).

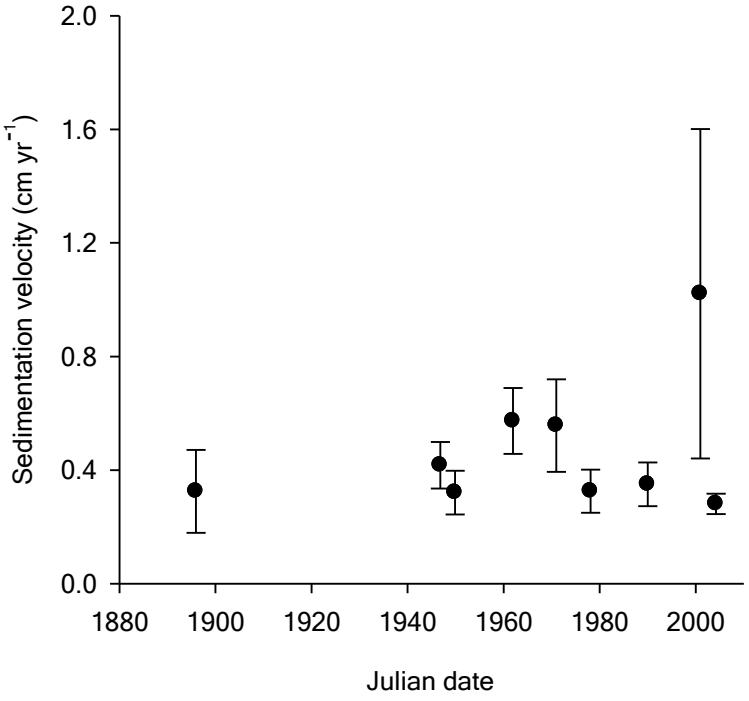

Figure 6.2. The baseline sedimentation velocities down the Upper Middle Basin sediment core LSPMB206 calculated by ^{210}Pb sediment isotope tomography (see Chapter 4).
The errors bars represent the standard deviations about their means.

Equation 6.2. $Sed = 1.584NTU - 0.985$

The equation was taken from a relationship within a marine environment subject to wind re-suspension (Almroth et al., 2009). *NTU* is Normal Turbidity Units, and *Sed* is the sediment load (mg L^{-1}).

The calculation assumes that:

1. there had been no re-suspension of deep-water sediments into surface waters (*cf.* sediment traps [Kozerski, 1994]), as implied from a persistent water column haline stability within this region (see Chapter 4);
2. there had been no significant changes in the sediment's particle size, outside the range of the 3 to 4 years of seasonal turbidity measurements (*i.e.* due to changes in micro-agal standing crop, river sources, wind and tide resuspension) as indicated a muddy sediment and no correlation of the results with long term wind proxies (see Chapter 5). A muddy sediment supports the view that there was no significant change in the modal particle size to a larger sandier fraction. Particle sorting of shallow muddy sediments

is primarily by the action of wind (Smith, 1975), thus, no correlation with wind fetch supports the view of no significant changes to particle sorting within the mud fraction;

3. there had been no slumping of sediments from shallow waters direct to the deep spot, as implied by no evidence of long-term sediment focusing (see Chapter 4).

The sediment load was then transformed to Secchi depth using a general relationship for shallow estuarine waters (Morris, 1983):

Equation 6.3. $$\frac{1}{Secchi} = 0.1 + 0.04Sed$$

The water column light extinction coefficient (*Kd)* was calculated from the Secchi depth for estuarine waters according to Holmes (1970):

Equation 6.4. $$Kd = \frac{1.44}{Secchi}$$

Finally, the depth to which ambient light is reduced to 22 % was calculated from the first order decay in light intensity with depth (Parsons *et al.*, 1984):

Equation 6.5. $$L_0 = L_{0.22}e^{-kd.D}$$

Where L_0 is ambient light fraction at the surface (100 %), $L_{0.22}$ is 22 % of ambient light, D is the depth at which the light is reduced to 22 % of the ambient for the value of the extinction coefficient k_d.

6.2.6. Data analysis

6.2.6.1. Regime change

Andersen *et al.* (2008) recognised that identifying ecosystem regime thresholds requires a two-stage process of exploration and inference, that is, an exploration of dissimilarity and a inference from a rapid change in the biome variables in relation to its external driver. The reasons are two fold: (1) a constrained cluster analysis may force a graded series into discrete structures, and (2) any rapid in the biome that is accompanied by rapid changes in external driver is consistent with a change driven by the driver and not the result of a threshold change to another biome regime (see Andersen *et al.*, 2008 for a range of hypothetical examples).

A constrained cluster analysis (PAST™) of the biome and process components proxies (see Section 6.2.1) was used for exploration. A change point analysis (Pettit, 1980; Taylor, 2000

[Variance™]) as the cumulative sum of the mean within an ordered series (CUSUM) of the two principal component's MAR[26] (seagrass pieces >315 μm and DBSi) was used for inference in relation to changes in the CPN (see Andersen *et al.*, 2008 for a survey of different methods).

6.2.6.2. The cause, stability and type of regime

The causes of regime transitions and the type of regime were determined by correlating changes in relationships between annual imputed time-series of the CPN (see Chapter 5), micro-algal proxies MAR, seagrass proxies MAR with the major events and changes to inferred nitrogen fixation or nitrogen mineralisation (*i.e.* $\delta^{15}N_{org}$ signatures [see Chapter 3]). Imputation of the interrupted time series was determined by singular spectrum analysis for missing data (SSAM) according to Golyandina and Osipov (2007 [Caterpillar™]). The changes of relationships between the CPN, micro-algal and seagrass proxies of MAR were calculated by a modified increasing window analysis of the type used for the estuary's surface sediment transect (see Chapter 3). The modifications were: (1) a change from a two-way to one-way best linear model from past to the present, and (2) the use of a minimum in the residual mean square error as a measure of fitness in place of the strength of a good correlation. In this way, changes in the bi-variant relationship as a regime changes from one of dependence to independence can be marked over time.

6.3. Results and discussion

6.3.1. Sediment signal depth profiles: Diagenetic corrections

6.3.1.1. Sediment content variables

Both the TOC and BSi had complex depth and dynamic profiles (see Figure 6.3), in which diagenetic corrections indicated that relative losses due to dissolution of BSi (DBSi) and particularly, losses due to mineralisation of TOC and POC (DTOC, DPOC) were only significant for the first 20 years. Indeed, without the corrections, the impression was that OM content had increased from around 1986 to the present (2006) in contrast to a more stationary BSi variance over this time.

---

[26] The MAR for micro-algae is a measure of a water body's net micro-algal production (*e.g.* Zimmerman and Canuel, 2002). However, MAR of seagrass pieces is a measure of seagrass abundance–basin coverage and/or productivity, as the two categories do not necessarily change in concert (*e.g.* Hauxwell *et al.*, 2003).

All the diagenetically corrected elemental content profiles within the baseline sediments (DBSi, DTOC and DPOC) while complex throughout the sediment core were marked by a clear transition from a smaller post-1960 content, to a larger content pre-1960 (see Figure 6.3). However, the relative differences of pre- and post-1960 DBSi and were noticeably greater for DBSi (173 %) than for DTOC (143 %).

The post-1938 baseline LOI 950 °C profile (calcareous epifauna [see Chapter 3]) broadly followed the profiles of DBSi and DTOC as far back as 1938, where the LOI 950 °C remained relatively high but invariant with respect to DBSi and DTOC (see Figure 6.3). This was in contrast to the post-1938 epifaunal density variance (LOI 950 °C/seagrass pieces >315 μm), which fell with increasing seagrass content towards the present (2006) after a generally higher but noticeable chaotic pre-1938 density.

The copepod faecal pellet content of base line sediments (100 μm and 150 μm) was a significant proportion of the fine fraction content and displayed a broad inverse relationship with each other down throughout the sediment core (see Figure 6.3). However, the faecal pellet content only varied inversely with the inferred planktivore predation (100 μm/150 μm) post-1938 but not pre-1938 (see Figure 6.3). The pre-1938 relationships appeared to alternate between a broad proportional response (1938 to 1929) and then back to a broad inverse response (1929 to 1923 [see Figure 6.3]).

6.3.1.2. Sediment quality variables

Overall, the $\delta^{13}C_{org}$ profiles of the total and fine fraction (<76 μm) followed each other with the same pre- and post-1960 flood transitions as DBSi and organic carbon content variables (DTOC and DPOC [see Figure 6.3]). $\delta^{13}C_{org}$ for baseline sediments post-1960 were noticeably isotopically lighter by 1.9 ‰ and 2.7 ‰ for the TOC and the fine fractions POC respectively. In contrast, the baseline total POC–PON ratios remained relatively constant (see Figure 6.3) but with a suggestion of a fall in the fine fraction's ratio post-1960 (CUSUM change from 9.4 to 8.4). The total POC–PON ratios (14.33, standard deviation 0.53) were significantly greater than the fine fraction's (8.9, standard deviation 0.56). The total fraction being closer to values represented by soils and seagrass leaves (see Chapter 3) and a fine fraction that lay within the range for both estuarine micro-algae (Cloern *et al.,* 2002; see Chapter 3) and the estuary's SPM.

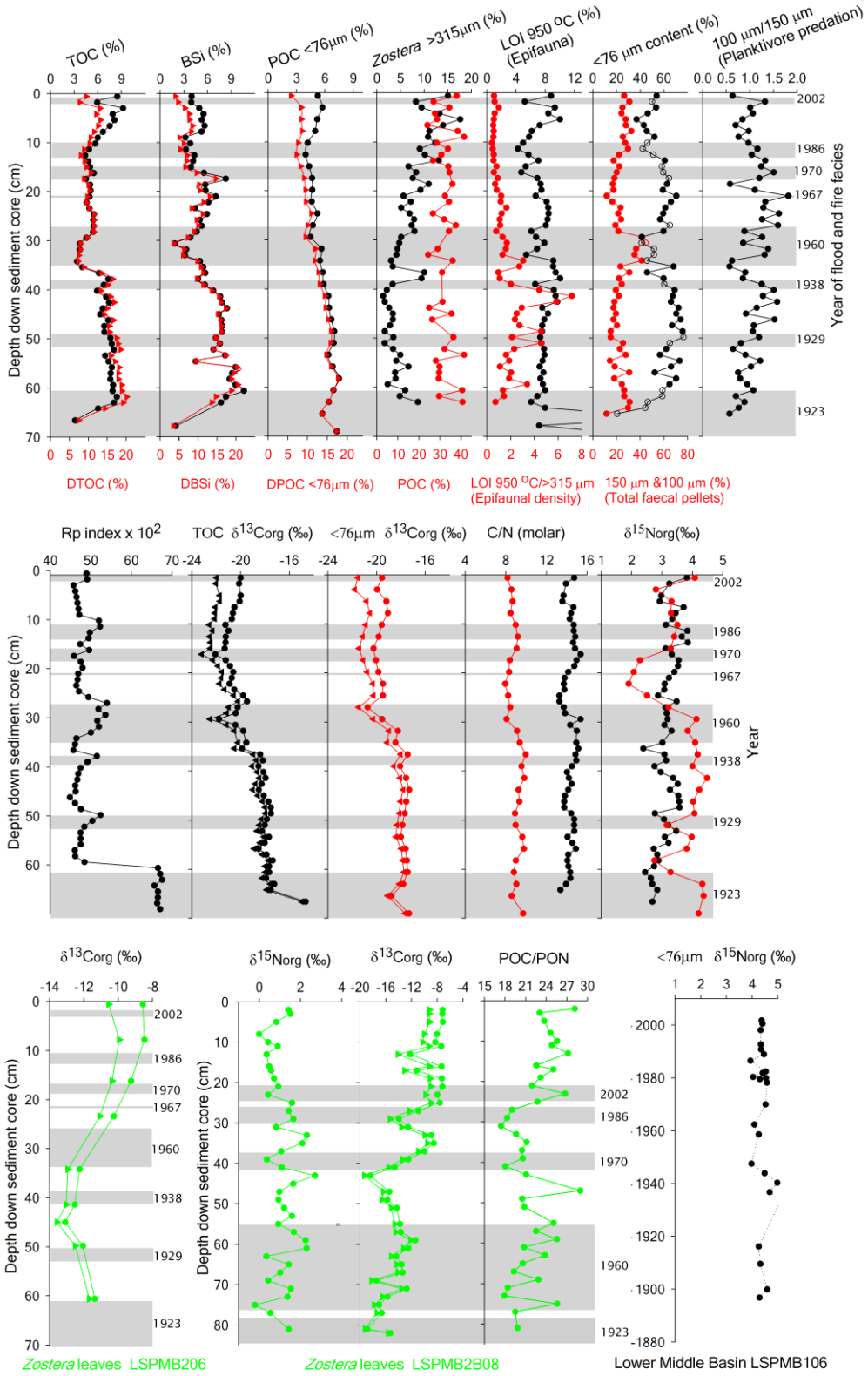

Figure 6.3. Sediment and fossil seagrass leaves (>315 µm) content and quality variables down the Upper Middle Basin and Lower Middle Basin sediment cores.
(Top) Sediment core LSPMB206: (▲) DBSi, DPOC and DTOC contents corrected for loss dissolution and mineralisation (see text); epifaunal density and faecal pellets refers only the baseline sediments. (Middle) Sediment core LSPMB206 quality variables: (●) Suess corrected $\delta^{13}C_{org}$; (●) for C/N ratios and $\delta^{15}N_{org}$ represent the fine fraction (<76 µm); (●) for C/N ratios and $\delta^{15}N_{org}$ represent the total sediment. (Bottom) Seagrass pieces (>315 µm) quality variables down the two Upper Middle Basin sediment cores (LSPMB206 and LSPMB2B08) and the fine fraction's $\delta^{15}N_{org}$ down the Lower Middle Basin sediment cores LSPM106. (●) Suess corrected $\delta^{13}C_{org}$. The chronologies was based on events evaluated by ^{210}Pb SIT chronology (upper cores) and SIT chronology evaluated by events (lower core); see Chapter 4.

The baseline total POC–PON ratios, however, did not fall with the absence of seagrass pieces (pre-1938) nor did the fine fraction and POC–PON ratio's increase (see Figure 6.3). Such a pattern was consistent with the transport of seagrass with high POC–PON ratios >14 (see Chapter 3) to the deep sediment core extraction sites predominantly within a size fraction between <315 μm and >76 μm. The few reliable baseline examples of the faecal pellet fraction's $\delta^{13}C_{org}$ and PON–POC ratios (see Figure 6.4) also suggested that there was an increased supply of seagrass over that of soils to this fraction sometime before 1953. This was in contrast to the heavier $\delta^{13}C_{org}$ and PON–POC ratios for faecal pellet fraction (150 μm and 100 μm) post-1953, which fell within the range of a mixture dominated by soils and micro-algae (see Figure 6.4 (○)).

The baseline $\delta^{15}N_{org}$ for the total and fine fractions was different in both value and profile variance (see Figure 6.3). Overall, there was little change in the total $\delta^{15}N_{org}$ down the sediment column; with the possible exception of a lighter $\delta^{15}N_{org}$ between the 1923 and 1929 floods (see Figure 6.3). In contrast, the fine fraction's $\delta^{15}N_{org}$ depth profile had a relatively complex set of potential transitions. Between 1960 and 1970, during the postulated entrance restriction period (see Chapter 4), the fine fractions $\delta^{15}N_{org}$ was lighter by 1.2 ‰ than all remaining sediment horizons. There were other noticeable periods of lighter $\delta^{15}N_{org}$ for the fine fraction between the 1923 and 1929 floods (mean 3.1 ‰) and after the 1970 flood (mean 3.5 ‰) compared to periods between the 1938 and 1960 floods (mean 4.4 ‰; see Figure 6.3). The latter were within the range of the coastal SPM and the fine fraction (mean 4.4.‰ [see Figure 6.3]) from a core adjacent to the Marine Flood/Tidal Delta coastal boundary (see Chapter 3) during the Anthropocene. The implication being that between 1938 and 1960 the supply of inorganic nitrogen for the upper estuary's primary production was ostensibly from coastal waters, that is, coastal waters with an invariant annual average $\delta^{15}N_{DIN}$ reflected by its micro-algal's annual average $\delta^{15}N_{org}$ (Francois *et al.*, 1997).

6.3.1.3. Seagrass quality variables

The compilation from reliable seagrass pieces (>315 μm) stable isotopes analysis and their TOC–TON ratios are shown Figure 6.3 for the two Upper Middle Basin sediment cores LSPMB206 and LSPMB2B08. It can be seen the data variance between the two cores appeared to be paired with their respective dated sediment horizons (see Chapter 4). The main point of difference between the sediments was that seagrass $\delta^{13}C_{org}$ and POC–PON ratios broadly followed each other down the core, with a heavier and greater post-1970 $\delta^{13}C_{org}$ and POC–PON ratios. Such a broad inverse relationship between the seagrass and sedimentary

$\delta^{13}C_{org}$ was seen across the estuarine surface sediment transect. Such a variance was found to be consistent with changes of carbon fixation between micro-algae (sediments) and seagrass, and not synonymous with changes in salinity (see Section 3.4.3.3). This contention is also supported by no common variance between sediment or seagrass $\delta^{13}C_{org}$ and the reconstructed surface salinity (*c.f.* Figure 5.4).

Like the sediment $\delta^{15}N_{org}$, the profile dynamics of seagrass $\delta^{15}N_{org}$ also differed from their $\delta^{13}C_{org}$ and POC–PON ratios. The seagrass $\delta^{15}N_{org}$ profile appeared to be noisier pre-1986 than post-1986. Further, the post 1986 $\delta^{15}N_{org}$ were on the average lighter than pre-1986. The impression was confirmed by a CUSUM change point analysis that also marked the change at 1986 from mean of 1.3 ‰ (pre-1986) to 0.7 ‰ (post-1986).

6.3.2. The palaeo-reconstruction

6.3.2.1. Seagrass and micro-algae ternary mixing models

Aside from possible diagenetic variance down the sediment core, the accuracy of the model depends on the accuracy of the value of the organic component signals. For example, the range of possible ternary mixing boundaries, illustrated in Figure 6.4, indicates that the traditional reliance on a statistical average of contemporary end-point (*e.g.* Gonneea *et al.*, 2004; Turner *et al.*, 2006) would result in most of the post-1960 sediments lying outside the model boundaries. Consequently, with the exception the old catchment soils, the organic components signatures were selected to closely represent their sediment horizons.

The mean $\delta^{13}C_{org}$ and PON/POC signals for seagrass component (see Figure 6.4) were chosen to reflect the seagrass pieces (>315 μm) profile transitions down the core (see Figure 6.3). For the micro-algal component, the mean $\delta^{13}C_{org}$ and POC–PON ratios were calculated from the fine fraction by using $\delta^{13}C_{org}$ *vs.* 1/DPOC Keeling plots (see Figures 6.5d) and the POC–PON down the sediment core (see Figure 6.5d). The Keeling plot removes the contamination of the $\delta^{13}C_{org}$ signal from the major organic fraction, assuming the fine fraction was dominated by micro-algae. The above assumption was supported by: (1) the close variance between the total BSi and the fine fraction's POC (see Figure 6.3), (2) most of the BSi residing within the fine fraction (see Figure 6.5a), (3) POC–PON ratios for the pre- and post-1960 flood (*calc.* 10 and 9.7, respectively) that were located within the range found for estuarine benthic micro-algae (see Chapter 3; Cloern *et al.*, 2002) as highly silicified diatoms (molar DBSi–POC *calc.* 0.35 and 0.46; Brzezinski, 1985; see Chapter 3).

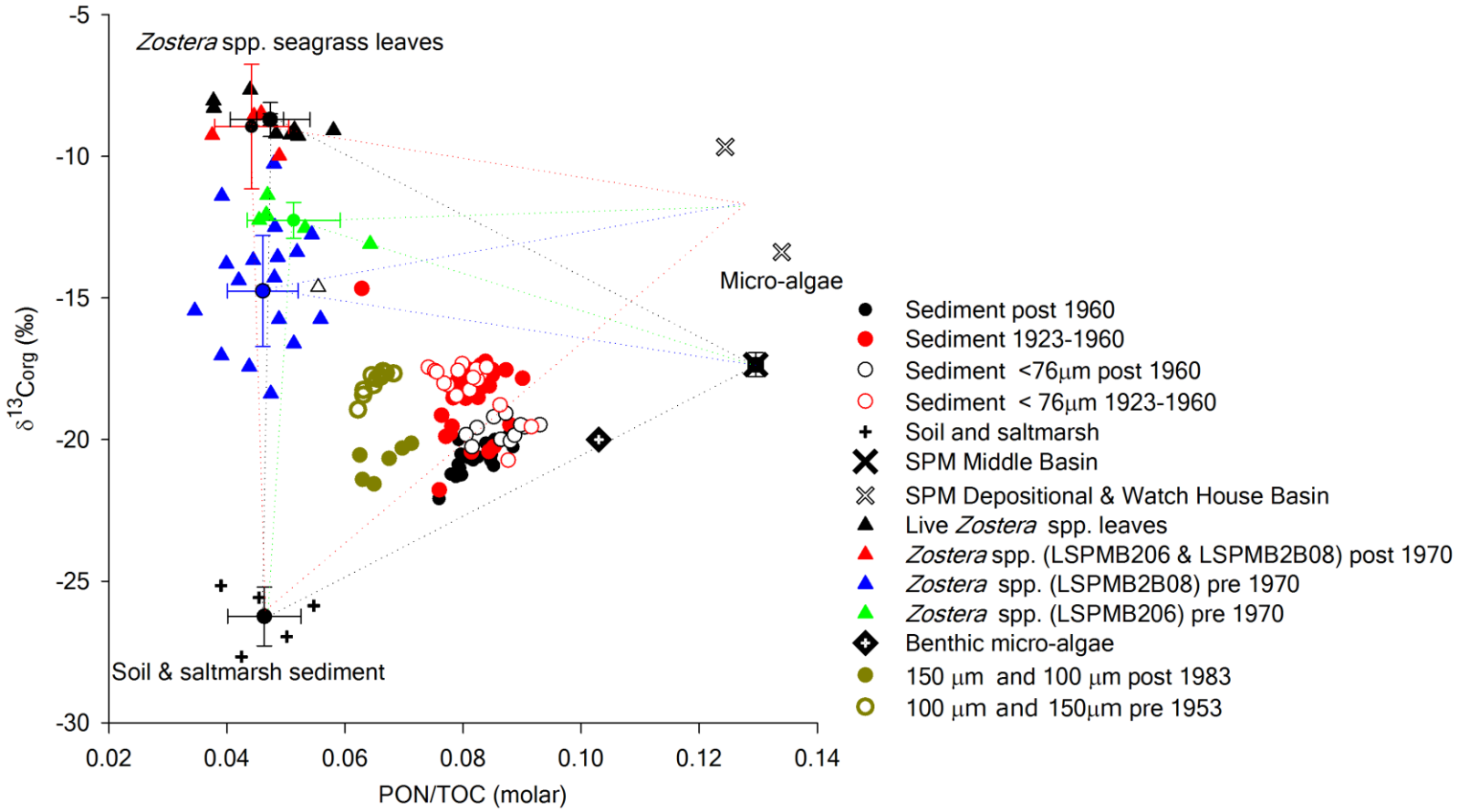

Figure 6.4. $\delta^{13}C_{org}$—PON/TOC linear ternary mixing models illustrating the different model boundaries that result from different choices of plausible organic component signals. Live *Zostera* spp and detrital *Zostera* spp leaves pre- and post-1970, together with soil and salt marsh sediments, and contemporary SPM samples across the estuarine transect (see Chapter 3). The benthic micro-algal data was taken from Cloern *et al.* (2002) for San Francisco Bay (USA). The error bars represent the standard deviation about the mean.

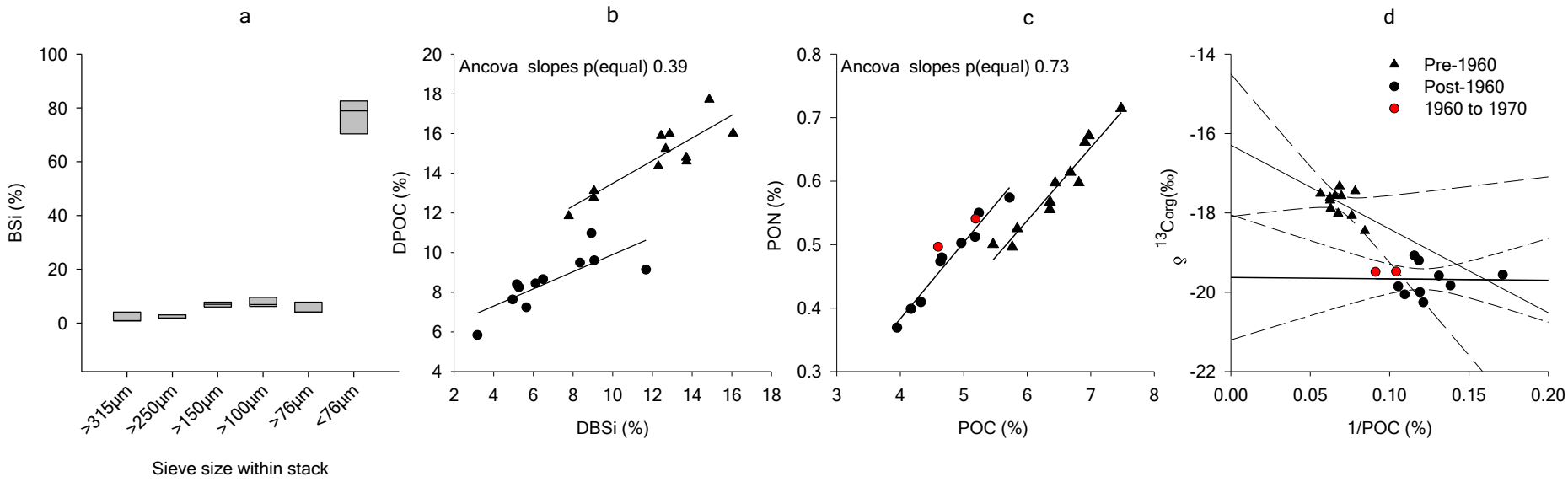

Figure 6.5. Organic carbon stable isotope Keeling plots and major elemental ratios down the Upper Middle Basin sediment core LSPMB206.
(a) The proportions of BSi within gently wet sieved size fractions from six baseline horizons haphazardly selected down through sediment core LSPMB206 indicating that most of the BSi resides in the <76 µm fraction; the box plots represent the medians and 95 % confidence limits. (b) Pre-and post-1960 flood baseline sediments DPOC (<76 µm)–DBSi ratios. (c) Pre- and post -1960 flood baseline sediment PON–POC ratios (<76 µm); the red circles represent baseline sediments over the period of entrance restriction. (d) Keeling plot $\delta^{13}C_{org}$ extrapolations of the baseline sediment's fine fraction to infinite addition of carbon from the major micro-algal components; the dashed lines (– – –) represent the 95 % confidence limits.

All the baseline sediment Rp index/TN–TOC ratio signals lay within the boundaries defined by the means of the organic components' signals (see Figure 6.6), in contrast to the deviation from a simple mixing criteria found for most of the flood shell and clay deposits (see Chapter 4). However, in contrast to the isotope and elemental ratio model, this model showed poor separation between the organic components as a group. In other words, a separation similar to the difference between the points of an equilateral and isosceles triangle. As a consequence, the sensitivity of the model was reduced for sediments dominated by the micro-algal component that would lead to greater errors for seagrass and soil proportions.

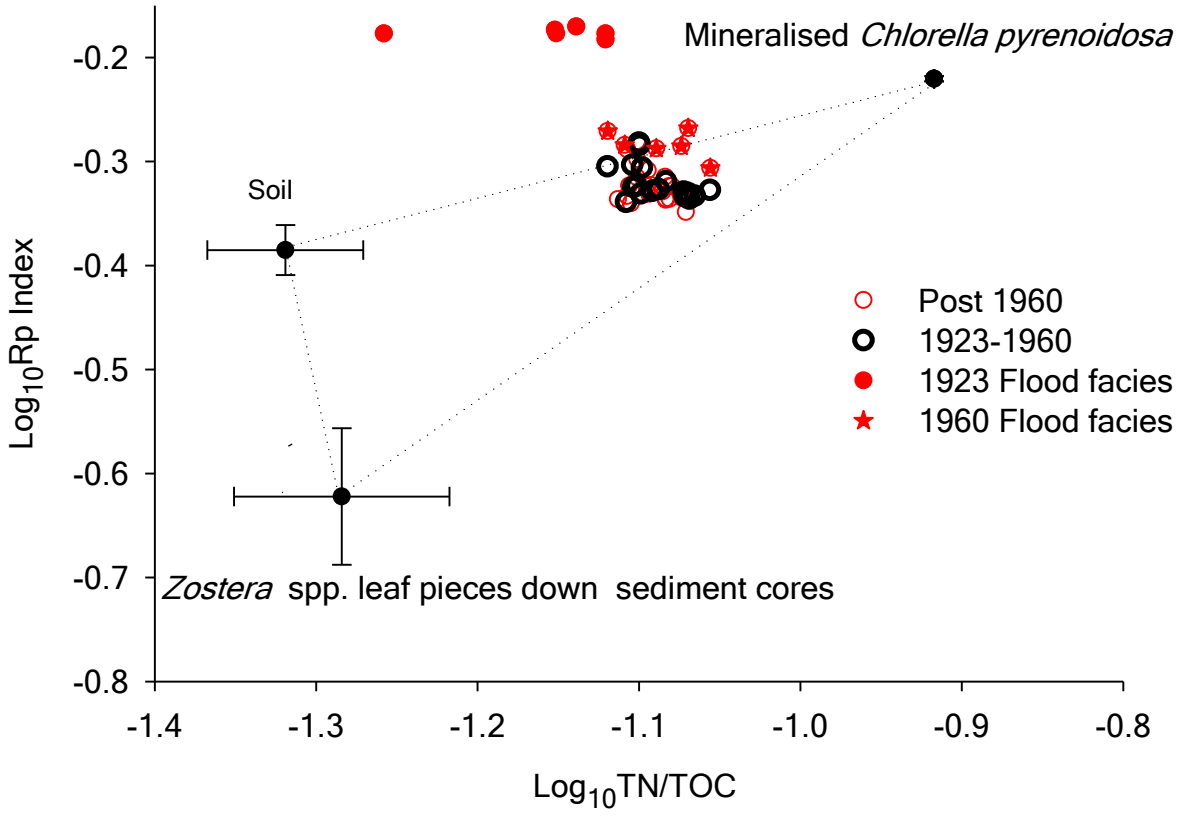

Figure 6.6. The Rp index/TN–TOC ratio ternary mixing model for baseline sediments and depositional facies down the Upper Middle Basin sediment core LSPMB206.
The error bars represent standard deviation about the mean for all organic source samples. The error bars for the mineralised *Chlorella pyrenoidosa* are too small to be displayed on the figure.

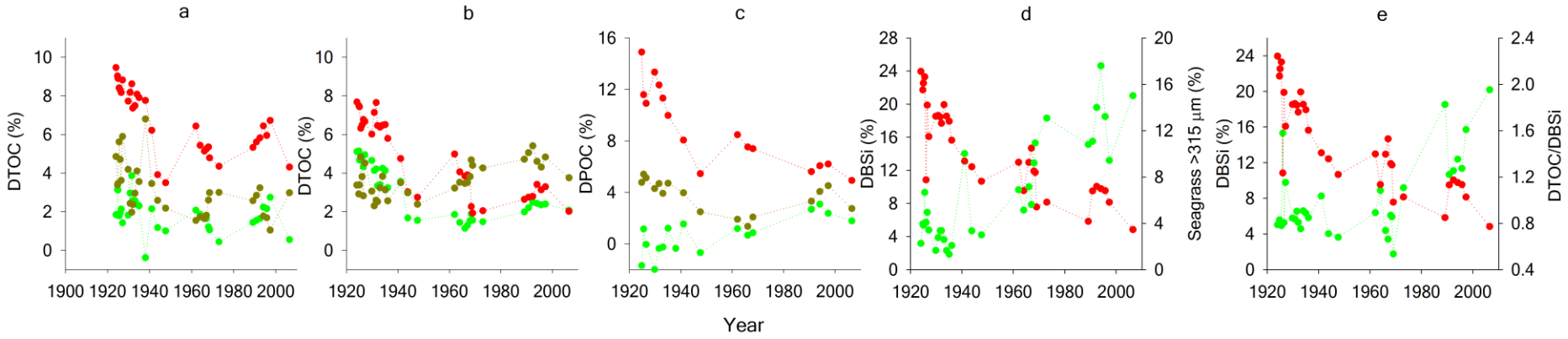

Figure 6.7. Organic matter mixing model time series for soil (●), micro-algae (●), and seagrass (●), within the total and fine fractions of baseline sediments down the Upper Middle Basin sediment core LSPMB206
(a) The $\log_{10}$ Rp index/TN–TOC ratio model; (b) $\delta^{13}C_{org}$/TON–TOC ratios for the total fraction; (c) $\delta^{13}C_{org}$/PON–POC ratios for the fine fraction (<76 µm); (d) Seagrass pieces content < 315 µm: DBSi; (e) seagrass proxy as DTOC/DBSi. The small negative seagrass values in (d) result from the repositioning of the micro-algal TOC/TON end-point after optimisation of the micro-algal result to the DBSi variance.

6.3.2.2. Seagrass, micro-algal and soil content down baseline sediments: A convergence and divergence of independent model solutions

All the models produced a similar time-series of micro-algal content (see Figure 6.7). However, there was a disagreement between the pre- and post-1960 flood ternary mixing models (see Figure 6.7a,b,c) and the remaining content and content ratio seagrass models (see Figure 6.7d,e). The ternary mixing models suggested that there was a larger seagrass content pre-1960 than post-1960, in contrast to a significantly larger seagrass content post-1960, as suggested by the abundance of seagrass pieces (>315 μm) and the seagrass DTOC–DBSi index.

Two lines of evidence suggest that the total sediment ternary mixing models were in error, at least concerning the concepts the measurements were assumed to represent. There was evidence that was counter to IBE, based on the standard model that increases in micro-algal production (pre-1960) are usually accompanied by falls rather than increases in seagrass productivity and coverage (Duarte, 1995; Borum and Sand-Jensen, 1996), and observations that the current shoot density and meadow coverage is already near its maximum (see Chapter 3). Given the latter scenario, it is unlikely that seagrass coverage and shoot density would have been much greater during pre-1960 than today.

The disagreement, however, is based on the assumption that the proxies represent a living seagrass meadow. The divergence does not rule out that all models are correct but that there was a change from a larger to a smaller seagrass size fraction (see Section 6.3.1.3 [Figure 6.4]) over the pre-1960 period. A change that has not been observed post-1960. This contention is further supported by the absence of significant seagrass content within the pre-1960 fine fraction (see Figure 6.7c) and a smaller proportion within the >315 μm fraction (see Figure 6.7d), thus implying that the seagrass signal lies somewhere between.

The explanation behind a smaller pre-1960 seagrass fragment size can be abductively reasoned by first setting an axiom of what has been observed. From the axiom, a series of hypothetical consequences can then be deducted and supported by further observations within the estuary and within the literature.

1. *The Axiom*: seagrass leaves from living *Zostera* spp. are damaged from physical processes of wind and tide that results in as a uni-modal size distribution >315 μm (Robertson and Mann, 1980).

Hence:

2. *Postulate:* seagrass detrital size variance peaked mainly between >76 μm and <315 μm and the faecal pellet fraction, and again at >315 μm[27]. Hence, seagrass was not supplied from the physical breakage of living seagrass leaves.
3. *Inductive support:* isopods and amphipods grazing on *Zostera* spp. leaves produced the above characteristic fragmentation spectra by grazing on dead leaves from the littoral zone (Robertson and Mann, 1980).
4. *Support from constraints or prior knowledge:* anoxic sediments within the deep spot do not harbour grazers.
5. *Deduction:* during the pre-1960 period, most of the seagrass meadow was dead.
6. *Support from constraints or prior knowledge*: transported detrital material within living seagrass meadows by wind re-suspension was restricted by a healthy shoot density (Ward *et al.*, 1984).
7. *Inductive support:* 1923 saw the largest flood of the century; with enough strength and duration to kill *Zostera* spp. by exposing the meadow to freshwater for over a month (see Chapter 4).

Consequently, it appears that the most appropriate set of proxies for describing the changes in the living primary productivity assemblage are the corrected total biogenic silica content (DBSi) and the seagrass fraction >315 μm. However, this is conditional on knowing carbon content of seagrass pieces or assuming it to be constant. Otherwise, the seagrass DTOC–DBSi ratio index should be used if most of the organic content within the fine fraction follows the DBSi content (*i.e.* relationship that is consistent with no significant contribution to the variance from soils [see Figure 6.7b]).

6.3.3. The synthesis: Ecosystem regimes

The results from the constrained cluster analysis identified a pair of regimes that were separated by what appeared to be separated by a period of transition set after 1937, and ended sometime between 1948 and 1962 (see Figure 6.8). An exploratory analysis of the timing of the regime changes with the major flood events suggested that floods might have been the cause of regime change. It appeared that the loss of the seagrass meadow occurred immediately after the 1923 flood and the major regime transitions, marked by the 1931, 1938 and 1962 horizons (see Figure 6.8) were close to the major 1929, 1938 and 1960 flood events

[27] Material captured on the 250 μm sieve down the sediment cores was a minor fraction of the total, an average of 3.1 % (standard deviation 1.8 %).

that were large enough to leave a depositional record. In contrast to these earlier horizons, however, the more recent regime change, marked by the 1989 horizon (see Figure 6.8), was separated by a large gap in chronological record. Consequently, the range of possible reasons is also extended. For example, the expansion of the entrance to increased coastal exchange by the 1969/1970 floods, the start of the drought (1979) or the development of the lower estuary's shellfish aquaculture immediately after the 1986 flood (see Chapter 4).

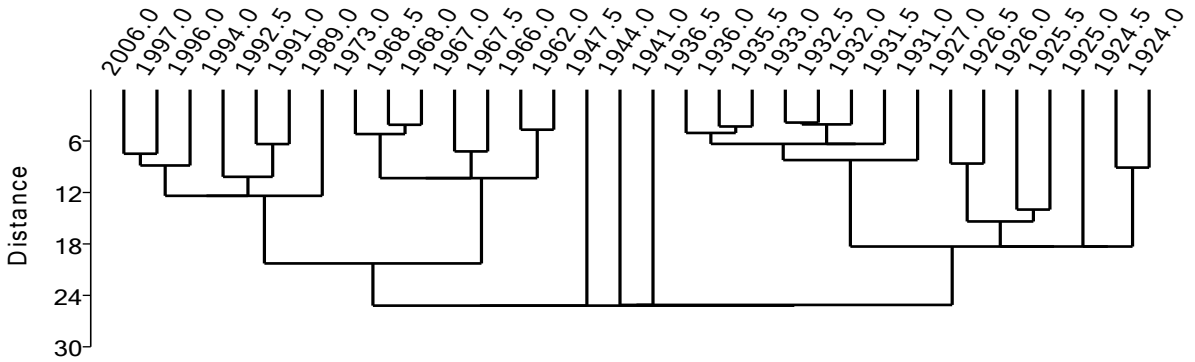

Figure 6.8. A constrained cluster analysis of biome and process proxies for times associated with their baseline sediments for the Upper Middle Basin sediment core LSPMB206.
See Section 6.3.2 for a list of inputs use to construct the constrained cluster analysis.

Individually, the CUSUM change points to the MAR of the two principal productivity components (*i.e.* seagrass pieces and micro-algae [DBSi]) did not completely converge nor did they conform to all of the above major cluster regimes (see Figure 6.9). The DBSi thresholds were located at the 1924, 1926, 1936, 1966, 1968 and 1973 horizons. The seagrass thresholds were located at the 1926, 1941 and 1962 horizons. Nevertheless, as a pair, the number and timing of the regime changes correlated to most of the cluster regimes and transitions. The notable exception being the regime change sometime between 1973 and 1989 marked by the cluster analysis, in spite of the suggestion of a fall in micro-algal and seagrass MAR's. The inability of CUSUM to recognise the earliest threshold might reflect the small quantity of data at the end of the series (*e.g.* see Chapter 5; Andersen *et al.*, 2008). Alternatively, the regime change recognised by the cluster analysis might not have been change to the structure of seagrass–micro-algal assemblage, but rather a switch in function to seagrass-mediated nitrogen fixation that maintained seagrass coverage close to previous levels (see Chapter 3).

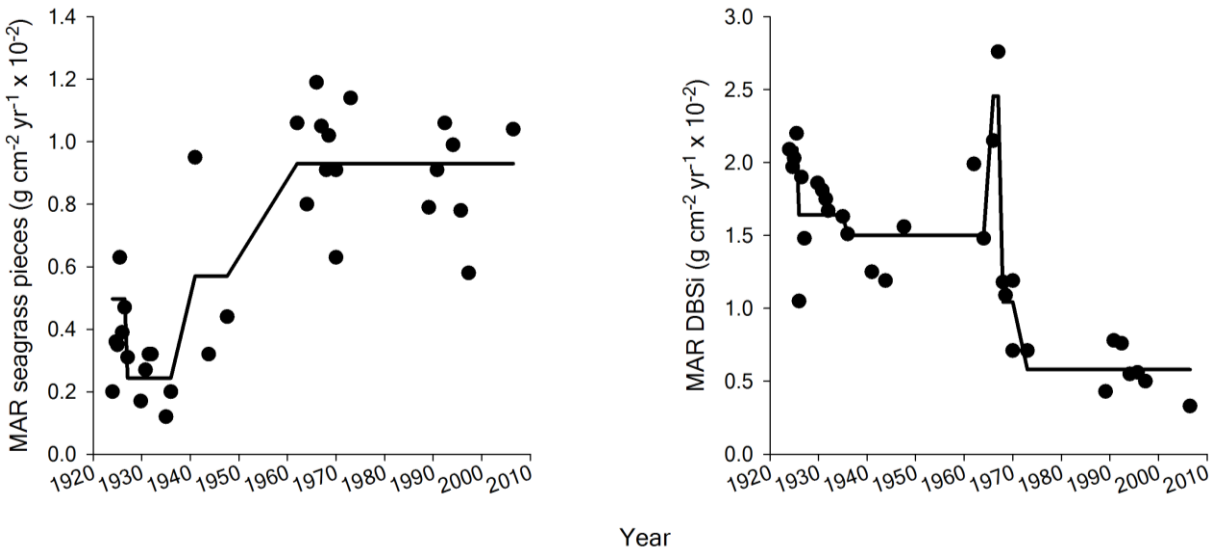

Figure 6.9. CUSUM change point analysis of the mean primary productivity assemblage for the baseline sediments down the Upper Middle Basin sediment core LSPMB206.
The diagonal lines linking the regimes highlight the uncertainty in the timing of the transitions due to both sediment erosion and the low annual sampling resolution and were not were part of the CUSUM analysis.

6.3.3.1. Causation

Clearly, the above transitions are suggestive but not sufficiently conclusive as to the causes of regime change owing to the relatively low temporal resolution and eroded baseline sediments (see Chapter 4). To help overcome the poor temporal resolution, best least square linear models between seagrass and micro-algal MAR were constructed from their annual imputed time-series. The SSAM imputation method has the advantage of being model independent, in that it does not force the variance to a assumed construct. Nevertheless, it can produce reasonable postulate of variance as it relies on information taken from the complete autoregressive time series (Kondrashov *et al.*, 2005). In this way, by using a narrative of unfolding events (*i.e.* floods, drought, and anthropogenic disturbance) a more precise test and explanation can made for intra-regime and inter regime changes.

The Narrative. After the death of the seagrass meadow, marked by the pivotal 1923 flood, the regimes productivity was clearly dominated by falling micro-algal production (see Figure 6.9), despite an increase in the external supply of inorganic nitrogen availability (CPN) (see Figure 6.10a,c). By 1946 micro-algal production had fallen to its lowest (see Figure 6.10b (●)) and marked the beginning of a recovery for both the seagrass meadow and micro-algal production (see Figure 6.10b (●)). Hence, based on the imputation of the two time-series, it appeared that a smaller but significant 1946 flood (see Figure 4.21), not placed within the sedimentary record, might have been responsible for the recovery of the seagrass meadow and

not the larger pivotal 1938 flood. Alternatively, the 1946 flood may be the last of a series of similar smaller floods in which the recovery was the result of their accumulative effects.

By 1960 the seagrass meadow had fully recovered and remained invariant to changes in micro-algal productivity (see Figure 6.10b (●)) and the CPN; in contrast to micro-algal productivity that continued to responded to changes in the CPN (see Figure 6.10a,c). The functional transition was coincident with the 1960 flood–tsunami confluence (see Chapter 4), events that were postulated as the cause of near closure of the estuary until it was re-opened by the 1969/70 pivotal floods (see Chapter 4).

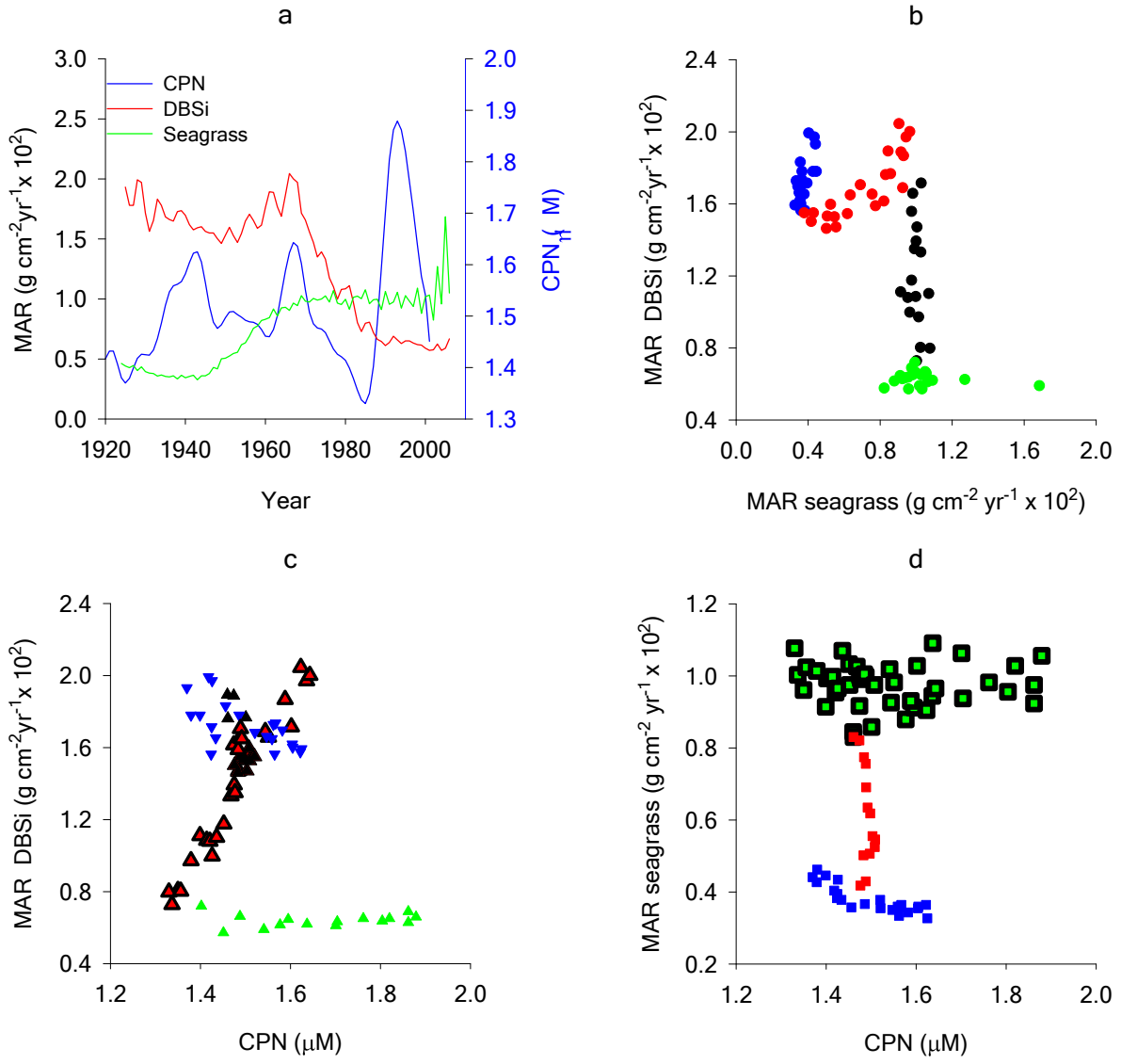

Figure 6.10. Imputed time-series and best least squares linear models for assemblage of primary producers and the CPN for the Upper Middle Basin sediment core LSPMB206.
(a) Annual imputed time series of seagrass, microalgae, and CPN estuary (SSAM). (b) Best least squares linear models between the seagrass and micro-algal (DBSi) MAR: (●) 1923 to 1945;(●) 1946 to 1959; (●) 1960 to 1985; (●) 1986 to 2006. (c) Best least squares linear models between micro-algae (DBSi) and the CPN: ▼ 1923 to 1945, ▲ 1964 to 1986, ▲ 1960 to 1963 and ▲ 1987 to 2006; (d) Best least squares linear models between seagrass (>315 µm) and the CPN: ■ 1923 to 1946, ■ 1946 to 1960 and ■ 1960 to 2006.

By 1986 and not 1969/70 (reopening of the entrance) or the start of the drought (1979) the regime had changed once more (see Figure 6.10b (●)) to a time when the CPN variance was decoupled from both seagrass and micro-algal production. However, 1986 was a time of two closely linked events, that is, a flood had forced the newly introduced shellfish aquaculture to re-locate to the Marine Flood/Tidal Delta (see Figure 4.2). Nevertheless, it is more likely to be the result of the shellfish aquaculture moderating supply of coastal nitrate to the upper estuary (Chapter 3). For the alternative, it is difficult to reconcile how the third largest flood of the 20th century could have changed the regime function without any apparent impact on seagrass shoot productivity (*i.e.* $\delta^{13}C_{org}$ [see Figure 6.3 and Section 3.4.3.3]) or abundance of the system contingency on a healthy seagrass state other than its destruction.

6.3.3.2. Stability and nature of the regime between 1923 and 1946

The traditional view is that a water body which changes to a more turbid state from the loss of seagrass, and is dominated by micro-algal production, is indicative of an alternative micro-stable state (Duarte, 1995; Scheffer and Carpenter, 2003; Kemp *et al.*, 2005). These states are stabilised through eutrophication and sediment wind suspension that leads to light attenuation sufficient to arrest the recovery of its previous seagrass meadow. Indeed, the relatively depleted $\delta^{15}N_{org}$ within the fine fraction during this time (see Figure 6.3) suggests an additional supply of nitrogen from the dead seagrass meadow (see Figure 6.3) over the usual coastal nitrate supply (see Chapter 5).

According to Kemp *et al.*, (2005) light attenuation >22 % of surface irradiance, as reconstructed over this period, is sufficient for the recovery of *Zostera* spp seagrass meadows (see Figure 6.11b). The reconstructed light attenuation could not be directly evaluated; nevertheless, the value is robust because conditions were consistent with the model's constraint. A constraint of no long-term correlation between light attenuation and long-term changes in wind fetch (*c.f.* Figure 5.5) supports the assumption of no significant particle sorting of the pre-1960 muddy fine fraction (see Section 6.2.5).

The regime state at this time does behave, however, in the manner of a seagrass transient regime. A seagrass transient regime can be expected to be partially maintained by the supply of nutrients from the sediments from the years of excess accumulation of organic material (Scheffer and Carpenter, 2003; Knowlton, 2004). For the Upper Middle Basin, it is a sudden deposition of organic material from the death of a seagrass meadow that had accumulated from years of shoot recruitment and expansion. The role of floods then becomes one that

initiates the seagrass transient state but also one that may also accelerate it towards full recovery by removing remnants of the dead seagrass meadow (*e.g.* Morris and Virnstein, 2004).

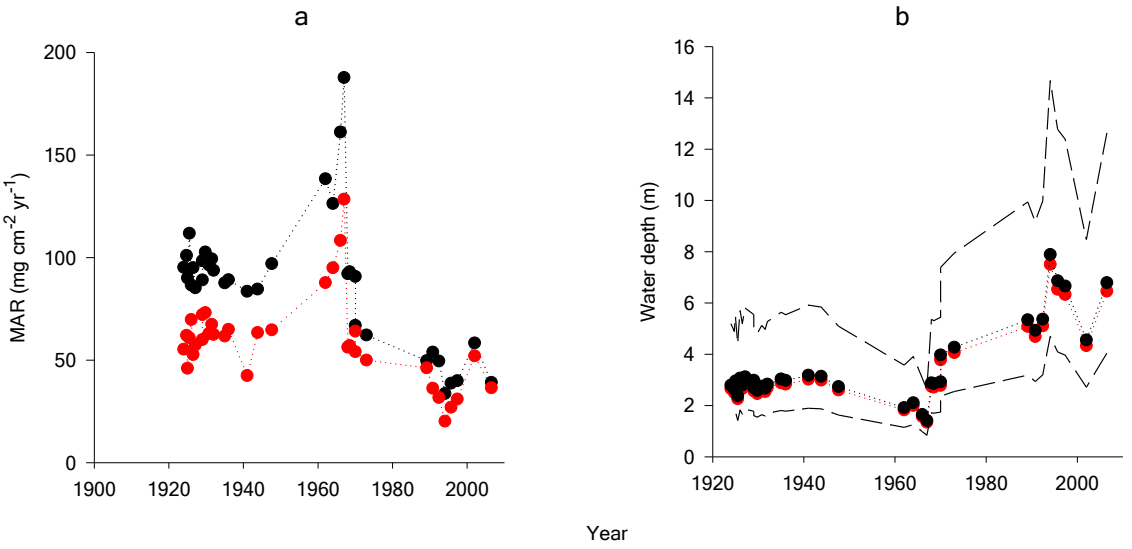

Figure 6.11. MAR of the fine fraction and critical depth light levels for the Upper Middle Basin sediment core LSPMB206.

(a) Diagenetically corrected MAR for the <76 µm fraction (●), uncorrected MAR for the <76 µm fraction (●). (b) Secchi depth (●), depth at 22 % of incident light (●), the 75 % and 25 % quartiles about the median 22 % incident light depths from the contemporary surface water turbidity statistics (———).

The reasons behind the maintenance of relatively high pre-1960 light levels are not clear. Perhaps re-suspension was kept in check by the dead seagrass meadow covering the sediment. Alternatively, the relatively high light levels are also consistent with evidence of an efficient rate of sestonic clearance by copepod egestion. The faecal pellet content represents a significant fraction of the total and is inversely correlated with the sestonic fine fraction throughout the baseline sediment horizons; although on a larger background turbidity than post 1960 (see Figure 6.12e). Such a change to a greater mean sestonic background suggests more efficient selective feeding on micro-algae during a time when there was a greater contribution of micro-algae to the seston. Further, the reason behind the greater copepod sestonic egestion is consistent with a low rate of planktivorous fish predation during the early existence of the transient (see Figure 6.12a). However, predation became weaker as the state aged towards the beginning of period of seagrass recovery (1946 to 1960).

6.3.3.3. Stability and nature of the regime between 1946 and 1960

The relative variance between the seagrass MAR, as a measure of meadow production, with DBSi MAR, as micro-algal production, is not consistent with the standard model of a seagrass light limited state at equilibrium with its nitrogen supply (*i.e.* an inverse relationship between

seagrass and micro-algal organic carbon production due to micro-algal shading of seagrass leaves [Borum and Sand-Jensen, 1996]). Nor is there evidence that the increase in the seagrass pieces MAR was a time of relatively high rates of carbon fixation in comparison to a time of stable seagrass MAR post 1960 (*i.e.* a lighter seagrass $\delta^{13}C_{org}$ pre-1960 than post-1960 [see Figure 6.3; see Section 3.4.3.3]). On the other hand, MAR of seagrass pieces during this may have been a proxy for seagrass abundance, when shoot recruitment and growth is greater than mortality (*vice versa*), a process irrespective of an increase in individual shoot productivity (*e.g.* Hauxwell *et al.*, 2003). Nevertheless, the continued inter-annual increase in micro-algal productivity does not appear to conform to the other tenet of the standard equilibrium model that there is constant carbon productivity for all coastal macrophyte–micro-algal systems (Borum and Sand-Jensen, 1996).

Clearly, this period of seagrass recovery did not behave in a manner that conforms to a regime state at equilibrium with it external nitrogen supply. Further, the constrained cluster analysis indicated that it is a regime that is separated from the others as a set of apparent transitions between pre- and post- 1960 regimes states (see Figure 6.8). The question remains what was driving the seagrass meadow expansion, as the CPN was relatively invariant during this time (see Figure 6.10).

The CPN did appear to be relatively invariant and the heavier fine fraction $\delta^{15}N_{org}$ indicated that there was no significant contribution of inorganic nitrogen from either nitrogen fixation, soil extracts or sedimentary mineralisation of organic matter over that of coastal supply (see Figure 6.3. and Section 6.3.1.2). Nevertheless, the fall in epifaunal density (see Figure 6.12d) might indicate that its availability to the seagrass leaves had increased over the period of seagrass recovery. However, the link between the planktivorous fish trophic cascade and its control over epifuanal coverage, as postulated in Chapter 3, appeared to be broken. The increase in MAR of sestonic turbidity with total micro-algae would have otherwise led to an increase in epifaunal coverage (see Figure 6.12c,d). This break in the relationship, however, need not imply that epifaunal production was no longer dependent on its micro-algal food supply. It is more likely that either the micro-algal population during this time (*e.g.* epiphytes) was increasingly unavailable for epifaunal bryozoan growth and/or the rate of growth of seagrass leaves was sufficient to overcome epifaunal production. Such a response is consistent with both nutrient limitation of seagrass meadow growth (*e.g.* Zieman *et al.*, 1999) and a role for top down control by a planktivorous fish trophic cascade (*i.e.* fish–copepods–seston–calcareous epifauna) in the progress of the nutrient limited transient regime.

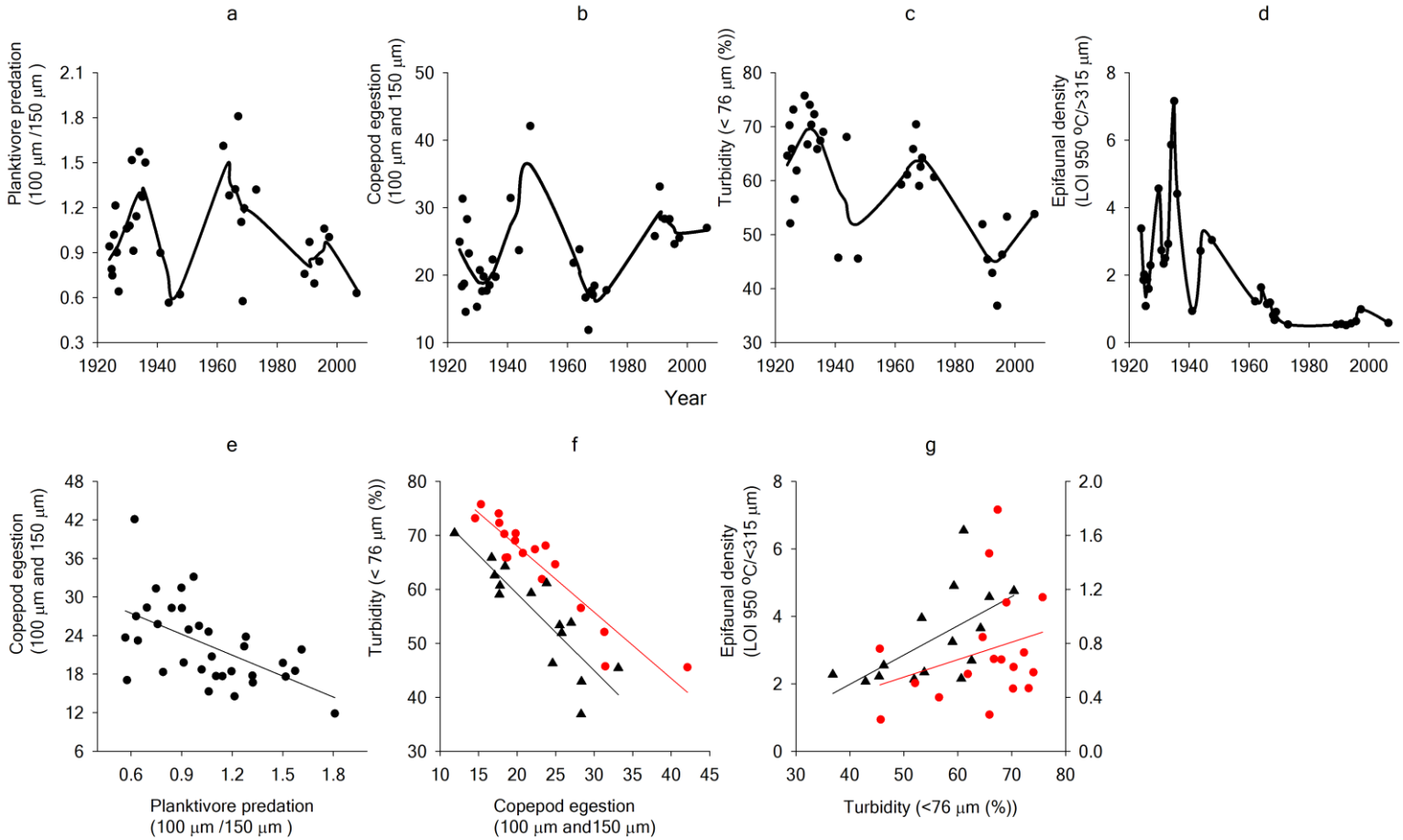

Figure 6.12. A time-series of elements consistent with a planktivorous fish trophic cascade and their relationship to each other down the Upper Middle Basin sediment core LSPMB206.

Top: (a) inferred planktivore predation as the ratio of the 100 µm and 150 µm copepod faecal pellet content; (b) copepod activity as the sum of the 100 µm and 150 faecal pellet content; (c) seston as the remaining fine faction content <76 µm; (d) the epifaunal seagrass leaf density as ratio of the LOI 950 °C: seagrass >315 µm. Bottom: the sequence of relationships between the above elements of the trophic cascade. (▲) post-1960 and (●) pre-1960. The smoothing procedure is based on a least squares criterion to a β-spline as a sequence of third-order polynomials continuous up to the second derivative (PAST™).

Reasons behind the large changes in the net predation of planktivorous fish were not clear. The lack of clarity results from a combination of no continuous and repeatable patterns over time or examples from other similar systems. The large periodic variance of planktivorous fish predation and copepod egestion may have forced the SSAM algorithm to fit only one major continuous symmetrical periodic component and trend (unpublished) and thus remove any temporal asymmetry (see Section 5.4.7), which may exist out phase with the assemblage of primary producers. Consequently, it is difficult to distinguish between two possible reasons behind the changes to the trophic cascade—stochastic variance in the external supply of planktivorous fish to the Upper Middle Basin or planktivorous fish predation that is coupled to the state and type of the regime.

Why micro-algal productivity should continue to increase was not clear. Certainly light attenuation increased to its highest levels over the period of study and this might indicate a form of co-limitation with nitrogen. Under these circumstances, the nitrogen requirements for the cell growth as less (*i.e.* greater POC–PON ratio) with increased light attenuation (*e.g.* Philippart and Cadee, 2000) and with it presumably BSi (see Figure 6.3).

6.3.3.4. Stability and nature of the regime between 1960 and 1986

It was not possible to know if or when the planktivorous fish trophic cascade started to strengthen during the latter period of the previous seagrass transient phase. Nevertheless, by 1960 and through to 1970—the postulated period of a reduced coastal exchange restriction—(see Chapter 4) saw a fall in epifaunal density (see Figure 6.12d). The fall in epifaunal density, however, did not reflect the factors previously synonymous with its previous seagrass recovery (transient regime state) a variable rate of micro-algal production, which was correlated to CPN, relatively high rates of planktivorous predation and low rates of copepod egestion (see Figure 6.12a,b,c), no change in seagrass abundance, and a switch to relatively high rate seagrass carbon fixation (heavier $\delta^{13}C_{org}$ [see Section 6.3.1.3]). In contrast to the previous increase of inorganic nitrogen availability for a constant ambient CPN variance, at a time of low sestonic turbidity, relatively low rates of planktivorous predation and high rates of copepod egestion at a time of low sestonic turbidity, increasing rates of seagrass abundance and micro-algal production and (*i.e.* MAR) a relatively low rate of seagrass shoot carbon fixation (lighter $\delta^{13}C_{org}$).

Interestingly, the mean micro-algal response to the CPN immediately after the 1960 was greater than other times after 1946 and before 1987 (see Figure 6.10c (▲)). The change to the

response parameter might be the result of the partial blockage of the entrance by the flood–tsunami confluence (see Chapter 4). The blockage would have increased the water residence time and consequently in the net basin micro-algal production. Indeed, an increased residence time is consistent with the lighter $\delta^{15}N_{org}$ micro-algal dominated fine fraction (see Figure 6.3) supplied from the undiluted mineralisation remnants of the dead seagrass meadow.

The reasons behind the regimes states ecosystem patterns were not clear, again, possibly the result of no information regarding changes to micro-algal forms (see Section 6.3.3.3). Alternatively, seagrass abundance may have simply reached its maximum extent within the confines and shallow depths of the basin, and with it a maximum shoot density (Duarte *et al.*, 2006). Under these conditions the meadow becomes subject to the combination of stabilising factors that emerge at high shoot densities. For example, leaf self-shading leads to an overall increase in the meadow's light attenuation of emerging shoots (Enriquez *et al.,* 2002), thereby maintaining individual shoot productivity but at the expense of an increase in mortality over recruitment (Hauxwell *et al.,* 2003). Alternatively a high shoot density may also lead to reduction in water exchange for the supply of waterborne micro-algae for epifaunal production (see Koch, 2001, also for a review of other mechanisms by which a reduction in water exchange limits seagrass growth).

Whichever stabilising mechanism or combination of the above predominates, the invariance with relatively large fluctuation with the CPN suggests that a seagrass meadow at its basin's full capacity might be a more resilient state to the effects of eutrophication than a meadow with a relatively low coverage and low shoot density.

6.3.3.5. Stability and nature of the regime between 1986 and 2008.

After 1986, both micro-algal MAR and seagrass MAR were invariant to the CPN variance, the largest variance currently experienced since 1923, and at a time the seagrass switched to light mediated nitrogen fixation, a time of a previously health seagrass meadow at full capacity (see Section 6.3.1.3). Such a pattern is consistent with the shellfish aquaculture hypothesis of system juvenilisation—an abundant seagrass meadow's switch to a near complete reliance on nitrogen fixation—because of the upper estuary's nitrogen impoverishment due to the drought (1979 to >2006) and the placement of the lower estuary shellfish aquaculture, which moderated the only other nitrogen supply from coastal waters.

It was not clear, however, if this response was specific to the previous state of the seagrass meadow. That is, a time of low epifaunal density and relatively high rates of carbon fixation for sugars to the bacterial nitrogen fixing symbiont (Welsh, 2000). For example, there may have been no similar response on the previous seagrass transient regime state because of: (1) a smaller seagrass nitrogen requirement for a smaller meadow, and (2) a reduced ability to fix nitrogen because of a higher epifaunal density and a lower rate of carbon fixation.

6.4. Summary and conclusions

The palaeo-reconstruction verified the postulate that nitrogen fixation within the Upper Middle Basin during 2006 was not a natural state, but rather an anthropogenic state consistent with the timing and location of the lower estuary shellfish aquaculture (1986) during the drought (1979 to <2006). During this time, the only other available nitrogen source from coastal resources appeared to be 'soaked up' by aquaculture production and harvesting (*e.g.* Songsangjinda *et al.*, 2000). This highlights the importance of coastal nitrate supply to the upper estuary ecosystem, as it also highlights the importance of historical contingency. It remains uncertain whether nitrogen fixation would have played such a significant role in maintaining seagrass abundance and/or production if the seagrass meadow coverage were smaller and/or less productive than its current state.

The palaeo-reconstruction also indicated that the Upper Middle Basin's long-term ecosystem variability was consistent with a sequence of three natural regime states and one anthropogenic regime state: a natural seagrass transient regime state, nitrogen limited and dominated by micro-algae; a natural seagrass transient regime state as seagrass meadow recovered, which may also be limited by nitrogen; a natural seagrass regime state at full basin capacity that is resilient to the effects of nitrogen eutrophication, possibly because of leaf self shading and reduction in the supply of micro-algae for epifaunal production; and an anthropogenic juvenilisation of the previous regime state, maintained by light mediated nitrogen fixation.

The presence of flood events, droughts, and anthropogenic disturbances was very informative as to the causes and mechanisms of regime change and produced a clear demonstration of historical contingency (*i.e.* floods were responsible for the death and recovery of the seagrass meadow). However, their interruption of a contiguous ecosystem time-series, together without a consideration of the variance between different micro-algal habitat forms made it difficult to postulate a general theory of seagrass variance. It was not possible to discern the reason

behind a fall in epifaunal growth as sestonic supply increased during the progression of the transient regime, without considering the role of epiphyte abundance. In addition, the low temporal resolution, loss of baseline information by erosion, together with the large changes in the strength of planktivorous fish cascade led to an uncertainty in correlating regime thresholds with changes in their top-down control. More importantly, it was not possible to ascertain the reasons behind the large asymmetric variance in the strength of the planktivore trophic cascade. In essence, the uncertainty is between changes in planktivorous fish predation as a function of changing numbers of migrating fish to and from the estuary or the rate of predation was the result of a long-term emergent property of the seagrass ecosystem. A property, which in some-way reflected the apparent, yet unproven, long-term asymmetry of planktivorous fish predation and the rate of copepod egestion.

Clearly, the development of general long-term theory of seagrass variance will require an continuous palaeo-reconstruction uninterrupted by events and erosion, long enough to oversee a number of complete cycles of decline and recovery of the seagrass–micro-algal assemblage stable state driven by the long-term cycles in inorganic nutrient supply (CPN). In this way, it may be possible to distinguish stochastic variance in the planktivore trophic cascade from variance due to some postulated long term emergent property associated with the meadows temporal and spatial landscape (see Section 1.3). In addition, a future study will need to examine the role of variance between epiphytes and water borne and micro-algal habitat forms for calcareous epifaunal production to determine any role for top down control of planktivorous fish trophic cascade (*i.e.* fish→copepods→trypton–water borne micro-algae→ calcareous epifauna) in relation to changes in bottom up eutrophication (*i.e.* CPN variance). It is such a future study, and the relation to an evolving landscape configuration, that frames the final data chapter of this thesis.

Chapter 7. Evidence of a neutral model for a general theory of seagrass meadow dynamics

7.1. Introduction

Seagrass ecosystems provide a high-value service to communities around the world, rivalling or exceeding that of many cultivated terrestrial systems (Costanza *et al.*, 1997; Orth *et al.*, 2006). Therefore, it is of concern that current data suggests a long-term global decline in seagrass meadows (Waycott *et al.*, 2009). Consequently, long-term theories of seagrass meadow dynamics have been developed to predict future impacts and remediation strategies. Outside of nebulous theories focusing on sequences of changes in natural historical conditions that might lead to stress and die off (Zieman *et al.*, 1999), current theories, at the landscape/meadow scale, focus on two seemingly disparate hypotheses of bottom-up control. These are: (1) algal eutrophication, leading to leaf shading and light limited seagrass meadow growth (Livingston, 1984; Duarte, 1995; Marbà and Duarte, 1997; Duarte *et al.*, 2006) and (2) a seagrass meadow that is limited by nutrient availability (Fourqurean and Zieman, 2002).

The current theories have not always been adequate to account for observed long-term changes in the size of a water body's seagrass meadow. For example, in Arcachon Bay (Western France), Martin *et al.* (2010) noted a significant decline in seagrass meadow coverage from 1988 to 2005, but could find no definitive reason for the decline. Similarly, faced with no significant change in water quality (temperature, salinity, dissolved inorganic nitrogen, suspended sediment and chlorophyll), Nienhuis *et al.* (1996) could find little evidence that environmental variables were responsible for the wax and wane of the eelgrass coverage (*Zostera marina*) in Grevelingen lagoon (The Netherlands) over 25 years. Further, periodic changes in eelgrass coverage in Danish coastal waters did not appear to directly correlate with the available long-term records of either natural or human-induced disturbance (Frederiksen *et al.*, 2004a). Indeed, the response of the seagrass abundance to external nitrogen supply and micro-algal productivity within the Little Swanport estuary's Upper Middle Basin was not always consistent with a strict delineation between the affects of algal eutrophication and external nitrogen forcing (see Chapter 6).

The above descriptions indicate that, in isolation, standard environmental variables and/or external disturbance parameters, tested by laboratory and limited field experiments, do not always account for seagrass ecosystem dynamics. This may be either due to a failure to account for long-term emergent properties or changes in external parameters. For example,

within lakes a large planktivorous fish year class can alter herbivory rates over the medium term (around 5 years) and subsequently net micro-algal production that reflects the lifespan of the fish population (Carpenter and Kitchell 1988; Carpenter and Leavitt, 1991). Alternatively, in more open estuarine systems, adult planktivorous fish or grazers may simply vary in numbers due to natural changes to the larger coastal ecosystem (Southward *et al.,* 1975; Southward, 1980; Jackson, 2001).

Irrespective of reasons behind the numbers of planktivorous fish, the inclusion of a planktivorous fish trophic cascade into seagrass dynamics is currently considered the most likely and universal mechanism, with sufficient power, to explain the failure of the above long-term studies. Indeed, based on open studies at the seagrass patch level (*e.g.* Jorgensen *et al.,* 2007; Macreadie *et al.,* 2009, 2010), it has been suggested that seagrass nutrient or light limited seagrass meadow growth may depend on the balance between the strength of a planktivorous fish trophic cascade and seagrass epibiont eutrophication. For example, low rates of planktivorous fish predation on mesograzers or copepods leads to a low rate of net epiphyte and gross epifaunal production respectively (top down control [*e.g.* Jorgensen *et al.,* 2007; see Chapter 6]), and thus maintains sufficient light resources for nutrient stimulation of seagrass growth (Baird and Middleton, 2004). Conversely, high rates of planktivorous predation leads to insufficient light resources for seagrass growth (bottom up control [Livingston, 1984; Heck *et al.,* 2000; Heck and Valentine, 2006; Jorgensen *et al.,* 2007; Moksnes *et al.,* 2008; see Chapter 6]).

Outside of changes in fishing pressure or introducing piscavores, no study has sufficiently addressed if endogenous or exogenous factors determine the numbers of planktivorous fish and the rate of planktivorous fish predation over the long term, despite empirical evidence from paleo-reconstructions within closed ecosystems (McGowan *et al.,* 2005). McGowen *et al.,* (2005) found that the planktivorous fish proxy varied with macrophyte coverage as integrated over the lakes and over the long-term.

.

7.1.1. A postulate for an emergent property: The role of landscape configuration

It is important to test for the long-term emergent properties that determine the true dynamics of the system before considering the affects of changes to external parameters. Indeed, there is anecdotal evidence from the long-term data set of Morris and Virnstein's (2004) to suggest an underlying emergent property. Morris and Virnstein (2004) recorded a repeatable series of natural recovery and decline phases of seagrass meadow (Turnbull Bay in Indian River

lagoon, Florida, USA), that did not appear to be linked to changes in external nitrogen forcing[28]. Each recovery phase, initiated by a hurricane, filled the Turnbull Bay's littoral zone with a homogenous seagrass meadow unencumbered by epiphyte or macrophyte shading (*i.e.* nitrogen limitation; *e.g.* Fourqurean and Zieman, 2002) and was immediately followed by an inevitable loss caused by the smothering of seagrass shoots by ephemeral macrophyte and micro-algal (*i.e.* light limitation; Duarte, 1995).

Morris and Virnstein's data also indicated an asymmetry in seagrass landscape configuration, as expressed by differences between seagrass patchy zones and homogenous zones within the bay during recovery and decline. Their data indicated that during recovery there were small homogenous zones and large patchy zones but during decline the homogenous zones with relatively larger and patchy zones were relatively smaller. Kendrick *et al.*, (2005) suggested that such natural changes in seagrass landscape patch configuration may be the result of self-organisation due to an accelerated growth of patches as an emergent property of seagrass ramet growth. Such results highlight that any theory of long-term variance of a rooted plant landscape will be incomplete without consideration of its landscape configuration (for aquatic modelling hypotheticals see van Nes and Scheffer, 2005; Dakos *et al.*, 2010, and for terrestrial systems see Hastings and Higgins, 1994; Kareiva and Wennergren, 1995; Pastor *et al.*, 1997; Dieckmann *et al.*, 2000; Rietkerk *et al.*, 2004). More specifically, it was the judgment of Robbins and Bell (1994) that '[g]given that marine researchers are investigating questions over large scales as well as examining patch characteristics, the stage is set for landscape-level analyses to emerge'. More recent reviews concluded, '[w]while knowledge at the molecular, organism, patch and community scale is pervasive, understanding of seagrass landscape ecology is more fragmentary and has not yet been synthesized' (Connolly and Hindell, 2006). '[C]Consequently, a better understanding of faunal–seascape relationships and threshold affects is urgently needed to support the holistic management actions in restoration, site prioritisation, and forecasting the impacts of environmental change' (Boström *et al.*, 2006; Boström *et al.*, 2011).

Current research continues to advance the realisation that there might be an internal reorganisation of planktivorous fish top-down control as a function of landscape configuration

[28] Morris and Virnstein's (2004) study did not have long-term nutrient data from within the bay. Nevertheless, their historical nutrient data set outside the bay indicated that the system was always eutrophic and that the periodicity was not a function of a periodicity in nutrient loading, but rather the result of hurricanes that had swept the sediment clean, restarting the natural cycle.

in unexpected and non-linear ways. Jelbart *et al.* (2007) found that smaller patches invite larger numbers and densities of planktivorous fish. Macreadie *et al.* (2009, 2010) showed that planktivore abundance did not fall as expected with smaller artificial seagrass patchy areas. It would be expected that rates of planktivorous fish predation are proportional with patch perimeter length because copepods swarm immediately outside the patch perimeter (*e.g.* Ueda *et al.,* 1983; Hicks, 1986) and are preyed upon by planktivorous fish from within the patches (Smith *et al.*, 2008; Macreadie *et al.*, 2009, 2010).

A similar edge affect between small and large submerged aquatic vegetation patch sizes, with respect to copepods numbers, was observed within a freshwater lake (Lauridsen *et al.*, 1996). Lauridsen *et al.* (1996) found a significantly greater density of free-swimming cladocerans around the edges of smaller patches (3430 indiv L^{-1}; 2 m diameter) compared with around larger patches (202 indiv L^{-1}; 25 m diameter). Scheffer (2004) commented on Lauridsen *et al.'s* (1996) result by suggesting that this would lead to a greater rate of planktivore predation on cladocerans around the smaller patches, given that freshwater planktivorous fish also feed at the edges from within the vegetation. Assuming that copepod behaviour between fresh and marine systems is axiomatic or mostly universal, smaller patches with longer perimeters would result in a greater predation rate, conceivably further amplified by higher planktivorous fish patch densities and copepod patch perimeter densities.

However, observations of individual seagrass patch dynamics are insufficient to explain the affect of such an emergent property across the landscape; that is, there is no evidence for a mechanism of a global connection[29]. Other studies (Habeeb *et al.*, 2007) have demonstrated a global connection between seagrass patches by a space–time semi-variogram procedure that determines the landscape characteristic length scale. However, the literature appears not to have discussed or suggested a vector for transferring information between the finer patch spatial–temporal scales to and from the broader spatial–temporal scales of landscape. Consequently, aquatic landscape modelling has relied on empirical coefficients, which only represent connection strength between individual units of patch ecologies (*e.g.* van Nes and Scheffer, 2005; Dakos *et al.,* 2010).

[29] Global connection is a term used in landscape ecology to describe a well connected structural and or biological landscape. In this study it is used to convey an unimpeded transfer of information between patch ecologies within a landscape unit.

For aquatic systems, horizontal advective dispersion of water and motile organisms are obvious candidates for transferring information across individual patch ecologies (Gouhier and Guichard, 2007). However, to fulfil the conditions of information transfer, there must be a net redistribution of the organism across the landscape. For example, planktivorous fish may swim freely around a seagrass meadow, but if there is no net movement among patches there will be no physical or chemical potential between individual patches and therefore no information transfer to effect change across the landscape. In other words, the patch ecologies are open to movement, but remains an effectively dynamically closed system, much like a chemical process at equilibrium. Indeed, the evidence suggests that planktivore abundance does appear to be at equilibrium with its available niche (*i.e.* number of patches and patch size). For example, Jelbart *et al.* (2007) found that individual fish numbers were related to patch size, did not significantly change between day and night and net movements of individual species were mixed and small. Macreadie *et al.* (2009, 2010) found that newly introduced artificial seagrass patches were quickly colonised to a constant fish density.

In contrast to planktivores, copepods migrate and disperse across open water for the night before returning to the perimeter of seagrass patches for the day (*e.g.* Hicks, 1986). Copepods also respond to changes in micro-algal primary productivity, but at a finer seasonal scale than the decadal scale of meadow dynamics (Scheffer, 2004). The mixing and dispersion of copepods within the main water body during the night, after various local planktivorous and copepod predation impacts during the day, could be expected to return a lower number to individual patches but in similar proportions to the previous total. The result is a change across the landscape (defined by copepod dispersion) in net water-borne micro-algal productivity and thus, epifaunal production (see Chapter 6). The result of copepod mediation is that information gained at fine scales can conceivably be extrapolated to broader temporal and spatial scales, and *vice versa,* across one organisational level to another *via* a planktivorous fish trophic cascade and from patch to meadow dynamics. Notwithstanding wave and water current structure (Fonseca *et al.*, 2002), how the growth, mortality and configuration of seagrass patches evolve in response to changes in available limiting nitrogen and light resources then arguably is common feature of a rooted aquatic angiosperm meadow (Duarte *et al.*, 2006).

7.1.2. Aims

The aims of the study were to:

- To construct complete range of natural patterns that are necessary to describe the seagrass ecosystem (*i.e.* bottom up and top down control on the seagrass–micro-algal assemblage) from an uninterrupted sediment core palaeo-reconstruction of the Lower Middle Basin (*circa* 1890 to 2007), and thereby identify its neutral model's unit of variance (see Section 1.2.1, foot note 2);
- Test for affects of shellfish aquaculture on the seagrass ecosystems unit of pattern and process (see Section 1.2.1);
- Determine any role for landscape configuration in the stability of the light and nitrogen limiting function regimes and;
- Develop a general theory of seagrass dynamics based on the neutral models' ecosystem's patterns and processes by testing a series of hypotheses relating to the balance between top down and bottom up control for predicting the seagrass meadow–micro-algal response in relation to changes to the natural evolution of a seagrass meadow's patch configuration.

7.1.3. Hypotheses

The aims were achieved using a series of expected ecosystem patterns, to test the conditions and the axiom on which the theory can be easily expressed and the hypotheses that are embedded in the theory's postulates. That is, conditions of no significant advective contribution to the basin's micro-algal production and a regime at equilibrium (*i.e.* no dynamic transient regimes [hypotheses 1 and 2]); postulates that relate to the type of top down control [hypotheses 3 and 4]); postulates that describe the relationship between the seagrass and the CPN to constrain the interpretation as either a light limited (inferred bottom up control) or a nitrogen limited regime (inferred top down control [hypotheses 5 and 6]); and postulates that connect the patterns and processes across a seagrass landscape (hypotheses 6 and 7).

- Hypothesis 1. The current standard model (Borum and Sand-Jensen, 1996). There is an inverse correlation down the sediment core between seagrass and micro-algal content as nitrogen resources are distributed between seagrass and micro-algal production, because of the constraint of a constant organic carbon productivity for a benthic–pelagic system at equilibrium with it nitrogen supply.
- Hypothesis 2. Seagrass epifaunal density down the sediment core is inversely correlated with seagrass content as effect (nitrogen limitation) and/or a cause (light limitation) of seagrass growth.

- Hypothesis 3. A stepwise multi-linear regression model of epifaunal density that excludes epiphytes from its dependence on waterborne micro-algae (facultative epipelics and phytoplankton) and seagrass growth is consistent with conditions of seagrass meadow nutrient limitation (*e.g.* Frankovich and Fourqurean, 1997).
- Hypothesis 4. A stepwise multi-linear regression model of epifaunal density that excludes seagrass and epiphytes suggests that changes in seagrass abundance down the sediment core depends on clean seagrass leaves relatively free from epifauna for sufficient light and nitrogen absorption (see postulates in Chapters 3 and 6).
- Hypothesis 5. Positive or negative correlations between CPN and seagrass or total micro-algae are consistent with patterns of nitrogen limitation and light limitation respectively.
- Hypothesis 6. A series of inverse relationships between inferred planktivorous fish predation, copepod feeding and sestonic turbidity (faecal pellets and the fine fraction), as a significant proportion of the total sediment content, is consistent the both the presence and ecological importance of a planktivorous fish trophic cascade (potential top down control [see Chapter 6]).
- Hypothesis 7. Any changes between nitrogen and light limited regime states connected by top down and bottom-up vectors are marked by peaks and troughs of elements of the planktivorous fish trophic cascade (as far as sestonic grazing [see Chapter 6]) at the same temporal scale. It should be noted, however, that this statement is not a strongly testable hypothesis because it is not a falsifiable statement, but rather a parsimonious expectation for an inference to the best explanation (see Chapter 1). In other words, it is conceivable that the control of epifaunal productivity may have equivalent degrees of top-down and bottom-up control. For example, a moderate trophic cascade with a moderate micro-algal production may be equivalent to a high trophic cascade and a low micro-algal production and so on.
- Hypothesis 8. Planktivorous fish predation correlations with total seagrass coverage within the sediment record converge with similar correlations of total edge length to total seagrass coverage from an ‘ideal’ seagrass configuration model (see below).

7.1.4. A Robustness Analysis

Hypothesis 7 and its relationship to hypotheses 6 is a test based on the logic of scientific justification of mixed Robustness Analysis ([RA] Bycroft, 2009; see Chapter 1). RA argues that the convergence of two plausible independent models/hypotheses, structured to test postulates to predict a common outcome of a common theory (see Section 7.1.1), will confirm

the core structure of each model as generally robust. In this case, the two lines of evidence (Model 1 and Model 2; see below) were structured to predict a common variance with a common temporal and spatial scale between total seagrass coverage and total meadow edge length. That is, by comparing relative planktivorous fish predation rates with total seagrass abundance (the Little Swanport estuary paleo-reconstruction) to a landscape configuration model, constructed from data across a similar seagrass landscape with landscape patch parameters taken from other similar systems. While each prediction is specific for their own systems, the convergence of the result from similar systems reinforces the two models core structures to give support as a general model for all similar systems.

Evidence to suggest that the strength of top down control is connected and controlled across a naturally evolving seagrass landscape (Model 1 [**see section 7.1.1])**. Planktivorous fish predation and seagrass proxies, integrated from their immediate surrounds (supply to the deep spot [see Section 2.1]) that significantly vary in strength over a number of recovery and decline phases, and at the same temporal scale suggests: (1) total seagrass edge length will vary in the same way with coverage (the model prediction [see Figure 7.1]), (2) the scale of the planktivorous fish behavioural response to seagrass coverage, and the inferred edge length, is integrated across the seagrass landscape (Greig-Smith, 1979; Schneider and Piatt, 1986), and (3) the relationships are likely to be the result of a natural internal re-organisation (evolution) of the seagrass landscape as a potential vector for controlling the relative importance of top down control, which may explain the switch from seagrass nitrogen limitation to light limitation.

Evidence to suggest that the seagrass patch perimeter length, connected across an evolving seagrass landscape, is greater during a recovery phase than the decline phase and thus, with the strength of top down control (Model 2 [see Section 7.1.1]). A total meadow edge length that varies significantly out of phase with total seagrass coverage (calculated for Tully Bay using data from Morris and Virnstein, 2004; Fonseca and Bell, 1998; Frederiksen *et al.*, 2004b) over a number of natural recovery and decline phases (the model prediction [see Figure 7.1]) suggests: (1) a long-term link between patchiness and top down control, consistent with the inferred switch from nitrogen stimulation to light inhibition of the seagrass meadow, and (2) the patch dynamics are connected across the seagrass landscape (*i.e.* adherence to a neutral model of edge density/number of patches [Fortin *et al.*, 2003]).

Robustness argument. A convergence between evidence of planktivorous fish predation over declines and recovery with the total edge length and seagrass abundance/coverage evidence from Model 1 and Model 2 reduces the likelihood that the common result (a link between landscape edge length and planktivorous fish predation) is due to some error that both techniques have in common, and consequently increases confidence in the evidence and both the models' underlying assumptions (see Figure 7.1). In other words, there was a process of self-organisation of seagrass patch configuration across the Tully Bay's seagrass meadow, and that planktivorous fish predation was part of the same landscape process of self-organisation.

Generalisation. Given the mutual support for each of the models assumptions, taken from evidence across two different times and two different seagrass meadows, then the convergence supports a result which is tentatively generally correct across similar seagrass ecologies within similar embayments and periods (see Figure 7.1).

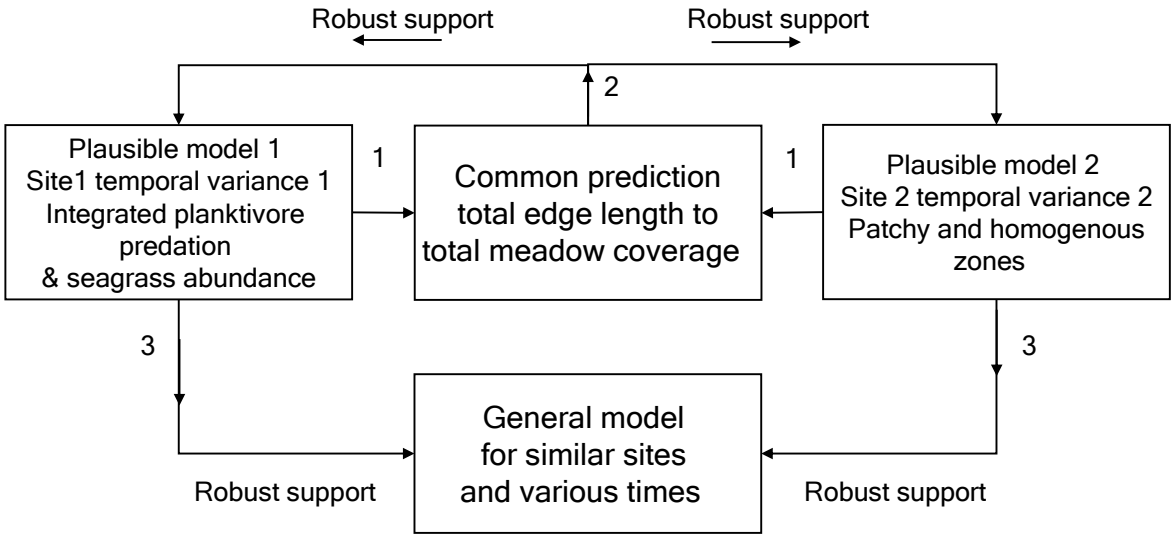

Figure 7.1. A logic schematic of a mixed Robustness Analysis used in the study. The schematic shows how site-specific plausible lines of evidence, in different spaces and times, converge to a spatial and temporal common result.
The convergence then supports the assumptions behind each individual theory for a general theory from different seagrass embayments and at various times, within the confines of their theories domain.

7.2. Materials and methods

The palaeo-reconstruction was carried out on sediment core (LSPMB106) from the Lower Middle Basin of the Little Swanport estuary (see Figure 7.2), immediately above the 1868 tsunami depositional facies. For site selection, sediment core extraction, processing and analysis of sediment components, see Chapter 2. See Chapter 4 for details of the geochronology and Chapter 5 for the reconstruction of CPN.

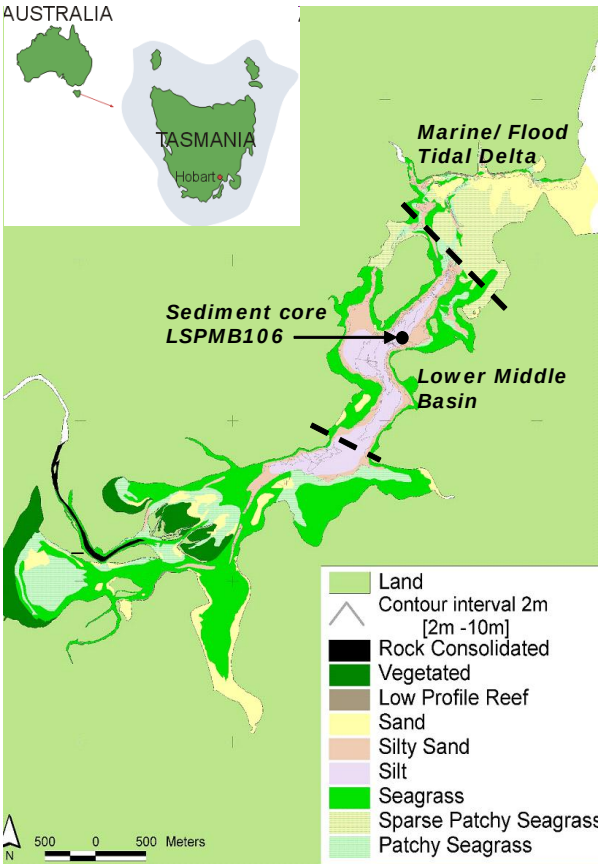

Figure 7.2. A habitat map of the Little Swanport estuary showing the boundaries for the Upper Middle Basin, the adjacent Marine Flood/Tidal Delta and the sediment core extraction site in the heterotrophic deep central basin (8 m).

7.2.1. Biome palaeo-reconstruction

The choice of plausible proxies was restricted to those successfully tested for the Upper Middle Basin (see Chapter 6): (1) total diagenetically corrected biogenic silica (DBSi), corrected for dissolution, to represent the total micro-algal population; (2) the washed >315 µm fraction, leaving the remnants of seagrass leaf pieces for live seagrass abundance, contingent on a constant OM content; and (3) the ratio of diagenetically corrected total organic carbon (DTOC) to DBSi as an index of seagrass abundance, assuming a relative constant BSi–C across the diatom population.

The DBSi was further divided between the proportion of micro-algal diatomaceous habitat forms: epiphytes, epipelics and facultative phytoplankton, according to Round *et al.* (1990). See Appendix B for the abundance of each species down the sediment column. Centric diatoms were not separated from the facultative phytoplanktonic pennates because the ratio of centric to pennate was found to be too small for statistical assessment (0.015 to 0.045).

Epifauna was represented by the total sediment loss of material on ignition between 550 °C and 950 °C (LOI 950 °C) without a diagenetic correction (see Chapter 6). Calanoid copepod feeding activity was represented by total faecal pellet content captured in 150 μm and 100 μm sieves, their ratios were used as an index of inferred planktivorous fish predation, and sestonic turbidity was then represented by the remains of the fine fraction content (<76 μm; see Chapter 6) not egested as copepod faecal pellets.

7.2.2. An ideal configuration model for a seagrass meadow (model 2; Section 7.1.3)

The model was expressed at a traditional landscape scale (1 km^2). However, the exact value is arbitrary. The construction of the model was based on data taken from an isolated embayment of the Indian River Lagoon (Florida, USA; Morris and Virnstein, 2004). The data was digitally extracted from a pdf file of Morris and Virnstein's figures (FindGraph™) as average changes in seagrass homogenous and patchy zones over a number of decadal cycles. The embayment was of a similar size and structure to the Little Swanport's Lower Middle Basin, in that the water bodies supported an extensive seagrass meadow located within their shallow littoral zones, surrounding a deeper central basin, postulated as needed for a copepod global transfer of information across the heterogeneous patchy seagrass meadow.

It was assumed that within the patchy zones, the seagrass coverage was 60 %. The percentage is a value that defined a break in benthic assemblage connectivity within a patchy seagrass meadow of Tampa Bay (USA; Fonseca and Bell, 1998). The size of the patches was fixed at 0.001 km^2 to set the number of patches on a scale of 100 within an arbitrary 1 km^2 landscape unit. Frederiksen *et al.* (2004b) found that *circa* 100 patches occupied 87 % of the seagrass meadow over an similar landscape range (around 0.5 km^2 to 2.5 km^2). Calculations of patch coverage and perimeter length were based on a circle, and the total seagrass edge across the landscape was calculated, as circles, by combining the homogenous zone and patchy zones.

7.2.3. Data analysis

All biome content depth profiles were optimally smoothed down the sediment core to facilitate pattern recognition between the ecosystem components. The smoothing procedure was carried out in PAST™ by fitting a least squares criterion to a β-spline, as a sequence of third-order polynomials continuous up to the second derivative.

A reduced major axis (RMA) linear regression was used for paired correlations between ecosystem components to minimise both the x and the y errors (PAST™). Stepwise

regressions were used to identify cause and effect of epifaunal densities from postulated selections of the independent biome components (Sigmaplot™).

Free-phase sinusoidal models (PAST™), based on the major periodic components, were fitted to the stationary sediment content time series to construct the temporal patterns between the long-term periodicities of concentration of potential inorganic nitrogen (CPN; see Chapter 5), the non-tautological representatives of the primary productivity assemblage and the planktivorous fish trophic cascade. The major inter-decadal frequencies were identified using a Lomb periodogram procedure for uneven sampling (PAST™). The presence of significant higher frequencies at the decadal scale (around 13 years) was not considered in the synthesis because not all time series could distinguish them as significant ($p < 0.05$ level) from white noise.

7.3. Results

7.3.1. Total edge length to total coverage model

The calculated variables for the construction of total edge length to total seagrass coverage periodicity over two cycles are presented in Table 7.1. The landscape reconstruction illustrated that patchy asymmetry, and thus the total edge length, between a declining and recovery phase, was primarily due to the differences in the number of patches, rather than the difference between the sizes of homogenous and patch zones (*c.f.* meadow areas at 0.4 km^2, see Table 7.1). Consequently, the edge density not only increased with the number of patches but also reached a maximum patch number asymptote near the completion of meadow recovery. Such a relationship between edge density and patch numbers was consistent with a neutral model simulation of a globally connected landscape (Fortin *et al.*, 2003) that supports a connection around Tully Bay's littoral zones and/or across the open water of its deeper central basin (see Morris and Virnstein, 2004).

The lag between the total meadow edge length and total seagrass coverage is clearly illustrated in Figure 7.3. The significance of the total edge asymmetry and lag reiterates that, based on the selected patch parameters, the loss of the homogenous zone was not primarily due to internal fragmentation (see Table 7.1), but to a loss from the edges from the deeper parts of the estuary (Morris and Virnstein, 2004). The recovery of the seagrass meadow was preceded by patch formation (see Table 7.1) and subsequent coalescence in a manner consistent with seed dispersal followed by rhizome expansion, as was the case for Tully Bay (Morris and Virnstein, 2004).

Table 7.1. Variables and parameters used in the construction of a seagrass landscape configuration ideal model. The relative extent of the meadow and the proportions of homogenous and patchy zones during a decadal recovery and decline phase were taken from Tully Bay (Morris and Virnstein, 2004). The median patch size was fixed at 0.001 km², as a circle, to match the maximum patch number within a landscape (Frederiksen *et al.,* 2004a), assuming that the seagrass coverage within the patchy zones was set at a maximum of 60 % (Fonseca and Bell, 1998). For the purpose of illustration, time is arbitrary and will depend on the species of seagrass and local conditions in question.

Meadow area (km^2)	Homogenous zone area (km^2)	Homogenous zone edge length (km)	Patch zone area (km^2)	Total number of patches (km^2)	Area of patches (km^2)	Total edge length of patches (km)	Total seagrass coverage (km^2)	Total meadow edge length (km)	Edge density (km^{-1})
1	1	3.54	0.00	1	0.000	0.00	1.00	3.54	3.5
0.6	0.6	2.74	0.00	1	0.000	0.00	0.6	2.74	4.6
0.4	0.38	2.18	0.02	20	0.012	2.24	0.39	4.42	11.3
0.2	0.15	1.37	0.05	50	0.03	5.60	0.16	6.97	38.8
0.4	0.2	1.58	0.20	200	0.120	22.41	0.32	24.00	75
0.6	0.4	2.24	0.20	200	0.120	22.41	0.52	24.65	47.4

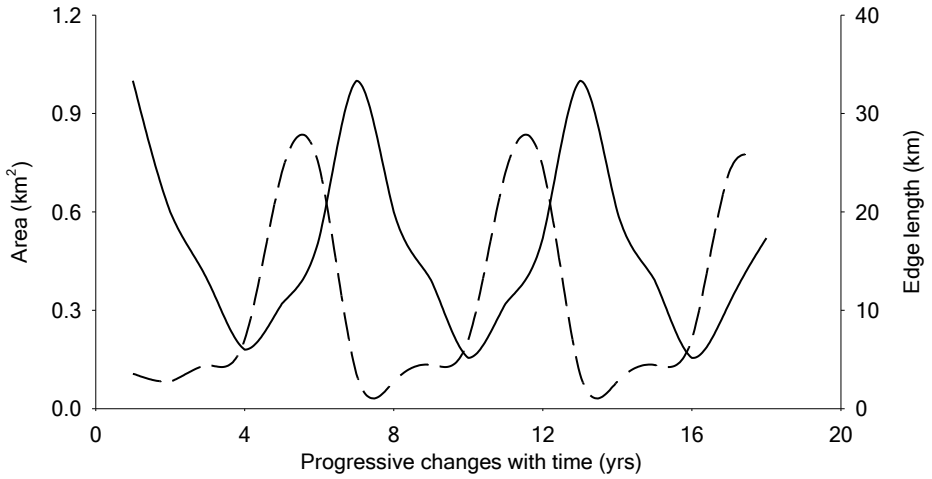

Figure 7.3. An ideal model of a seagrass landscape expressed as a time series of total edge length (— —) with total coverage (——) for a 1 km² unit.
The proportions of homogenous and patchy zones during a recovery and decline phase were taken from Morris and Virnstein (2004). Individual circular patch areas were assumed to be constant (0.001 km²) based on a maximum median patch number over a landscape unit (Frederiksen *et al.,* 2004b) occupying 60 % of the patchy zone (Fonesca and Bell, 1998).

7.3.2. Palaeo-reconstruction of the primary productivity assemblage

There were clear differences in the early dynamics from the last 15 years between TOC and DTOC (see Figure 7.4). These differences included an early fall in DTOC in contrast to a relatively invariant concurrent trend for uncorrected TOC. The same reversal of trends applied to a lesser extent for uncorrected total biogenic silica (TBSi) and corrected TBSi for losses from dissolution (DBSi). The difference between the above relative changes reflects the more variable BSi surface profile and thus content gradient dependence (see Chapter 6; Equation 6) buffered any changes in trend over the last 15 years or so.

Both the >315 µm fraction, dominated by seagrass pieces, and the DTOC–DBSi seagrass index recorded a large peak as seagrass content that was centred around 15 cm. However, the OM content within the >315 µm fraction was not constant (see Figure 7.4). Consequently, this precluded the use of dry weight as a reliable proxy for seagrass carbon productivity, given that there was insufficient reliable OM data for a contiguous profile. Therefore, as a value judgment, seagrass proxy index (DTOC–DBSi), which assumes a constant BSi–C ratio (see Chapter 3), was chosen in preference to >315 µm content to represent seagrass variance for the ecosystem synthesis of events and theory.

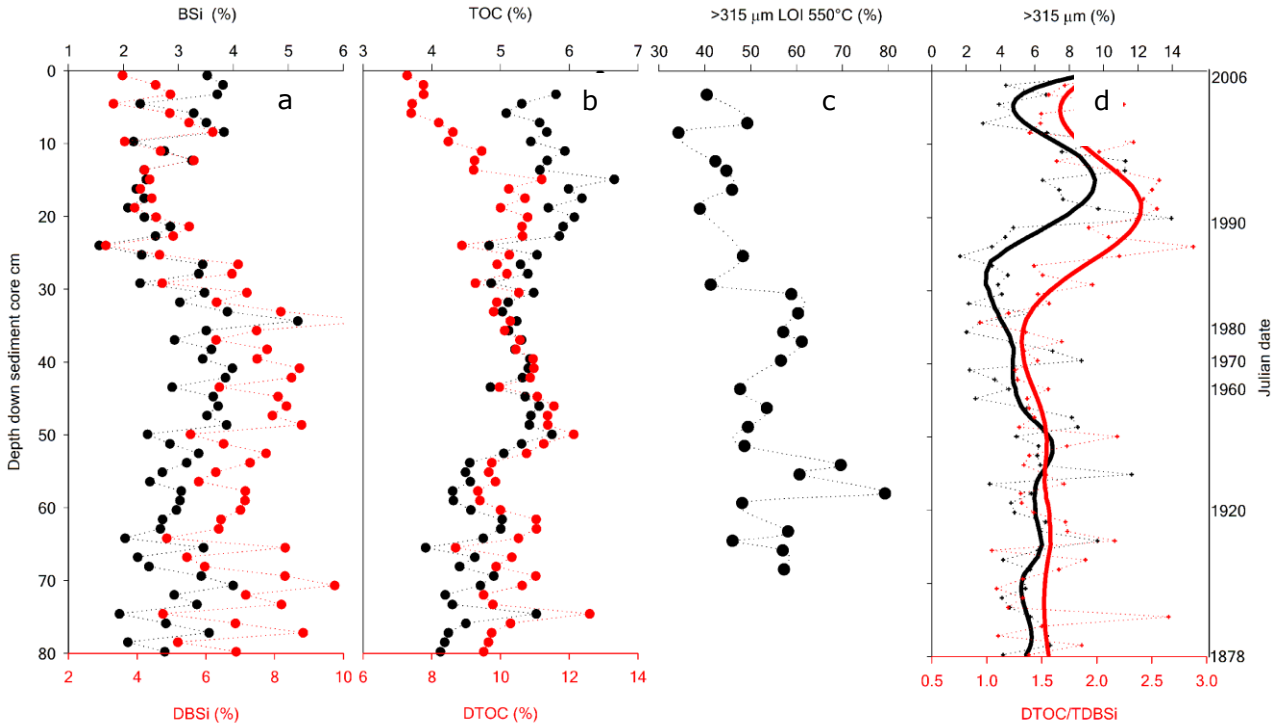

Figure 7.4. Total organic carbon and total biogenic silica before and after diagenetic corrections together with seagrass proxies for Lower Middle Basin sediment core LSPMB106.
(a) TBSi corrected for dissolution as TDBSi; (b) TOC correction for dissolution as DTOC; (c) organic carbon content (LOI 550 °C) of the >315 µm seagrass fraction; (d) proxies for live seagrass meadows based on seagrass content from the >315 µm fraction and the ratio of DTOC–DBSi. See Chapter 6 for details of the diagenetic models. The date of sediment horizons were determined by ^{210}Pb sediment isotope tomography (see Chapter 4).

7.3.3. Relative changes of biome components down the sediment column

A cross-correlation analysis with depth indicated that seagrass and total micro-algal proxies down the sediment core were negatively correlated to each other without any lag with depth (see Figure 7.5 [top panel]; Table 7.1). Inverse correlations of that nature were consistent with patterns that result from a transfer of excess nitrogen resources from seagrass to micro-algae, dictated by a constant total carbon primary production (Borum and Sand-Jensen, 1996). Although, in the deeper sections of the sediment core, below 60 cm, the seagrass index was

relatively invariant. This invariance was probably not the result of a break down in the theory of benthic/pelagic coupling, but rather due to an increasing proportion of epipelic diatoms below 60 cm (see Figure 7.5) with a heavier silicon to organic carbon content (Brzezinski, 1985).

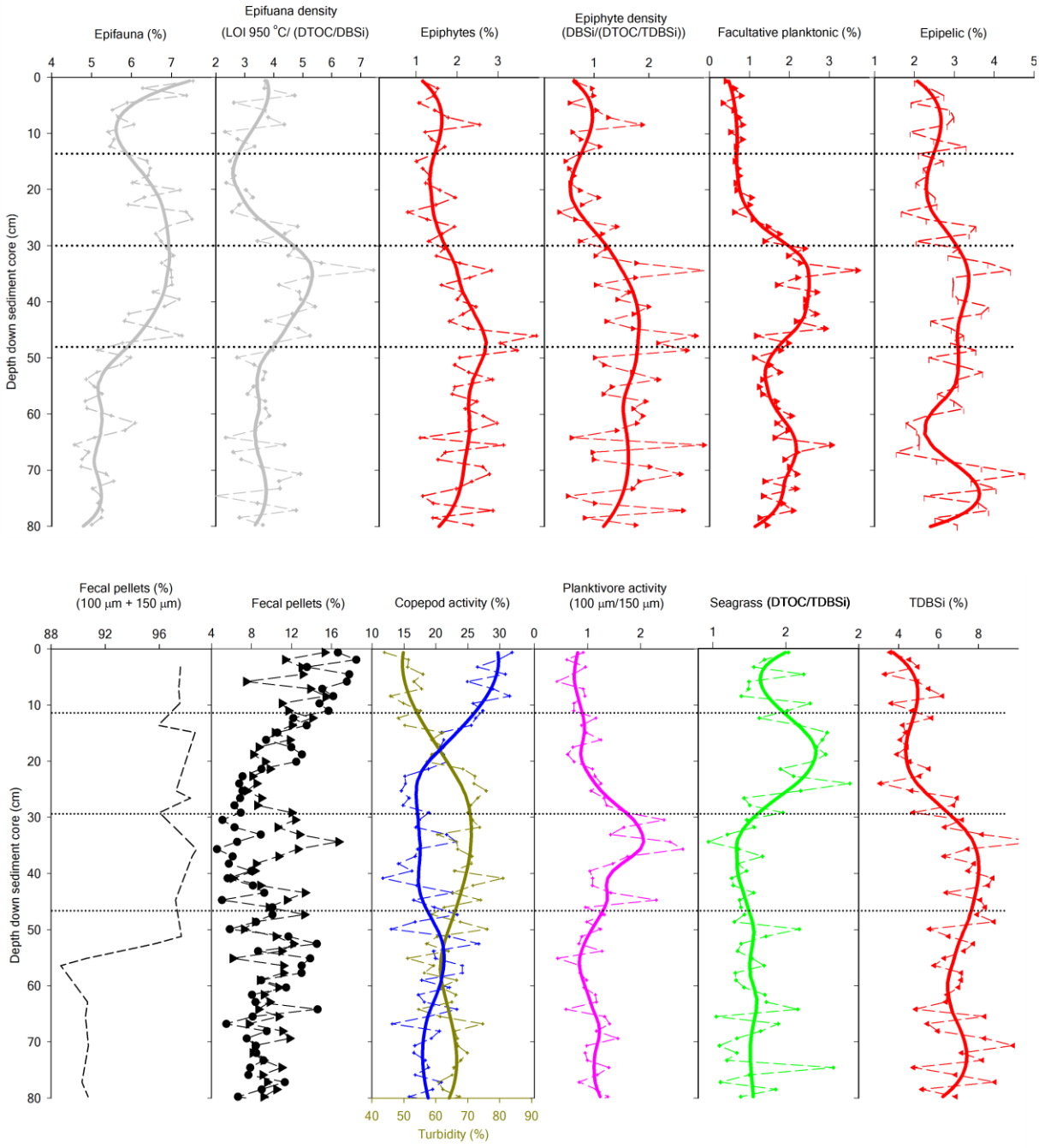

Figure 7.5. Content variance down sediment core LSPMB106 from the Lower Middle Basin of the Little Swanport estuary.
►faecal pellets captured on 100 µm sieves, ● faecal pellets on the 150 µm sieve. The dotted lines refer to approximate positions of high and low relative abundance of seagrass and total micro-algae as TDBSi, and the apparent alternating relationships between micro-algal epiphytes and epifauna. The non-linear trend lines were calculated with an optimal β-spline smoothing procedure (see Section 7.2).

Interestingly, the total micro-algal variability adherence to theory (*i.e.* the best inverse relationship to seagrass productivity; see Table 7.1, Figure 7.6a) was the result of a complex

succession between epiphytes and the relative contributions from other diatom habitat forms (see Figure 7.5 [bottom panel]). The epiphytes diverged from a peak in total diatom content during a period of relatively low seagrass content, whereas the remaining habitat forms were synchronous with the seagrass–micro-algal couple, but only as a pair did they represent all of the total micro-algal peaks and troughs. Most of the large-scale variability of the total micro-algal fraction was represented by centric/facultative pelagic forms and the finer scale variability from the epipelics and epiphytes.

Table 7.2. Non-tautological examples of synchronistic Spearman rank (r) correlations between the primary productivity assemblage and the tropic cascade, identified as such from cross correlations with sampling depth (PAST™)

	Total micro-algae (DTBSi)	Facultative and centric micro-algae (%DBSi)	Epipelic micro-algae (%DBSi)	Epiphytic micro-algae (%DBSi)	Epiphytic micro-algal density (%DBSi–Seagrass index)	Epifaunal density (LOI 950 °C–Seagrass index)
Seagrass proxy (DTOC/DTBSi)	-0.88	-0.69	-0.74	-0.81	-0.84	-0.80
			Copepod feeding (faecal pellets)		Sestonic turbidity (<76 μm)	
Planktivorous fish predation			-0.41		0.52	

In contrast, a first impression of the two seagrass leaf epibiont contents, sessile calcareous epifauna and epiphytes, showed little similarity at the whole sediment core scale, despite their high-density correlations to seagrass content (see Table 7.2). However, in terms of effective coverage, the transect study (see Chapter 3) indicated that sessile epifauna, as bryozoans[30], was likely to be a more effective in light attenuation and nitrogen sorption inhibition than micro-algal epiphytes. Nevertheless, both epifaunal and epiphyte densities had strong synchronistic negative correlations between seagrass abundance and their seagrass densities (see Table 7.2).

The inverse relationship between epifaunal density and seagrass abundance cannot distinguish between cause and effect, or as to whether there was a change from effect to cause along the time series. A cursory increasing window examination from the past to the present (see

[30] The occasional remnants of bryozoans down sediment core LSPMB106 were found to survive seagrass on seagrass pieces (>315 μm) in accord with what had been observed from seagrass leaves across the transect.

Section 6.2.5 for further explanation of the construction) indicated a functional regime change transition, which may have some bearing on the driver of seagrass variance. The epifaunal and epiphyte contents were relatively proportional to each other during a period of quite low seagrass content (dotted lines from 13 cm to 30 cm, Figure 7.5). However, during a period of relative high seagrass content (dotted lines from 30 cm and 48 cm, Figure 7.5) the epifaunal and epiphyte content were inversely proportional.

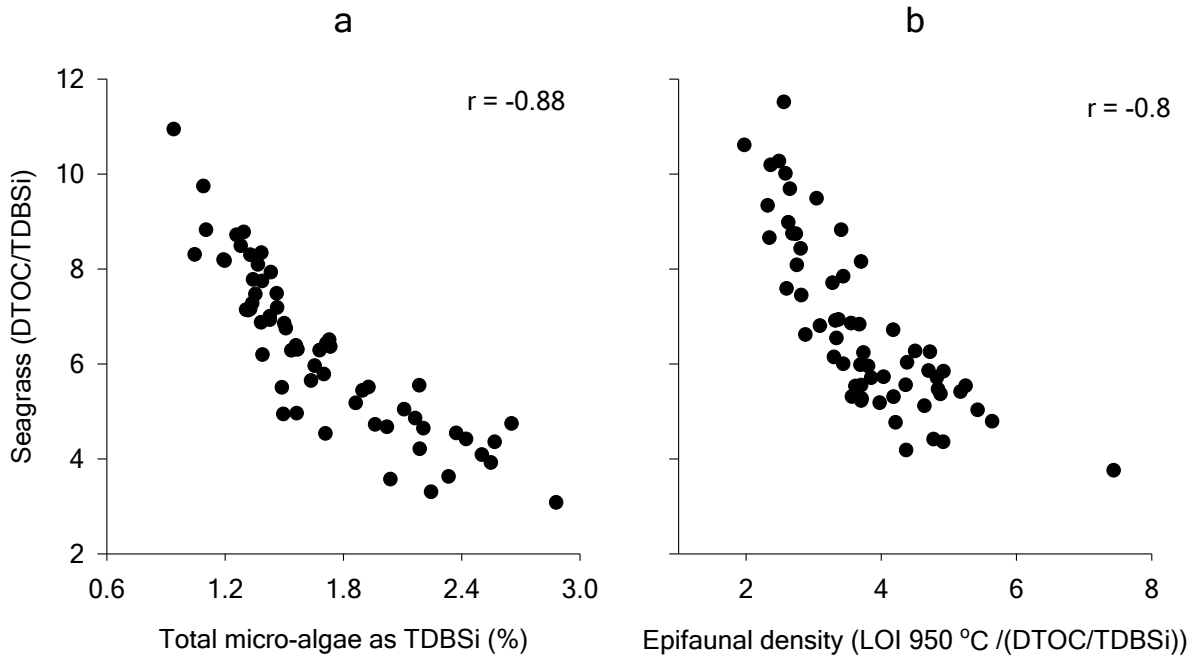

Figure 7.6. Synchronistic correlations between a) the primary productivity assemblage and b) the sessile epifaunal density (b) down sediment core LSPMB106, extracted from the Lower Middle Basin of the Little Swanport estuary.

The timing of the above transition and the nature of the regime change was tested from the dependence of epifaunal density on micro-algal forms and seagrass by stepwise multi-linear regression models. Table 7.3 shows the summary statistics of the two best models that explored the dependency of epifaunal density down the whole core. The models of seagrass and micro-algal habitat forms both rejected epiphytes as an independent variable. It appeared that epiphyte variance was a consequence or epifaunal and seagrass production, rather than the cause.

Table 7.3. Selected summary statistics from backwards stepwise multiple linear regression within sediment core LSPMB106, extracted from the Lower Middle Basin of the Little Swanport estuary.
The first column represents the two independent variables for predicting epifaunal density. In both models epiphyte variance was rejected as a necessary independent variable.

Significant independent variables for epifaunal density	Adjusted r^2	Mean square error
Seagrass and micro-algae bar epiphytes	0.577	13.142
Micro-algae bar epiphytes	0.676	10.726

Both epifaunal density models were independent of epiphyte production, and both had strong correlations (adj. r^2) and similar residual errors in spite of a different set of independent variables (see Table 7.2). The observation that there were two good plausible models that spanned one to two complete cycles of seagrass–micro-algal periodicity suggested an equivalence borne of a switch between seagrass dependence and independence distributed over half of the time series.

Indeed, a 're-analysis' of the above two models' de-trended depth profiles showed the transition was located half way between maximum and minimum epifaunal density (see Figure 7.7). There was a transition from a 1:1 high correlation below seagrass and epifaunal density mean abundance during the seagrass recovery and subsequent decline by the removal of seagrass growth as an independent variable on epifaunal density. Thus, the temporal unit of seagrass variance (*i.e.* complete description of two functional regimes) was bordered not by maximum and minimum seagrass abundance, but by half the potential maximum seagrass abundance between a decline and recovery phase. During the decline phase, seagrass growth was limited by epifaunal coverage, which was fed from waterborne micro-algae, consistent with significant light attenuation. During a recovery phase, epifaunal density was a consequence of seagrass growth, consistent with nitrogen availability for seagrass meadow growth.

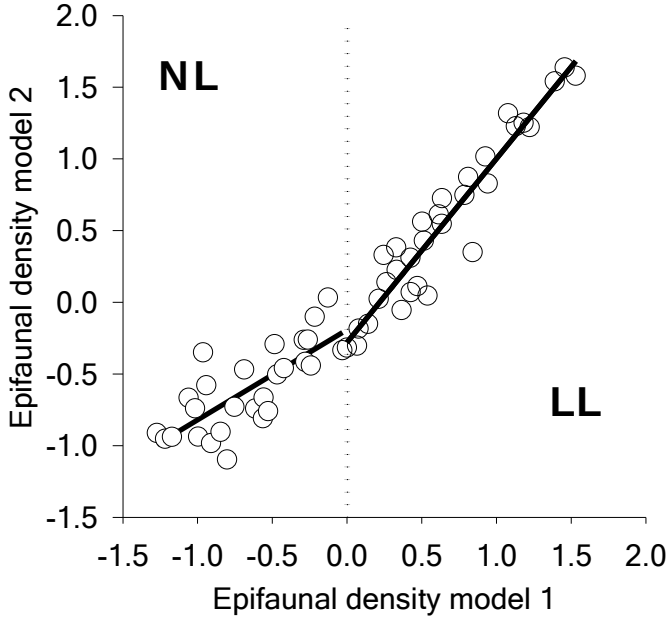

Figure 7.7. Relationship between two stationary model predictions of epifaunal density (see Table 7.3) down the sediment core LSPMB106, extracted from the Lower Middle Basin of the Little Swanport estuary.
LL and NL represent relative states of epifaunal density during potential light limitation and nitrogen limitation, respectively.

7.3.3.1. Trophic cascade variance

The faecal pellet elements of the planktivorous fish trophic cascade (*i.e.* the inferred planktivorous fish predation, copepod faecal pellet egestion and sestonic turbidity; see Chapter 6) were synchronous down the sediment cores (see Figures 7.6) and similar to those found in the Upper Middle Basin of the Little Swanport estuary (see Chapter 6). The inferred planktivorous fish predation proxy was supported by agreement with the observed dominance of the larger copepod *Paracalanus indicus* over the smaller morph form *Arcatia tranteri* (Crawford *et al.*, 2005; Swadling K., 2006, unpublished data, University of Tasmania) over the same period in the core stratigraphy (1999 to 2006).

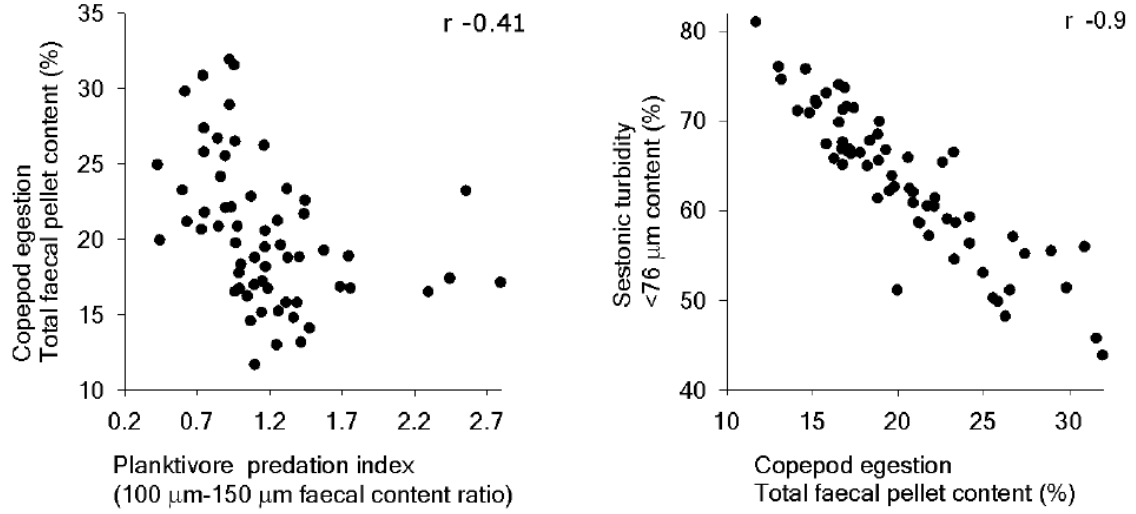

Figure 7.8. Correlations between the elements of a planktivorous fish trophic cascade down the Lower Middle Basin sediment core LSPMB106 within the Little Swanport estuary.
The total faecal pellet content is the combined content of the 150μm and 100μm fractions after they had been corrected for their individual faecal pellet content (see Figure 7.5).

7.3.4. Pattern and process: A neutral model for seagrass ecosystem

The planktivorous fish trophic cascade was not synchronous with the periodicity of the primary productivity assemblage down the sediment core. Cross correlations with depth indicated the average depth lag of 10.2 cm produced the maximum correlation within a variable sedimentation velocity. Figure 7.9 shows the results of the time-series analysis and puts the planktivorous fish predation lag with the seagrass–micro-algal abundance, as approximated by a simple sine wave model, as an average of 13 years. Further, the planktivorous fish trophic cascade had a similar long-term inter-decadal temporal variance as the seagrass–micro-algal abundance, consistent with the hypothesis of a global connection between individual patch ecologies.

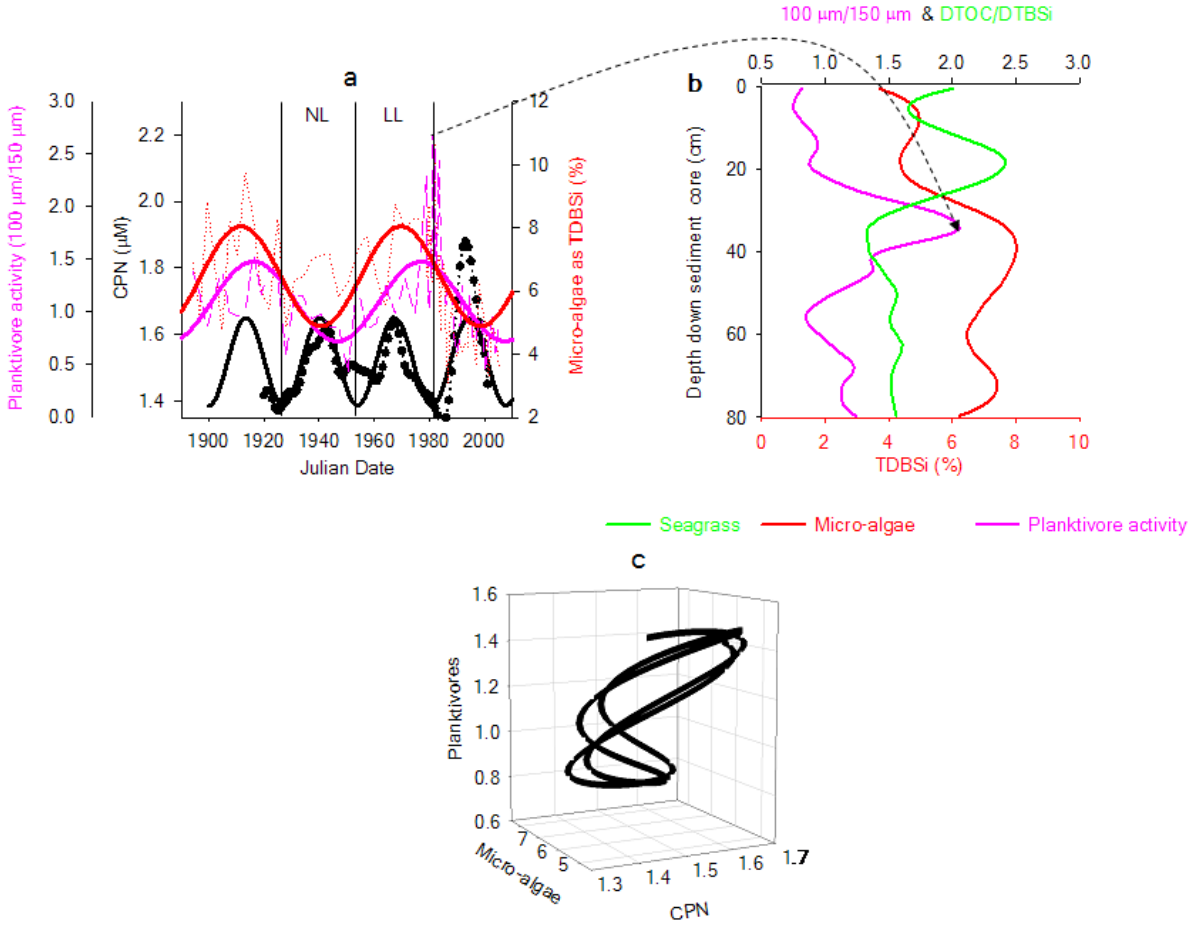

Figure 7.9. Time series models and stratigraphy of ecosystem periodicity as resented by proxies of planktivorous fish, micro-algae and the availability of inorganic nitrogen down the Lower Middle Basin sediment core LSPMB106.
(a) Shows the ecosystem components fitted to a floating sine wave model, evaluated by a Fourier analysis of its major periodic components (see Section 7.2): (—) the CPN, (—) inferred planktivorous fish predation, (—) total micro-algal content. (b) smoothed (optimal β-spline) biome components of the primary productivity assemblage and the planktivorous fish predation down the sediment core: (—) seagrass content, (—) inferred planktivorous fish predation, (—) total micro-algal content. (c) three ecosystem variables that determine the state of the ecology: elements of the planktivorous fish trophic cascade, inorganic nitrogen availability as the CPN and representative of the micro-algal–seagrass couple as its 3-D attractor in phase space. Note the timing of the largest peak in inferred planktivorous fish predation is referenced to its position down the sediment core by the dotted line (---).

The time-series sine wave models gave further support for the contention that the broad-scale variance of the seagrass–micro-algal couple alternated between seagrass meadow growth limited by CPN (*i.e.* a proportional relationship with seagrass) and one controlled by net micro-algal nitrogen eutrophication as food for epifaunal production (*i.e.* a positive relationship with micro-algae; DBSi). Because the regime transition occurred at around half the maximum seagrass–micro-algal abundance during recovery and decline, the pattern of response resulted in a CPN variance that was synchronous with the primary productivity assemblage peaks and troughs, but at twice frequency (27 years *c.f.* 57 years; see Figure 7.9a). In other words, the regime switch depended not only on a particular dynamic state of the seagrass meadow, but on a historical sequence of its ecosystem and not its absolute

abundance/coverage. It should be noted there was some suggestion of a significant finer scale intra-decadal periodicity for both the seagrass and micro-algae (unpublished analysis) as seen in the residual variability about the sine wave (see Figure 7.9). However, there was sufficient resolution to link their dynamics with the other ecosystem components.

7.3.5. A general theory of seagrass variance

The planktivorous fish trophic cascade lag with the seagrass–micro-algal abundance, as approximated by a simple sine wave model (around 13 year), was synonymous with the globally connected evolving ideal landscape configuration model (see Figure 7.3). Further, the lag in the total edge length and the trophic cascade marked a specific patch ecotone at the time of ecosystem thresholds between seagrass nitrogen and light limitation. In other words, thresholds were synonymous with two ecotones with different combinations of planktivorous fish predation and CPN with the same total seagrass abundance/coverage; that is, (1) a low CPN together with a strong planktivorous fish trophic cascade and a long total edge within a relatively patchy landscape and (2) a low CPN together with a weak planktivorous fish trophic cascade and a short total edge length within a relatively less patchy environment than the previous ecotone.

7.3.5.1. A mechanism of regime stability

Outside the ecotones, it is important to understand the feedbacks that maintain the regime's stability at the landscape scale, should society wish to remediate or maintain coverage under pressure from eutrophication, fishing, introduction or removal of additional trophic levels, direct damage that leads to loss of total coverage and, importantly, changes to the patchiness of the meadow (anchor drag, boat moorings, dredging). Figure 7.10 outlines the details of a proposed mechanism. For brevity, the proportional relationship of the seagrass meadow's configuration to planktivorous fish predation was omitted but assumed. In the construction, care was taken to assure that none of the feedbacks were contradictory. However, the exception was a fall in copepod grazing that offset the fall in available phytoplankton productivity (facultative and obligate phytoplankton) within the light limitation regime (see Figure 7.10A). However, value judgment was required to determine whether (1) the fall in phytoplankton was more than offset by an increase in the supply of epipelics in an increasingly patchy landscape and/or (2) light co-limitation of micro-algae reduced their nitrogen quota at low substrate concentrations and *vice versa* (*e.g.* Philippart and Cadee, 2000).

A light limited regime (see Figure 7.10A) illustrates a reinforcement of water micro-algal variability on nitrogen availability *via* two potential feedbacks: (1) the fall in seagrass coverage by increased epifaunal shading caused by nitrogen stimulation of waterborne micro-algal productivity, reinforced by the supply of obligate epipelics as coverage becomes more patchy; or (2) an increase in the planktivorous fish predation within the patchy landscape, which in turn increases the availability of waterborne micro-algae for epifaunal production by reducing the copepod population. Overall, the effect was to maintain a light limited state by maximising epifaunal coverage.

The nitrogen limited regime (see Figure 7.10B) illustrates how the nitrogen stimulation of seagrass coverage results in a fall in planktivorous fish predation, contingent on the natural evolution of the landscapes total edge length, and how it sets up feedbacks that maintain a low epifaunal production. The fall in planktivorous fish predation results in an increase in copepod feeding, thereby reducing the available micro-algal forms and maintaining epifaunal production at a minimum for efficient nitrogen absorption and seagrass growth. Note that no feedback of seagrass abundance with obligate epipelic re-suspension variance was included. The exclusion was a value judgment, based on parsimony, the relatively high seagrass abundance and large homogenous zones within this state (see Table 7.1). In other words, re-suspension of sediments was mostly invariant with shoot density, as found for other *Zostera* meadows above a certain low shoot density threshold (Ward *et al.*, 1984).

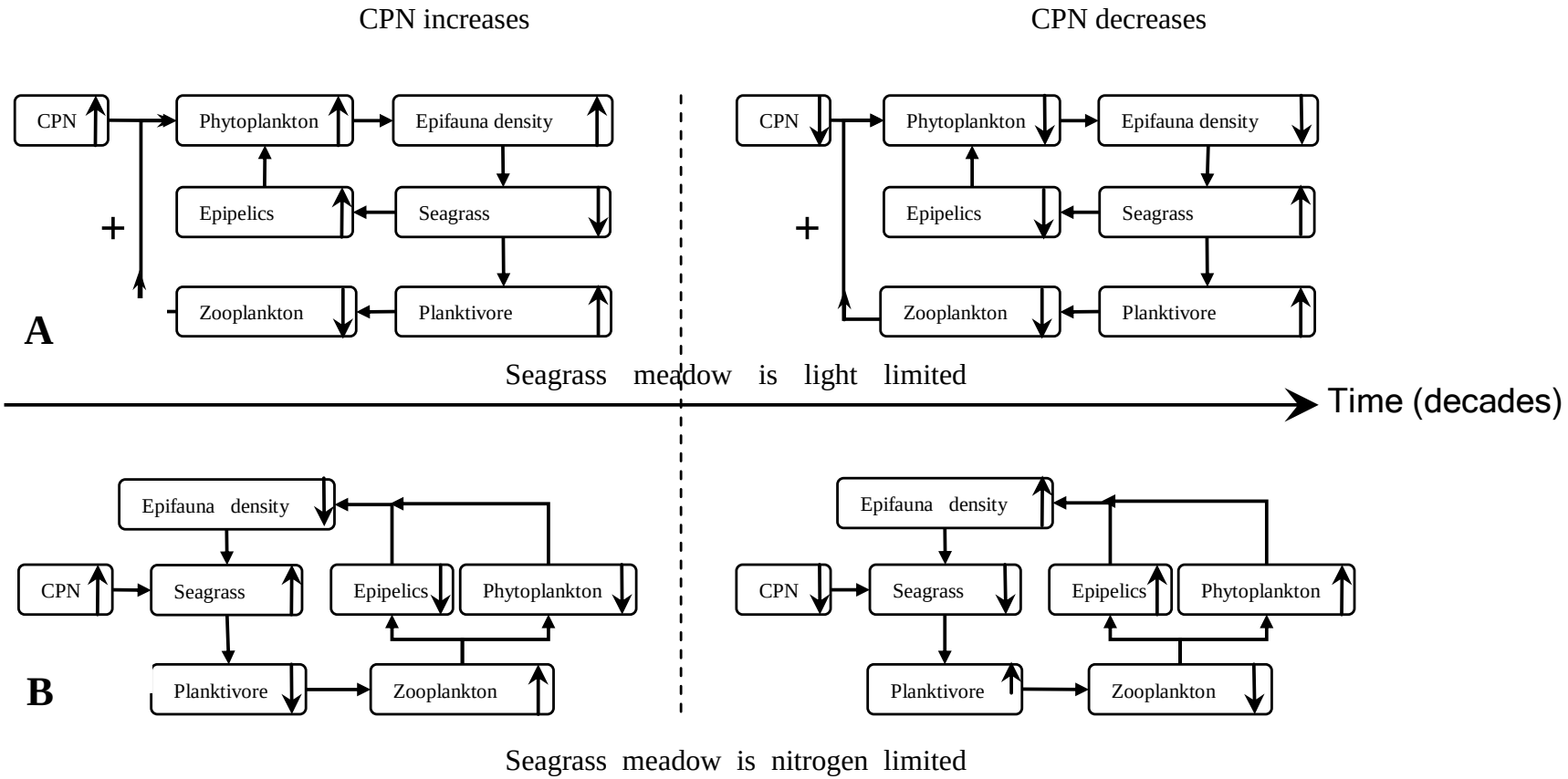

Figure 7.10. Stochastic nitrogen forcing and feedbacks leading to the transfer of nitrogen and light resources between seagrass and total micro-algae within the water column leading to a seagrass light limited growth regime and a nitrogen limited growth regime.
The half arrow in regime B refers to the relative strength of planktivorous fish predation at this time as a consequence of its temporal asymmetry with edge length (see text). Epipelics and phytoplankton refer to micro-algae re-suspended from the sediments and both facultative phytoplanktonic and obligate phytoplanktonic habitat forms, respectively.

7.4. Effects on the ecosystem's pattern and process by the lower estuary's aquaculture

There was no doubt that shellfish aquaculture activities had increased the rate of deep-water sedimentation (see Chapter 4). Indeed, the resultant increase in supply of re-suspended viable or detrital micro-algae might serve to supply food for both oyster production and seagrass epifaunal production. However, this was only one of many possible effects on individual ecosystem components and processes, with others including changes to zooplankton and micro-algal species, rates of sediment denitrification, net basin micro-algal productivity and the removal of nitrogen during harvesting and burial (Dumbauld *et al.*, 2009). Nevertheless, in spite of the above potential effects, the results of the study suggested that aquaculture, at the current intensity, did not appear to effect the sequence of patterns and processes that defined the nitrogen limited seagrass regime state at the time of impact (1986 to 2007). This was a robust conclusion. The assessment was based on a complete cycle of CPN variance, and was consistent with the conclusions of a recent review (Dumbauld *et al.*, 2009) that bivalve aquaculture has not been implicated in shifts to alternate states or reduced adaptive capacity of the larger ecological system by replacing seagrass or degrade water quality.

The Lower Middle Basin ecosystem appeared to have sufficient buffer capacity to moderate epifaunal production. It appeared that there was a proportional response in copepod feeding/production, with similar content within an increasing rate of sediment accretion (see Chapter 4), and a subsequent increase in planktivorous fish predation that locked microbiological organic carbon away from the leaf epifauna. Ironically, the only apparent impact from shellfish aquaculture was postulated as on the Upper Middle Basin, which was not a site of shellfish aquaculture, by moderating its supply of coastal nitrogen resources, contingent on a drought (see Chapter 6).

7.5. Conclusions

A general theory of long-term landscape seagrass variance was developed, expressed as a temporal neutral model of ecosystem patterns and processes within an evolving landscape configuration. It was found that the neutral model's patterns and processes were not interrupted by the presence of the lower estuary's oyster aquaculture, in spite of it contributing the greatest increase in the supply of all destabilising ecosystem components over the last 20 years (*i.e.* the CPN and seston supply; see Chapter 4).

It was postulated that the evolving landscape configuration, with its extent determined by copepod dispersion, was responsible for a threshold change in the strength of a planktivorous fish trophic cascade, which was necessary to maintain one or the other of the seagrass meadow light and nitrogen limited regimes *via* epifaunal production. The patterns were consistent with a weak planktivorous fish trophic cascade, which led to relatively low epifaunal production and nitrogen limitation, and a strong trophic cascade, which led to relatively high epifaunal production and seagrass light limitation. The functional thresholds were marked by ecotones of equivalent moderate seagrass abundance, differentiated by relatively homogenous and patchy meadows at times of low CPN. The result was a long-term seagrass–micro-algal abundance periodicity (57 years) at half the frequency of CPN (27 years), synchronous with the peaks in maximum and minimum seagrass coverage.

The postulated theory for the first time unified the two disparate approaches for predicting and understanding long-term seagrass meadow variance by the inclusion of landscape configuration on a planktivorous fish trophic cascade in determining the switch between two forms of bottom-up control: light limited growth and nitrogen limited growth. Consequently, for a long-term predictive ecology of seagrass meadow variance, the state of the ecosystem along its attractor needs to be identified by considering a significant proportion of its past long-term variance, and that the future changes need to be framed with respect to predictions of decadal long-term nitrogen supply. Further, the study highlighted that any affect to the seagrass ecosystem from the onset of a potential anthropogenic disturbance must assessed on the basis of long term deviations from its biphasic dynamic attractor and not just to changes in the primary productivity assemblage. This can be best achieved from temporal patterns of functionally coupled units (neutral model), that is, planktivorous fish predation, nutrients and the targeted seagrass—micro-algal couple. Alternatively, more accessible proximate covariants with the above variables may be used as proxies in place of more difficult planktivorous fish predation rates, for example, the aerial determination of total edge length of the seagrass meadow, turbidity and copepod abundance.

Chapter 8. Discussion and conclusions

8.1. Chronology

The study has demonstrated the value of applying palaeoecological techniques to a dynamic shallow estuary to better understand long-term variability in the system. Long-term environmental conditions at the landscape scale were reconstructed to test the impacts of shellfish aquaculture on the ecosystem patterns and processes and to postulate the effects of the long-term emergent properties of landscape configuration. Central to the study's success was the development of an accurate geochronology within a non-ideal sedimentological environment using the convergence of event-based dating and a robust ^{210}Pb geochronological model; namely, sediment isotope tomography. In this way, the reconstructed internal dynamics could be untangled from the effects of external nitrogen supply.

8.2. Pattern and process

It was found that shallow bar-built estuaries such as the Little Swanport estuary should be managed with the recognition that the estuary's upper and lower zones have two functionally separate sets of regimes determined by different sets of historical events. Nevertheless, there was strong evidence that persistent decadal regime changes caused by flood events, in the upper estuary, still exhibited the same underlying processes of competing top down and bottom up stabilisation directed towards eventually reaching seagrass stable state. That is, the micro-algal standing crop, fed through the mineralisation of the dead seagrass meadow killed by a previous flood, was ameliorated by weak planktivorous fish predation on copepods, thus maintaining a seagrass dynamic transient state. This state then appeared to be accelerated through a series of punctuated flood induced flushing periods, which led to a stable light limited lush seagrass regime.

The study also highlighted that anthropogenic changes to patterns and processes that operate on decadal scales only became apparent after the seagrass system had been impacted over a similar decadal scale for both dynamic transient states and to changes in the seagrass stable state. That is, in the upper estuary a lush seagrass regime originally supported by external supply of inorganic nitrogen, as the concentration of potential inorganic nitrogen (CPN), appeared to fall into juvenile state maintained by nitrogen fixation, due to a period of drought and the presence of the lower estuary shellfish aquaculture (*i.e.* from the late 1980's to 2007). This was consistent with the moderating effects of lower estuary shellfish aquaculture on the

supply of coastal nitrogen resources to the upper estuary. In other words, anthropogenic impacts were highly dependent on historical contingency, which suggests that Vollenweider predictive models, based on compilation of contemporary responses to nitrogen loading across different shallow estuarine systems (*e.g.* Peters 1991), may not be sufficiently precise or accurate when applied to individual systems.

The importance of historical contingency was further highlighted by the lower estuary ecosystem reconstruction. The evidence was consistent with the lower estuary's stable seagrass state being affected by the asynchronous changes in the strength of the planktivorous fish trophic cascade (13 years) within a periodic naturally evolving seagrass landscape (57 years). This led to a switch from seagrass light limited growth to nitrogen limited growth caused by a long-term coastal nitrogen periodicity at twice the frequency (27 years) of the biome. There was also some evidence to suggest an inter-annual periodicity in the biome. However, the sediment core temporal resolution was insufficient to correlate with other possible inter-annual internal or external forcing factors such as the periodicity of El Niño southern oscillation index or internal factors such as the life history of planktivorous fish that can determine the periodicity of the lower components of the food web (Carpenter and Leavitt, 1991).

Interestingly, it was the position of the shellfish aquaculture relative to coastal waters that determined the its impact only the upper estuary and only during extended periods of drought. Direct effects by the shellfish aquaculture on the lower estuary were not apparent, despite an increase in sestonic sediment accretion consistent with increased aquaculture activity. The cause of this regime stability was not clear from the data; nevertheless, within the framework of the developed general theory, it was postulated to be due to the ability of copepods to maintain a clear water state from either an increase in population or grazing efficiency.

8.3. A general theory of seagrass variance

The temporal patterns and processes associated with the upper estuary and lower estuary were used in conjunction with data from similar systems to develop a testable general theory that; (1) recognises the importance of known biome feedbacks for the persistence of seagrass transient states and (2) the importance of an evolving seagrass landscape configuration on top down control in the switch from the seagrass meadows nitrogen limitation to light limitation In essence, long-term nutrient variance is the driver of change to seagrass meadow abundance that leads to changes in edge length that controls the rate of planktivorous fish predation of

copepods, which in turn controls the amount of seston available for calcareous epifaunal growth. It is the extent of epifaunal growth that determines the availability of light resources over nutrient resources for seagrass production and its response to external nutrient supply (see Figure 8.1).

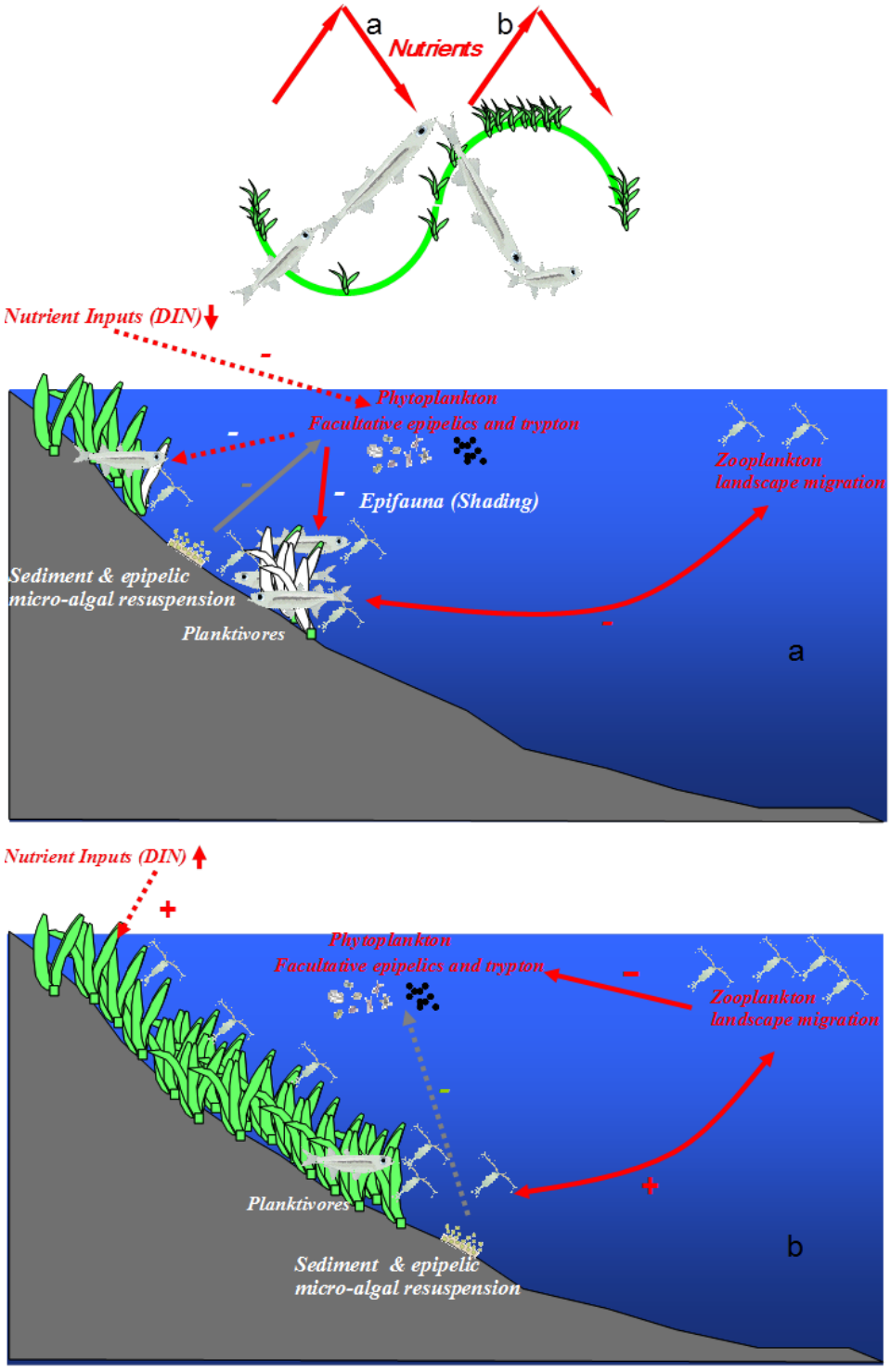

Figure 8.1. A conceptual diagram of the seagrass landscape and its ecosystem elements at the two extreme positions of light and nutrient limited regimes.
(a) The seagrass light limited regime at a minimum seagrass abundance and maximum nitrogen supply; (b) the seagrass nitrogen limited regime at a maximum seagrass abundance and maximum nitrogen supply. The top figure illustrates the ideal temporal unit of ecosystem patterns (*i.e.* the neutral model) in relation to changes in landscape configuration, that is, a homogenous average coverage followed by a patchy sparse coverage, a patchy average coverage and a homogenous maximum coverage).

The type of inter-dependence between bottom up and top down control with respect to an evolving landscape configuration is characteristic of a dynamically stable non-point ecosystem. In other words, its future states are determined largely by its own current state, with little or no reference to outside (*e.g.* disturbance by the shellfish aquaculture). Furthermore, there is anecdotal evidence to suggest that the theory may apply to other types of macrophyte landscapes. McGowan *et al.* (2005) paleo-reconstruction of total planktivorous fish and macrophyte abundance proxies of a number of freshwater lakes showed similar lags as the Little Swanport estuary seagrass meadow, although no explanation was volunteered.

The theory is limited, however, in that is does not include a mechanism by which the landscape configuration changes or the effects of seagrass grazing by animals in non detrital systems. Nevertheless, there was anecdotal evidence from the modelled configuration metrics to suggest that the changes in patch configuration were a naturally evolving process of self-organisation (see Section 7.3.1) and any long-term affects due to animal grazing should be evident from a change in the neutral models ecosystems temporal patterns. Any such affect can then be used as starting point to postulate underlying mechanisms behind grazing, on those patterns and processes.

The study indicates that managers of seagrass meadows should be cogent of coastal climatic periodicities and trends before assigning changes to local anthropogenic impacts (see also Glémarec *et al.*, 1997; Marbà and Duarte, 1997) and cautious of using nitrogen loading as a predictor of a particular stable seagrass or micro-algal regime state or its effect on seagrass meadow dynamics, without *a priori* knowledge of its ecosystem history or the current landscape configuration. For example, in undisturbed systems there is a positive or negative cyclic trajectory in to nitrogen loading on the seagrass meadow, which is dependent on the state of the seagrass meadow's patch configuration (see Figure 8.1). In disturbed systems, however, the biome response (*i.e.* transient and stable regimes) is dependent on its previous state that is determined by its history of nitrogen loading and external perturbations on the biome, from either direct damage by events or estuary use on the seagrass meadow, over fishing of planktivorous fish or the indirect impacts of aquaculture.

The theory also highlights that there may be unexpected consequences to ecosystem services on popular recreational catch by not taking into account seagrass landscape configuration, irrespective of a successful prediction of meadow coverage with external nutrient loading (see Figure 8.1). In other words, a reduction in nitrogen loading can lead to different degrees of

patchiness for the same level of coverage and lead to different levels of fish abundance and diversity. For example, Salita *et al.* (2003) found that there was a difference in dominant fish species but little difference in the total fish abundance between a homogenous and a broken landscape (100 m^2), possibly similar to the light limited ecotone (see Figure 8.1(top) and Table 7.1) comprising of relatively small and numerous patches with a moderate seagrass coverage. Salita *et al.* (2003) and Jelbart *et al.* (2007) also found, however, a landscape with a high seagrass coverage with a few large patches, possibly similar to the nitrogen limited ecotone; (see Figure 8.1 (top) and Table 7.1) contained a significantly smaller fish abundance. Nevertheless, any falls in coverage need to be treated with caution and the total loss may still still overwhelm compensating non-linear responses to fish dynamics, such as the 96 % fall in juvenile cod that led to a loss of about 6 million individuals per year associated with a 60 % fall in seagrass coverage from the Swedish Skagerrak coast (Pihl *et al.*, 2006).

8.4. Future work

The paleo-reconstruction led to the formulation of a testable theory of long-term ecosystem variance for shallow estuaries within a sub-aquatic vegetation regime state. However, to corroborate or falsify a general theory of seagrass variance that involves such long, undisturbed periods over relatively large areas is a formidable task. Nonetheless, the predictions from its postulates can be used to test the underlying structure without the need to follow the full temporal sequence (Ford, 2000). Before such an undertaking, postulates need to be linked within a formally constructed theory that has a name, a narrative, a domain in which the theory sits, a list of the theory's necessary axioms and postulates, and possibly a mechanism. Although, it has been argued that a detailed mechanism is not necessary for a predictive ecology (Peters, 1991), it can conceivably be used to identify possible engineering solutions for management of the biome ecosystem services.

The name. Seagrass landscape theory

The narrative. Biome periodicity is driven by external DIN by stimulating seagrass coverage or inhibiting seagrass coverage due to calcareous epifaunal growth fed by micro-algal productivity at twice the biome frequency but asynchronous with a planktivorous fish trophic to sestonic cascade in proportion to the evolving seagrass meadow's edge length.

The domain. A planktivore-dominated detrital system (*i.e.* no significant loss caused by direct seagrass grazing) and bounded by a continuous regime shift within a single stable state. The system can be considered at equilibrium (dynamically closed), meaning that micro-algal

productivity is mainly autochthonous, planktivorous fish are always at capacity within patches and are not totally reliant on copepod resources. Copepods are, however, significantly affected by planktivorous fish predation. There should be sufficient room for meadow expansion in order to restrict top down and or bottom up parameters changes associated with high shoot densities (see Section 6.3.3.4) and homogenous coverage on fish abundance dynamics (Salita *et al.*, 2003). The temporal unit of the seagrass ecosystem pattern and process is expressed with external DIN forcing as the same scale of the seagrass meadow dynamics. Biome variance is driven by new DIN supply *via* seagrass leaf and micro-algal absorption.

Postulate 1. There is an intrinsic self-organising seagrass landscape configuration over a decline and recovery that is expressed as temporal asymmetry in the total landscape edge area to total landscape coverage.

Postulate 2. Landscape planktivorous fish predation is proportional to total landscape edge length, as planktivorous fish feed from within patches on copepods distributed outside patch perimeters.

Postulate 3. There is an inter-annual synchronous planktivorous fish/copepod/sestonic cascade that integrates local patch ecologies to the whole of the landscape *via* copepod diurnal dispersal and migration between the seagrass littoral zones and the deeper water body. Thus, the extent of copepod dispersal defines the size and shape of the meadow landscape.

Axiom 1. Carbon primary productivity of the biome is always constant and distributed between seagrass and micro-algae by external DIN availability (CPN) as a consequence of different C/N stoichiometry between that of seagrass and micro-algae (Borum and Sand-Jensen, 1996).

Postulate 4. The total net micro-algal productivity's temporal variance is an expression of a succession between epiphytic, epipelic and facultative phytoplanktonic forms.

Postulate 5. Calcareous epifaunal density is dependent on the availability of water borne micro-algae or seagrass growth resulting in seagrass light limitation or nutrient limitation respectively.

Postulate 6. The temporal unit of ecosystem patterns and processes is marked by a relatively low CPN, a moderate seagrass coverage and net micro-algal productivity but with relatively low and high sestonic turbidity, synchronous with planktivorous fish–copepod predation, for seagrass light and nutrient limited growth respectively.

The mechanism. Biome periodicity depends on the existence of both bottom-up (external DIN availability) and top-down control (planktivorous fish–copepod–sestonic cascade), leading to a DIN and light resource transfer between the total micro-algae and seagrass meadow at twice the biome frequency. The transfer is driven by the dynamics of an evolving seagrass meadow configuration at the landscape scale, globally connected by the dispersal of copepods, where intrinsic self-organisation leads to a changing total edge length that determines the strength of top down control over bottom up control.

8.4.1. Testing hypotheses

The most striking change, in both space and time, was the switch of the seagrass to nitrogen fixation, as indicated by the seagrass leaf $\delta^{15}N_{org}$ signature close to 0 ‰. It was suggested that the upper estuary's dependence on nitrogen fixation was due to loss of catchment nitrogen resources during the extended drought and coastal resources moderated by the lower estuary's oyster aquaculture. Indeed, seagrass-mediated nitrogen fixation in the lower estuary to maintain seagrass coverage during low coastal supply was also a necessary construct to explain the determinacy of the long-term pattern and process.

The hypotheses are:

1. During sustained baseline flows over the lifetime of seagrass shoots (70 days), the $\delta^{15}N_{org}$ of seagrass shoots within the upper estuary should become heavier than their presently depleted nitrogen fixation signatures.
2. The seagrass $\delta^{15}N_{org}$ in the upper estuary should be currently lighter than its heavier signature (around +5 ‰) due to the long-term falls in coastal nitrate concentrations over the present El Nino phase, as well as the general trend towards more consistent, warmer and less productive waters of the East Australian Current (Hill *et al.*, 2008).

In addition to the long-term coastal monitoring program east of Maria Island, there is currently an ongoing water quality monitoring program within the Little Swanport estuary. Consequently, a number of hypotheses can be tested, based on the expected changes in water quality, meadow coverage, configuration and the type of functional regime (light or nitrogen limitation). Two of these are: (1) a post-2007 fall in the lower estuary seagrass coverage (light

limiting regime) and total edge length, contingent on an expected increase in coastal annual average nitrate, (2) an increase in the relative abundance of the smaller copepod *Acartia tranteri*, with an increase in water column turbidity caused by an increase in planktivore predation.

Unfortunately, inconsistent water column clarity and the intermittent low frequency of aerial photographs mean a lack of sufficient data to measure patch configuration as it defines the landscape unit (Habeeb *et al.*, 2007), let alone coverage. The use of remote-controlled drones, blimps and kites may provide enough flexibility for sufficient data collection. However, aerial observations need to be regularly validated by measurements on the ground. SeagrassNet is an example of a program designed to involve the local community in monitoring water quality and seagrass coverage to identify long-term trends. It is also conceivable that aerial surveillance can encourage a new level of engagement and interest in those on the ground monitoring activities, as the results become immediately apparent.

8.5. Conclusions

Both landscape spatial and temporal approaches are needed as convergent lines of evidence to evaluate the theory, to identify ecotone regime instability in order to manage a seagrass meadow. This convergence approach has been the central theme of the palaeo-reconstruction, but it can also be a powerful way of managing risk to an ecosystem by increasing confidence when multiple risk assessments based on different lines of evidence yield similar qualitative results (Nagy *et al.*, 2007). In this way changes to Little Swanport estuary's ecology should be based on testing the effects of two separate external forcing factors on the future spatial and temporal patterns and processes from its current regime state: future long-term nitrogen loading from the catchment to the upper estuary, contingent on the continued presence of the lower estuary's shellfish aquaculture; and future long-term nitrogen loading to the lower estuary from coastal waters.

The amount of monitoring data needed to detect changes to the seagrass landscape will require several years of past and future data. Long-term past data are needed to identify the landscape's position on the ecosystem's attractor trajectory and the present functional state of the seagrass (light or nitrogen limited) in relation to previous flood events and anthropogenic stressors (droughts and aquaculture). Several years of annual average coastal and river-flow nitrogen data are also required to identify the direction of the long-term trend from the inter-annual periodicity (*e.g.* for coastal waters around 7 years; see Chapter 4). Moreover, with a

long-term record available for coastal inorganic supply, the main driver of nitrogen variance, the recent developments in time-series analysis used in this study (Singular spectrum analysis of missing data; Golyandina and Osipov, 2007) can potentially be applied to predict several years into the future. This is invaluable, both as part of a long-term adaptive management program for the environment, and for the users of the estuary for the ecosystem services that a seagrass meadow and its evolving landscape coverage and configuration provides.

Appendices

Appendix A. Mineralogical examination of sediment

Little Swanport
An unpublished Mineral Resources Tasmania report

for J B Gallagher

University of Tasmania
MRT Min/Pet Job No. M08/063
5/07/13 [*sic*]

Introduction

Two sediment samples from the above area were submitted for analysis with respect to their mineral content and colour change during heating. Sample details are:

21 (sediment)	21 (heated)
LSP MB2 (sediment)	LSP MB2 (heated)

Results
The samples were examined by X-ray diffraction in the MRT laboratories, MRT.

The raw samples are quite similar mineralogically: mixtures of quartz, halloysite (clay), halite (salt), pyrite and plagioclase, with traces of clinopyroxene and possibly K-feldspar. The major difference between the two samples is that sample 21 (yellow on heating) contains aragonite and sample 2 (red on heating) does not. The aragonite probably represents shell detritus.

The heated samples are complex and difficult to determine fully but both contain plagioclase ($NaAlSi_3O_8$), quartz and clinopyroxene ($(Ca,Na)(Mg,Fe)Si_2O_6$). There is much more pyroxene in sample 21, probably reflecting the calcium content, and this and other unidentified Ca +/- Al silicates are perhaps causing the yellow colour. The red colour is due to hematite (ferric oxide), more prevalent in sample 2.

R.S. Bottrill

Disclaimers

While every care has been taken in the preparation of this report, no warranty is given as to the correctness of the information and no liability is accepted for any statement or opinion or for any error or omission. No reader should act or fail to act on the basis of any material contained herein. Readers should consult professional advisers. As a result the Crown in Right of the State of Tasmania and its employees, contractors and agents expressly disclaim all and any liability (including all liability from or attributable to any negligent or wrongful act or omission) to any persons whatsoever in respect of anything done or omitted to be done by any such person in reliance whether in whole or in part upon any of the material in this report.

This and other data collected in MRT laboratories may enter the MRT databases but every attempt will be made to ensure it remains closed file and not be available externally, unless at your request.

Appendix B. Diatoms species and transfer function for salinity and pH, within Little Swanport estuary for sediment core LSPMB106

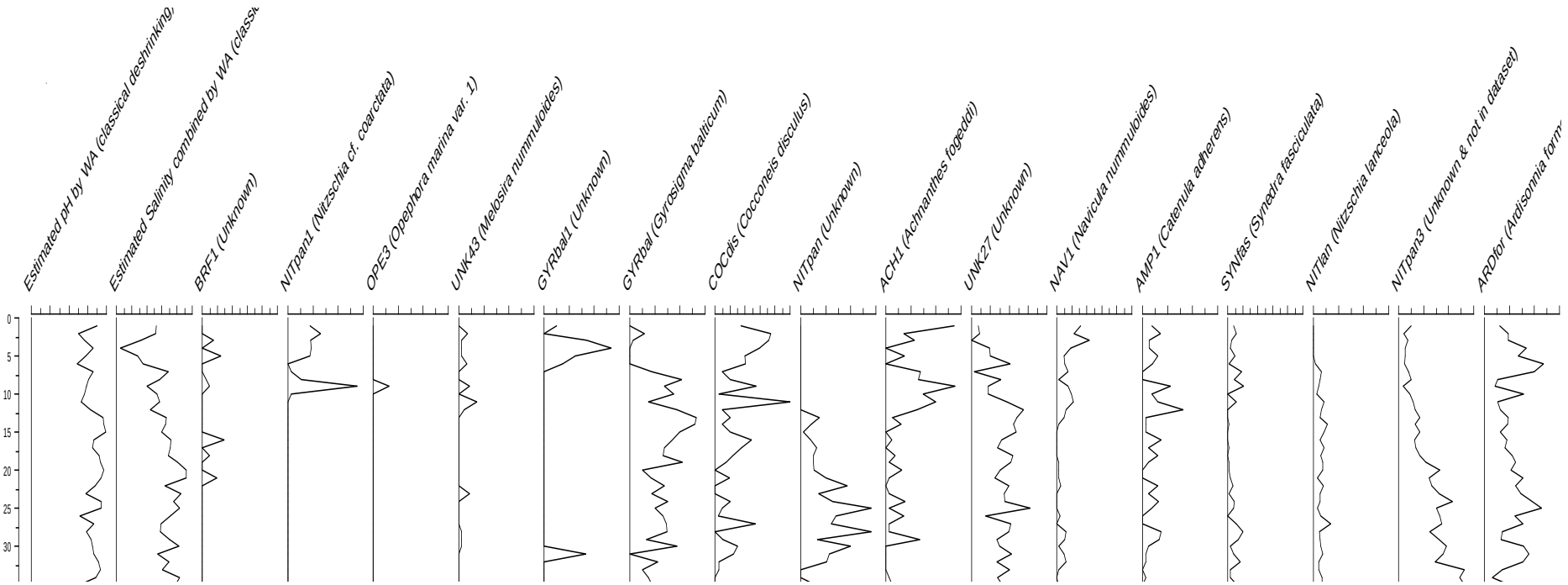

All diatom species found down the Lower Middle Basin sediment core (LSPMB106) of Little Swanport estuary

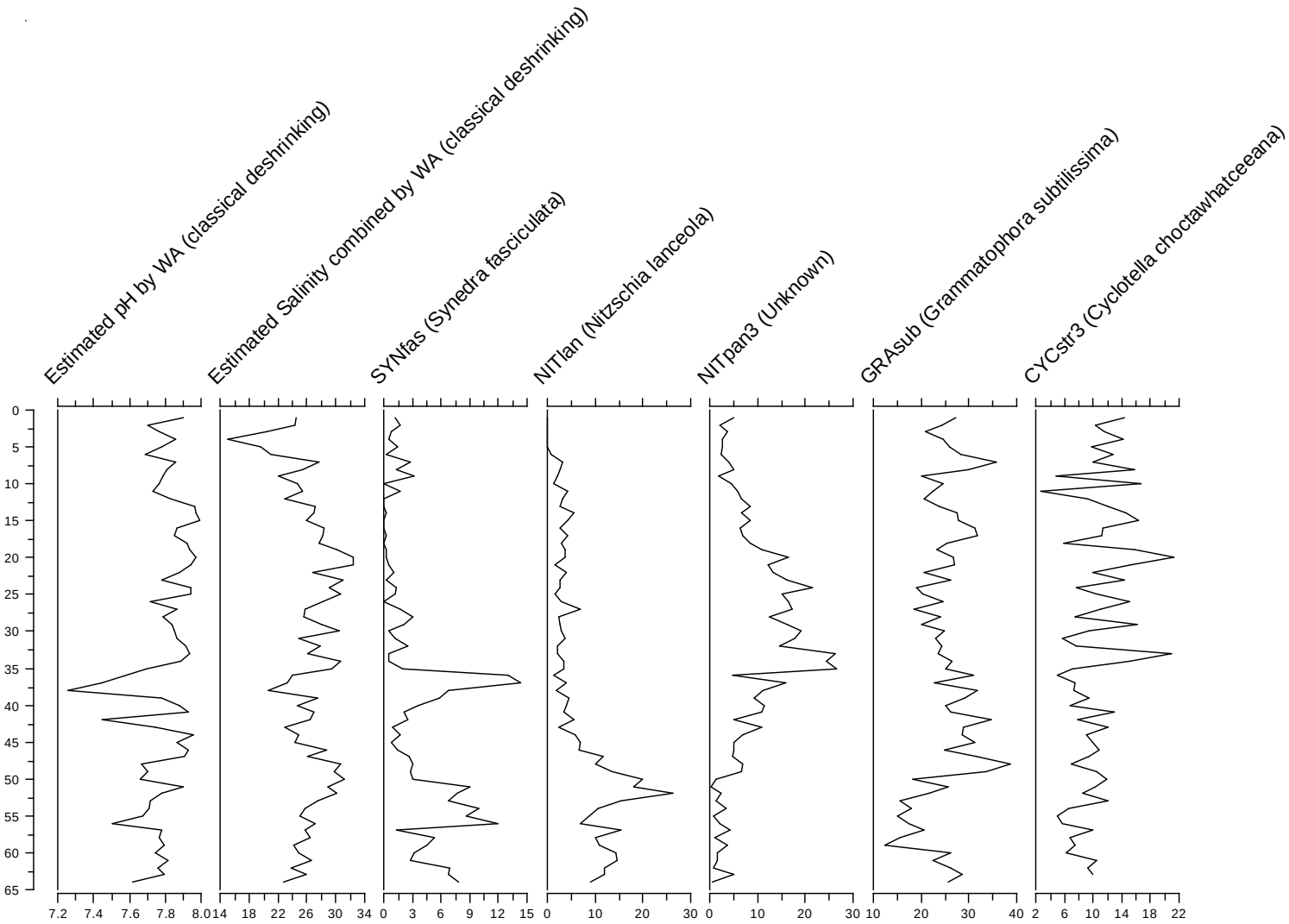

Species occurring ≥ 10 % maximum relative abundance in ≥ 1 sample, down the Lower Middle basin sediment core (LSPMB106) of Little Swanport estuary

References

Abril, J.M., 2004, Constraints on the use of ^{137}Cs as a time-marker to support CRS and SIT chronologies: Environmental Pollution, v. 129, p. 31–37.

Andersen, T., Carstensen, J., Hernandez-Garcia, E., and Duarte, C.M., 2008: Ecological thresholds and regime shifts: Approaches to identification: Trends in Ecology and Evolution, v. 21, p. 49–57.

Adkins, J.F., and Schrag, D.P., 2003, Reconstructing last glacial maximum bottom water salinities from deep-sea sediment pore fluid profiles: Earth and Planetary Science Letters, v. 216, p. 109–123.

Alber, M., and Sheldon, J.E., 1999, Use of a date-specific method to examine variability in the flushing times of Georgia estuaries: Estuarine Coastal and Shelf Science, v. 49, p. 469–482.

Allen, T.F.H., and Hoekstra, T.W., 1990, The confusion between scale-defined levels and conventional levels of organization: Ecology Journal of Vegetation Science, v. 1, p. 5–12.

Almroth, E., Tengberg, A., Andersson, J.H., Pakhomova, S., and Hall, P.O.J., 2009, Effects of resuspension on benthic fluxes of oxygen, nutrients, dissolved inorganic carbon, iron and manganese in the Gulf of Finland, Baltic Sea: Continental Shelf Research, v. 29, p. 807–818.

Appleby, P.G., 2001, Chronostratigraphic techniques in recent sediments, *in* Smol, J.P., and Last, W.M., eds., Tracking environmental change using lakesediments: Dordrecht, Kluwer Academic Publishers, v. 1, p. 171–203.

—, 2008, Three decades of dating recent sediments by fallout radionuclides: A review: Holocene, v. 18, p. 83–93.

Arnaud, F., Lignier, V., Revel, M., Desmet, M., Beck, C., Pourchet, M., Charlet, F., Trentesaux, A., and Tribovillard, N., 2002, Flood and earthquake disturbance of Pb-210 geochronology (Lake Anterne, NW Alps): Terra Nova, v. 14, p. 225–232.

Atkinson, M.J., and Smith, S.V., 1983, C:N:P ratios of benthic marine plants: Limnology and Oceanography, v. 28, p. 568–574.

Baird, M.E., and Middleton, J.H., 2004, On relating physical limits to the carbon: nitrogen ratio of unicellular algae and benthic plants: Journal of Marine Systems, v. 49, p.169–175 .

Bayley, S.E., Creed, I.F., Sass, G.Z., and Wong, A.S., 2007, Frequent regime shifts in trophic states in shallow lakes on the Boreal Plain: Alternative 'unstable' states: Limnoloy and Oceanography, v. 5, p. 202–212.

Bayley, S., Stotts, V.D., Springer, D.F., and Steenis, J., 1978, Changes in subaquatic macrophyte populations at the head of Chesapeake Bay, 1958–1975: Estuaries, v. 1, p 73–84.

Bard, E., Arnold, M., Duprat, J., Moyes, J., and Duplessy, J.C., 1987, Reconstruction of the last deglaciation: Deconvolved records of δ^{18}O profiles, micropalaeontological variations and accelerator mass spectrometric dating ^{14}C: Climate Dynamics, v. 1, p. 101–112.

Beaumont, K.L., Nash, G.V., and Davidson, A.T., 2002, Ultrastructure, morphology and flux of microzooplankton faecal pellets in an east Antarctic fjord: Marine Ecology progress Series, v. 245, p. 133-148.

Benoit, G., and Hemond, H.F., 1990, Po-210 and Pb-210 remobilization from Lake-sediments in relation to iron and manganese cycling: Environmental Science & Technology, v. 24, p. 1224–1234.

Berner, R.A., 1980, Early diagenesis: Princeton, N.J., Princeton University Press, 241 p.

Binford, M.W., 1990, Calculation and uncertainty analysis of ^{210}Pb dates for the PIRLA project lakesediment cores*: Journal of Palaeolimnology, v. 3, p. 253–267.

Boer, W.F., 2007, Seagrass–sediment interactions, positive feedbacks and critical thresholds for occurrence: A review: Hydrobiologia, v. 591, p. 5–24.

Borum, J., and Sand-Jensen, K., 1996, Is total primary production in shallow coastal marine waters stimulated by nitrogen loading?: Oikos, v. 76, p. 406–410.

Boström, C., Jackson, E.L., and Simenstad, C.A., 2006, Seagrass landscapes and their effects on associated fauna: A review: Estuarine, Coastal and Shelf Science, v. 68, p. 383–403.

Boström, C., Pittma, S.J., Simenstad, C., and Kneib, T.R., 2011, Seascape ecology of coastal biogenic habitats: Advances, gaps, and challenges: Marine Ecology-Progress Series, v. 427, p. 191–217.

Box, J.D., 1984, Observations on the use of iron(ii) complexing agents to fractionate the total filterable iron in natural water samples: Water Research, v. 18, p. 397–402.

Bruner, J., 1991, The narrative construction of reality: Critical Inquiry, v. 18, p. 1–21.

Brush, G.S., 1989, Rates and patterns of estuarine sediment accumulation: Limnology and Oceanography, v. 34, p. 1235–1246.

Brzezinski, M.A., 1985, The Si:C:N ratio of marine diatoms: interspecific variability and the effect of some environmental variables: Journal of Phycology, v. 21, p. 347–357.

Burdige, D.J., 2006, Geochemistry of marine sediments: Princeton, Princeton University Press.

Burkhardt, S., Riebesell, U., and Zondervan, I., 1999, Stable carbon isotope fractionation by marine phytoplankton in response to daylength, growth rate, and CO_2 availability: Marine Ecology-Progress Series, v. 184, p. 31–41.

Burkholder, J.M., Tomasko, D.A., and Touchette, B.W., 2007, Seagrasses and eutrophication: Journal of Experimental Marine Biology and Ecology, v. 350, p. 46–72.

Bycroft, M., 2009, Going outside the model: Robustness analysis and experimental science: Spontaneous Generations: A Journal for the History and Philosophy of Science, v. 3, p. 123–141.

Byron, D., and Heck, K., 2006, Hurricane effects on seagrasses along Alabama's Gulf coast: Estuaries and Coasts, v. 29, p. 939–942.

Callender, W.R., Staff, G.M., Parsons-Hubbard, K.M., Powell, E.N., Rowe, G.T., Walker, S.E., Brett, C.E., Raymond, A., Carlson, D.D., White, S., and Heise, E.A., 2002, Taphonomic trends along a forereef slope: Lee Stocking Island, Bahamas. I. Location and water depth: Palaios, v. 17, p. 50–65.

Carcaillet, C., Almquist, H., Asnong, H., Bradshaw, R.H.W., Carrión, J.S., Gaillard, M.J., Gajewski, K., Haas, J.N., Haberle, S.G., Hadorn, P., Müller, S.D., Richard, P.J.H., Richoz, I., Rösch, M., Sánchez Goñi, M.F., von Stedingk, H., Stevenson, A.C., Talon, B., Tardy, C., Tinner, W., Tryterud, E., Wick, L., and Willis, K.J., 2002, Holocene biomass burning and global dynamics of the carbon cycle: Chemosphere, v. 49, p. 845–863.

Carey, L., Alexandre, A., Meunier, J.D., Boeglin, J.L., and Braun, J.J., 2005, Contribution of phytoliths to the suspended load of biogenic silica in the Nyong basin rivers (Cameroon): Biogeochemistry, v. 74, p. 101–114.

Carpenter, S.R, and Kitchell, J.F., 1988, Consumer control of lake productivity: Bioscience, v. 38, p. 764–769.

Carpenter, S.R., and Leavitt, P.R., 1991, Temporal variation in a palaeolimnological record arising from a trophic cascade: Ecology, v. 72, p. 277–285.

Carroll, J.L, Lerche, I., Abraham, J.D., and Cisar, D.J., 1999a, Sediment ages and flux variations from depth profiles of Pb-210: Lake and marine examples: Applied Radiation and Isotopes, v. 50, p. 793–804.

Carroll, J.L., and Lerche, I., 2003, Sedimentary processes: Quantification using radionuclides: Oxford, Elsevier.

Carroll, J.L., Lerche, I., Abraham, J.D., and Cisar, D.J., 1995, Model-determined sediment ages from Pb-210 profiles in un-mixed sediments: Nuclear Geophysics, v. 9, p. 553–565.

Carroll, J.L, Williamson, M., Lerche, I., Karabanov, E., and Williams, D.F., 1999b, Geochronology of Lake Baikal from Pb-210 and Cs-137 radioisotopes: Applied Radiation and Isotopes, v. 50, p. 1105–1119.

Carslow, H.S., and Jaeger, J.C., 1959, Conduction of heat in solids: Oxford University Press.

Caswell, H., 1976, Community structure: A neutral model analysis: Ecological Monographs, v. 46, p. 327–354.

CBD, 1998, Ecosystem approach: www.cbd.int/ecosystem/ (accessed June 2011).

Chanton, J.P., Martens, C.S., and Kipphut, G.W., 1983, Pb-210 sediment geochronology in a changing coastal environment: Geochimica et Cosmochimica Acta, v. 47, p. 1791–1804.

Chen, Y.C., and Windom, H.L., 1997, Sediment manganese and biogenic silica as geochemical indicators in estuarine salt marshes of coastal Georgia, USA: Environmental Geochemistry and Health, v. 19, p. 29–38.

Childers, D.L., Sklar, F.H., and Hutchinson, S.E., 1994, Statistical treatment and comparative analysis of scale-dependent aquatic transect data in estuarine landscapes: Landscape Ecology, v. 9, p. 127–141.

Cloern, J.E., Canuel, E.A., and Harris, D., 2002, Stable carbon and nitrogen isotope composition of aquatic and terrestrial plants of the San Francisco Bay estuarine system: Limnology and Oceanography, v. 47, p. 713–729.

Cloern, J.E., Jassby, A.D., Thompson, J.K., and Hieb, K.A., 2007, A cold phase of the east Pacific triggers new phytoplankton blooms in San Francisco Bay: Proceedings of the National Academy of Sciences of the United States of America, v. 104, p. 18561–18565.

Conley, D.J., 1988, Biogenic silica as an estimate of siliceous microfossil abundance in Great-Lakes sediments: Biogeochemistry, v. 6, p. 161–179.

Conley, D.J., and Schelske, C.L., 1993, Potential role of sponge spicules in influencing the silicon biogeochemistry of Florida lakes: Canadian Journal of Fisheries and Aquatic Science, v. 50, p. 296–302.

Connolly, R.M., and Hindell, J.S., 2006, Review of nekton patterns and ecological processes in seagrass landscapes: Estuarine, Coastal and Shelf Science, v. 68, p. 433–444.

Cooper, J.A.G., 2002, The role of extreme floods in estuary-coastal behaviour: Contrasts between river- and tide-dominated microtidal estuaries: Sedimentary Geology, v. 150, p. 123–137.

Cooper, S.R., McGlothlin, K.S., Madritch, M., and Jones, D.L., 2004, Palaeoecological evidence of human impacts on the Neuse and Pamlico Estuaries of North Carolina, USA: Estuaries, v. 27, p. 617–633.

Costanza, R., d'Arge, R., De Groot, R., Fraber, S., Grasso, M.,Hannon, B., Limburg, K., Naeem, S., O'Neill, R.V., Paruelo, J.,Raskin, R.G., Sutton, P., and Van den Belt, M., 1997, The value of the world's ecosystem services and natural capital: Nature, v. 387, p. 253–60.

Costanza, R., and Mageau, M., 1999, What is a healthy ecosystem?: Aquatic Ecology, v. 33, p. 105–115.

Costanza, R., Fisher, B., Mulder, K., Liu, S., and Treg, C., 2007, Biodiversity and ecosystem services: A multi-scale empirical study of the relationship between species richness and net primary production: Ecological Economics, v. 61, p. 478-491.

Coull, B.C., 1985, The use of long-term biological data to generate testable hypotheses: Estuaries, v. 8, p. 84–92.

Crawford, C., Neira, F.J., and White, C.A., 2005, Environmental flows in the Little Swanport estuary: Tasmanian Aquaculture and Fisheries Insitute, University of Tasmania.

Crawford, C., and Mitchell, I., 1999, Physical and chemical parameters of several oyster growing areas in Tasmania: Tech report series 155m 1441-8487, Tasmanian Aquaculture and Fisheries Insitute, University of Tasmania.

Cromer, L., Gibson, J.A.E., Swadling, K.M., and Ritz, D.A., 2005, Faunal microfossils: Indicators of Holocene ecological change in a saline Antarctic Lake: Palaeogeography, Palaeoclimatology, Palaeoecology, v. 221, p. 83–97.

Cunha, A.H., Santos, R.P., Gaspar, A.P., and Bairros, M.F., 2005, Seagrass landscape-scale changes in response to disturbance created by the dynamics of barrier-Islands: A case study from Ria Formosa (southern Portugal): Estuarine Coastal and Shelf Science, v. 64, p. 636–644.

Dakos, V., van Nes, E.H., Donangelo, R., Fort, H., and Scheffer, M., 2010, Spatial correlation as leading indicator of catastrophic shifts: Theoretical Ecology, v. 3, p. 163–174.

Davison, W., and Heaney, S.I., 1978, Ferrous iron-sulfide interactions in anoxic hypolimnetic waters: Limnology and Oceanography, v. 23, p. 1194–1200.

Davidson, T.A., Sayer, C.D., Bennion, H., David, C., Rose, N., and Wade, M.P., 1995, A 250 year comparison of historical, macrofossil and pollen records of aquatic plants in a shallow lake: Freshwater Biology, v. 50, p. 1671–1686.

Dawson, A.G., and Shi, S.Z., 2000, Tsunami deposits: Pure and Applied Geophysics, v. 157, p. 875–897.

Dean, J.M., Kemp, A.E.S., and Pearce, R.B., 2001, Palaeo-flux records from electron microscope studies of Holocene laminated sediments, saanich Inlet, British Columbia: Marine Geology, v. 174, p. 139–158.

Dieckmann, U., Law, R., and Metz, J.A.J., editors, 2000, The geometry of ecological interactions, Cambridge University Press.

Deevy, E.S., 1969, Coaxing history to conduct experiments: Bioscience, v. 19, p. 40–43.

DeMaster, D.J., 1981, The supply and accumulation of silica in the marine-environment: Geochimica Et Cosmochimica Acta, v. 45, p. 1715–1732.

Dent, S.R., and Uhen, M.D., 1993, Tidal reorientation and transport of recent bivalves on a temperate tidal flat, north western United-States: Palaios, v. 8, p. 244–249.

Dettmann, E.H., 2001, Effect of water residence time on annual export and denitrification of nitrogen in estuaries: A model analysis: Estuaries, v. 24, p. 481–490.

Dominey-Howes, D., 2007, Geological and historical records of tsunami in Australia: Marine Geology, v. 239, p. 99–123.

Donato, S.V., Reinhardt, E.G., Boyce, J.I., Pilarczyk, J.E., and Jupp, B.P., 2009, Particle-size distribution of inferred tsunami deposits in Sur Lagoon, Sultanate of Oman: Marine Geology, v. 257, p. 54–64.

Donato, S.V., Reinhardt, E.G., Boyce, J.I., Rothaus, R., and Vosmer, T., 2008, Identifying tsunami deposits using bivalve shell taphonomy: Geology, v. 36, p. 199–202.

Douglass, J.G., France, K.E., Richardson, J.P. and Duffy, J.E., 2010, Seasonal and interannual change in a Chesapeake Bay eelgrass comminity: Insight into biotic and abiotic control of community structure.

DPIW, 1998, Great Oyster Bay and mercury passage marine farming development plan: www.dpiw.tas.gov.au.

DPIPWE, 2006, Water quality—lower catchment and coastal catchments: www.dpipwe.tas.gov.au/.../SwanportSOR_Chpt4c_Lwr%20catchment.pdf.

Drexler, T.M., and Nittrouer, C.A., 2008, Stratigraphic signatures due to flood deposition near the rhone river: Gulf of Lions, northwest Mediterranean Sea: Continental Shelf Research, v. 28, p. 1877–1894.

Duarte, C.M., 1990, Seagrass nutrient content: Marine Ecology-Progress Series, v. 67, p. 201–207.

—, 1992, Nutrient concentration of aquatic plants—Patterns across species: Limnology and Oceanography, v. 37, p. 882–889.

—, 1995, Submerged aquatic vegetation in relation to different nutrient regimes: Ophelia, v. 41, p. 87–112.

Duarte, C.M., Fourqurean, J.W., Kruase-Jensen, D., and Olesen, B., 2006, Dynamics of seagrass stability and change: *in* Larkum, W.D., ed., Seagrasses: Biology, Ecology and Conservation, p. 271–294.

Dumbauld, B.R, Ruesink, J.L., and Rumrill, S.S., 2009, The ecological role of bivalve shellfish aquaculture in the estuarine environment: A review with application to oyster and clam culture in West Coast (USA) estuaries: Aquaculture, p. 196–223.

Duncan, S.L., McComb, B.C., and Johnson, K.N., 2010, Integrating ecological and social ranges of variability in conservation of biodiversity: Past, present, and future: Ecology and Society, v. 15, 5. [online] www.ecologyandsociety.org/vol5/iss5/.

Dyer, K.R., 1973, Estuaries: A physical introduction: New York, John Wiley and Sons.

Elwany, M.H.S., Flick, R.E., and Aijaz, S., 1998, Opening and closure of a marginal southern California lagoon inlet: Estuaries, v. 21, p. 246–254.

Engstrom, D.R., and Wright, H.E., 1984, Chemical stratigraphy of lake sediments as a record of environmental change, *in* Haworth, E.Y., and Lund, J.W.G., eds., Lake sediments and environmental history: Studies in palaeolimnology and palaeoecology in honour of Winifred Tutin: Leicester, Leicester University Press.

Enrıquez, S., Merino, M., Iglesias-Prieto, R., 2002, Variations in the photosynthetic performance along the leaves of the tropical seagrass Thalassia testudinum: Marine Biology, v. 140, p. 891–900.

Evans, K., Thresher, R., Warneke, R.M., Bradshaw, C.J.A., Pook, M., Thiele, D., and Hindell, M.A., 2005, Periodic variability in cetacean strandings: Links to large-scale climate events: Biology Letters, v. 1, p. 147–150.

Eyre, B., and Twigg, C., 1997, Nutrient behaviour during post-flood recovery of the Richmond river estuary northern NSW, Australia: Estuarine Coastal and Shelf Science, v. 44, p. 311–326.

Fagerström, T., 1987, On theory, data and mathematics in ecology: Oikos, v. 50, p. 258–261.

Ferreira, J.G., Wolff, W.J., Simas, T.C., and Bricker, S.B., 2005, Does biodiversity of estuarine phytoplankton depend on hydrology?: Ecological Modelling, v. 187, p. 513–523.

Fonseca, M.S., and Bell, S.S., 1998, Influence of physical setting on seagrass landscapes near Beaufort, North Carolina, USA: Marine Ecology-Progress Series, v. 171, p. 109–121.

Fonseca, M.S., Whitfield, P.E., Kelly, N.M., and Bell, S.S., 2002,Modeling seagrass landscape pattern and associated ecological attributes: Ecological Applications, v. 12, p. 218–237.

Ford, E.D., 2000, Scientific methods for ecological research: Cambridge, UK, Cambridge University Press.

Fortin, M.J., Boots, B., Csillag, F., and Remmel, T.K., 2003, On the role of spatial stochastic models in understanding landscape indices in ecology: Oikos, v. 102, p. 203–212.

Foster, I.D.L., Mighall, T.M., Proffitt, H., Walling, D.E., and Owens, P.N., 2006, Post-depositional Cs-137 mobility in the sediments of three shallow coastal lagoons, SW England: Journal of Palaeolimnology, v. 35, p. 881–895.

Fourqurean, J.W., and Schrlau, J.E., 2003, Changes in nutrient content and stable isotope ratios of C and N during decomposition of seagrasses and mangrove leaves along a nutrient availability gradient in Florida Bay, USA: Abingdon, Taylor & Francis, 18 p.

Fourqurean, J.W., and Zieman, J.C., 2002, N:P study of Florida bay nutrient content of the seagrass Thalassia testudinum reveals regional patterns of relative availability of nitrogen and phosphorus in the Florida Keys USA: Biogeochemistry, v. 61, p. 229–245.

Francois R., Altabet, M.A., Yu, E.-F., Sigman, D.M., Bacon, M.P., Frank M., Bohrmann G., Bareille G., and Labeyrie, L.D., 1997, Contribution of Southern Ocean surface-water

stratification to low atmospheric CO2 concentrations during the last glacial period: Nature, v. 389, p. 929–935.

Frankovich, T.A., and Fourqurean, J.W., 1997, Seagrass epiphyte loads along a nutrient availability gradient, Florida Bay, USA: Marine Ecology-Progress Series, v. 159, p. 37–50.

Franks, S.W., 2002, Identification of a change in climate state using regional flood data: Hydrology and Earth System Sciences, v. 6, p. 11–16.

Franks, S.W., and Kuczera, G., 2002, Flood frequency analysis: Evidence and implications of secular climate variability, New South Wales: Water Resources Research, v. 38, p. 1062.

Frederiksen, M., Krause-Jensen, D., Holmer, M., and Laursen, J.S., 2004a, Long-term changes in area distribution of eelgrass (Zostera marina) in Danish coastal waters: Aquatic Botany, v. 78, p. 167–181.

—, 2004b, Spatial and temporal variation in eelgrass (Zostera marina) landscapes: Influence of physical setting: Aquatic Botany, v. 78, p. 147–165.

Fry, B., 2006, Stable isotope ecology: New York, Springer.

Fry, B., Bern, A.L., Ross, M.S., and Meeder, J.F., 2000, Studies of $\delta^{15}N$ use by the red mangrove, Rhizophora mangle in South Florida: Estuarine, Coastal and Shelf Science, v. 50, p. 291–296.

Fulton, R.S III, 1984, Distribution and community structure of estuarine copepods: Estuaries, v. 7, p. 38-50.

Galman, V., Rydberg, J., and Bigler, C., 2009, Decadal diagenetic effects on delta $\delta^{13}C$ and $\delta^{15}N$ studied in varved lake sediment: Limnology and Oceanography, v. 54, p. 917–924.

Garces, B.L.V., Moreno, A., Navas, A., Mata, P., Machin, J., Huertas, A.D., Samperiz, P.G., Schwalb, A., Morellon, M., Cheng, H., and Edwards, R.L., 2008, The Taravilla lake and tufa deposits (central Iberian Range, Spain) as palaeohydrological and palaeoclimatic indicators: Palaeogeography, Palaeoclimatology, Palaeoecology, v. 259, p. 136–156.

Gardner, L.R., and Bohn, M., 1980, Geomorphic and hydraulic evolution of tidal creeks on a subsiding beach ridge plain, North-Inlet, sc: Marine Geology, v. 34, p. M91–M97.

Gardner, R.H., Mime, B.T., Turner, M.G., and O'Neil, R.V., 1987, Neutral models for the analysis of broad-scale landscape pattern: Landscape Ecology, v. 1, p. 19–28.

Giese, G.S., 1988., Cyclical behavior of the tidal inlet at Nauset Beach, Chatham, Massachusetts, *in* Aubrey, D.G., Weishar, J., eds., Hydrodynamics and sediment dynamics of tidal inlets: New York, Springer Verlag, p. 26–283.

Gilbert, R., Crookshanks, S., Hodder, K.R., Spagno, J., and Stull, R.B., 2006, The record of an extreme flood in the sediments of Montane Lillooet Lake British Columbia: Implications for palaeoenvironmental assessment: Journal of Palaeolimnology, v. 35, p. 737–745.

Glémarec, M., Le Faou, Y., and François, C.U.Q., 1997, Long-term changes of seagrass beds in Glenan Archipeligo (South Britanny): Oceanologica Acta, v. 20, p. 217-227.

Greenwood, J.E., Truesdale, V.W., and Rendell, A.R., 2005, Toward an understanding of biogenic-silica dissolution in seawater: An initial rate approach applied between 40 and 90°C: Aquatic Geochemistry, v. 1, p. 1–20.

Gunderson L., and Holling C., editors, 2002. Panarchy: Understanding transformations in human and natural systems: Washington (DC), Island Press.

Gibson, J.A.E., 1994, Kinetics of silicon and aluminum release from soils during extraction with 0.01m calcium-chloride: Communications in Soil Science and Plant Analysis, v. 25, p. 3393–3403.

Goff, J., McFadgen, B.G., and Chague-Goff, C., 2004, Sedimentary differences between the 2002 easter storm and the 15th-century Okoropunga tsunami, southeastern North Island, New Zealand: Marine Geology, v. 204, p. 235–250.

Golyandina, N., and Osipov, E., 2007, The 'Caterpillar'-SSA method for analysis of time series with missing values: Kidlington, Royaume-Uni, Elsevier, 12 p.

Gonneea, M.E., Paytan, A., and Herrera-Silveira, J.A., 2004, Tracing organic matter sources and carbon burial in mangrove sediments over the past 160 years: Estuarine Coastal and Shelf Science, v. 61, p. 211–227.

Gouhier, T., and Guichard, F., 2007, Local disturbance cycles and the maintenance of heterogeneity across scales in marine metapopulations: Ecology, v. 88, p. 647–657.

Graf, W.L., 2003, Dam removal research: Status and prospects: Washington, The John Heinz Center for Science, Economics and the Environment.

Green, M.A., and Aller, R.C., 2001, Early diagenesis of calcium carbonate in Long Island sound sediments: Benthic fluxes of Ca^{2+} and minor elements during seasonal periods of net dissolution: Journal of Marine Research, v. 59, p. 769–794.

Greig-Smith, P.,1979, Pattern in vegetation: Journal of Ecology, v.67, p. 755-779.

Groffman, P.M., Baron, J.S., and others, 2006, Ecological thresholds: The key to successful environmental management or an important concept with no practical application?: Ecosystems, v. 9, p. 1–13.

Guinasso, N.L., and Schink, D.R., 1975, Quantitative estimates of biological mixing rates in abyssal sediments: Journal of Geophysical Research-Oceans and Atmospheres, v. 80, p. 3032–3043.

Habeeb, R.L., Johnson, C.R., Wotherspoon, S., and Mumby, P., 2007, Optimal scales to observe habitat dynamics: A coral reef example: Ecological Applications, v. 17, p. 641–647.

Haberyan, K.A., 1985, The role of copepod faecal pellets in the deposition of diatoms in Lake Tanganyika: Limnology and Oceanography, v. 30, p. 1010–1023.

Hancock, G., Edgington, D.N., Robbins, J.A., Smith, J.N., Brunskil, G.L., and Pfitzner, J., 2000, Workshop on radiological techniques in sedimentation studies: Methods and applications, *in* Fernandez, J.M., and Fichez, R., eds., Environmental changes and radioactive tracers: Paris, SPERA, IRD.

Hancock, J.G., Olley, J.M., and Wallbrink, P.J., 2001, Sediment transport and accumulation in Western Port, report on phase 1 of a study determining the sources of sediment to Western Port: Canberra, CSIRO Land and Water, Environment Hydrology.

Harris, G., Nilsson, C., Clementson, L., and Thomas, D., 1987, The water masses of the east-coast of Tasmania—Seasonal and interannual variability and the influence on phytoplankton biomass and productivity: Australian Journal of Marine and Freshwater Research, v. 38, p. 569–590.

Harris, G.P., 1999, Comparison of the biogeochemistry of lakes and estuaries: Ecosystem processes, functional groups, hysteresis effects and interactions between macro- and microbiology: Marine and Freshwater Research, v. 50, p. 791–811.

—, 2001, Biogeochemistry of nitrogen and phosphorus in Australian catchments, rivers and estuaries: Effects of land use and flow regulation and comparisons with global patterns: Marine and Freshwater Research, v. 52, p. 139–149.

Harris, G.P., Davies, P., Nunez, M., and Meyers, G., 1988, Interannual variability in climate and fisheries in Tasmania: Nature, v. 333, p. 754–757.

Harrison, P.G., 1989, Detrital processing in seagrass systems: A review of factors affecting decay rates, remineralization and detritivory: Aquatic Botany, v. 35, p. 263–288.

Hastings, A., and Higgins, K., 1994, Persistence of transients in spatially structured ecological models: Science, v. 263, p. 1133–1136.

Hauxwell, J., Cebrián1, J., and Valiela, I, 2003, Eelgrass Zostera marina loss in temperate estuaries: relationship to land-derived nitrogen loads and effect of light limitation imposed by algae: Marine ecology progress series, v. 247, p.59 –73.

Heck, K.L., Pennock, J.R., Valentine, J.F., Coen, L.D., and Sklenar, S.A., 2000, Effects of nutrient enrichment and small predator density on seagrass ecosystems: An experimental assessment: Limnology and Oceanography, v. 45, p. 1041–1057.

Heck, K.L., and Valentine, J.F., 2006, Plant–herbivore interactions in seagrass meadows: Journal of Experimental Marine Biology and Ecology, v. 330, p. 420–436.

Heiri, O., Lotter, A.F., and Lemcke, G., 2001, Loss on ignition as a method for estimating organic and carbonate content in sediments: Reproducibility and comparability of results: Journal of Palaeolimnology, v. 25, p. 101–110.

Hicks, G.R.F., 1986, Distribution and behaviour of meiofaunal copepods inside and outside seagrass beds: Marine Ecology-Progress Series, v. 31, p. 159–170.

Hill, K.L., Rintoul, S.R., Coleman, R., and Ridgway, K.R., 2008, Wind forced low frequency variability of the east Australia current: Geophysical Research Letters, v. 35.

Hiromi, J., Hiyama, H., and Kadota S., 1988, Morphological observations of fecal pellets produced by inlet water copepods under experimental conditions: Bulletin of the College of Agriculture and Veternary Medicine, Nihon Unversity, v. 45, p. 219-226.

Holmer, M., and Olsen, A.B., 2002, Role of decomposition of mangrove and seagrass detritus in sediment carbon and nitrogen cycling in a tropical mangrove forest: Oldendorf, Allemagne, Inter-Research.

Holmes, R.W., 1970, Secchi disk in turbid coastal waters: Limnology and Oceanography, v. 15, p. 688–694.

Inkpen, R., and Wilson, G.P., 2009, Explaining the past: Abductive and Bayesian reasoning: Holocene, v. 19, p. 329–334.

Jackson, M.L., 1975, Soil chemical analysis advanced course (second edition): Wisconsin, M.L. Jackson.

Jackson, J.B.C., 2001, What was natural in the coastal oceans?: Proceedings of the National Academy of Sciences of the United States of America, v. 98, p. 5411–5418.

James, W.F., Best, E.P., and Barko, J.W., 2004, Sediment resuspension and light attenuation in Peoria Lake: Can macrophytes improve water quality in this shallow system?: Hydrobiologia, v. 515, p. 193–201.

James, N.P., Bone, Y., Brown, K.M., and Cheshire, A., 2009, Calcareous epiphyte production in cool-water carbonate seagrass depositional environments-south Australia, *in* Swart, P.K., Gregor, P.E., and McKenzie, J.A., eds., Perspectives in carbonate geology, Wiley-Blackwell, p. 123–148.

Jelbart, J.E., Ross, P.M., and Connolly, R.M., 2007, Patterns of small fish distributions in seagrass beds in a temperate Australian estuary: Journal of the Marine Biological Association of the United Kingdom, v. 87, p. 1297–1307.

Jorgensen, P., Ibarra-Obando, S.E., and Carriquiry, J.D., 2007, Top-down and bottom-up stabilizing mechanisms in eelgrass meadows differentially affected by coastal upwelling: Marine Ecology-Progress Series, v. 333, p. 81–93.

Karbassi, A.R., Nouri, J., Mehrdadi, N., and Ayaz, G.O., 2008, Flocculation of heavy metals during mixing of freshwater with Caspian Sea water: Environmental Geology, v. 53, p. 1811–1816.

Kareiva, P., and Wennergren, U., 1995, Connecting landscape patterns to ecosystem and population processes: Nature, v. 373, p. 299–302.

Kashima, K., 1990, Diatom assemblages in the surface sediments of Lake Shinji and Lake Nakaumi, Shimane Prefecture, Japan: Diatom, v. 5, p. 51–58.

Kemp, W.M., Boynton, W.R., Adolf, J.E., Boesch, D.F., Boicourt, W.C., Brush, G., Cornwell, J.C., Fisher, T.R., Glibert, P.M., Hagy, J.D., Harding, L.W., Houde, E.D., Kimmel, D.G., Miller, W.D., Newell, R.I.E., Roman, M.R., Smith, E.M., and Stevenson, J.C., 2005, Eutrophication of Chesapeake Bay: Historical trends and ecological interactions: Marine Ecology-Progress Series, v. 303, p. 1–29.

Kendrick, G, Duarte, C.M., and Marbà, N., 2005, Clonality in seagrasses, emergent properties and seagrass landscapes: Marine Ecology Progress Series, v. 290, p. 291-296.

Khalia, J.H., Santoso, A., and England, M.H., 2009, Interannual Tasmanian rainfall variability associated with large-scale climate modes: American Meteorological Society, v. 22, p. 4383–4397.

Khalil, K., Rabouille, C., Gallinari, M., Soetaert, K., DeMaster, D.J., and Ragueneau, O., 2007, Constraining biogenic silica dissolution in marine sediments: A comparison between diagenetic models and experimental dissolution rates: Marine Chemistry, v. 106, p. 223–238.

Kimmerer, W.J., and McKinnon, A.D., 1985, A comparative study of the zooplankton in two adjacent embayments, Port Phillip and Westernport Bay Australia: Estuarine Coastal and Shelf Science, v. 21, p.145–159.

—, 1987, Growth, mortality, and secondary production of the copepod acartia-tranteri in Western Port Bay, Australia: Limnology and Oceanography, v. 32, p. 14–28.

Knowlton, N., 2004, Multiple 'stable' states and the conservation of marine ecosystems: Progress in Oceanography, v. 60, p. 387–396.

Koch, E.W., 2001, Beyond light: Physical, geological, and geochemical parameters as possible submersed aquatic vegetation habitat requirements: Estuaries, v. 24, p. 1–17.

Kok, M.V., and Gundogar, A.S., 2010, Effect of different clay concentrations on crude oil combustion kinetics by thermogravimetry: Journal of Thermal Analysis and Calorimetry, v. 99, p. 779–783.

Kondrashov, D., Feliks, Y., and Ghil, M., 2005, Oscillatory modes of extended Nile River records (A.D. 622–1922): Geophysical Research Letters, v. 32, L10702, doi:10.1029/2004GL022156.

Kondrashov, D., and Ghil, M., 2006, Spatio-temporal filling of missing points in geophysical data sets: Non-linear Processes in Geophysics, v. 13, p. 151–159.

Kozerski, H.P., 1994, Possibilities and limitations of sediment traps to measure sedimentation and resuspension: Hydrobiologia, v. 284, p. 93–100.

Krishnaswami, S.D., Lal, D., Martin, J.M., and Meybeck, M., 1971, Geochronology of lake sediments: Earth and Planetary Science Letters, v. 11, p. 407–414.

Kristensen, E., 1990, Characterization of biogenic organic-matter by stepwise thermogravimetry (stg): Biogeochemistry, v. 9, p. 135–159.

—, 1994, Decomposition of microalage, vascular plants and sediment detritus in seawater-use of stepwise thermogravimetry: Biogeochemistry, v. 26, p. 1–24.

Kristensen, E., King, G.M., Holmer, M., Banta, G.T., Jensen, M.H., Hansen, K., and Bussarawit, N., 1994, Sulfate reduction, acetate turnover and carbon metabolism in sediments of the Ao-nam-bor mangrove, Phuket, Thailand: Marine Ecology-Progress Series, v. 109, p. 245–255.

Landres, P.B., Morgan, P., and Swanson, F.J., 1999, Overview of the use of natural variability concepts in managing ecological systems: Ecological Applications, v. 9, p. 1179–1188.

Larkum, A.W.D., and West, R.J., 1983, Stability, depletion and restoration of seagrass beds. Proceedings of Limnological Society New South Wales, Australia, v. 106, p. 202–212.

Lauridsen, T.L., Pedersen, L.J., Jeppsen, E., and Søndergaard, M., 1996, The importance of macrophyte bed size for cladoceran composition and horizontal migration in a shallow lake: Journal of Plankton Research, v. 18, p. 2283-2294.

Lavelle, J.W., Massoth, G.J., and Crecelius, E.A., 1985, Sedimentation rates in Puget Sound from ^{210}Pb measurements: Sequim, Pacific Marine Research Laboratory.

Leavitt, P.R., Hann, B.J., Smol, J.P., Zeeb, B.A., Christie, C.E., Wolfe, B., and Kling, H.J., 1994, Palaeolimnological analysis of whole-lake experiments—An overview of results from experimental lakes area 227: Canadian Journal of Fisheries and Aquatic Sciences, v. 51, p. 2322–2332.

Lecroart, P., Schmidt, I.S., Jouanneau, J.M., and Weber, O., 2005, Be-7 and Th-234 as tracers of sediment mixing on seasonal time scale at the water-sediment interface of the Thau Lagoon: Radioprotection, Suppl. 1, v. 40, p. 661–667.

Lee, K.S., Short, F.T., and Burdick, D.M., 2004, Development of a nutrient pollution indicator using the seagrass, Zostera marina, along nutrient gradients in three New England estuaries: Aquatic Botany, v. 78, p. 197–216.

Lehmann, M.F., Bernasconi, S.M., Barbieri, A., and McKenzie, J.C., 2002, Preservation of organic matter and alteration of its carbon and nitrogen isotope composition during simulated and in situ early sedimentary diagenesis: Geochimica et Cosmochimica Acta, v. 66, p. 3573–3584.

Levins, R., 1966, Strategy of model building in population bioogy: American Scientist, v. 54, p. 421–431.

Lindberg, S.E., and Harriss, R.C., 1973, Mechanisms controlling pore water salinities in a salt marsh: Limnology and Oceanography, v. 18, p. 788–791.

Livingston, R.J., 1984, The relationship of physical factor and biological responses in coastal seagrass meadows: Estuaries, v. 7, p. 377–390.

Lipton, P., 2000, Inference to the best explanation, *in* Newton-Smith, W.H., ed., A companion to the philosophy of science: Blackwell, p. 184–193.

Liu, J., Carroll, J.L., and Lerche, I., 1991, A technique for distentangling temporal source and sediment variations from radioactive isotope measrements with depth: Nuclear Geophysics, v. 5, p. 31–45.

Loh, P.S., Reeves, A.D., Harvey, S.M., Overnell, J., and Miller, A.E.J., 2008, The fate of terrestrial organic matter in two Scottish sea lochs: Estuarine Coastal and Shelf Science, v. 76, p. 566–579.

Longmore, M.E., O'Leary, B.M., and Rose, C.W., 1983, Caesium-137 profiles in the sediments of a partial-meromictic lakeon Great Sandy Island (Fraser Island), Queensland, Australia: Hydrobiologia, v. 103, p. 21–27.

Lu, X.Q., and Matsumoto, E., 2005, Recent sedimentation rates derived from Pb-210 and Cs-137 methods in Ise Bay, Japan: Estuarine Coastal and Shelf Science, v. 65, p. 83–93.

Lu, H., and Liu, K., 2003, Phytoliths of common grasses in the coastal environments of southeastern USA: Estuarine, Coastal and Shelf Science, v. 58, p. 587–600.

Mader, C.L., 2008, Numerical modeling of water waves: Boca Raton, CRS Press.

Maire, O., Lecroart, P., Meysman, F., Rosenberg, R., Duchene, J.C., and Gremare, A., 2008, Quantification of sediment reworking rates in bioturbation research: A review: Aquatic Biology, v. 2, p. 219–238.

Marbà, N., and Duarte, C.M., 1997, Interannual changes in seagrass (Posidonia oceanica) growth and environmental change in the spanish Mediterranean littoral zone: Limnology and Oceanography, v. 42, p. 800–810.

Marsden-Smedley, J.B., 1997, Fire and fuel in Tasmania button grass moorlands: Gegime characteristics, behavior and management: PhD thesis, Hobart, University of Tasmania.

Martin, P., Sebastien, D., Gilles, T., Isabelle, A., de Montaudouin, X., Emery, E., Claire, N., and Christophe, V., 2010, Long-term evolution (1988–2008) of Zostera spp. Meadows in France Bay (Bay of Biscay): Estuarine Coastal and Shelf Science, v. 87, p. 357–366.

Matisoff, G., 1980, Time-dependent transport in Chesapeake Bay sediments: Temperature and chloride: American Journal of Science, v. 280, p. 1–25.

Macreadie, P.I., Hindell, J.S., Perkins, G.P., Connolly, R.M., and Keough, J., 2009, Fish responses to experimental fragmentationof seagrass habitat: Conservation Biology, v. 23, p. 644–652.

Macreadie, P.I., Rod, M., Connolly, C., Gregory, P., Jenkins, A.D., Jeremy, S., Hindell, A.E., and Keough, M.J., 2010, Edge patterns in aquatic invertebrates explained by predictive models: Marine and Freshwater Research, v. 61, p. 214–218.

Mayr, E., 1982, The growth of biological thought: Cambridge: Harvard University Press.

McGowan, S., Leavitt, P.R., Hall, R.I., Anderson, N.J., Jeppesen, E., and Odgaard, B.V., 2005, Controls of algal abundance and community composition during ecosystem state change: Ecology, v. 86, p. 2200–2211.

McGuinness, K.A., 1988, Explaining patterns in abundances of organisms on boulders: The failure of 'natural experiments': Marine Ecology-Progress Series, v. 48, p. 199–204.

McIntosh, P.D., Laffan, M., and Hewitt, A.E., 2005, The role of fire and nutrient loss in the genesis of the forest soils of Tasmania and southern New Zealand: Forest Ecology and Management, v. 220, p. 185–215.

Michalopoulos, P., and Aller, R.C., 2004, Early diagenesis of biogenic silica in the Amazon Delta: Alteration, authigenic clay formation, and storage: Geochimica Et Cosmochimica Acta, v. 68, p. 1061–1085.

Middelburg, J.J., 1989, A simple rate model for organic matter decompostion in marine sediments: Geochimica et Cosmochimica Acta, v. 53, p. 1577–1581.

Middleton, G.V., 1993, Sediment deposition from turbidity currents: Annual Review of Earth and Planetary Sciences, v. 21, p. 89–114.

Milly, P.C.D., wetherrald, R.T., Dunne, K.A., Delworth, T.L., 2002, Increasing risk of great floods in a changing climate: Nature, v 415, p514-517.

Mohr, L.B., 1982, Explaining organizational behavior: The limits of possibilities of theory and research: San Francisco, Jossey-Bass.

Moksnes, P.-O., Gullström, M., Tryman, K., and Baden, S., 2008, Trophic cascades in a temperate seagrass community: Oikos, v. 117, p. 763–777.

MOLTEN, 2004, Monitoring long-term trends in eutrophication and nutrients in the coastal zone: Creation of guidelines for the evaluation of background conditions, anthropogenic influence and recovery: www.Craticula.ncl.ac.uk:8000/Molten/jsp/index.jsp.

Mook, D.H., and Hoskin, C.M., 1982, Organic determinations by ignition: Caution advised: Estuarine Coastal and Shelf Science, v. 15, p. 697–699.

Morales, J.A., Borrego, J., Miguel, E.G.S., Lopez-Gonzalez, N., and Carro, B., 2008, Sedimentary record of recent tsunamis in the Huelva estuary (southwestern Spain): Quaternary Science Reviews, v. 27, p. 734–746.

Moreno, A., Valero-Garces, B.L., Gonzalez-Samperiz, P., and Rico, M., 2008, Flood response to rainfall variability during the last 2000 years inferred from the Taravilla lake record (central Iberian range, Spain): Journal of Palaeolimnology, v. 40, p. 943–961.

Morris, A.W., 1983, Practical procedures for estuarine studies: The Natural Environmental Research Council.

Morris, L., and Virnstein, R.W., 2004, The demise and recovery of seagrass in the northern Indian River Lagoon, Florida: Estuaries, v. 27, p. 915–922.

Morton, R.A., and Donaldson, A.C., 1973, Sediment distribution and evolution of tidal deltas along a tide-dominated shoreline, Wachapreague, Virginia: Sedimentary Geology, v. 10, p. 285–299.

Mount, R., Lucieer, V., Lawler M., and Jordan, A., 2005, Mapping of estuarine and marine habitats in the southern NRM regio: Marine Research Laboratories, Tasmanian Aquaculture and Fisheries Institute, University of Tasmania.

Nagy, L., Fairbrother, A., Etterson, M., and Orme-Zavaleta, J., 2007, The intersection of independent lies: Increasing realism in ecological risk assessment: Human and Ecological Risk Assessment, v. 13, p. 355–369.

NRC, 2000, Clean coastal waters understanding and reducing the effects of nutrient pollution committee on the causes and management of coastal eutrophication ocean studies board and water science and technology board: Washington, D.C., National Acadamy Press, 428 p.

Nelson, C.S., and Smith, A.M., 1996, Stable oxygen and carbon isotope compositional fields for skeletal anddiagenetic components in New Zealand Cenozoic nontropical carbonatesediments and limestones: A synthesis and review: New Zealand Journal of Geology and Geophysics, v. 39, p. 93–107.

Nienhuis, P., De Bree, B., Herman, P., Holland, A., Verschuure, J., and Wessel, E., 1996, Twenty five years of changes in the distribution and biomass of eelgrass: Zostera marina in Grevelingen Lagoon, The Netherlands: Aquatic Ecology, v. 30, p. 107–117.

Nunez, M., and Li, Y., 2008, A cloud-based reconstruction of surface solar radiation trends for Australia: Theoretical and Applied Climatology, v. 91, p. 59–75.

Nunez, M., and McGregor, J.L., 2007, Modelling future water environments of Tasmania, Australia: Climate Research, v. 34, p. 25–37.

Nyqvist, A., André, C., Gullström, M., Baden, S.P., and Åberg, P., 2009, Dynamics of seagrass meadows on the Swedish Skagerrack Coast: Ambio, v. 38, p. 85-88.

Oldfield, F., and Appleby, P.G., 1984, Empirical testing of ^{210}Pb-dating models for lakesediments, *in* Haworth, E.Y., and Lund, J.W.G., eds., Lake sediments and environmental history, studies in palaeolimnology and palaeoecology in honour of Winifred Tutin: Leicester, Leicester University Press, p. 93–124.

Orem, W.H., Holmes, C.W., Kendall, C., Lerch, H.E., Bates, A.L., Silva, S.R., Boylan, A., Corum, M., Marot, M., and Hedgman, C., 1999, Geochemistry of Florida Bay sediments: Nutrient history at five sites in eastern and central Florida Bay: Journal of Coastal Research, v. 15, p. 1055–1071.

Orth, R.J., Carruthers, T.J.B., Dennison, W.C., Duarte, C.M., Fourqurean, J.W., Heck Jr, K.L., Hughes, A.R., Olyarnik, S., Williams, S.L., Kendrick, G.A., Kenworthy, W.J., Short, F.T., and Waycott, M., 2006, A global crisis for seagrass ecosystems: Bioscience, v. 56, p. 987–996.

OzCoasts, 2006, Australian online coastal information: www.Ozcoasts.org.au.

Papadimitriou, S., Kennedy, H., Kennedy, D.P., and Borum, J., 2005, Seasonal and spatial variation in the organic carbon and nitrogen concentration and their stable isotopic composition in Zostera marina (Denmark): Limnology and Oceanography, v. 50, p. 1084–1095.

Parsons, T.R., Takahashi, M., and Hargrave, B., 1984., Biological oceanographic processes: Oxford, Pergamon Press.

Pastor, J., Mladenoff, D.J., Haila, Y., Bryant, J., and Payette S., 1996, Biodiversity and ecosystem processes in boreal regions: *in* Mooney, H.A., Cushman, J.H., Medina, E., Sala, O.E., and Schulze, E.-D., editors, Functional roles of biodiversity: A global perspective: New York, John Wiley.

Paulsen, S.C., List, E.J., and Santschi, P.H., 1999, Modeling variability in Pb-210 and sediment fluxes near the whites point outfalls, palaeo verdes shelf, California: Environmental Science & Technology, v. 33, p. 3077–3085.

Perdue, E.M., and Koprivnjak, J.F., 2007, Using the C/N ratio to estimate terrigenous inputs of organic matter to aquatic environments: Estuarine, Coastal and Shelf Science, v. 73, p. 65–72.

Perry, C.T., and Beavington-Penney, S.J., 2005, Epiphytic calcium carbonate production and facies development within sub-tropical seagrass beds, Inhaca Island, Mozambique: Sedimentary Geology, v. 174, p. 161–176.

Peters, R.H., 1986. The role of prediction in limnology: Limnology and Oceanography, v. 31, p. 1143–1159.

—, 1991, A critique for ecology: New York, Cambridge University Press.

Pettit, A.N., 1980, A simple cumulative sum type statistic for the change-point problem with zero-one observations: Biometrika, v. 67, p. 79–84.

Pihl, L., Baden, S., Kausky, N., Rönnbilck, P., Söderqvist, T., Troell, M., and Wennhage, H., 2006, Shift in fish assemblage structure due to loss of seagrass *Zostera marina* habitats in Sweden: Estuarine Coastal and Shelf Science, v. 67, p. 123-132.

Plew, D.R., 2011, Shellfish farm-induced changes to tidal circulation in an embayment, and implications for seston depletion: Aquaculture Environment Interactions, v. 1, p. 201–214.

Philippart, C.J.M., and Cadee, G.C., 2000, Was total primary production in the western Wadden Sea stimulated by nitrogen loading?: Helgoland Marine Research, v. 54, p. 55–62.

Polkinghorne, D.E., 1988, Narrative knowing and the human sciences: Albany, State University of New York Press.

Pook, M.J., 1992, A note on the variability of the mid-tropospheric flow over the southern ocean in the Australian region: Australian Meteorological Magazine, v. 40, p. 169–177.

Priyadarshana, T., Asaeda, T., and Manatunge, J., 2001, Foraging behaviour of planktivorous fish in artificial vegetation: The effects on swimming and feeding: Hydrobiologia, v. 442, p. 231–239.

Redfield, A.C., Ketchum, B.H., and Richards, F.A., 1963, The influence of organisms on the composition of sea water, *in* Hill, M.N., ed., The Sea: London, Wiley, v. 2, p. 26–77.

Ray, R.D., 2007, Decadal climate variability: Is there a tidal connection?: Journal of Climatology, v. 20, p. 3542-3560.

Rees, C.G., 1993, Tasmanian seagrass communities [M.Sc. thesis]: Hobart, University of Tasmania.

Reeves, G., and Duncan, S., 2009, Ecological history vs. Social expectations: Managing aquatic ecosystems: Ecology and Society, v. 14.

Reimer, P.J., and Reimer, R.W., 2006, Marine Resevoir Correction Database: www.calib.qub.ac.uk/marine/

Report of the Commissioners, 1883, Royal commission on the fisheries of Tasmania: Hobart, William Thomas Strutt, Government printer.

Rietkerk, M., Dekker, S.C, de Ruiter, P.C, van de Koppel J., 2004, Self-organized patchiness and catastrophic shifts in ecosystems: Science, v. 305, p. 1926–1929.

Riley, J.P., and Chester, R., 1971, Introduction to marine chemistry (third edition): Academic Press.

Robbins, J.A., 1978, Biogeochemistry of lead in the environment: Amsterdam, Elsevier Scientific, p. 285–393.

Robbins, B.D., and Bell, S.S., 1994, Seagrass landscapes: A terrestrial approach to the marine subtidal environment: Trends in Ecology and Evolution, v. 9, p. 301–303.

Robertson, A.I., and Mann, K.H., 1980, The role of isopods and amphipods in the initial fragmentation of eelgrass detritus in Nova-Scotia, Canada: Marine Biology, v. 59, p. 63–69.

Round, F., Crawford, R.M., and Mann, D.G., 1990, The diatoms: Biology and morphology of the genera: Cambridge, Cambridge University Press.

Roy, P.S., and Thom, B.G., 1981, Late quaternary marine deposition in new-south-wales and southern queenslan—An evolutionary model: Journal of the Geological Society of Australia, v. 28, p. 471–489.

Roy, P.S., Williams, R.J., Jones, A.R., Yassini, I., Gibbs, P.J., Coates, B., West, R.J., Scanes, P.R., Hudson, J.P., and Nichol, S., 2001, Structure and function of south-east Australian estuaries: Estuarine Coastal and Shelf Science, v. 53, p. 351–384.

Ruddiman, W.F., Molfino, B., Esmay, A., and Pokras, E., 1980, Evidence bearing on the mechanism of rapid deglaciation: Climatic Change, v. 3, p. 65–87.

Ruiz-Fernandez, A.C., Hillaire-Marcel, C., Ghaleb, B., Soto-Jimene´z, M., and Pa´ez-Osuna, F., 2002, Recent sedimentary history of anthropogenic impacts on the Culiacan River estuary, north western Mexico: Geochemical evidence from organic matter and nutrients: Environmental Pollution, v. 118, p. 365– 377.

Rustomji, P., 2007, Flood and drought impacts on the opening regime of a wave-dominated estuary: Marine and Freshwater Research, v. 58, p. 1108–1119.

Salita, J.T., Ekau, W., and Saint-Paul, U, 2003, Field evidence on the influence of seagrass landscapes on fish adundance in Bolinao, northern Philipines: Marine Ecology Progress Series, v. 247, p. 183-195.

Santisteban, J.I., Mediavilla, R., Lopez-Pamo, E., Dabrio, C.J., Zapata, M.B.R., Garcia, M.J.G., Castano, S., and Martinez-Alfaro, P.E., 2004, Loss on ignition: A qualitative

or quantitative method for organic matter and carbonate mineral content in sediments: Journal of Palaeolimnology, v. 32, p. 287–299.

Saunders, K.M., McMinn, A., Roberts, D., Hodgson, D.A., and Heijnis, H., 2007, Recent human-induced salinity changes in Ramsar-listed Orielton Lagoon, south-east Tasmania, Australia: A new approach for coastal lagoon conservation and management: Aquatic Conservation-Marine and Freshwater Ecosystems, v. 17, p. 51–70.

Scanes, P., Coade, G., Doherty, M., and Hill, R., 2007, Evaluation of the utility of water based indicators of estuarine lagoon condition in NSW, Australia: Estuarine, Coastal, and Shelf Science, v. 74, p. 306–319.

Scheffer, M., 2004, Ecology of shallow lakes, Dordrecht: Boston, Kluwer Academic.

Scheffer, M., and Carpenter, S.R., 2003, Catastrophic regime shifts in ecosystems: Linking theory to observation: Trends in Ecology and Evolution, v. 18, p. 648–656.

Schelske, C.L., and Hodell, D.A., 1995. Using carbon isotopes of bulk sedimentary organic matter to reconstruct the history of nutrient loading and eutrophication in Lake Erie: Limnology and Oceanography, v. 40, p. 918–929.

Schiffelbein, P., 1985, Extracting the benthic mixing impulse-response function—A constrained deconvolution technique: Marine Geology, v. 64, p. 313–336.

Schleppi, P., Bucher-Wallin, I., Saurer, M., Jäggi, M., and Landolt, W., 2006, Citric acid traps to replace sulphuric acid in the ammonia diffusion of dilute water samples for $\delta^{15}N$ analysis: Rapid Communications in Mass Spectrometry, v. 20, p. 629-634.

Schneider, D.C., and Piatt, J.F., 1986, Scale-dependent correlation of seabirds with schooling fish in a coastal ecosystem: Marine Ecology Progress Series, v. 32, p. 237-246.

Schröder, A., Persson, L., and De Roos, A.M., 2005, Direct experimental evidence for alternative stable states: A review: Oikos, v. 110, p. 3-19.

Schröder, W.W., Dinnel, S.P., and Wiseman, W.J., Jr., 1990, Salinity stratification in a river-dominated estuary: Estuaries, v. 13, p. 145–154.

Sharma, P., Gardner, L.R., Moore, W.S., and Bollinger, M.S., 1987, Sedimentation and bioturbation in a salt-marsh as revealed by Pb-210, Cs-137, and Be-7 studies: Limnology and Oceanography, v. 32, p. 313–326.

Sholkovitz, E.R., and Copland, D., 1981, The coagulation, solubility and adsorption properties of Fe, Mn, Cu, Ni, Cd, Co and humic acids in river water: Geochimica et Cosmochimica Acta, v. 45, p. 181–189.

Shumway, S.E., 2011, Shellfish aquaculture and the environment, ed. Shumway, S.E., Chester: Wiley Blackwell.

Sigmon, D.E., and Cahoon, L.B., 1997, Comparative effects of benthic microalgae and phytoplankton on dissolved silica fluxes: Aquatic Microbial Ecology, v. 13, p. 275–284.

SKM, 2004, Little swanport river catchment—Water balance model and scenario assessment Armadale, Victoria: www.DPIW.tas.gov.au.

Sloss, C.R., Murray-Wallace, C.V., and Jones, B.G., 2007, Holocene sea-level change on the southeast coast of Australia: A review: Holocene, v. 17, p. 999–1014.

Smith, I.R, 1975, Behaviour of small particles in turbulent flow: Freshwater Biological Association, issue 29 of Scientific Publications.

Smith, J.N., 2001, Why should we believe Pb-210 sediment geochronologies?: Journal of Environmental Radioactivity, v. 55, p. 121–123.

Smith, N.D., and Syvitski, J.P.M., 1982, Sedimentation in a glacier-fed lake—The role of pelletization on deposition of fine-grained suspensates: Journal of Sedimentary Petrology, v. 52, p. 503–513.

Smith, T.M., Hindell, J.S., Jenkins, G.P., and Connolly, R.M., 2008, Edge effects on fish associated with seagrass and sand patches: Marine Ecology-Progress Series, v. 359, p. 203–213.

Smol, J.P., Birks, H.J.B., and Last, W.M., 2001, Using biology to study long-term environmental change, *in* Smol, J.P., Birks, H.J.B., and Last, W.M., eds., Tracking environmental change using lake sediments: Terrestrial, algal and siliceous indicators, v. 3: Dordrecht, The Netherlands.

Somayajulu, B.L.K., Bhushan, R., Sarkar, A., Burr, G.S., and Jull, A.J.T., 1999, Sediment deposition rates on the continental margins of the eastern Arabian Sea using Pb-210, Cs-137 and c-14: Science of the Total Environment, v. 238, p. 429–439.

Sommer, F, Stibor, H., Sommer, U., and Velimirov, B., 2000, Grazing by mesozooplankton from Kiel Bight, Baltic Sea, on different sized algae and natural seston size fractions: Marine Ecology Progress Series, v. 199, p. 43-53.

Songsangjinda, P., Matsuda, O., Yamamoto, T., Rajendran, N., and Maeda, H., 2000, The role of suspended oyster culture on nitrogen cycle in Hiroshima Bay: Journal of Oceanography, v. 56, p. 223-231.

Sørensen, P., and Jensen, E.S., 1991, Sequential diffusion of ammonium and nitrate from soil extracts to a polytetrafluoroethylene trap for 15n determination: Analytica Chimica Acta, v. 252, p. 201-203.

Soulet, G., Delaygue, G., Vallet-Coulomb, C., Böttcher, M.E., Sonzogni, C., Lericolais, G., and Bard, E., 2010, Glacial hydrologic conditions in the Black Sea reconstructed using geochemical pore water profiles: Earth and Planetary Science Letters, v. 296, p. 57–66.

Southward A.J., E.I. Butler, L., and Cuick, P., 1975, Recent cyclic changes in climate and in abundance of marine life: Nature, v. 253, p. 710-715.

Southward A.J., 1980, The Western English Channel, an inconstant ecosystcm?: Nature, v. 285, p. 361-366.

Staff, G.M., Callender, R.W., Powell, E.N., Parsons-Hubbard, K.M., Brett, C.E., Walker, S.E., Carlson, D.D., White, S., Raymond, A., and Heise, E.A., 2002, Taphonomic trends along a forereef slope: Lee Stocking Island, Bahamas: Palaios, v. 17, p. 66–83.

Stenseth, N.C., Ottersen, G., Hurrell, J.W., Mysterud, A., Lima, M., Chan, K.S., Yoccoz, N.G., and Adlandsvik, B., 2003, Studying climate effects on ecology through the use of climate indices: The North Atlantic oscillation, EL Nino southern oscillation and beyond: Proceedings of the Royal Society of London Series B-Biological Sciences, v. 270, p. 2087–2096.

Steffen, W., Grinevald, J., Crutzen, P., and Mcneill, J., 2011, The Anthropocene: Conceptual and historical perspectives: Philisophical Transaction of the Royal Society, v. 369, p. 842–867.

Stiller, M., Kaushansky, P., and Carmi, I., 1983, Recent climatic changes recorded by the salinity of pore waters in the Dead Sea sediments: Hydrobiologia, v. 103, p. 75–79.

Strayer, D.L., Glitzenstein, J.S., Jones, C., Kolasa, J., Likens, G.E., McDonnell, M., Parker, G.G., and Pickett, S.T.A. (1986). Long term ecological studies: An illustrated account of their design, operation, and importance to ecology: Occasional Publication of the Institute of Ecosystem Studies, No. 2., Millbrook, New York.

Suess, E., 1978, Distinction between natural and anthropogenic material in sediments: Biogeochemistry of Estuarine Sediments: Melreux, Belgium, UNESCO/SCOR, p. 224–237.

Sugihara, G., May, R., Ye, H., Haleh, C.H., Deyle, E., Fogarty, M., and Munch, S., 2012, Detecting causality in complex ecosystems: Science, www.sciencemag.org/content/early/2012/09/19/science.1227079.

Swart, P.K., Burns, S.J., and Leder, J.J., 1991, Fractionation of stable isotopes of oxygen and carbon in carbon dioxide during the reaction of calcite with phosphoric acid as a function of temperature and technique: Chemical Geology, v. 86, p 89–96.

Switzer, A.D., and Jones, B.G., 2008, Large-scale washover sedimentation in a freshwater lagoon from the southeast Australian coast: Sea-level change, tsunami or exceptionally large storm?: Holocene, v. 18, p. 1014–1016.

Taylor, W., 2000, Change-point analyzer 2.0 shareware program: Libertyville, Illinois, Taylor Enterprises: www.variation.com/cpa.

Toba, Y., Suzuki, N., and Komori, S., 2008, Discrimination of spurious self-Correlation innondimensionalized analyses of fluid dynamical data: Journal of Oceanography, v. 64, p. 393-397.

Thompson, P.A., Baird, M.E., Ingleton, T., and Doblin, M.A., 2009, Long-term changes in temperate Australian coastal waters: Implications for phytoplankton: Marine Ecology-Progress Series, v. 394, p. 1–19.

Thorndycraft, V., Hu, Y., Oldfield, F., Crooks, P.R.J., and Appleby, P.G., 1998, Individual flood events detected in the recent sediments of the Petit Lac d'Annecy, eastern France: The Holocene, v. 8, p. 741–746.

Trull, T.W., Davies, D., and Casciotti, K., 2008, Insights into nutrient assimilation and export in naturally iron-fertilized waters of the Southern Ocean from nitrogenm carbon and oxygen isotopes: Deep-Sea Research, v. 55, p. 820–840.

Tukey, J. W., 1977, Exploratory Data Analysis: Addison-Wesley, Reading.

Tully, J.P., 1949, Oceanography and prediction of pulpmill pollution in Alberni Inlet: Bulletin of the Fisheries Research Board of Canada, v. 83.

Turekian, K.K., Nozaki, Y., and Benninger, L.K., 1977, Geochemistry of atmospheric radon and radon products: Annual Review of Earth and Planetary Sciences, v. 5, p. 227–255.

Turner, R.E., Rabalais, N.N., Fry, B., Atilla, N., Milan, C.S., Lee, J.M., Normandeau, C., Oswald, T.A., Swenson, E.M., and Tomasko, D.A., 2006, Palaeo-indicators and water quality change in the Charlotte Harbor estuary (Florida): Limnology and Oceanography, v. 51, p. 518–533.

Ueda, H., Kuwahara, A., Tanaka, M., and Azeta, M., 1983, Underwater observations on copepod swarms in temperate and sub-tropical waters: Marine Ecology-Progress Series, v. 11, p. 165–171.

Uye, S., and Kaname, K., 1994, Relations between faecal pellet volume and body size for major zooplankters of the Inland Sea of Japan: Journal of Oceanography, v. 50, p. 43–49.

Valentine, J.F.,and Duffy, J.E., 2006, The central role of grazing in seagrass ecology: Seagrasses: biology, ecology and conservation, Lakum, W.D., Orth, R.J., and Duarte, C.M. eds., p 463-50.

van Nes, E.H., and Scheffer, M., 2005, Implications of spatial heterogeneity for catastrophic regime shifts in ecosystems: Ecology, v. 86, p. 1797–1807.

van Nes, E.H., Rip, W.J., and Scheffer, M., 2007, A theory for cyclic shifts between alternative states in shallow lakes: Ecosystems, v. 10, p. 17–27.

Vautard, R., Yiou, P., and Ghil, M., 1992, Singular-spectrum analysis: A toolkit for short, noisy chaotic signals: Physica D: Non-linear Phenomena, v. 58, p. 95–126.

Viitasalo, M., Rosenberg, M., Heiskanen, A-S., and Marja, K., 1999, Sedimentation of copepod fecal material in the coastal northern Baltic Sea: Where did all the pellets go?: Limology and Oceanography, v. 44, p. 1388-1399.

von Gunten, L., Grosjean, M., Beer, J., Grob, P., Morales, A., and Urrutia, R., 2009, Age modeling of young non-varved lake sediments: Methods and limits. Examples from two lakes in central Chile: Journal of Palaeolimnology, v. 42, p. 401–412.

von Platen, J., 2008, A history and interpretation of fire frequency in dry eucalypt forests and woodlands of eastern Tasmania, University of Tasmania.

Wan, G.J., Chen, J.A., Xu, S.Q., Wu, F.C., Wan, E.Y., Yang, W., and Santschi, P.H., 2004, The coupling relation between Pb-210(ex) and organic matter in sediments of enrichment nutrient lake: An example from Lake Chenghai, China: Geochimica Et Cosmochimica Acta, v. 68, p. A397–A397.

Ward, L.G., Kemp, W.M., and Boynton, W.R., 1984, The influence of waves and seagrass communities on suspended particulates in an estuarine embayment: Marine Geology, v. 59, p. 85–103.

Waycott, M., Duarte, C.M., Carruthers, T.J.B., Orth, R.J., Dennison, W.C., Olyarnik, S., Calladine, A., Fourqurean, J.W., Heck, K.L., Hughes, A.R., Kendrick, G.A., Kenworthy, W.J., Short, F.T., Williams, S.L., 2009, Accelerating loss of seagrasses across the globe threatens coastal ecosystems: Proceedings of the National Academy of Sciences of United States of America, v. 106, p. 12377–12381.

Wiens, J.A., 1989, Spatial scaling in ecology: Functional Ecology, v. 3, p. 385–397.

Weisberg, M., 2006, Forty years of 'the strategy': Levins on model-building and idealization: Biology and Philosophy, v. 21, p. 623–645.

Welsh, D.T., 2000, Nitrogen fixation in seagrass meadows: Regulation, plant–bacteria interactions and significance to primary productivity: Ecology Letters, v. 3, p. 58–71.

Wheatcroft, R.A., 1992, Experimental tests for particle size-dependent bioturbation in the deep ocean: Limnology and Oceanography, v. 37, p. 90–104.

Wolfe, D.A., Champ, M.A., Flemer, D.A., and Mearns, A.J., 1987, Long-term biological data sets: Their role in research, monitoring, and management of estuarine and coastal marine systems: Estuaries, v. 10, p. 181–193.

Woodward, I.O, Gallagher, J.B., Ruston, M., Machin, J., and Milalenko J., 1992, Salmon Farming and the environment of the Huon Estuary: Tech Report 45 Division of Seafisheries, Crayfish point, Taroona Hobart, Tasmania.

Willis, K.J., and Birks, H.J.B., 2006, What is natural? The need for a long-term perspective in biodiversity conservation: Science, v. 314, p. 1261–1265.

Wu, Y.H., Lucke, A., and Wang, S.M., 2008, Assessment of nutrient sources and palaeoproductivity during the past century in Longgan Lake, middle reaches of the Yangtze River, China: Journal of Palaeolimnology, v. 39, p. 451–462.

Yamakita, T., Watanabe, K., and Nakaoka, M., 2010, Asynchronous local dynamics contributes to stability of a seagrass bed in Tokyo Bay: Ecography, v. 34, p. 519–528.

Xinping, H., and Burdige, D.J., 2007, Enriched stable carbon isotopes in the pore waters of carbonate sediments dominated by seagrasses: Evidence for coupled carbonate dissolution and reprecipitation: Geochimica et Cosmochimica Acta, v. 71, p. 129–144.

Zieman, J.C., Fourqurean, J., and Frankovich, T.A., 1999, Seagrass die off in Florida Bay(USA): Long-term trends in abundance and growth of Thalassia testudinum and the role of hypersalinity and temperature: Estuaries, v. 22, p. 460–470.

Zimmerman, A.R., and Canuel, E.A., 2002, Sediment geochemical records of eutrophication in the mesohaline Chesapeake Bay: Limnology and Oceanography, v. 47, p. 1084–1093.

Zimmerman, G.M., Lean, D.R.S., and Charlton, S.M, 1987, Differential thermal and thermo-gravimetric analysis of sediment forming materials from Lake Ontario: Canadian Journal of Fisheries and Aquatic Science, v. 44, p. 2216–2224.

Zong, Y., Lloyd, J.M., Leng, M.J., Yim, W.W.S., and Huang, G., 2006, Reconstruction of Holocene monsoon history from the Pearl River estuary, southern China, using diatoms and carbon isotope ratios: Holocene, v. 16, p. 251–263.